Philipp Eisenbach

PROCESSING OF SLENDER CONCRETE SHELLS — FABRICATION AND INSTALLATION

Philipp Eisenbach

PROCESSING OF SLENDER CONCRETE SHELLS — FABRICATION AND INSTALLATION

This work has been accepted by the *Faculty of Architecture – Urban and Regional Planning – Landscape Architecture and Landscape Planning* of the *University of Kassel* as a thesis for acquiring the academic degree of *Doktor der Ingenieurwissenschaften* (Dr.-Ing.).

Philipp Eisenbach (philipp@eisenbach.info)

Preface

Today the whole construction industry is facing tremendous challenges. It already is responsible for the major parts of emissions, resource and energy consumption as well as waste disposal. Taking into account the upcoming global demographic changes we are facing big challenges to satisfy the upcoming infrastructure demands without exhausting resources and without diminishing ambitions of structural aesthetics. With this background the significance of lightweight structures, for which Frei Otto had already created the foundations in the last century, could hardly be more recent.

The building practice, particularly in concrete construction, is dominated by repetitive standards of industrial production. The built environment does not reflect possibilities provided by developments in computation and material science. As current chair of the scientific committee of the International Association for Shell and Spatial Structures (IASS) I can acknowledge that responsibility is increasingly identified in science and constitutes the focus of several research efforts.

Philipp Eisenbach intensely and creatively dealt with the matter of how to implement slender concrete structures in the environment. In my Department of Structural Design we have positive experience in linking science and teaching by integrating the creativity and curiosity of students in our research. With Philipp's methodology to demonstrate constructive principals with design-and-built ventures inconsistencies cannot be blurred away. Financial or facility constraints are not contradictory for the creation of aesthetic structures since constraints typically necessitate unconventional solutions.

I am sure that his work is a significant contribution to the realization of contemporary lightweight concrete structures that opens up a wide range of possibilities and inspiration for architects and engineers.

Kassel, January 2017   Manfred Grohmann

Acknowledgements

Frankfurt, January 2017   Philipp Eisenbach

Abstract

Lightweight structures and material optimized systems are the key objectives of several research efforts. This is not only for aesthetic reasons, but also to use materials in a more resource conserving way.

Minimization of cross-section dimensions is achieved by two measures: Firstly the increase of strength and stiffness characteristics, secondly the directed allocation of material within a given design-space in order to create form dependent structures. For both, the material and the form-giving aspects, progresses have been made recently.

Technical advances in computation allow digitized form finding processes and the analysis of complex geometries, as well as the transfer to computer-aided manufacturing. Improvements in material science, focusing on cementitious materials, lead to high- and ultra-high performance concrete, with compressive strength characteristics, closing up with the properties of steel. In combination with respective reinforcement strategies, high tensile and bending tensile capacities and ductile material behaviour are also enabled.

Despite the possibilities at hand, it can be observed that the potential is not reflected in built architecture. One reason is a lack of experience and the consequent economical risks, but also implementation features on site: The greater the material performance, the higher the requirements of precision in manufacturing and post-treatment, necessitating a prefabrication under laboratory conditions.

This thesis examines the contradiction of the possibility to reduce cross-section dimensions, and the complexity of the discontinued homogeneity arising from segmentation. The objective is to expand the planning and the variety of contemporary concrete shells.

Connection typologies are categorized according to their mechanical behaviour, to enable the development of jointing strategies. Selected case studies, all of them either exhibited or surrendered to the public, are demonstrating approaches, about how to implement prefabricated concrete elements on site.

Two developed connection methods are investigated in detail, and their applicability is verified by the evaluation of experimental examinations.

The 'seamless rigid connection technique' is a fully load bearing connection, in which the necessary overlapping of micro reinforcement layers within the joint zone is enabled by two subsequent casting steps and the associated invention of a stop-end technique.

The 'micro prestressing connection technique' is based on the idea to scale system dimensions of concrete sections. In analogy to mesh wire reinforcement, small prestressing media with small axial distances are constructed and embedded in slender concrete elements.

Zusammenfassung

Konstruktiver Leichtbau und materialoptimierte Tragwerke dienen als Motivation diverser Forschungsvorhaben. Neben direkter Kosteneinsparung und gestalterischen Gründen ist ein ressourcenschonender Materialeinsatz von zentraler Bedeutung.

Die Reduzierung von Querschnittsdimensionen wird durch zwei Maßnahmen erreicht: Erstens die Verbesserung von Materialeigenschaften, und zweitens die gezielte stoffliche Anordnung innerhalb eines vorgegebenen Entwurfsraums zur Erschaffung formabhängiger Tragwerke. Für beide Ansätze wurden in den vergangen Jahren große Fortschritte erzielt.

Möglich sind nicht nur digitale Formfindungsprozesse komplexer Strukturen und deren Berechnung, sondern auch der Datentransfer zu einer computergestützten Fabrikation. Errungenschaften in der Betontechnologie ermöglichen den Einsatz von hoch- und ultrahochfesten Betonen, mit Druckfestigkeiten, die denen von Stahl nahekommen. Kombiniert mit innovativen Bewehrungstechniken werden zusätzlich hohe Zug- und Biegezugfestigkeiten bei duktilem Materialverhalten erreicht.

Dennoch wird das vorhandene Potenzial im aktuellen Architekturgeschehen kaum reflektiert. Gründe dafür sind, neben mangelnder Erfahrung, Besonderheiten bei der baupraktischen Umsetzung: Mit zunehmenden Festigkeiten steigen die Anforderungen an die Verarbeitung und Nachbehandlung zementgebundener Werkstoffe, und setzen eine Vorfertigung unter Laborbedingungen voraus.

Die vorliegende Arbeit setzt sich mit dem Widerspruch auseinander, dass Querschnitte zwar reduziert werden können, durch die Segmentierung jedoch eine Komplexität, bedingt durch die Unterbrechung der Strukturhomogenität, entsteht. Ziel ist die Erweiterung von Anwendungen zur Umsetzung zeitgenössischer Betonschalen.

Grundlagen von Verbindungen werden anhand ihrer mechanischen Wirkung kategorisiert, um Fügungsstrategien entwickeln zu können. Ausgewählte Fallstudien dienen als Demonstratoren für Lösungsansätze einer Installation vorgefertigter, dünnwandiger Betonbauteile. Zwei Fügungstechniken werden detailliert betrachtet und deren Anwendbarkeit anhand experimenteller Untersuchungen verifiziert.

Eine Lösung beschreibt eine biegesteife Verbindung von Betonelementen, bei der das Übergreifen der Bewehrung auf separaten Betoniersequenzen basiert. Grundlage hierfür ist die Ausarbeitung einer Abstelltechnik für den Einsatz einer Mikro-Maschenbewehrung. Ein weiterer Ansatz überträgt die Skalierung von Querschnittsdimensionen, analog zu maschenbewehrtem Beton, auf den Spannbetonbau. Kleine Spannmedien mit kleinen Achsabständen, in dünnwandige Betonelemente integriert, dienen als Grundlage dieses neuen Fügungskonzepts.

Contents

Nomenclatures

Abbreviations

ACI	–	American Concrete Institute
AMPA	–	Amtliche Materialprüfanstalt
AR	–	alkaline resistant
ASL	–	Architektur Stadtplanung und Landschaftsplanung
ASTM	–	American Society for Testing and Materials
B+G	–	B+G Ingenieure Bollinger und Grohmann GmbH
BRG	–	Block Research Group
CAD	–	computer aided design
CAM	–	computer aided manufacturing
C.A.S.T	–	Centre for Architectural Structures and Technology
CiA	–	Composites in Architecture
CNC	–	computerized numerical control
comb	–	combination
Co. KG	–	Compagnie Kommanditgesellschaft
DAfStb	–	Deutscher Ausschuss für Stahlbeton
DDU	–	Digital Design Unit
DIN	–	Deutsches Institut für Normung
DR	–	dynamic relaxation
DUCON	–	Ductile Concrete
Dywidag	–	Dyckerhoff & Widmann AG
EC	–	Eurocode
EN	–	European Norm
EP	–	epoxy
EPFL	–	École polytechnique fédérale de Lausanne
et al.	–	et alia (and others)
ETH	–	Eidgenössische Technische Hochschule (Zurich)

expo	–	exposition
FB	–	Fachbereich (faculty)
FDM	–	force-density method
FEM	–	finite element method
fib	–	Fédération internationale du béton
fltr	–	from left to right
FRP	–	fiber reinforced polymers
FU	–	*Fuge* - casting sequence in two steps
GmbH	–	Gesellschaft mit beschränkter Haftung
HiLo	–	High performance, Low energy
HiPerMat	–	UHPC and High Performance Construction Materials
HPC	–	high performance concrete
IASS	–	International Association for Shell and Spatial Structures
iBMB	–	Institut für Baustoffe, Massivbau und Brandschutz (Braunschweig)
ILEK	–	Institut für Leichtbau Entwerfen und Konstruieren
imp	–	imperfection
ITE	–	Institut für Tragwerksentwurf (Braunschweig)
itke	–	Institut für Tragkonstruktion und Konstruktives Entwerfen
LC	–	load case
LG	–	load group
MDF	–	medium density fiberboard
MIT	–	Massachusetts Institute of Technology
MO	–	*Monolithic* - casting sequence in one step
NEST	–	Next Evolution in Sustainable Building Technologies
NURBS	–	non-uniform rational b-spline
OSB	–	oriented strand boards
pH	–	potentia Hydrogenii
PS	–	particle spring
PU	–	polyurethane
PS	–	polystyrene
PVC	–	polyvinyl chloride
RH	–	relative humidity
Rhino	–	Rhinoceros®
RPC	–	reactive powder concrete
RWTH	–	Rheinisch-Westfälische Technische Hochschule (Aachen)
sec	–	second

SLS	–	serviceability limit state
TNA	–	thrust network analysis
TRC	–	textile reinforced concrete
TU	–	Technische Universität
UHPC	–	ultra high performance concrete
UHPFRC	–	ultra high performance fiber reinforced concrete
ULS	–	ultimate limit state
UNESCO	–	United Nations Educational, Scientific and Cultural Organization
UniK	–	University of Kassel
Vol	–	volume
ZiE	–	Zustimmung im Einzelfall

Latin letters

Upper case

A	–	area
b	–	width
C	–	cement
°C	–	degrees Celsius
c	–	concrete cover
cm	–	centimeter
D	–	diameter
d	–	day
dm	–	decimeter
E	–	modulus of elasticity
e	–	eccentricity, axial spacing
F	–	force
f	–	strength
f	–	factor
G	–	shear modulus
GPa	–	gigapascal
g	–	gravity
g	–	gram
h	–	hour
h	–	height

k	–	kilo
k	–	curvature
kg	–	kilogram
kN	–	kilonewton
ksi	–	kilopound per square inch
l	–	length
M	–	metric thread
M	–	moment
m	–	meter
mm	–	millimeter
MPa	–	megapascal
N	–	Newton
N	–	axial force
n	–	number of
Ø	–	diameter
P	–	pitch of threads
p	–	page
Pa	–	Pascal
q	–	life load
®	–	registered trademark
R	–	radius of curvature
r	–	radius
S	–	snow load on the roof
s	–	snow load on the ground
t	–	thickness, time
u	–	perimeter length
V	–	shear force, volume
W	–	water
W	–	section modulus
x, y, z	–	cartesian coordinate directions

Subscripted characters

b	–	bolt, bottom
BT	–	bending tensile
c	–	concrete, creep

cc	–	concrete creep
comp	–	compression
cs	–	concrete shrinkage
cs,∞	–	concrete shrinkage end value
c,cube	–	concrete cube
c,cyl	–	concrete cylinder
d	–	design value
eff	–	effective
el	–	elastic
f	–	fiber
FE	–	finite elements
found	–	foundation
G	–	Gaussian
G	–	dead load
i	–	integer
imp	–	imperfection
k	–	characteristic value
l	–	left
M	–	median
$\overline{\text{M}}$	–	median (value range)
m	–	median
max	–	maximum
min	–	minimum
p	–	prestressing
proj	–	projected
Q	–	live load
R	–	resistance, Resultant
r	–	right
ref	–	reference
s	–	steel, tensile stress area of bolts
surf	–	surface
t	–	tension, top
tot	–	total
u	–	ultimate
x, y, z	–	cartesian coordinate directions
y	–	yield

Greek letters

α	–	angle, factor for cement strength development
β	–	stress capacity, time based development of creep deformation
γ_G	–	security factor for dead loads
γ_Q	–	security factor for live loads
γ_M	–	reduction factor for steel
γ_{M2}	–	reduction factor for screws/bolts
Δ	–	deviation
ε	–	strain
η_{gl}	–	global safety factor
ϑ	–	angle of rotation, shell coordinate direction
μ	–	snow load shape coefficient
ν	–	Poisson's ratio
Π	–	strain energy potential
π	–	3,14159...
ρ	–	density
Σ	–	summation
σ	–	stress
τ	–	shear stress
φ	–	coefficient of creep, shell coordinate direction

1 Introduction

1.1 Motivation

1.1.1 Responsible use of concrete materials

Structurally optimized systems, and lightweight concrete structures in particular, are in focus of several research efforts. Besides direct cost savings from a lower material consumption, there are aesthetic benefits in architecture and design. A key objective though, is the use of material in a resource conserving way. The building industry is directly affected by current global challenges, based on climatic and demographic changes [GERW16].

One major aspect is the achievement of sustainability[1] in structural design. A significant portion of the energy consumed during the life cycle of our buildings, is covered within the 'grey energy', which is the embodied energy of each building element. It comprises the extraction of constituents, the production and manufacturing of building components, the transportation of men, machines and materials, the installation on site as well as the removal and disposal of construction waste. The reduction of the 'carbon footprint' is also an objective. $5-10\%$ of the worldwide CO_2-emission is induced by concrete and respectively the production of cement, with an upward trend. In contrast, the emission of air traffic accounts to 4% [For13, 47].

Further aspects are the installation of discrete elements on site and a provided ability of de- and reconstruction. An increasing frequency of changes of user demands of our built environment, directs to an inevitable rethinking of design practice and building technology [GERW16].

---

[1]Sustainable development describes a development, meeting the needs of a present generation, without affecting future generations in satisfying their own needs [P$^+$13, 116]

1.1.2 Rebirth of concrete shells ?

The application of thin-walled concrete elements and filigree structures is one approach to enhance the utilization of construction materials. An aesthetic appearance is a beneficial side effect, by realizing filigree structures, although not scope of this research.

In [ABVW14, 1], *Adriaessens* et al. indicate the renaissance of shells in recent years. De facto, there have been several progresses in latest design and building technologies, streamlining processes in shell construction.

Slender structures, and thus material savings, are achieved by both, increasing the material performance, as well as the directed arrangement of material within the design-space, in order to predetermine the force flow of form dependent systems[2].

Enormous advances in computational power, storage, handling and cross-linking of data networks, enable automated steps from planning to fabrication, in undisturbed, digitized process-chains.

'Computer aided design' (CAD) has almost comprehensively entered the sector of building construction. Software developments provide methods of form-finding and generation of complex geometries, under consideration of multiple boundary conditions. Standardized formats and interfaces allow not only the capturing of geometrical data, but also the structural analysis and transference to 'computer aided manufacturing' (CAM), without sources of errors due to scale changes.

Accomplished and ongoing research attempts also lead to improvements in material science. Focusing on cementitious materials, the strength characteristics of ultra-high performance concrete are almost closing up with properties of steel, due to the discovery of superplasticizers and reactive silica fume. Innovations in reinforcement strategies, like the development of high-strength fibers or micro-meshes, enable the application of composite materials, with high tensile and bending-tensile strength capacities, and a ductile material behaviour, of this initially brittle basis material.

Despite the fact that innovative opportunities and prerequisites are available, it can be observed that concrete shells, realized with contemporary technologies, are hardly imple-

---

[2]'Form-dependent' structures in this thesis are separated in 'form-active' and 'form-passive' systems. Form-active systems, like cable-nets, are actively changing the shape by varying load conditions. Form-passive systems, like concrete shells, passively keep their shape with changing states of loading [ABVW14]. Although the efficiency of form-passive structures is dependent on the shape, the reaction to varying loads is inherent stress conditions, whereas form-active systems emerge a structurally optimized geometry

mented on site. The possibilities in combining high-tech materials and digital tools, are not reflected in built architecture. As *Mainka* et al. state in [MLBK13], the way of thinking of the building industry is dominated by standards of industrial production, and buildings are generally assembled of repetitive, massive elements, exposed to bending impacts.

The rebirth of innovative concrete shells is often limited to a pavilion-scale and demonstrators, developed within academic environments, where the currency of labour costs are credit-points and publications.

1.1.3 Implementation features of thin-walled concrete elements

One reason for the low establishment of high performance materials is a lack of knowledge of the participants involved. Missing guidelines and design rules, the non-coverage of high-performance materials in the building codes[3] and fragmentary cost-calculations, not considering life-cycle costs, are accumulating risks that architects, engineers, clients and contractors are not willing to bear.

Another, more technical reason, can be constituted by the handling during the construction process. The greater the capability of cementitious materials, the higher the requirements of precision in manufacturing and (post-) treatment.
A predefined fluidity is necessary, ensuring the concrete slurry being able to flow into narrow, and usually closed, formworks, passing and covering the (mesh-) reinforcement.
The fluidity, defined by the slump size, is highly sensible to air and water temperatures, ingredients and the mixing devices. Mixing processes, casting methods and post-treatment[4] require a neat monitoring. This postulates a manufacturing of prefabricated elements under laboratory conditions.

A further argument for a prefabrication of concrete elements is the minimization of construction times on site, especially in densified urban areas. For event architecture, temporary structures and exhibition objects, it is even more important to ensure an efficient mounting concept. Not only a quick assembly, but also a de- and reassembly may be nec-

---

[3]UHPC, applicable in construction, has a strength capacity of about $200 - 300 \, \text{N/mm}^2$; concrete grades, exceeding a compressive strength of $90 \, \text{N/mm}^2$ are not covered within European standards

[4]heat treatments and steam curing at $90°$ are beneficial for the strength development

essary, presuming a non-destructive concept.

Consequently the problem arises of how to connect prefabricated concrete elements in a load bearing manner. A special consideration focusses on jointing methods on site and the respective constructional design.

1.2 Objectives and approach

The aim of this research approach is an expansion of the application range for slender concrete shells, realized in architecture. Based on innovative design procedures and materials, reflecting the state of the art, thin-walled shell structures are investigated for implementation. This premises the contradictory dispute of the possibilities to reduce cross-section dimensions on the one hand, and the arising complexity of discontinued homogeneity, due to segmentation, on the other hand.

General classifications of connection methods, according to their mechanical bonding behavior, need to be analyzed in order to develop design strategies of novel connection techniques. These methods investigated need to be aligned with the state of stress and the material involved.

As key aspects for both, problem identification and research verification, case studies are used. Objects, to be realized, require a consequent detailing and implementation of envisaged concepts, with no potential of blurring inconsistencies.

The current trend in architectural marketing, stated by *Laurent Ney* and *Sigrid Adriannsens* in [NA14], to reduce "... *sketch–plan–build–reality–picture–publish*" to "*sketch–render–publish*" is consequently obviated in this thesis.

Financial limits, naturally affecting design decisions of objects to be realized, presuppose an economical way of thinking, generating innovative engineering solutions. *David Billington* attests in *The Tower and the Bridge* [Bil14, 3], that structural engineers ever since excelled themselves under economic pressure, competing among each other for lowest costs. Furthermore he states, that economic demands are no obstacles but stimulations for 'structural art'.

1.3 Structure of this thesis

As a general guidance, a superior structuring describes the arrangement of the thesis.
Starting with 'Why?', an outline of the relevance of the present research field is given, and the motivation to pursue the progression is communicated. The classification of slender shells in architecture, as well as the historical and contemporary development, is exposed. The part 'State of the art' comprises the processing and fabrication of concrete shells. Formfinding methods, design features and structural characteristics, as well as a detailed compendium of concrete materials, and the implementation of concrete shells on site, are presented.
Eventually, the part 'Own research' is a comprehensive report of the research investigations undertaken. Four selected and realized case studies, serving for both, raising the problem and demonstrating the solution, are illustrated. Two construction joint techniques are developed and experimentally verified.
A descriptive flow-chart in fig. 1.1, illustrates the structure and arrangement of the thesis.

After the introduction and the outline of the research question in chapter 1, chapter 2, *Slender shells in architecture*, provides the terminology and classifications of shell structures, focusing on thin-walled concrete shells. The historical development of shells, indicating ground breaking milestones, is described. Contemporary trends and positions in modern shell design, are summarized and discussed.

Chapter 3, *Designing of concrete shells*, summarizes measures and peculiarities of the non-linear design process of concrete shells. The complex assignment, to create one entity of form, structure and construction, considering the architectural idea, and the necessity of integrative and interdisciplinary planning-processes, is argued. Experimental and numerical form finding methods, as well as optimization strategies, are described, and structural characteristics of shells, including shell-theory and buckling behavior, are given.

Specifics of the implementation of concrete shells on site are presented in chapter 4, *Fabrication of concrete shells*. With special focus on concrete as a construction material, the development of hydraulicity and, in combination with reinforcement strategies, attributes of cementitious composites are described. Classifications, development and application of formwork systems are outlined and discussed, from plane (system-) formwork, to double-curved master- and disposable moulds, as well as current investigations on flexible and adaptive formwork. Furthermore, mechanical principles of load bearing connections

are identified, and connection methods for prefabricated concrete elements are outlined.

Key aspects, determining the problem-identification and methodology of the research attempts, are selected demonstration objects, which are reported in chapter 5, *Case studies*. Four realized structures are illustrating research questions and their proposals for solutions.

Parapluie is a roof structure for a bus stop shelter. It describes a thin concrete shell that is realized by activating membrane effects.

A public outdoor seating-accommodation, *Möbiusban(k)d*, on the university campus, follows the shape of an infinite loop. Special consideration is given by the load bearing connection of segmental, prefabricated concrete elements.

The concrete mobile, *Stable Equilibrium*, is an exhibition object designed for a competition, announced by the IASS, where the short time frame provided for the installation at the venue required a special connection technique. Therefore a dry-fit prestressing system is developed.

Furthermore, the approaches of the *concrete table substructure* are design-wise augmenting the prestressing connection technique, in order to hide any visible prestressing devices.

Two connection strategies in chapter 6, *Seamless rigid connections for prefabricated shell elements*, and chapter 7, *Micro prestressing connections of prefabricated shell elements*, comprise comprehensive investigations of connection methods for thin-walled concrete elements. Whereas in chapter 6, the development of a specifically designed stop-end technique is a key aspect, in chapter 7, the scaling concept of prestressing dimensions leads to 'micro prestressing approaches', applicable as a joint technique. Both attempts include concept developments and prototyping, as well as experimental verifications and evaluations.

Finally, in chapter 8, *Conclusion*, the outcome of all investigations is summarized and discussed. Further research prospects are outlined.

Introduction and outlining of research idea

Why?   **Slender shells in architecture**

Classification & terminology   **Historical outline**   **Current slender shells**

Shell typologies (principles)   From Romans to   Contemporary concrete
Slenderness criteria   concrete shells of   Developments and positions
categorization of shells   20th century   in shell design

State of the art   **Designing of concrete shells**

Form finding methods   **Structural characteristics**

Experimental form finding   Fundamentals and shell theory
Numerical form generation   Buckling phenomenon

Fabrication of concrete shells

Concrete construction material   **Formwork systems**   **Connection methods**

Historic development   Master moulds   Mechanical principals
Composition & ingredients   Flexible moulds   Jointing concrete elements

---

Own research   **Case studies**

Parapluie   Möbiusban(k)d   Concrete mobile   Concrete table legs

Construction joint techniques for slender concrete shells

Seamless rigid constructions   **Micro prestressing connections**

Fully load bearing joint concept   Concept of scaling prestressing
Development of stop end technique   Prestressing joint technique
Prototyping and arrangements   Constructive formation and detailing
Experimental verification   Experimental verification

Conclusion and further research prospects

Figure 1.1   Structure of this thesis as flow-chart

2 Slender shells in architecture

2.1 What is a shell ?

2.1.1 Terminology 'slender shells'

The term 'shell', German: 'Schale', is originating from the old-high German word 'scala'. Analogously it is translated to 'cutting-off'. Early drinking vessels have been made of cut-off skulls of killed enemies or have been carved out of wood [Dud16]. Thus the shell was a cut-off part of a larger quantity.

In flora, the shell is understood as a protecting cover separating its content from the outside, like seeds, nuts or fruits. In fauna, the shell is carapace-like housing of mollusks, like mussels or snails.

The shell is a structure often used and adapted in nature, an evidence of its efficiency. Notwithstanding that all structures in nature are optimized carrying structures, rather evolutionary developed considering multiple impacts and side conditions, it can be observed that nature does not apply the construction principle of a beam supported by two columns [SK07]. Forms developed by nature are following the rational attempt to achieve distinct functionalities with smallest possible material- and energy consumption. An impressive example is the phenomenon of egg-shells, combining a protective envelope of the embryo and structural cover with a shell thickness of only $0{,}2 - 0{,}4$ mm. The shell principle is adopted by humans in a various objects of daily use, and also in building construction, in order to achieve wide spanning and material saving 'slender' structures.

Strain energy in shell structures　The design of shells is a complex and nonlinear assignment, excluding a sequential planning process of architects and engineers. Beside formal and functional aspects, the design of shells implicates the design of internal stress fields of form dependent shapes. The consequent perseverance by meeting the compatibilities of all boundary conditions is essential.

For concrete shells, the membrane action is an inherent restriction to achieve slender

(a) Linear elastic stress gradients, for strain- and bending-exposure. In case of bending, the inner areas are marginally contributing to the load take-down

(b) Demonstration of the difference in the required effort to break a pencil, by applying axial- and bending impact
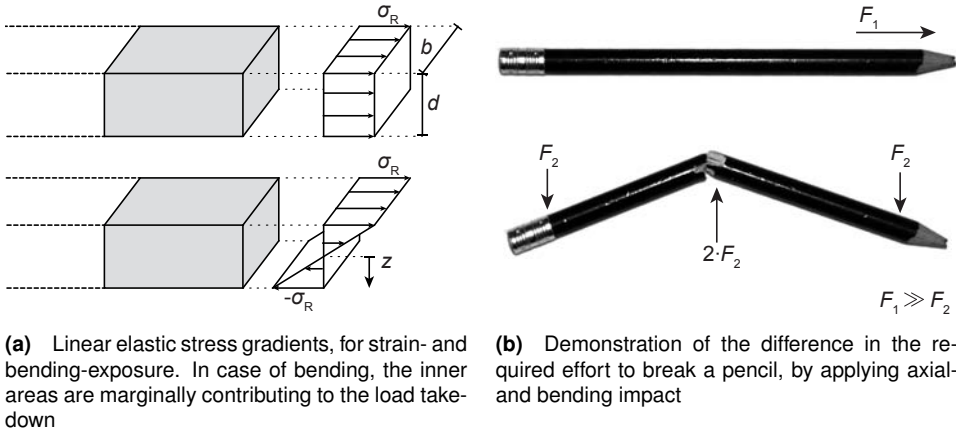
Figure 2.1 Strain energy potential using the example of the beam analogy

structures. Considering the loading impact, shells are combining 'plate action' (bending), where loads are acting perpendicular to the surface, as well as 'membrane action' (strain), where loads are acting in surface direction. The membrane stress theory for double curved shells, as described in section 3.2.2.2 on page 41, is based on a state of strain, avoiding bending actions.

The capability of the load bearing compensation to axial stresses, can be clarified with the energy theorem [Gru06]. States of bending and strain are compared by means of the beam analogy: Inner strain energy, gained in a cross section of a beam increment per unit length, as a stored potential Π^*, is obtained as:

$$\Pi^* = \frac{1}{2} \int \sigma \varepsilon \, \mathrm{dA} = \frac{1}{2} \int \frac{1}{E} \sigma^2 \, \mathrm{dA} \quad [\text{J/m}] \tag{2.1}$$

The stress gradient over the section height d, refer fig. 2.1a, for the bending stress state is determined as:

$$\sigma = \frac{2\,\sigma_R}{d} \cdot z \equiv \text{linear} \tag{2.2}$$

For the state of strain (axial impact):

$$\sigma = \sigma_R \equiv \text{const.} \tag{2.3}$$

with σ_R as a reference stress value. Inserting eq. (2.2) in eq. (2.1) gives:

$$\Pi_{\text{bending}}^* = \frac{1}{2}b \int_{-d/2}^{d/2} \frac{1}{E}\left(\frac{2\,\sigma_R}{d}z\right)^2 dz$$

$$= \frac{4\,b\,\sigma_R^2}{2\,d^2\,E}\left[\frac{z^3}{3}\right]_{-d/2}^{d/2}$$

$$= \frac{1}{6}\frac{bd}{E}\cdot\sigma_R^2$$

Inserting eq. (2.3) in eq. (2.1) gives:

$$\Pi_{\text{strain}}^* = \frac{1}{2}b \int_{-d/2}^{d/2} \frac{1}{E}\,\sigma_R^2\,dz$$

$$= \frac{1}{2}\frac{bd}{E}\cdot\sigma_R^2$$

It is obtained, that $\Pi_{\text{strain}}^* = 3\cdot\Pi_{\text{bending}}^*$. In other words, a cross section, with an imposed reference stress σ_R, incorporates an inner energy three times greater in case of an impose with an axial force compared to an impose of a bending moment. As a reversal conclusion, the energy required (with applied loads) to reach the material stress capacity, hence the resistance of a system is three times higher for axial- in comparison to bending impacts. The illustrative example shown in fig. 2.1b demonstrates the considerably higher energy required: If one wants to break a pencil, a bending impact is more applicable instead of pulling at it.

Definition of 'slender'   The statement above implicates the necessity of utilizing a membrane action, when slender shell structures are achieved, due to the absence of an inner lever-arm required for a bending resistance.   What is the definition of slender in literature?   According *Chris Williams* [Wil14] there is no absolute rule, as to how thin a shell has to be.   It is *"… a curved surface, thin in the direction perpendicular to the surface."*
A common allocation to 'thick', 'thin' and 'very thin' concrete shells results from the proportion of the shell thickness t to the curvature radius R. The values vary dependent on the source. *Werner Sobek* confines in [SK07] the following categories:

thick shells $t/R > 1/50$

thin shells $1/50 \geq t/R \geq 1/1000$

very thin shells $t/R < 1/1000$

This categorisation is well applicable for consistent geometries but comes to its limits for more complex topologies and freeform shapes. A further allocation is regarding the 'vault boldness', defined by the proportion of the span-length l, or median diameter Ø, and the shell thickness t. The following examples provide a notion of these values Ø/t, nowadays reaching magnitudes > 1000 [Gru06]:

Pantheon in Rome (125 AD), p. 47 $Ø/t = 43\,\mathrm{m}/1{,}4\,\mathrm{m} = 31$

Absprengerei Fa. Schott, Jena (1923), p. 17 $Ø/t = 40\,\mathrm{m}/0{,}06\,\mathrm{m} = 667$

hen's egg $Ø/t = 50\,\mathrm{mm}/0{,}2\,\mathrm{mm} = 250$

The criteria described are considering the shell thickness in relation to reference building characteristics as there are the span lengths or the curvature radii. An additional approach might be the treatment of the element thickness as an absolute value, dependent on the production method. For conventional reinforced concrete, the thinness of a cast surface is limited by the bar diameter plus twice the concrete cover. Consequently, sections smaller than 5 cm are hardly possible. In that sense, it might be discussed, whether the pushing of limits, as given from the material compilation side, is also an indicator of slenderness in a concrete construction.

2.1.2 Classification of shell structures

There are several definitions and classifications of shells in literature.
A starting point is the determination of the slenderness or vault boldness, given by the quotient of the shell thickness t and radius of curvature R or respectively the median diameter Ø, as discussed in section 2.1.1.
A common method of categorization is the origin of generation of the achieved shape. This analytic approach separates according to the mathematical descriptiveness in 'algebraic' and 'transcendent' shells. Mathematical derived 'algebraic' shapes are described by analytical functions, simplifying the handling of shape-geometry and analytical calculations, see [ABVW14, 2]. These are also 'rotational surfaces' or 'translational surfaces' (gliding planes). The counterparts are 'form-found' surfaces and 'freeform surfaces'.
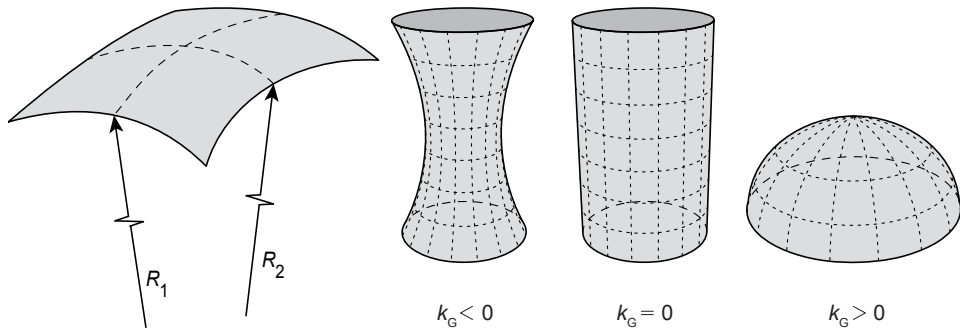
Figure 2.2 *Gaussian* curvature k_G obtained with main curvature radii R_1 and R_2.

'Form-found' results from a digitally or experimentally achieved state of static equilibrium, a common example is given by hanging models, as further described in section 3.1.1. 'Freeform surfaces', derived from architectural demands, are not necessarily considering a structural performance.

A functional classification distinguishes according to the potential of curvature, defined by the *Gaussian* curvature, determined with the main curvature radii R_1 and R_2 via following equation:

$$k_G = k_1 \cdot k_2 \tag{2.4}$$

with

$$k_1 = \frac{1}{R_1} \ \text{ and } \ k_2 = \frac{1}{R_2} \tag{2.5}$$

$k_G = 0$ describes no or 'one directional curvature', as given for cylinders, cones or barrel shells, thus shapes that can be laid out flat. 'Double curvature' is sub-categorized to $k_G > 0$, leading to 'synclastic' shapes with curvature radii on one side, like paraboloids or domes. $k_G < 0$ leads to 'anticlastic' shapes with curvature radii located on opposite sides. Well-known examples of the latter are saddles and the hyperbolic paraboloid.[1]

Franz Dischinger (1887–1953), a pioneering German shell designer, acting at the beginning of the 20th century, formulated his shell definition in 1928: *"Shells are structures,*

---

[1] A descriptive example for the terms 'synclastic' and 'anticlastic' is a torus: The inner portion of a donut is 'anticlastic', the outer one 'synclastic'.

formed with single- or double curvature with a thickness small in relation to surface extents" [Dis28, own translation].

Joachim Born adds in [Bor62] the necessity of edge enhancements, in order to maintain the application of the membrane theory.

The Spanish architect *Félix Candela* (1910–1997), who realized numerous concrete shells in Mexico in the middle of the 20th century, even separated between 'true' and 'false' shells, where true shells are double curved and load bearing under membrane stress state, excluding any bending action, see [Joe62, 20].

It may be added, that pure membrane stress states for form passive structures are achievable for the form-determining load case only, which is usually the self weight for the design of concrete shells. Additional live loads, point loads or imperfections may initiate unwanted bending actions.

The definition of *Dischinger* includes tensile structures like the minimal surface of the *Expo Pavilion* in Montreal by *Frei Otto* (1925–2015), fig. 2.3a, to the category of shell structures. Excluding sole stress modes, however, would consequently exclude pure compressive structures like the service station in Deitingen by *Heinz Isler*, fig. 2.3b, where the form is defined by an inverted hanging fabric. An example of a membrane structure, bearing loads with both, compressive and tensile stresses is the *Oceanarium* in Valencia, fig. 2.3c, that has been built posthumously according to *Candela*'s design.

A reasonable categorization seems to be the expansion of *Dischinger*'s definition, stated above, by constraining shells to 'form-passive' structures, as specified by *Sigrid Adriaenssens* et al. in [ABVW14, 1]. Contrary to 'form-active' systems, the shape of the structure does not adapt in dependency on the outer loading applied. In literature it is not uncommon for authors of handbooks summarizing the design of shells, to point out, that bending impacts have to be diminished to achieve 'good shells' in order to utilize the cross sections. Potentially, it is questionable, whether the example of the *Crematory* roof in Kakamigahara by *Toyo Ito*, fig. 2.3d, is a good shell or not. As a freeform shell, it is a hybrid system, bearing axial- and bending stresses, legitimated by the design, supplying and usage concept. Nevertheless, this present load takedown has to be considered by the constructing engineer for the implementation and choice of material.

It may be concluded by the author, that the design of shells should not be reduced to the demands of technical engineering. A shell in service is rather informed by multiple criteria derived from design, technical aspects and the application in practice. In every case, a certain bending capacity has to be provided by the design of form-passive struc-

(a) Form active and solely tensile structure – German Pavilion Expo 1967, Montreal, Canada by *Frei Otto*, *©ILEK*, *University of Stuttgart*

(b) Form passive and solely compressive structure – Service station in Deitingen 1968, Switzerland by *Heinz Isler*

(c) Form passive membrane structure with compressive and tensile stresses – Oceanarium Valencia, posthumous construction after the design of *Félix Candela*, *©CMD Ingenieros*

(d) Freeform structure with compressive, tensile and bending stresses – Crematory in Kakamigahara, Japan 2006 by *Toyo Ito*, Photo: *Toyo Ito & Associates, Architects*

Figure 2.3   Categorization of shells according to the basic load takedown

tures. Imperfections, buckling impacts and concentrated loads need to be counteracted. The design of hybrid systems, with a combination of axial- and bending stresses, postulates a comprehensive design of stress fields, in order to achieve a consistent distribution of stress utilization. Achieving a structure, appropriate for the material involved, requires a close collaboration of the architect and structural engineer from the beginning of the design process.

2.2 Historical outline of concrete shells

2.2.1 Masonry domes as precursors

Single and double curved structures have been well-known and realized from ancient times. Vaults and cupolas have been implemented as roofing and structural elements for the spanning of large, column-free spaces. Predominantly used for prestigious and sacral buildings, the visual appearance was always a main focus of attention. Barrel-vaults, cross-shaped vaults and especially cupolas, as a special type of vault, have been known as form dependent structures, appropriate for large span lengths with highly aesthetic effects of the inside space and representative from the outside.

Due to the predominantly compressive load transfer of cupolas, masonry and cast stone was most suitable because of the compressive strength. The 43,30 m spherical cupola of the *Pantheon* in Rome (p. 47), completed in 125 AD, is an impressive and still preserved witness of history.

To provide lighting inside the domes, round openings or roofed lanterns have been provided. The additional loading of these lanterns led to the development of double-shells, braced with webs, placed in between. The cupola of *St. Peter's Basilica* in Rome, designed by *Michelangelo* in the middle of the 16th century, initially was planned with even three shells.

Cupolas are usually double-curved formations of rotational symmetry, continuously supported at the bottom edges. Under self-weight loading, compressive stresses occur in direction of the meridians. Thus, orthogonal to the meridians, hoop-stresses develop within the shell surface: Compression stresses at the zenith, decreasing along the meridians, with a zero-crossing at the fraction point, changing to tension at the lower part of the cupola. The location of this fraction point is dependent on the shape and the loading of the shell. Occurring tension in masonry is taken by friction only, thus often cracks orthogonal to the hoops (equivalent to the force direction) emerged. Anchors of hardwood and iron as well as horizontal bearings parallel to the meridians at the support were attempts to counteract this effect.

The development of reinforced concrete construction in the beginning of the 19th century was an answer to this problem: Well distributed reinforcement leads to homogeneous stress fields and consistent shell utilization [SK07].

2.2.2 Appearance of concrete shells

2.2.2.1 *Gaudi*'s hanging model

The Italian mathematician *Giovanni Poleni* (1683–1761) was ordered by pontifex *Benedict XIV* to investigate structural defects in the cupola of *St. Peter's Basilica* in 1743. He identified that the thrust line[2] should be located within the masonry section and proposed a meridian shape, derived from a catenary curve, preventing the development of cracks [Lug02, 50].

The extensive application of hanging models as a formfinding method is inevitably associated with the catalan master-builder *Antoni Gaudi* (1852–1926).

Gaudi, supported by the *Güell* family, worked on a chapel for *Colònia Güell* from 1898, a working-class estate of the textile industry of the family west of Barcelona. The design of the high roof was based on a hanging model M 1:10, 6 m wide and 4 m high, with interconnected filaments, loaded with pellet-filled sacs (p. 33). All dimensions of the (unfinished) building could be quantified out of this model.

Gaudi, averting historicism of facades of the 19th century, succeeded in establishing new shapes congruent to rationally structures [Bil14, 168].

2.2.2.2 German precedents *Bauersfeld*, *Dischinger* and *Finsterwalder*

In the beginning of the 20th century, three development directions intersected: Research of reinforced concrete as a composite material, advances in production possibilities and increasingly theory-guided analysis methods. The developments in reinforced concrete, for the first time published 1887 in the *Monier brochure*, see also section 4.1.1, enabled the construction of frames and panel-walls, made of ferroconcrete, and the range of application expanded to double-axis load transfer in plane and shell constructions [Pes09].

A remarkable milestone in that sense is the *Centennial Hall* in Wrocław, Poland from *Max Berg*, completed in 1913. What is revolutionary about this building, listed by UNESCO, is both, the early and audacious application of reinforced concrete (naturally there was no long-term experience at hand), and the aesthetics, emphasised by the construction. No decoration element embellishes the rough material. The enormous span, 65 m, of the domed structure, beat the record that has been held for more than thousand years by the *Pantheon* with an increase of fifty percent.

---

[2]thrust lines are theoretical lines representing the location and direction of resultant force vectors of structures

Reducible cross section dimensions inevitably demanded higher precision of formwork construction to avoid unconsidered bending, in case of the thrust line being located outside the cross section.

An innovative approach, to increase lightness and preciseness, valid as the initiation of shell constructions in Germany, is given with the construction of a planetarium for the optical factory *Zeiss* in Jena in 1922, shown in fig. 2.4.

Encouraged by the founder of the *Deutsches Museum* in Munich, *Oscar von Miller* (1855–1934), the physicist *Walther Bauersfeld* (1879–1959), affiliated with *Zeiss*, was commissioned with the design of a planetarium. *Bauersfeld* entered into a joint-venture with *Franz Dischinger* (1887–1953), a structural engineer from the building company *Dyckerhoff & Widmann AG* (*Dywidag*)[3]. The complementary collaboration of these two characters was enabled by the technical skills and attention to details of *Bauersfeld* in combination with the mathematically-scientific preference of *Dischinger*[4]. Together they developed a construction method, later patented as the *Zeiss-Dywidag-System*, that enabled a realization accurate to the mathematically derived shapes, avoiding hazardous stress states from stripping the scaffolding.

The envisaged planetarium was a spherical projection screen, planned onto an existent building, demanding low superimposed loads. The triangulated sphere, shown in fig. 2.4, with a span of 16 m, was assembled with specific-formed and individual produced steel bars. According a statistic survey of *Peseke* et al. in [PRGB15], about 4600 bars with 72 different lengths have been installed. Special attention is given to the construction of the nodes, designed to enable the varying distribution of intersecting angles.

A mesh of reinforcement bars was bound onto the steel grid, coated with sprayed concrete. Wooden shields of 3×3 m inside the dome were shifted as a backing to prevent spray-through. The result was an unprecedented thin shell with a thickness of 3 cm only.

Dischinger and *Bauersfeld* repeated the application of their *Zeiss-Dywidag-System*, looking for opportunities to boost the span dimensions. Such opportunity was offered by the associated company *Schott*, also located in Jena. On a circular footprint area, with a diameter of 40 m, they realized a cupola with a curvature radius of 35 m and a thickness of 6 cm [Hub64, 155]. The *Schott*-dome, finished in 1924, unclosed further questions of the edge treatment. *Dischinger*, convinced of the practicability of shell construction also for

---

[3]*Dywidag* was the contractor responsible for the construction of the *Centennial Hall* a few years before.

[4]*Dischinger* developed calculation methods for cupolas and was able to present a complete mathematical derivation of the analysis of cupolas proved by applications in practice [Bil14, 159].

Figure 2.4 Planetarium in Jena by *Dischinger* and *Bauersfeld* from 1922 with a diameter of 16 m. The assembled steel grind facilitates the accuracy of the spherical geometry
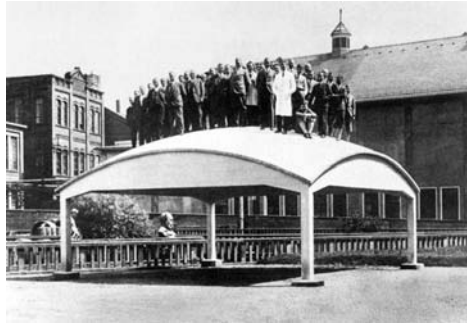

Figure 2.5 *Dischinger*'s test shell from 1931 on the property of *Dywidag*. With a thickness of $\leq 2{,}5\,\text{cm}$ it demonstrates the efficiency of double curvature in shell construction

rectangular plans, supplemented his surveys with a test shell in 1931, investigating edge beams enhancing the shell edges. Figure 2.5 shows the tested shell loaded with 50 people: Spanning $7{,}3 \times 7{,}3\,\text{m}$ the shell had a thickness, ranging from $1{,}5 - 2{,}5\,\text{cm}$. The shell is considered as the evidence of the positive effect of double curvature in surface structures, see [Hub64, 156].

In 1923, the young engineer *Ulrich Finsterwalder*, just graduated, joined *Dyckerhoff & Widmann AG*, spending his entire career in this company. He significantly contributed to the development of shell theory. He concentrated on calculation methods of barrel-shells and transversely braced cylinder-shells. His results were implemented at the *Great Market Hall* in Frankfurt / Main, opened in 1928. The architecture of *Martin Elsaesser* (1884–1957), was part of the 'New Frankfurt'. The $220 \times 50\,\text{m}$ large market hall was biggest building complex to that time. Today it houses parts of the *European Central Bank*. Fifteen barrel-shaped roof elements, 14 m wide and 37 m long, have been built by applying the *Zeiss-Dywidag* method[5]. The shell thickness at the zenith was 6 cm. The proof of the load bearing capacity of this prototype in building industry (beside the structural analysis) was carried out at a scaled mock-up of a barrel M 1:3 where the deformations and behaviour were monitored.

---

[5]During the construction work, *Finsterwalder* reduced the height of the barrels from 6 m to 4 m without informing *Dischinger*. The result is a non-orthogonal end-tangent of the edges, a substantial discrepancy of the two engineers, leading to heavy disputes, carried out in public. [Dic13]

(a) Shell stresses are transferred by inclined Y-shape buttresses to a prestressed concrete ring below ground to bear the horizontal shear
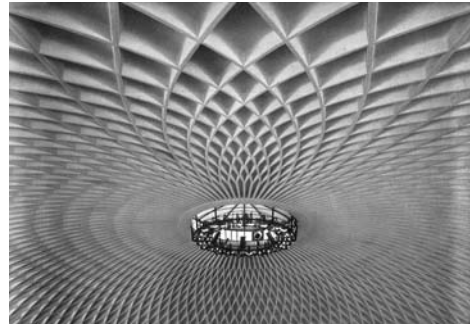
(b) Cross shapes rips stiffening the shell to prevent stability failure without increase of material efforts

Figure 2.6 *Palazzetto dello Sport* by *Pier Luigi Nervi* from 1957, spanning 60 m

The experiences made at the *Great Market Hall* was basis for further related buildings, like the great market halls in Leipzig, Basel and Budapest.[6] The work, publications and the engineering attitude of *Finsterwalder* and *Dischinger* were vastly renown, motivating young engineers to gain experience in their company, like the Austrian engineer *Anton Tedesko*, who was sent to the USA in 1932, responsible for various shell structures in the 'New World' [Bec08, 35].

2.2.3 Golden age of concrete shells

2.2.3.1 Italian tradition and *Nervi*'s structural art

In contrast to German approaches in the design of shell structures, as described in section 2.2.2.2, which have been motivated from a mathematically and theoretically background, the design methods of *Pier Luigi Nervi* (1891–1979) are characterized by his artistic incitements. Educated as an engineer, his working procedures, publications and intellectual positions have been highly influenced by aesthetic ambitions.
Analog to the Italian building tradition, recognizable in ancient domes and cupolas, *Nervi* was engaged with ribs as structural- and design-elements. In a playful and simultane-

---

[6]A setback of shell construction happened 1934, when a thin shell hangar collapsed in Cottbus, due to extensive creep deformation, un-experienced to that time. *Finsterwalder* was threatened by death penalty by reason of sabotage. The expert opinion, written by *Dischinger*, confirming the correctness of statical calculations, procured his release from remand. [Dic13]

ously meticulous manner, he developed various layouts of intersecting ribs for plates and shells, which became a remarkable characteristic of his personal style. Always keeping cost-efficiency in mind[7], he focused on the combination of minimum material efforts and structural necessities, satisfying his demands for high-quality appearance.

His work is widely discussed by people involved in the building industry, since his ornamental constructions have not always been coherently following a structural logic.

Nervi was responsible for several hangars in the 1930s, where he developed construction methods and reflected the same by monitoring the behaviour of the built structures.

His most recognizable building is the *Palazzetto dello Sport* in Rome, see fig. 2.6, built in 1957. A system of two sets of intersecting ribs creates a decorative and structural pattern of the cupola, spanning 60 m. The ribs follow a technical necessity to gain bending stiffness in order to prevent buckling without increasing the self-weight. He thereby invented a significant enhancement of stiffness by redistribution of material, without increasing the same and developed an innovative construction method for the implementation on site. Prefabricated, lightweight, rhombic elements of 'ferrocement' (thin-walled mesh-reinforces cement-based composites), were placed onto the shuttering and filled with concrete in situ, becoming integral of the finished structure. With *Nervi*'s ribbed shells, novel solutions appeared, to bring daylight into large spaces, avoiding the central oculus. In some cases, for example at the *Terme di Chianciano* in central Italy, he provided openings between the ribs. At the *Palazzetto dello Sport*, the shell is supported on 36 Y-shaped buttresses, inclined analog the angle of the thrust-lines. The horizontal component of the buttress forces at the ground is bore with a prestressed ring, $\emptyset = 80\,\text{m}$, below ground.

In *The Tower and the Bridge* [Bil14], *David Billington* denotes *Nervi*'s *Palazzetto dello Sport* as the high point of 'Structural Art' in concrete construction.

2.2.3.2 Spanish craft and ruled surfaces of *Torroja* and *Candela*

Developments in the design of shells, proceeding to the same time in Spain, significantly vary from German and Italian trends. The ambition to realize slender concrete structures is expressed with smooth surfaces from above and below without the use of ribs. This may be manifested in the old-established tradition of Catalan workmanship, where vaults are built with layers of tiles, stuck together [Bil14, 168].

The investigation of shapes, rooted in traditional construction techniques lead to remark-

---

[7]The majority of *Nervis*'s projects emanated from design competitions.

Figure 2.7 Market hall in Algeciras, Spain by *Eduardo Torroja* from 1933 spanning of 47,6 m, to the time largest spanning spherical shell
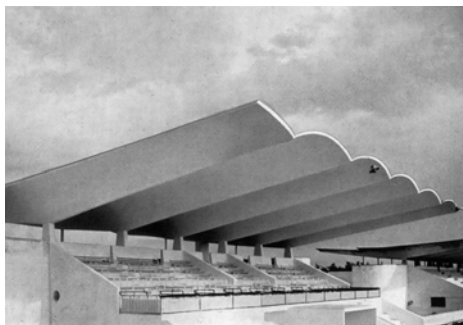
Figure 2.8 Spectator roof of the racetrack *La Zarzuela* in Madrid, Spain by *Eduardo Torroja* from 1935

able contributions in the ongoing developments of shells in Spain.

The structural engineer *Eduardo Torroja* (1899–1961) is considered to be a pioneer in the design of smooth double-curved shells, made of reinforced concrete and a key figure in the development of shell structures[8].

A notably structure of *Torroja*, is the market hall in Algeciras (1933), Spain (fig. 2.7), to this time the largest spanning spherical shell. In collaboration with *Manuel Sánchez*, he designed a double curved shell, with a curvature radius of 44 m, spanning 47,6 m. The shell has a varying thickness of 9 to 45 cm [Hub64, 10] and is supported on eight circular arranged columns. To counteract the horizontal shear from the shell, a polygonal, pre-stressed, tension ring connects the column heads. The extreme unprecedented slenderness involved challenges and risks. *Torroja* tested the structural behaviour with a scale model M 1:10, a working approach, he followed for much of his work [Bec08, 36].

The most famous design and structural approach is the cantilevered roof of the racetrack *La Zarzuela* in Madrid, Spain (fig. 2.8), from 1935, finished in 1941, due to a frozen construction during the wartime. The roof, cantilevering 13 m towards to front and 7 m backwards, is a hyperbolic double curvature with a thickness at the front edge of 5 cm, resulting in its filigree appearance.
Here *Torroja* tested the structural behaviour at an unscaled mock-up section, proving the

---

[8]*Eduardo Torroja* founded the *International Association for Shell and Spatial Structures, IASS* in 1959.

shell carrying triple the load desired. Even though bombardments during the Spanish civil war in fact injured the structure, they did not lead to global failure.

A further creator of thin concrete shells with Spanish roots significantly involved in the contribution of form variations, is the architect, engineer and building contractor *Félix Candela* (1910–1997). He graduated in architecture in Madrid, Spain. His interests in thin-walled concrete shells lead to a scholarship aiming to meet *Finsterwalder* and *Dischinger* in Germany. However, the progressions of the Spanish civil war forced *Candela* to leave his country. In 1939 he emigrated to Mexico, recalling his former engagement in concrete shells.

Candela's work is inseparably associated with the comprehensive application of shapes derived from one geometric form, the hyperbolic paraboloid (hypar). Motivated in the construction of economic, thin concrete structures, and focusing on unpretentious construction processes, he soon concentrated almost solely on this type of ruled surfaces. Applying hypars in an unprecedented variety of arrays and configurations, he invented some of the most memorable shell structures to date, see [Bec08, 38].
Beside the aesthetic appearance of thin concrete shells, *Candela*, typically approached as the architect, structural engineer and builder in one person, identified the economic advantages of his shapes, operating in a country with low labour and high material costs. Hyperbolic paraboloids, a special form of double-curved, anticlastic surfaces, are developed from two straight line generators, and consequently convertible with straight materials, enabling a construction without curved boards for formwork and shuttering, that he was able to utilize.

His first such structure of *Candela* is the *Cosmic Rays Laboratory* of the *University of Mexico City*, see fig. 2.9a. To be able to measure cosmic rays inside the building, the structure needs to be as thin as possible. The roof, spanning over an area of $10 \times 11{,}8\,\text{m}$, had already been designed as a barrel shell, by an architect involved. *Candela* changed the shape to two hypar shells strung together with a shell thickness of $1{,}5\,\text{cm}$ at the zenith and $5\,\text{cm}$ at the imposts. This thinness of the roofing skin achieved has been unprecedented to that date.
With increasing attention from the building industry, *Candela* was responsible for the design of several churches in Mexico. One example, the *Iglesia de la Virgen de la Medalla Milagrosa* in Narvarte, Mexico, was built in 1955 (fig. 2.9b). The whole structure of the roof and the walls was composed of hypar shapes, which he was able to design within one

(a) *Cosmic Rays Laboratory*, Mexico City, 1951

(b) *Iglesia de la Virgen de la Medalla Milagrosa*, Narvarte, Mexico, 1955

(c) Restaurant *Los Manantiales*, Xochimilco, Mexico, 1957

(d) *Bacardi Bottling Plant*, Cuautitlán, Mexico, 1960

Figure 2.9 The hyperbolic paraboloid as design-principle for most buildings of *Félix Candela*

afternoon [Bil14, 175].

His design research with several umbrella shapes, again developed from hypars (he was the first to realize concrete-made umbrellas), led to large and wide spanning factory spaces, like the *High Life Textile Factory*, 1954, assembled by repetitive concrete umbrellas, one after the other.

The construction of *Los Manantiales* in Xochimilco, Mexico (fig. 2.9c), completed in 1957, pushed the limits of achievable lightness in the design of concrete shells. The restaurant, an almost 'structure-only' building, was *Candela*'s favourite work.

Eight hypar shells, with a thickness of 4 cm are arranged in a circle, on an area with a di-

ameter of 43 m. The backwards located façades and the free edges emphasise the extreme slenderness of the structure.

The *Bacardi Bottling Plant*, designed by *Candela* in collaboration with *Ludwig Mies Van Der Rohe* (1886–1969) in 1960 (fig. 2.9d), is a factory building in Cuautitlán, north of Mexico City. Inspired by the St. Louis Airport terminal building designed by the architect *Minoru Yamasaki* and the engineer *Anton Tedesko*, *Candela* created a pure structure in a series of hypar cross-shaped vaults [GB09]. As a result, he disclaimed to ribs on the edges and showed that the terminal could be done more simply and elegantly. Initially, three adjacent vaults were built, followed by another three in a second stage about ten years later. The six hypars, spanning 26 m, form two large bays covering about 5000 m^2, with skylight gaps between the adjacent shells. The shells have a thickness of 4 cm, again representing the great slenderness which characterizes *Candela*'s work.

2.2.3.3 Swiss precision and *Isler*-shells

With more than 1400 realized shells of about 40 different shapes, the Swiss engineer *Heinz Isler* (1926–2009) is considered as the most eminent shell builder [SK07]. His main work period is during the 1950s and 1970s.

As *Stefan Polónyi* sums up in his obituary [Pol09], *Isler* was born at the time when *Dischinger* and *Bauersfeld* were finalizing the planetarium shells in Jena. When he was about ten years old, *Torroja*'s market hall in Algeciras was completed and during *Candela*'s work period realizing hypar-shells, *Isler* graduated in civil engineering at the *ETH-Zurich*. After three years assisting *Pierre Lardy*, he established his own engineering firm in 1954 in Burgdorf, Switzerland.

Notwithstanding the preliminary work of his colleagues mentioned above, *Isler* fundamentally stretched the diversity of expedient shapes in concrete shell construction. His revolutionary form finding approaches are no longer based on mathematically derivable shapes, his forms are rather developed from physical principles. In this context, *Isler* comprehensively investigated experimental form finding methods, leading to structurally-effective, mostly compressive-only shells, under pure membrane utilization.

His shells are adapted to the climate conditions of the Swiss environment and are thereby not as thin as the precedent Mexican shells by *Candela*. The frequently used thickness of 8 cm, see [GB14, 251], remains in its uncracked state under compression, enabling water-tightness while omitting sealing devices.
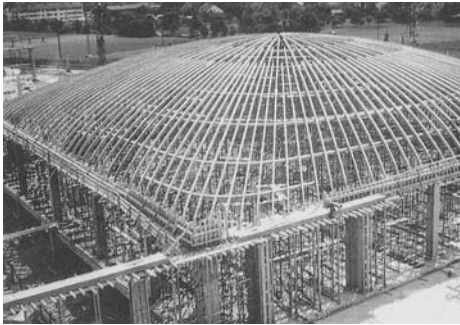
(a) Falsework for the *Coop Warehouse*, Wangen, Switzerland, 1960. The form of the shell, $54{,}6 \times 58{,}8\,\text{m}$, is a 'bubble-shapes', derived from a pressurized membrane pillow
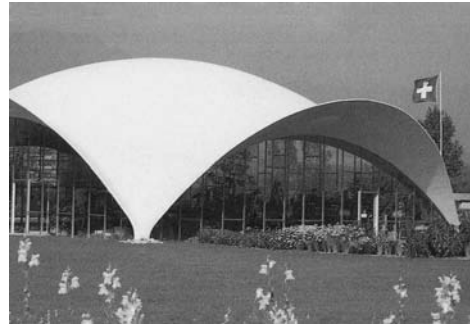
(b) *Wyss Garden Center*, Solothurn, Switzerland, 1962. *Isler*´s first free-shaped shell generated by circles, the structure is stiffened with cantilevers along the edges, orthogonal to the surface
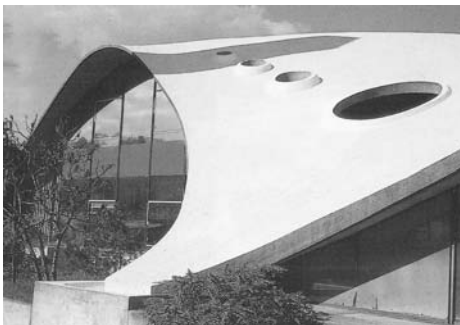
(c) Factory roof shell for *Sicli SA*, Geneva, Switzerland, 1969. The membrane shape, containing circular lightning openings and supported on seven points on an irregular plan, is derived from an inverted hanging model

(d) *Tennis courts*, Heimberg, Switzerland, 1979. The four adjacent shells are derived from inverted hanging models, with a shape following the flying-line of tennis balls

Figure 2.10 The hyperbolic paraboloid as design-principle for most buildings of *Heinz Isler*

The form finding methods, derived from *Isler*'s experimental surveys, can be separated to three principle categories.

The 'bubble-shapes', derived from pressurized membrane pillows, were an observation by *Isler* of the shape of a plumped-up pillow on his bed in 1954. A sheet of pliable rubber is sandwiched between a frame and a baseboard made of wood. Using a hand-pump, he inflated the rubber membrane to a double-curved synclastic surface. *Isler* adapted the shape

by rounding the corners to avoid a negative curvature in these areas. These types of shells usually were supported continuously or on edge beams. However, as he discovered later, when investigating the stress distribution within the shells, 90 % of the total weight was carried by the corners [Chi00, 33–34]. *Isler* applied this form finding method with pressurized pillows in combination with prestressed edge beams for various industrial complexes with dimensions up to $54 \times 58\,\text{m}$ (fig. 2.10a).

A further natural phenomenon, *Isler* observed in 1955, is the shape arising from 'hanging fabrics'. Inspired from a wet jute cloth, hanging over a grid of reinforcement, he undertook experiments with wet fabrics which froze during the cold periods of his home country. Related on the knowledge obtained by *Robert Hooke* and applied by former precedents like *Gaudi*, *Isler* transferred this method to concrete shells, by inverting the shape achieved and brought it to perfection. Since the hanging fabric naturally is a tensile only structure, the inverted system is of pure compression, with the unrivaled advantage of uncracked, self-sealing surfaces. In comparison to the bubble-shells described above, the load vectors of the form generating force is exactly the same as for the structure under self weight, whereas the force vectors of the internal pressure is orthogonal to the surface of the membrane.
Well known examples of shapes developed with hanging fabrics are the service station in Deitingen (p. 15) finished in 1968 and the factory building of *Sicli* in Geneva (fig. 2.10c), built in 1969, with a diagonal span length of $58\,\text{m}$ and a shell thickness of $10\,\text{cm}$.
A critical area of all compressive shells is the free edges, which are sensitive for buckling. At unsupported edges, the loads are transferred not biaxial, but in single direction, resulting in a tendency of wrinkling of the cloth, creating the characteristic reversals, stiffening the inverted shape [Bec08, 122]. *Isler* utilized these enhancing folding as design strategy for edges without beams, as in the *Wyss-Gardening-center* in Solothurn, Switzerland (fig. 2.10b), built in 1961 and the *Tennis courts* in Heimberg, Switzerland (fig. 2.10d), built in 1997. The latter is a remarkable building, assembled from a series of four identical shells, spanning $60\,\text{m}$, derived from hanging fabric shapes, following the flying line of tennis balls.

The third category of his form finding methods is 'extrusion- or flow shapes', based on a phenomenon *Isler* discovered in 1964, when observing polyurethane foam expanding out of a rectangular pipe, facilitating a further design principle.

Isler personally supervised all planning and execution phases of his projects, aiming to minimize sources of errors. His work did not end with the completion of a building. He precisely observed his buildings, executing long term measurements to draw conclusions from the behaviour of his structures.

2.2.4 Current slender concrete shells

With proceeding industrialization, the distribution of buildings costs shifted, expressed by an increase of labour compared to material costs. In consequence, the realization of concrete shells significantly decreased from the 1970s [SK07].

From the middle of the 20th century electric arc-welding established, with the first industrial welding robot developed in 1980 [PHF10, 15]. Progressively the structural steel engineering advanced from riveted steel plate sections to today's steel structures. Large spanning roofs were increasingly realized in the form of lightweight, spatial steel structures; a tendency observed up to the present time.

Notwithstanding, there are several realized examples of form dependent concrete shell structures, with a shape development based on a comprehensive understanding of the force flow and material behaviour. Representative examples of concrete shell construction being carried forward are the *Alster-Schwimmhalle* in Hamburg, designed by *Horst Niessen*, *Rolf Strömer* and structurally developed by *Fritz Leonhardt* and *Jörg Schlaich* in 1967; the *St. Paulus Church* in Neuss from 1969 designed by *Fritz Schaller* and *Stefan Polónyi*, a spatial structure assembled by folded plates, or the roof shells of the commercial building of *P&C* in Lübeck from 2005, designed by *Ingenhoven Architects* and the engineers of *Werner Sobek*.

Experimental formfinding methods for pure tensile structures have been transferred to compressive concrete elements. The shell-formed substructure of the *Ponte Musmeci* in Potenza, Italy, designed by *Sergio Musmeci* in 1975, is based on minimal surfaces aiming a compressive-only behaviour of the structure in service.

The horseshoe-shapes of the concrete shell columns in the underground station *Stuttgart 21* were developed with soap-film models by the form-finding pioneer and *Pritzker*-awardee *Frei Otto* in 2000[9].

The development of digital design tools and increased computational power are perceivable in the conception, development and realization of architectural designs. Architecture, designed with digital design tools, lacking in practical relevance, derogatively has

---

[9]The first column was completed in August 2016.

Figure 2.11 *Music Theatre* in Graz, Austria by *UNStudio* and *Arup*, completed in 2008, Photo: *Iwan Baan*

Figure 2.12 *Desert Learning Center* in Al Ain, Abu Dhabi, by *Chalabi Architects* and *Bollinger + Grohmann*, completed in 2013

been termed 'blob-architecture'. Starting with animation software from the film industry, architects tried to design and capture complex shapes, finally enabled by the introduction of 'Non-Uniform Rational B-Splines' (NURBS). The representation of architecture in two-dimensional projections, like plan-views and sections, was expanded to three-dimensional techniques in conception, representation and realization. Moreover, the movement towards parametric design procedures shifted formfinding from morphology to evolution, as an optimization by selection and recombination of various parameters [Wal13].

Freeform concrete structures of unprecedented complexity and accurateness in fabrication arose from the end of the 20th century.

Prominent examples are the *Phaeno Science Center* in Wolfsburg, Germany by *Zaha Hadid Architects*, finished 2005; the *Mercedes-Benz Museum* in Stuttgart, Germany, by *UNStudio* and the engineers of *Werner Sobek*, finished in 2006; the *Music Theatre* in Graz, Austria by *UNStudio* and *Arup* (fig. 2.11), completed in 2008; the *EPFL Rolex Learning Center* in Lausanne, Switzerland by *SANAA* and *Bollinger + Grohmann Ingenieure* (p. 69), built in 2010 and the *Desert Learning Center* in Al Ain, Abu Dhabi by *Chalabi Architects* and *Bollinger + Grohmann Ingenieure* (fig. 2.12), built in 2013.

Current attempts in research and practice are concentrating on computational form-finding methods, in particular for concrete shell structures, generating shapes informed and optimized according to structural parameters. Software plug-ins, picking up on associated models, are optimizing shapes with evolutionary solvers, manipulating predetermined parameters of the geometry. Developments of the *Block Research Group* of the *ETH* Zurich,

are based on the theory of vector-based graphic statics, enabling a generation of complex structures without tension, as further described in section 3.1.2.

It can be observed that innovative shell structures are hardly implemented in practice. Material possibilities and shape generation developments are not reflected in built architecture. The rebirth of concrete shells is limited to a pavilion-scale, and the realization is often reserved to demonstrators, developed in academic environments.

Despite that, trends are emerging in practice, focusing on morphological coherence from structural design logics, not only for overall spacial forms, but also for sub-articulations such as grids, ribs, perforations and tessellations, as *Patrick Schumacher*, director of *Zaha Hadid Architects* states in [Sch14]: "*In my design work I am now trying more and more to move away from the freedom play with complex curvature towards the disciplined use of structural form-finding algorithms...*"

3 Designing of concrete shells

3.1 Form finding methods

3.1.1 Experimental form finding

The design of concrete shells excludes a separation of form, structural behaviour and construction within the design process. A subsequent treatment of procedural design steps, as common in traditional design procedures, where the architect defines the valued space and appearance and the engineer takes charge of the stability analysis, is not feasible for form dependent structures. The construction is the form, defining the structural behaviour and vice versa. In order to fulfill the inherent restrictions of shell structures, as there is the slenderness or aspired membrane action, design methodologies are necessary to achieve structures in equilibrium for occurring design loading. As *Werner Sobek* states in [SK07], this process, termed 'form finding' does not imply a random finding of a solution, but rather a scientific and strategic iteration of quantifying results of variable parameters. As a result, there is a form, fulfilling material and statical requirements, taking the architectural approach as a basis. Whereas in obsolete design methods, stress states are conditioned by the form ('force follows form'), a form finding leads to a geometry fulfilling given restrictions for occurring stress fields ('form follows force').

Adriaessens et al. define form finding as *"a forward process in which parameters are explicitly/directly controlled to find an 'optimal' geometry of a structure which is in static equilibrium with a design loading."* [ABVW14, 2]. Beside 'freeform' shapes, not considering structural performance, geometries of shell structures can be categorized in 'mathematical' definable shapes and 'natural' or 'experimental' form found shells. Shapes defined by mathematical expressions are beneficial in order to describe geometrical data for analysis and fabrication purposes. Shapes can be spheres, ellipsoids, cones, toroids or hyperbolic paraboloids. As a backdrop, only in exceptional cases do these shapes fulfill statical requirements and respectively do not have an optimal structural behaviour.

Experimentally shapes are derived with physical models simulating the material conditions on the basis of natural and physically laws. This demonstrative procedure allows an
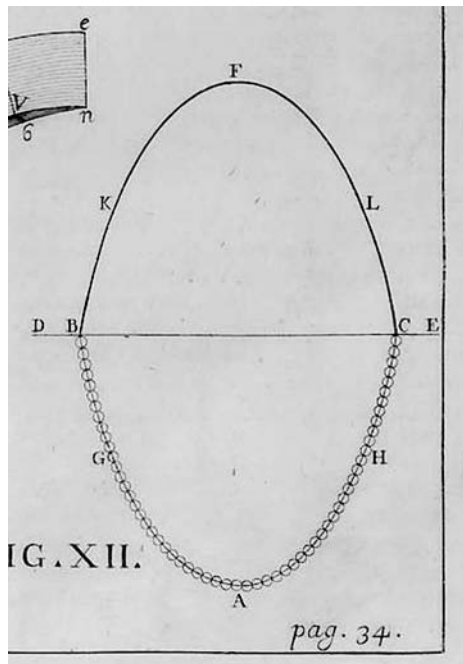
**(a)** *Hooke*'s hanging chain and the inverted rigid arch
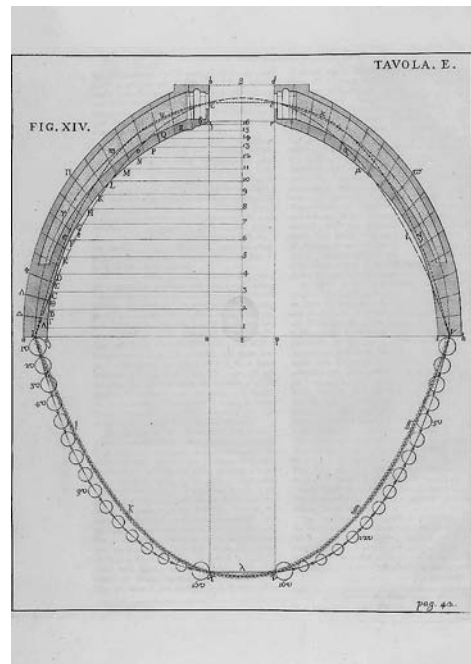
**(b)** Investigations of thrust line and masonry section of *St. Peter's Basilica*, Rome

Figure 3.1 As hangs the flexible line: *Robert Hooke*'s 'law of inversion' as depicted by *Giovanni Poleni* in 1748 [Pol48]

investigation of the structural behaviour. The transfer of the geometry achieved requires a neat measuring of the model, which is a source of inaccuracy since errors are multiplied by scaling up. Often adjustment activities are necessary thereafter. In [Add14], *Bill Addis* separates physical models in 'scale-dependent' and 'scale-independent'. Models are 'scale-dependent' as soon as both, stiffness and strength proportions need to be considered, whereas 'scale-independent' models are valuing as an exact inference of the structural behaviour.

Addis summarizes most considerable experimental formfinding methods. These include hanging cable-nets (section 2.2.2.1), hanging fabrics (fig. 3.2c), pneumatic or bubble shapes by inflated membranes (fig. 3.2b), extrusion- or flow shapes or minimal surfaces achieved
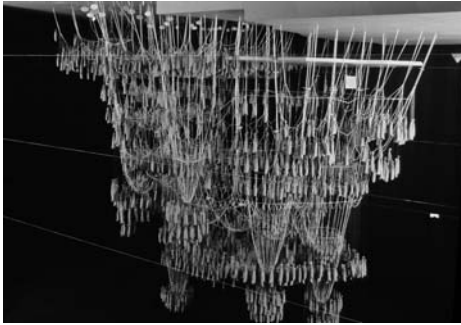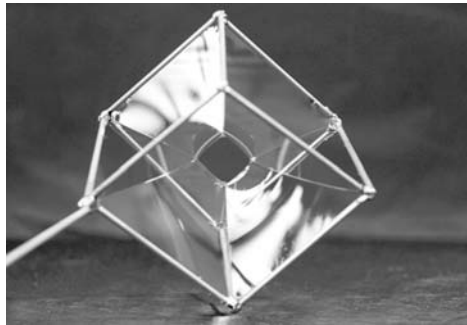
(a) Hanging cable-net model of the chapel *Colò-nia Güell* by *Antonio Gaudi*
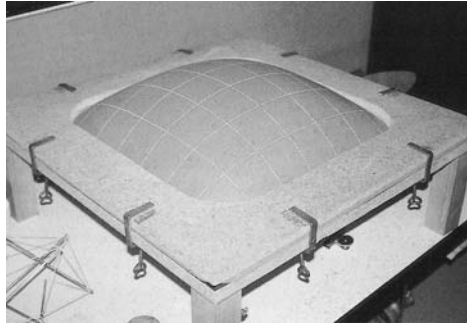
(b) Pneumatic bubble shape formfinding with in-flated membranes by *Heinz Isler*
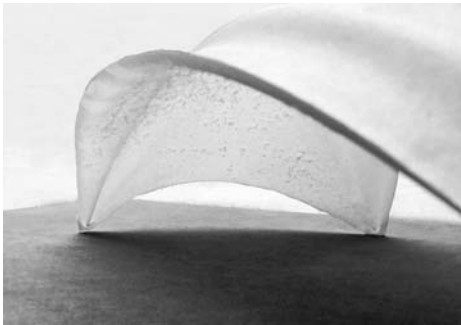
(c) Inverted hanging fabric made of ice

(d) Minimal surfaces achieved with soap film models

Figure 3.2   Examples of experimental form finding methods

with soap films (fig. 3.2d).

Hanging models, as the most considerable experimental form finding method, have already been applied over the centuries. Already in 1675, the structural form finding of an arch was invented by *Robert Hooke* (1635–1703). He published his ten inventions in the form of anagrams of Latin phrases. The second[1], solved in 1705, is cutting-edge for the hanging model as design method: *"As hangs the flexible line, so but inverted will stand*

---

[1]The third invention is the common '*Hooke*'s law of elasticity'

the rigid arch[2] ", see [OB14, 7]. Arch shapes respectively follow the line of the inverted hanging chain, which naturally is free of bending, considering permanent loading.

In 1743 *Giovanni Poleni* adapted *Hooke*'s analogy between the hanging chain and the rigid arch for an investigation of the dome of *St. Peter*'s in Rome (fig. 3.1). He used hanging chains weighted proportional to the sections of the vault, with the cognition that the thrust line should be located within the masonry section (see section 2.2.2.1).

The transfer of the hanging chain as a form finding method from two dimensional approaches to complex spatial structures, has significantly been pushed forward by *Antonio Gaudi* in Spain, as described in section 2.2.2.1. A reconstructed spacial hanging model, used by *Gaudi* for the development of the chapel *Colònia Güell* (fig. 3.2a), is exhibited in the *Sagrada Familia*, Barcelona.

From the middle of the 20th century, the Swiss engineer *Heinz Isler* expedited form finding techniques. Amongst other techniques, he elaborately investigated inverted hanging models with fabrics instead of chains to achieve funicular[3] structures (refer to section 2.2.3.3). The second dimension of the hanging surface leads to multiple possibilities of the load transfer with the structural surface. *Isler* dealt with the complication that occurs when the one-dimensional chain is replaced by materials with distinct two-dimensional stress states. The geometry achieved is highly dependent on the elastic properties and shear capacity of the fabric involved, for example in the tendency of wrinkling.

3.1.2 Numerical form finding

The design process of shell structures, as abstracted by *Werner Sobek* in [SK07], begins with the specification of boundary conditions. This may be the size, the geometry of the edges, the footprint area and the definition of a form-giving and design-driving load case. The self-weight is a common basis to initialise the process, but it becomes less relevant for lightweight constructions. For extreme lightweight structures, the domination of a single load case is no longer ensured and the form finding process has to be generally adapted. A preliminary achieved shape is then analysed under consideration of further load cases and combinations with a following evaluation of predefined target values, informing the initial shape as a curtailing iteration step.

---

[2]The anagram of the Latin phrase *Ut pendet continuum flexible, sic stabit contiguum rigidum inversum* is *abcccddeeeeefggiiiiiiiiillmmmmmnnnnnnooprrsssstttttttuuuuuuuuux.*

[3]In the context of shell structures, the term 'funicular' means 'tension-only' respectively 'compression-only' for a given loading [OB14]

With increasing significance of digitizing design processes, form finding is shifted to numerical methods to a greater extent. The essential benefit is the high accuracy due to standardized interfaces and interchange formats which enable not only the form finding and capturing of complex geometries, but also the structural analysis and the transmitting of data to Computer Aided Manufacturing (CAM).

Nevertheless, experimental and numerical form finding methods are often applied parallel. It is not unusual to use physical models as form finding tools, especially in early design stages, due to the comprehensibility which is not necessarily given in a digital simulation. In this sense, principle structural shapes can be evaluated under consideration of the flux of forces.

Sobek separates computer aided formfinding methods in 'indirect' and 'direct' methods, see [Sob90] and [SK07]. 'Indirect' methods are numerical simulations of the experimental methods, where a given configuration is deformed iteratively, until a final geometry is achieved that satisfies predefined design specifications. On account of this, this method is also termed 'deformation method'. A result fulfilling design requirements is enhanced by manipulation of input parameters and a corresponding reanalysis, thus in an indirect procedure. The achievement of distinct intended stress states is hardly possible, and the results are not fully sufficient. Indirect methods include 'dynamic relaxation' methods based on vector analysis, and predominantly 'finite element methods'.

Whereas indirect methods always lead to a solution due to the existence of an initial geometry, with indirect methods the non-existence of a solution is just as possible as multiple solutions, since desired stress states are defined without initialization of a starting geometry. The result is an unknown system, fulfilling a stress field from the predefined design load case. Direct methods include deformation methods combined with distinct optimization strategies and predominantly the 'force-density method'.

Most relevant numerical form finding strategies are abstracted in following paragraphs.

Force density method (FDM)   This mathematical method was developed at the *University of Stuttgart* in 1971 and is common in the design practice of cable-nets and tensioned membrane roofs. It generates solutions of discrete networks in exact equilibrium with linear independent systems of equations, without needs of iterations or convergence criteria. The basis of this method is the adjustment calculus of all nodes within the network, where equilibrium conditions are determined according compatibility criteria of the neighboring nodes. A solvable system of linear equations is achieved by the introduction of a constant force density q, which is defined as $q = F/l$, where F is the force and l the

Figure 3.3 *British Museum Great Court* by *Foster+Partners* and *Buro Happold*, London, UK

Figure 3.4 Canopy shell structure by *ZHA CODE*, Mexico City

stressed length of the bar. The procedure is entirely independent from material properties and allows design processes that are materialized arbitrarily. The force density method is described in detail by *Klaus Linkwitz* in [Lin14]. Prominent structures beside tensile membrane structures are the *Multihalle* in Mannheim, Germany (p. 83) from 1975 and the *Solemar Therme* in Bad Dürrheim, Germany from 1987.

Dynamic relaxation (DR)   In contrast to the FDM described above, the dynamic relaxation is based on a numerical iteration of non-linear equations, where the structural behaviour is analysed in result of external loads. An initial system is dynamically deformed by applying external loads. The movement of the nodes from their origin are determined with deviation vectors. Caused by an introduced viscous or kinematic damping, the dynamic system is iteratively converted to a final equilibrium state [Wal11].
A remarkable built example is the roof structure of the *British Museum Great Court* in London, UK (fig. 3.3) by *Foster+Partners*, *Buro Happold* and *Chris Williams*, completed in 2000. With the online publication of his work and corresponding source codes, *Chris Williams* provided this form finding method to a wider community of designers, whereby it was not limited to expert systems but became a design tool.

Particle spring (PS) systems   The idea of this method, developed in 2005 at the MIT in Cambridge, USA, is the generation of digital hanging models, analog to the experimental procedures of *Gaudi*, *Isler* and *Otto*. Embedded in parametric design tools, particle spring systems allow an exposure to physical loading, where effects of changing boundaries are visible in real time. The structure is transferred to a system of lines, as

axial springs, with a predefined maximum length, which allow no bending and points as mass-particles. Spring-mass systems are based on the determination of equilibrium within the system. If the equilibrium is disturbed by applying external loads, the length of the springs is adapted iteratively until an adjusted state is re-established.

The calculus of form deformation is based on *Newton*'s second law of motion, $\vec{F} = m \cdot \vec{a}$. The forces in the springs follow *Hooke*'s law of elasticity $F = D \cdot \Delta l$ where D is the predefined spring constant $D = E \cdot A / l$.

A demonstrative built concrete shell structure designed with form finding methods based on PS systems are the canopy structures by the design group *ZHA CODE* built in Bangalore, India and Mexico City (fig. 3.4) from 2011.

Finite element method (FEM)   To simulate the structural behaviour of complex, sometimes severalfold statically indeterminate systems, this method is widely established in engineering practice. Established in the 1950s in the aviation industry, the finite element method paved its way via the automotive to the building industry from the 1970s.

The structure is subdivided, 'meshed', in discrete finite elements. Based on a correlation of stiffnesses of the interconnected elements in the mesh, the action of force on a deformable solid state body can be determined. Manyfold types of elements have been established over the years, ranging from one-dimensional bar elements with a start and end node, up to volume elements with 20 integration points [Wal11]. Implemented in the environment of parametric modelling software, a live analysis and real-time response of the structural behaviour is enabled. In combination with optimization strategies, like evolutionary algorithm solvers, manipulating the input parameters according predefined fitness criteria, this deformation method can be used as a direct form finding tool.

Thrust network analysis (TNA)   Developed by the *Block Research Group* of the *ETH* Zurich, TNA is derived from the theory of vector-based graphic statics (see section 2.2.4). It is appropriate for the design of funicular, compressive-only shells, thus for vaulted systems of unreinforced masonry, as described by *Philippe Block* et al. [BLR14]. Graphic statics are based on the geometrical relationship between a form diagram, representing the geometry, and the force diagram representing the force magnitudes by measuring the vector lengths. The system can be informed bi-directional, thus the form can drive the force and vice versa. It generates thrust lines, visualizing compressive flow of forces if fitted within the middle-third zone of the masonry cross section. The expansion of the thrust line to a three-dimensional system is a thrust network that allows a spacial exploration of funicular forms in static equilibrium.

3.1.3 Structural optimization

"*... do not optimize a bad system – it will stay bad!*"
(*René Motro*, at the time president of the IASS in his conference lecture at the IASS symposium in Brasilia, 2014)

The structural behaviour of shells is essentially influenced from the geometry of the examined form dependent structure. Thus the optimization of the structural form is a fundamental step within the design procedure of shells, in order to increase the efficiency and utilize material saving potentials without functional drawbacks of the building in service. The aim of optimization is the achievement of a minimum or maximum value of a defined target function. The classical procedure in structural design is the determination of the structural response (stresses, deflections, etc.) caused by an applied loading. In structural optimization the problem is inverse, since the aim is an optimum response by varying the structural system within the design space. *Adriaessens* et al. define structural optimization as *"an inverse process in which parameters are implicitly/indirectly optimized to find the geometry of a structure such that an objective or fitness criterion is minimized."* [ABVW14, 3].
Fitness criteria, as defined for evolutionary solving algorithms and generic optimization, may be the deformation, support reactions or internal stress variables. An approach of *Walser* in [Wal11] is the minimization of the strain energy within the concrete section, in order to minimize in-plane bending, since membrane deformations imply a low strain energy level, see section 2.1.1.
Structural optimization can be classified according to the type of optimization variables to 'topology optimization', 'form optimization', 'sizing optimization' and 'material optimization' [Mau98, 20].

Topology optimization   This is the general layout information of a structure, thus the position and allocation of structural elements within the design space. The topology of the structure is not predefined by the designer. The approach is a development of an optimized structure inside a defined design space by a free allocation of material, hence the connectivity of nodes and the existence or absence of elements [ABVW14].

Form optimization   The optimization of form or shape deals with the elaboration of an optimum of a given topology, according to the load takedown. In discrete structures the adaptation of node coordinates may be an approach, without changing the principle nature

of the structure. A predefined structure is geometrically informed by design variables, where the origination of new elements or material openings is not possible [Wal11].

Sizing optimization   Also termed as 'cross section optimization' the sizing optimization is the determination of optimal cross sections, bar diameters or shell and plate thicknesses within a predefined structural system, where the overall geometry remains unchanged.

Material optimization   Material optimization is the optimization of material distribution and adjustment of their characteristics at a predefined location. This includes the content of reinforcement or fiber orientations.

As stated by *Maute* in [Mau98], the order of the optimization strategies described above are following a hierarchy within the optimization process. The general constellation of a system is defined with the topology optimization. Form and sizing optimization define the details, with the sizing optimization being a special case of form optimization. Material optimization can be classified as the final working step of the design process.
Lipka states in [Lip07, 39] that the reverse influence of material adaptations to the effect on the target function can be considered in an iterative process of optimization of topology, form, size, and material.

3.2 Structural characteristics of concrete shells

3.2.1 Design fundamentals of surface structures

Shell structures are surface structures, such as membranes and plates. The load bearing capacity of shells is not primarily defined by the material strength, but rather achieved by a spatially directed allocation of material within the design space. Due to the single or double curvature, as discussed in section 2.1.1, the shell has the ability to bear loads in a membrane stress state with a lower strain energy level compared to bending systems. A demonstrative example is a slice of an orange peel or a piece of an egg shell, where an inextensional deformation without changing the in-plane length of the surface is impossible. A shell structure is even more capable than just a spacial version of a two-dimensional arch (see fig. 3.5). Arches are able to bear loads without bending, provided a geometry balanced with the outer loads. Other loads will cause bending moments, as a product of the thrust and its eccentricity from the axis. In contrast, the three-dimensional thrust surface
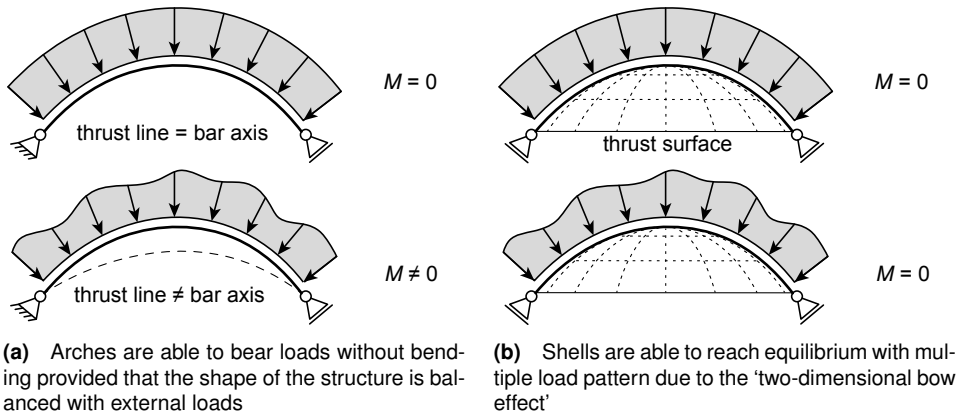
(a) Arches are able to bear loads without bending provided that the shape of the structure is balanced with external loads

(b) Shells are able to reach equilibrium with multiple load pattern due to the 'two-dimensional bow effect'

Figure 3.5 Comparison of arches and shells, see [Gru06]. The load takedown of shells is via hoop and meridian forces

provides multiple possibilities of stress fields in statical equilibrium without bending, due to the load takedown via both, hoop and meridian forces.

The analysis of shells is based on the convention of 'median surface models', which is defined as the surface that orthogonally bisects the shell thickness t at any position and the thinness hypothesis, $t \ll l_x, l_y, R_1, R_2$ [Zas05, 15], that implies a thickness which is small compared to shell extents and curvature radii.
The thickness is considered to be proximate constant by avoiding abrupt changes. The curvatures are supposed to be steady and the material homogeneous, isotropic and linear elastic. The shell form, the edges as well as the supporting, is one structural entity. *Hooke*'s law of elasticity is applied, as well as the hypothesis of *Bernoulli* [Rae01, 2], that implies that flat surfaces remain flat, disregarding the transverse shear strain.
Occurring shell forces are membrane forces, transversal shear forces and bending and twisting moments.

3.2.2 Theory of diaphragms, plates and shells

3.2.2.1 Plane stress and plate bending

Diaphragm structures Planar, rigid membrane structures, also termed 'discs', 'diaphragms' or imprecisely 'shells', are surface structures with an in-plane load bearing, such as shear walls. All loads are applied parallel to the median surface. The occurring
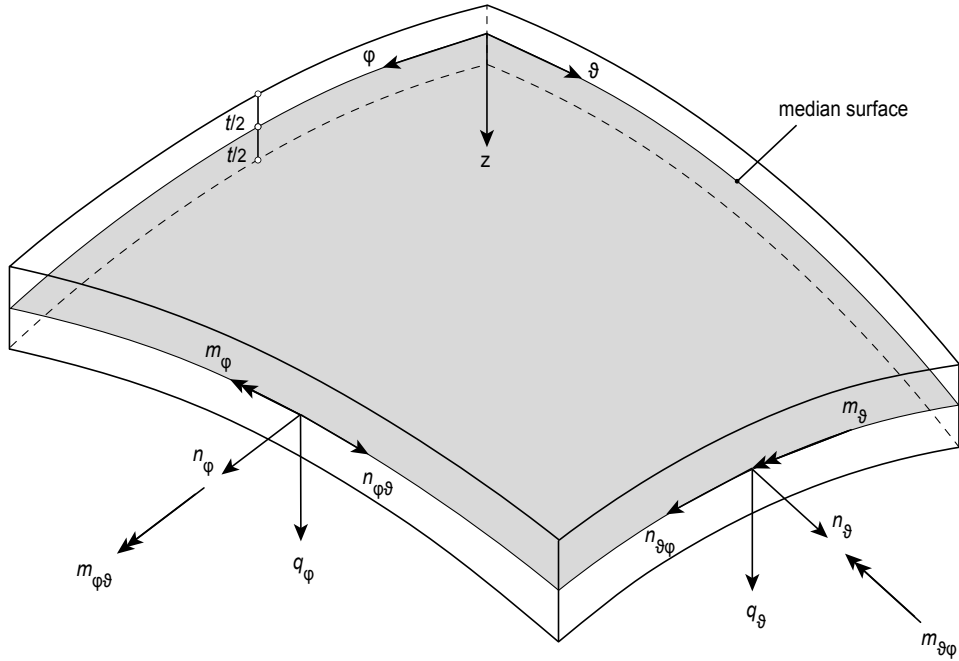
Figure 3.6   Internal forces of a shell element result to ten unknown with six equations of equilibrium

membrane forces in [kN/m], given cartesian coordinates, are n_x, n_y, n_{xy} and n_{yx}. Any bending and twisting moments, as well as transversal shear forces are considered to zero.

Plate structures   Plate structures are also planar, rigid surface structures, exposed to bending action, such as floor slabs. All loads are acting orthogonal to the median surface, and transferred via bending to the supports. The occurring plate resultants, given in carte-sian coordinates, are bending and twisting moments m_x, m_y, m_{xy} and m_{yx} in [kNm/m], as well as transversal shear forces q_x and q_y. Any membrane forces as stated above are considered to zero.

3.2.2.2 Shell theory

Planar rigid surface structures, as described above, are simplified to solely in-plane mem-brane systems as for diaphragm structures and bending systems like plates. In shell theory

the load bearing systems are aggregated and the number of internal load resultants are added up. Thus, in addition to a new introduced coordinate system, considering the double curvature, shell action is a combination of membrane- and bending systems:

$$\text{membranes} >> \text{shells} << \text{plates}$$

In membrane systems the number of unknown force resultants is four and the number of equilibrium equations is three, thus the statical indetermination is one. Bending systems have six unknowns for also three equations, leading to a three-fold indeterminacy.

For shell elements the directional coordinates are defined as φ, ϑ and z. Occurring shell forces are membrane forces n_φ, n_ϑ, $n_{\varphi\vartheta}$, $n_{\vartheta\varphi}$, transversal shear forces q_φ, q_ϑ, bending moments m_φ, m_ϑ and twisting moments $m_{\varphi\vartheta}$, $m_{\vartheta\varphi}$, see fig. 3.6.
Six equations of equilibrium for ten unknown force resultants can be constituted, consequently shells are four-fold statically indeterminate [Gru06, 7].

3.2.2.3 The membrane stress state

The reduction of shells to 'membrane shells' is the negligence of occurring bending, twisting and transversal shear. This paradigm is termed 'membrane stress state'. It is warranted to the very small shell thickness compared to the surface extents, where the bending stiffness converges to zero. The occurring force resultants are congruent with the diaphragm systems, as described in section 3.2.2.1. Considering the coordinate system for double curved systems, occurring membrane forces are n_φ, n_ϑ, $n_{\varphi\vartheta}$ and $n_{\vartheta\varphi}$. With $n_{\varphi\vartheta} = n_{\vartheta\varphi}$, a statical determined system is achieved.
The membrane stress state is based on the adherence of prerequisites, described in section 3.2.1. An appropriate hinged line supporting, disposed according the thrust line tangent, as well as steady load and geometry requirements are essential. It may be noticed, that even when perfectly shaped, a shell must have a certain bending stiffness to prevent buckling in compressive areas.

3.2.3 Buckling behaviour of shells

3.2.3.1 Phenomenology of stability failure

The structural response of a system is dependent on stiffness allocations, support conditions and the level of impact. Whereas 'well-tempered' structures will fail due to (well predictable) exceeding of the corresponding strength capacity, a sudden failure, attributed

to the loss of stability, is much more problematic. Stability failure is the deficiency of stable equilibrium within the system. *Matthias Andres* describes in [And04, 6–8] the analogy to the ball behaviour on a surface area: The ball in a valley is exposed to stable equilibrium, even when contacted, it will return to its initial position. The state of the ball on a plane is indifferent, thus indeterminate, whereas the ball on the peak of a hill describes an unstable state.

Stability failure of a structure is synonymic to the loss of stable equilibrium of the system. Gaining the first point of this impact level is the indifferent state, where at least two system responses are possible. With reaching unstable equilibrium, the system is unable to maintain the present state.

The simplest example of a well-tempered structure is the tension rod that never experiences buckling, whereas the simplest example of stability exposure is the compression bar which buckles as soon as the applied load exceeds the critical load.

According to *Andres*, stability failure of concrete shells can be separated to 'snap-through buckling' where the compressive arch from a critical impact level suddenly flips to a respectively tensile arrangement, and 'bifurcation buckling' where the system response branches to multiple possible states.

3.2.3.2 Measures preventing shell buckling

Stability failure may become design driving for shell structures. With increasing slenderness and material performance, the more relevant the investigation of stability. In [Wil14, 26], *Chris Williams* states: *"Shell buckling is particulary nasty because shell structures are so efficient. Almost no deflection occurs and suddenly there is total collapse."* Furthermore he concludes the paradox: *"The less efficient the shell, in terms of shape, triangulation of the surface and boundary support, the better it behaves in buckling."*

Possible stability failure modes are lateral buckling of edges, overturning of segments and local buckling of shell areas.

Werner Sobek describes in [SK07], that the transition to double curvature leads to an increase of stability capacity, since the prevention of buckling is not predominantly given by the bending capacity of the cross section, but rather by geometrical conditions of the shell. *Sobek* specifies the quotient of the squared thickness over the curvature radius t^2/R, influencing the enhancement of stability failure capacity. Thus buckling stability is gained by increasing the shell curvature $1/R$ (if possible from architectural and usage point of view) or increasing of shell thickness t. Since the increase of the shell thickness naturally results

in an increase of self weight, an alternative solution is the reallocation of material by introducing rips, as applied by *Nervi* (section 2.2.3.1), or the construction of multi-cellular, double-layered shells with connective webs.

4 Fabrication of concrete shells

4.1 Concrete construction materials

4.1.1 History of concrete technology

From beginning of human settlement, building construction is an elementary constituent for the ambition to encourage culture, society and prosperity. The knowledge of handling and production of building materials is the central aspect in construction. The use of natural and artificial stones for housing has ever since been the preferred choice to emphasize strength and durability, see [Hae64, 3].

The development in stone construction lasted several thousand years, starting from dry masonry and quarrystone work, followed by filling and casting masonry walls. The processing of binders has extensive significance; clay and mud fillers, limes and later lime mortar, and eventually the discovery of hydraulicity, led to the cements and thus the concrete characterizing the built environment these days.

There are different notions of the origin of the German word 'Beton'. Some are of the opinion that it is deduced from the Latin term 'bitumen' (mud sand). Others say it is derived from the French term 'beter' (solidification). The latter is favoured in the English term 'concrete', that is derived from the Latin 'concrescere' (also solidification). However, the first application of the term 'béton' is used 1753 in *Architecture Hydraulique*, by the French engineer *Bernard de Bélidor*, see [Hae64, 5].

Concrete in ancient times   Lime mortar has already been used by nomadic people. One theory describes that hearth areas and fireplaces, made of lime rocks, softened in the rain and accidently hardened when heated by the fire. The resultant burnt lime had a certain strength to be used as a filler, but still had no water resistance. The oldest known applications of lime mortar from 12 000 BC have been found in Turkey. Opinions in literature differ about the beginning of lime mortar as a construction material. Some sources indicate that ancient Egyptians have used lime mortars for their eminent examples of architecture, see [KBKPB02]. Others refer that lime, by way of example detected in the

Khafre pyramid from 2700 BC, is added accidently as an impurity of gypsum. In the Old Testament of the Bible, lime is mentioned in parts that can be dated around 1200 BC, see [Hae64, 8].

The invention and propagation of water resistant mortar can be accredited to the Phoenicians, a Semitic tribe with prosperity from 1000 to 600 BC. Coming from the coastal area of the Lebanon, these maritime and tradespeople colonized the southern and western areas of the Mediterranean Sea. The Phoenicians used brick flour as hydraulic additive of lime for a tightening plaster in the cisterns of Jerusalem of *King David*. They also recognized the water resistant properties of mortars, mixed with ground stones of the island Santorin, where the underground volcanic action carries out the burning process.

The ancient Greeks knew burnt lime from the Phoenicians and used it as whitewash with color additives and later as plaster. In 300 to 200 BC, a new masonry technique, called *Emplekton* developed in Greek colonies in lower Italy. Two wall layers were filled with quarry stones of different sizes. This agglomeration is filled up and compacted with lime mortar. To stabilize the two outer masonry formwork walls, anchors made of stone or iron have been implemented.
When the Romans banished the Greeks, they adopted and refined the *Emplekton* and complemented the construction of arches and vaults made of manufactured arch bricks with *Opus Caementitium*, a material that comes close to contemporary concrete of similar compressive strength.

Opus Caementitium   The technical expression *Opus Caementitium* is generally associated with Roman concrete, although it describes a construction technique (invented by the Greeks) for compression resistant building elements, made of mortar and stones. The Latin term is put together with 'Opus' (building, work) and 'Caementitium' (broken stone, aggregate). However, the Roman concrete is a significant invention in the history of building construction and is also termed as the 'revolution of building technique' or the 'turning point in history of architecture' [Lam93, 33].
Opus Caementitium is, depending on the binder, mostly water resistant and has aggregate sizes up to 70 mm, the reason for the visual similarity with concrete. The binder is a lime stone with or without clay and occasional added pozzolans (volcanic soil). The main differences to contemporary concrete are the burning temperatures. Present cements are burnt at about 1400 °C (until sintering) whereas the binders of Roman concrete are burned at about 800 – 1000 °C, a temperature below sintering [Lam93]. This is the reason for

Figure 4.1 Inside view of the rotunda in the *Pantheon* in Rome. The spherical cupola is built with *Opus Caementitium*

smaller strength and lower water resistance and inappropriate ability to cast underwater, that was not always guaranteed.

The technically talented Romans advanced the Greek *Emplekton* in the way of rationalizing the formwork masonry, and even substituted it with wooden formwork, as still apparent at the 12 m thick ring foundation of the *Colosseum*, the largest amphitheatre in ancient Rome, accomplished 80 AD.

 The highlight of the described building culture, merging the construction technique of *Opus Caementitium* and perfect utilization of the material characteristics, appertains to the *Pantheon* in Rome, as shown in fig. 4.1. The spherical cupola with a diameter of 43,30 m completed in 125 AD is still preserved and has been the largest spanning concrete dome in the world for more than thousand years, not relieved until the construction of the *Centennial Hall* in 1913 in Wrocław, Poland. The construction of the *Pantheon* is *Opus Caementitium* with a lost brick formwork, forming cassette reliefs reducing the self

weight. The cross sections are exactly adapted to the force flow, so that the arch thrust is transferred to the cylindrical substructure without further buttresses. Investigations have shown the application of different aggregate materials with variable densities that are diminishing towards the top of the shell.

Particular attention should be paid to the Roman architect, engineer and theoretician *Vitruv*, who lived in the first century BC. In his work *De Architectura Libri Decem* (ten books about architecture) he compiles the knowledge and experience of Roman master builders at the time in a scientific approach. Besides neat descriptions of mortar composition and fabrication, he gives explanations about architecture, technology and spatial design and describes his prospects about humanely habitation, combined with efficient constructions.
The three postulations of *Vitruv* to an entire building construction, are 'firmitas' (stability), 'utilitas' (expediency) and 'venustas' (prettiness) [Lam93, 17].

Exposing hydraulicity   The decline of the Roman empire in the 5th century led to a recession of the building technology in the occident. In contrast, the construction of the Byzantine *Hagia Sophia* in Istanbul, completed in 537, is a further high point in the construction of *Opus Caementitium*. In fact the cupola with a diameter of 31 m is smaller than the cupola of the *Pantheon*, but the construction is without the cylindric substructure. It is supported by four buttresses only.

During the middle age, the Roman construction traditions sank into oblivion. Although hydraulic binders existed, the technique of cast masonry had no relevance. Approaches to increase mortar strengths, ended as setbacks from current point of view. Some sources describe the admixture of mortar with eggs, milk, vinegar, wine or urine [Hae64, 28].

In the 16th century the Dutch gained naval, trading and economic power in Europe. An increase in prosperity of science and art, but also construction activity increased, all above harbor and watergate constructions. The Dutch were the first, recognizing the economic and technical significance of trass, milled volcanic tuff [Hae64, 32], without comprehensive knowledge about hydraulic activity. In the following decades an ambitious trading with tuff and trass becomes a significant economic factor, not only in Holland and Germany but in all of Europe.
With the beginning of the 17th century, manifold approaches by diverse scientists followed up to investigate the composition and connectivity of binders, in order to enter the market.

All these research efforts have been of empiric nature.

Elsewise *John Smeaton* (1724–1792), a British engineer and member of the *Royal Society of Civil Engineers*, was commissioned to build the third of so far demolished lighthouses on a small rock near Plymouth. The construction of the *Edystone Lighthouse*, completed 1759, and the extreme environmental site conditions motivated extensive laboratory investigations of hydraulic lime. Opposite to other scientists, he was critical concerning publications at the time and applied a scientific methodology with a series of experiments. He analyzed different sources of lime and identified the beneficial effect of existing clay for the water resistance of the construction material that is able to harden under water. With that he disclosed the secret of hydraulicity.

His promise, to create a material for the *Edystone Lighthouse*, with a strength equal to high quality Portland rocks (at that time the favoured construction material in London), later resulted in the term *Portland-Cement*.

Portland cement   Based on *Smeaton*'s expertise, inventions can be accented as a matter of significance, in contemporary cement development.

In 1796 the British *James Parker* invented the *Romancement*, a hydraulic binder produced with a clayey lime marl, obtained near London, that hardens without addition of lime. The name of the later patented material resulted in the similar color of Roman pozzolans. For the first time, the term 'cement' is not used for the pozzolanic components, but for the binder itself. It is still used for restorations and sealing constructions in flowing waters, due to its fast hardening as the main characteristic.

The French engineer *Louis-Joseph Vicat* invented an artificial hydraulic lime in 1818 and provided therefore the basis for the originating of *Portland-Cement* by the British bricklayer *Joseph Aspdin* in 1824. He adopted the still existing term *Portland-Cement* from *Smeaton*'s strengths comparison with Portland rocks, as mentioned above.

A further invention, leading to significant higher compressive strengths of the cements, is for the first time exposed by *Isaac Charles Johnson*, in 1844. He was the manager of a cement factory, competing against the factory of *Aspdin*. After failed spying and misdirections by his opponents, he invented the sintering process by an accidental overheating, contrary to the firing at lower temperatures, the practice until then [KBKPB02, 12].

Concrete in the 19th century   With the development of cements that guaranteed higher strengths at early and end stages of the concrete to the beginning of the 19th century, the industrial application of cements began. An important step in the history of concrete

technology is the awareness of explicit higher stability of concrete constructions with embedded inlays of iron and the insight of concrete being able to withstand high compression by insufficient tension resistance [vdH15].

The initiation of the application of iron reinforcement, a technology opening the gates to modernity, began in the middle of the 19th century, simultaneously in England and France. Several engineers and scientists worked on that idea to combine concrete with embedded iron elements. The British plasterer *William Boutland Wilkinson* and the French gardener *Joseph Monier* may be pointed out. 1854 *Wilkinson* claimed a patent on ferroconcrete in fire resistant slabs. The meshwork of ropes and rods was already placed below the central axis of the cross section. *Monier* investigated methods to improve the stability of planting buckets. He formed buckets of wire meshes and covered them with mortar mixtures. In 1867 he claimed a patent for a "*system of mobile container boxes made of iron and cement for horticulture*".

Prior to *Monier*'s patents, seminal innovations were patented in France. In 1855 *Joseph-Louis Lambot* invented the production of 'Ferciment', iron reinforced objects as a replacement of timber in shipbuilding. *François Coignet* developed a tamped concrete applications 'Beton aggloméré' and published in 1861 with *Betons agglomerés appliqués à l'art de construire*, applications and guidelines of the enhancement of concrete with embedded iron. Also the American lawyer and businessman *Thaddeus Hyatt* investigated ferroconcrete beams. One of his inventions from 1843 is a walkable concrete construction with glass grids that is already reinforced. His main focus was on fire resistant constructions, and from 1871 he claimed several patents on basics of ferroconcrete [Jür00].

Monier pursued and expanded his idea. In the following years he claimed additional patents, amongst others for bridges. In 1881 he got the patent of more general nature, that secured his technology for the "*production of various kinds of objects*", fig. 4.2. His inventions are characterized by iron embedments in the center of the cross sections (functional for buckets or filled reservoirs, but not for bending actions), a reason for the criticism of a lack of mechanical understanding. As mentioned in [Hub64], the life of *Monier* is shaped by various familiar blows and financial shortages, despite the success of his innovations. His first patents expired, since he did not pay the corresponding fees.

In 1884 he German engineer *Conrad Freytag*, who ran a company together with *Carl Heidschuh*, acquired the rights to the *Monier* patent and surrendered this pre-emption right, free of charge, to the Frankfurt engineer and businessman *Gustav Adolf Wayss*, director of *Diss & Wayss*, later *Wayss & Cie* in 1885. Together with *Matthias Koenen*, con-
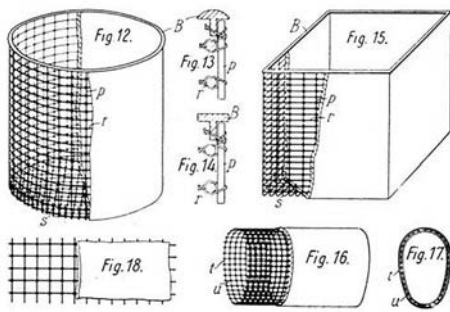
Figure 4.2 'Various kinds of objects from a bonding of metal grids with cement', patent of *Joseph Monier* from 1981
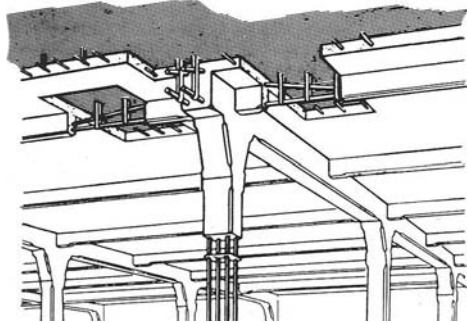
Figure 4.3 The *Système Hennebique*, monolithic building construction with continuous reinforcement

sidered as the 'spiritual father' of reinforced concrete construction, the so called *Monier brochure* is published in 1887. This work contained results of various investigations and is a basis for the propagation of reinforced concrete construction. The still active company *Wayss & Freytag* was established in 1893. [Way16]

With reinforced concrete, the first time a heterogeneous material is available, combining the positive material characteristics of iron and concrete. The French engineer and contractor *François Hennebique*, who operated international competitively to *Wayss & Freytag*, identified the fire protection of steel, covered with concrete and invented the idea of downstand beams. With his *Système Hennebique* (fig. 4.3) he successfully licensed the integral building approach with monolithic transitions of columns and slabs, made of reinforced concrete.

A further essential development, emphasizing the possibilities of concrete constructions, is the prestressing of concrete where the capacity of building elements is significantly increased. For further information refer to chapter 7 on page 183.

4.1.2 Concrete, an artificial stone

4.1.2.1 Lime, pozzolans, brick flour

White limestone, after burning and slaking, together with sand gives an air hardening lime mortar. This non water resistant mortar is used for plaster work and masonry.

The same limestone, together with clay, again burned and slaked and then milled to flour,

gives a hydraulic and water resistant mortar that hardens also under water.

If burnt clay fragments, like potsherds and roof tiles, are ground to red powder and mixed with lime, the same result, a hydraulic mortar, is achieved.

If the burning process is driven until sintering at about $1400\,°C$, the intermixture of lime and clay glazes. The achieved clinker milled to flour is the basic formation of Portland cement.

In some volcanic areas, the burning process has been carried out by the volcanic underground activity. In this way the originated and broken tuff results to pozzolana when milled to flour. The German equivalent is named trass [Hae64, 4].

4.1.2.2 Three$^+$ ingredients

Concrete is an artificially produced stone, initially considered as a 'three component mixture', consisting of aggregates, cement as a binder and water. To reach a better workability and plasticity without increasing the delicate water-cement ratio, that negatively affects the concrete strength to be achieved, additional ingredients have been developed in ongoing research efforts from the middle of the 20th century. The application of admixtures, like plasticisers and retarders as well as additives, like fly ashes, silica and fibers, means that concrete is nowadays considered as a 'five component mixture' or 'multi component mixture'. One additional component is air voids.

Concrete is characterized by a high compressive strength and high durability. The ready-mix concrete hardens both, by exposure to air and also under water, and the hardened concrete is water resistant.

Cements   Cements are fine milled hydraulic binders, substances that are durable and able to harden under water. In reaction with water, stable and insoluble connections are built, developing spicular crystals which are interlocking with each other, leading to the strength of the cement mortar.

The required ingredients, as mentioned above, are lime and clay. Some geological sediments already contain both substances and are referred to as clay or lime marl. Burning beyond sintering, gives the Portland cement clinker. Milled, and with addition of gypsum, used to control the hardening process, gives Portland cement.

Beside the natural conglomerates, like lime, clay and pozzolana, industrial originated products are used for the production of cement. These are blast-furnace slag or granulated cinder, that emerge by melting irony ore and residues of bituminous rocks.

The raw materials and production is regulated in the European Norm DIN EN 197-1. It classifies five principle types of cement according to the composition:

CEM I	Portland cements
CEM II	Portland composite cements
CEM III	blast furnace cements
CEM IV	pozzolanic cements
CEM V	composite cements

The strength of cements is also regulated in this code. Three strength categories are differed: $32,5\,N/mm^2$, $42,5\,N/mm^2$ and $52,5\,N/mm^2$ after 28 days. Within these categories, the curing speed is separated in slow (L), normal (N) and rapid (R). The Germans separate the strength categories and the curing speed with the colours of the bags and the labeling respectively.

The strength category of cement should not be mistaken with the strength capacity of concrete. The concrete strength is furthermore dependent on other issues, like the water – cement ratio, the compaction, and the post treatment of the cast concrete.

Aggregates Aggregates are conglomerates of stones in various grain sizes, regulated in DIN EN 12620. The grains can be natural or artificial, rounded or crushed. Also, recycled material from old concrete is used. The aggregates are glued together with the cement paste and build the main component of concrete.

Aggregates are graduated in grain categories, defined by the grain-sizes. In these categories the smallest and biggest grain diameter is labelled, e.g. 0/2, 2/4, 4/8 and so forth. The maximum conventional grain size for normal concrete is 32 mm. Mixed products with grading curves with maximum grain size smaller 4 mm are formally labelled as 'mortar' and not as 'concrete'. It may be noticed by the author, that in this script the term 'concrete' is also used for mixtures with maximum grain sizes even $\leq 1,2\,mm$. This decision is made due to the common practice of industrial suppliers.

Concrete additives and admixtures The terms 'additives' and 'admixtures' have different characteristics. 'Additives' are added to the cement during manufacturing, to achieve new cement properties. 'Admixtures' are added during the mixing, to achieve new properties of fresh concrete.

Admixtures are high efficient chemical substances, usually added as a fluid, to enhance the characteristics of the fresh concrete facilitating the construction workflow on site. Admixtures are categorized according to the effect to fresh concrete. The main application is plasticisers. Even self-levelling and self-compacting concrete is achieved and allows a casting in face of dense reinforcement or inaccessible formwork.

Further chemical or physical outcomes are of pore builders and compactors, retarders and catalysts, stabilizers and injection aids.

In contrast to admixtures, additives have an impact to the concrete characteristics in the final state, like strength capacity, durability or colour. Admixtures are fine particles like trass, stone flour, silica fume or fly ashes that have to be considered in volume calculations [KBKPB02, 50]. They are separated in two categories: 'Type I' for inactive admixtures, like stone flour or pigments and 'Type II' for hydraulic and latent hydraulic materials. Main components of 'Type II' are latent hydraulic fly ashes, that are initiated to hydration, in combination with a reaction partner-substance in the cement. The application of silica fume, also known as microsilica, leads to concrete characteristics with high compressive strength higher $100 \, \text{N/mm}^2$ and high durability. Because of its extreme fineness, it fills interstices of cement particles and increases the bonding between gravel and cement matrix.

4.1.2.3 Ultra High Performance Concrete

Specification and Development   In the last decades, the development in concrete technology has advanced significantly. Major influence factor is the development of superplasticizers and the discovery of the positive effect of reactive silica fume. In the late 1980s, for the first time a strength category of C100/115 was produced. The implementation of high performance concrete and thus the appropriation to construction practise took place in 1988 [FSW+13]. The classification of strength categories of usually applied concrete grades is given in table 4.1.

Concrete with higher strength is used for high loaded constructions, where the benefits due to the reduction of cross section dimensions pay back the higher material costs. Typical applications are advanced engineering structures, like bridges and multi-storey buildings, where smaller elements lead to both, a space-saving construction, influencing the slenderness and usable space, as well as the reduction of gravity loads that have to be transferred to the foundation. Not least, reduced transportation efforts have a positive influence to total building costs.

Table 4.1 Classification of strength categories according DIN EN 206

Type of concrete	category	$f_{c,cyl}$ [N/mm^2]	$f_{c,cube}$ [N/mm^2]
Normal and heavy concrete	C16/20	16	20
	C20/25	20	25
	C25/30	25	30
	C30/37	30	37
	C35/45	35	45
	C40/50	40	50
	C45/55	45	55
	C50/60	50	60
High Performance Concrete	C55/67	55	67
	C60/75	60	75
	C70/85	70	85
	C80/95	80	95
	C90/105[a]	90	105
	C100/115[a]	100	115
Ultra High Performance Concrete	>C100/115		>115

$f_{c,cyl}$: Compressive strength of cylinders, ø = 150 mm; length = 300 mm, age = 28 d
$f_{c,cube}$: Compressive strength of cubes, edge length = 150 mm, age = 28 d
[a] individual approval (ZiE)

The current development, feasible for the application on site, is 'Ultra High Performance Concrete' UHPC, with a compressive strength of about $200 - 300$ N/mm^2, a scaling magnitude of ten, compared to normal concrete, closing up with the properties of steel.

The dense and optimized packing fraction leads to impervious material characteristics, with almost zero capillary voids. The so achieved high durability is the reason for the generally used terminology 'Ultra High Performance Concrete' instead of 'Ultra High Strength Concrete'.

UHPC is not covered within European building codes, design rules and guidelines, thus an individual approval is required for the application. As *Nguyen Viet Tue* states in his plenary speech [Tue16], this is one reason for the still moderate spread of UHPC. As further reasons he states a lacking know-how of designers, clients and construction companies, the non-sufficient utilization of advantages of UHPC, and a non-appropriate justification of increased material costs (factor $4 - 5$, compared to conventional concrete, see [FSW$^+$13]),

where the life cycle costs are not considered.

Currently a task group of the *International Federation for Structural Concrete* (fib) is working on an international code of UHPC.

Consistence and behaviour   UHPC is a cementitious composite material, with an optimized gradation of granular constituents. The consistence is characterized by a dense cement matrix, with a balanced particle size distribution, especially in the fine particle sector. The application of superplasticizers allows workable mixtures with a low water over cement ratio of about 0,2 (conventional concrete 0,4 – 0,7). The areas of fine gaps $< 0,125$ mm are filled with cement, silica fume and quartz powder, as well as inert and reactive powders. Usually the cement grade of $52,5$ N/mm^2 is chosen.

Furthermore, the grain size of aggregates is usually limited to 1 mm. The inner structure of the so produced material is very homogeneous, and compression loads are distributed equally over the agglomerate. Initial cracking is carried forward straight through the matrix and gravels, thus UHPC is brittle, with an abrupt failure behaviour in contrast to ordinary concrete, which has a certain post-failure capacity, due to internal structural shifting. This brittleness can be counteracted with the admixture of steel fibers, refer to section 4.1.3.4. A further issue is the fire resistance. The dense material leads to flaking caused by sudden discharging of internal vapour pressure. This is faced with the admixture of plastic fibers, resulting a formation of pores by melting, in case of heat impact [FSW$^+$13]. Current research efforts are working on the reduction of brittleness, by the targeted use of fly ash to create predetermined breaking points. Furthermore, the application of superabsorbent polymers leads to internal curing of non-hydrated contents of cements [Mec16].

The material behaviour is characterized by an almost linear elastic stress-strain relationship with an elastic modulus of $45 - 55$ GPa. With higher strengths of concrete, the brittleness increases and the failure, especially for UHPC, occurs explosively. The admixture of high strength steel fibers does not effect the ascending section of the stress – strain curve, but the post peak behaviour and the descending section is enhanced significantly, depending on the amount, consistency and orientation of the fibers. The admixture of steel fibers, leading to 'Ultra High Performance Fiber Reinforced Concrete', UHPFRC, is applied, to achieve ductile compression failure behaviour, and is also used for structural improvement in tension zones of the section.

When initial cracking occurs, the fibers are connecting both banks of crack and take over the load transition of the tension force. With increasing load, both, a fiber utilization

Figure 4.4 The *Gärtnerplatzbrücke* in Kassel is a pilot project with glued UHPC construction elements
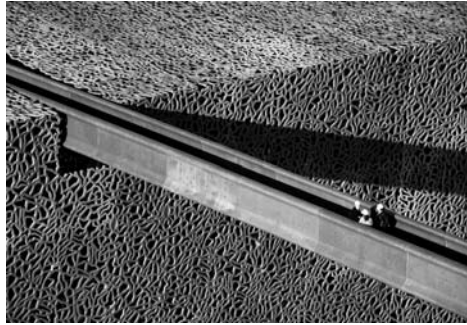
Figure 4.5 Major structural elements of the *MuCEM* in Marseille are constructed in UHPC. Photo: *Lisa Ricciotti*

(breaking of fiber) as well as a delamination process (pulling out of fibers) starts. An effect of tensile utilized stress strain curves is a strain hardening, after first formation of cracks, followed by a softening.

Design principals   The design concept of UHPC, recommended by *Ekkehard Fehling* et al. [FSW+14], is based on the partial safety factor concept, similar to the design of conventional concrete. Adaptations of the safety factors have been implemented on the material side, considering the sensitivity of the production process, the brittleness and the unpredictability of the fiber location and orientation. It is differentiated, whether alternative load paths can be formed (e.g. design of slabs), or if the absence of fibers leads to structural collapse (e.g. load introduction points).

Similar to the approach of reinforced concrete for the tensile and bending-tensile design, ultimate limit state investigations are carried out in the cracked state, where the concrete matrix has no carrying tensile contribution. It is a preassumption that flat surfaces remain flat.

The force equilibrium of the load bearing components is formed with the compressive stress block resultant of the concrete F_{cd}, the steel rebar tension force F_{sd} and the resultant of the equivalent tensile stress block of the fibers F_{fd}.

Benefits and applications   Low coefficients of permeability, high diffusion resistance and low capillary drawing are the basis for the high durability, characterizing the benefits of UHPC. In combination with the high achievable compressive strength and the

good workability, UHPC has been established in several application fields of structural and mechanical engineering, where these benefits are utilized.

The carbonation resistance and the resistance against freeze- and thaw cycles, sulfates and acid attacks, leads to a trafficability without further treating and thus an appropriate material for the repair and enhancement of bridge- and parking decks. The repair of reinforced concrete decks with UHPFRC gets along with layers of $20-30$ mm for waterproofing, and $40-70$ mm for waterproofing plus structural strengthening [Brü16]. Also the substitution of steel in aggressive environments as well as the construction of composite elements, load introduction points, and punching enhancements, are prospective applications.

A prominent pilot project is the *Gärtnerplatzbrücke* in Kassel (fig. 4.4), built in 2007. The bridge deck, made of UHPC elements, is glued onto the top chords, also UHPC, of the global truss structure. The first UHPC bridge was built in Sherbrooke, Canada in 1997 [FSW$^+$14].

Grouted installations of pylons in the foundation of off-shore power stations are executed in UHPC. For grouted joints, in the case of conventional concrete constructions, UHPC allows short lap splice lengths and shifts the weak point out of the joints. The *Musée des civilisations de l'Europe et de la Méditerranée – MuCEM*, by *Rudy Ricciotti*, opened in 2013, is a famous UHPC-application in building construction, where structural elements, like tree-shaped columns, as well as facade elements and the access bridge are constructed in UHPC.

The dramatically reduced carbonation depth leads to a reduced concrete cover required for corrosion protection. In combination with the high strength and good workability, the possibility is given to minimize cross sections of structural elements, widening options also in realization of slender concrete shells. However, new failure criteria may become design decisive, that have not been considered so far in the design of concrete structures, like stability failure and buckling, as well as the dynamic behaviour, caused by reduced damping masses.

4.1.3 Heterogeneity by means of reinforcement

4.1.3.1 The cracked state of concrete

With the comprehending of reinforcement, for the first time an artificial and heterogeneous construction material is provided. Design concepts are based on the assignment of load bearing tasks. Concrete is well suited to the bearing of compression forces, but has a low and unpredictable tensile capacity, that remains unconsidered in tensile and bending tensile

design. Occurrent tension forces are allocated to the reinforcement, an embedded material with appropriate tensile strength capacity. In the tension zones the present concrete still acts as location security and (corrosion-) protection of the inlays. Even compressive building elements have minimum reinforcing contents, to achieve durability and a good distribution of cracks.

Cracking occurs in the tensile zone of a concrete bending element and the load transfer of the tension forces is taken over by the reinforcement. The uncracked state is termed 'state I' and the cracked state 'state II'. This elongation defines the crack distribution and the crack width that has to be limited by the amount of reinforcement.

Beside the widely spread use of steel bar reinforcement, several approaches have been investigated, to produce concrete composite materials, as some have been established in construction industry.

4.1.3.2 Carbon Steel reinforcement

For conventional concrete structures, carbon steel reinforcement is used, either as bars or ready welded mesh-wire reinforcement for surface elements. The steel bars are placed horizontally to take over bending tensile forces, orthogonal stirrups are used as shear reinforcement. Reinforcement, in the compressive section of a concrete element, increases the load bearing capacity of compression.

Steel reinforcement, as covered in DIN 488, is available in diameters from 6 mm to 40 mm. To assure a sufficient bonding between steel and concrete matrix, the steel bars are ripped, increasing the required space for placing by 15 %. The construction site conditions are considered by the determination of the concrete cover. This surrounding layer is crucial for both, the load introduction of tensile forces, as well as protection against fire and corrosion. The cement matrix builds an alkaline environment with am pH-value of $12-14$. With carbonation over the long term of a building element, exposed to carbon dioxide and humidity, the pH-value decreases. With incipient corrosion the steel expands, leading to flaking of the concrete cover. The concrete cover assures the reinforcement to be placed beyond this critical zone.

The labeling, according to European codes, is 'B500S' for steel bars and 'B500M' for mat reinforcement. The label includes the characteristic strength category of $f_{yk} = 500 \, \text{N/mm}^2$. In the USA and Arabic countries, reinforcement steel grades are specified in [ksi] according to ACI and ASTM as 'grade 40' ($280 \, \text{N/mm}^2$), 'grade 60' ($420 \, \text{N/mm}^2$), 'grade 75' ($520 \, \text{N/mm}^2$) and newly 'grade 80' ($550 \, \text{N/mm}^2$) whereas 'grade 60' is the most common steel used [Sch11].

In Germany, even higher strength reinforcement grades have been developed. Individually approved for the *OpernTurm Frankfurt*, a 'SAS 670' with $f_{yk} = 670 \, N/mm^2$ and bar diameters of $\text{Ø} = 75 \, mm$ have been applied as compression reinforcement, as an alternative solution to steel composite columns [BBF+08].

4.1.3.3 Micro mesh reinforced concrete

Scaling down dimensions of conventional reinforced concrete by a crude factor of around ten, in order to achieve narrow structural concrete elements, leads to concrete sections with micro reinforcement. As further described in section 7.1 on page 183, geometrical dimensions, such as the element thickness and the concrete cover, as well as corresponding material components, can be downsized, like concrete grains, reinforcement diameters and distances. A denser cement matrix, as achieved by applying HPC and UHPC, allows smaller concrete cover for the sake of corrosion protection. The use of stainless steel in areas close to the surface even allows omitting this protective covering. Ready welded micro mesh reinforcement wires provide bi-axial reinforcing, with small diameters and small axial bar distances respectively.

A concrete technology, based on the downsized geometry of concrete components, is developed by *Stephan Hauser*, founder of *DUCON*, a material supplying company. *DUCON* stands for 'Ductile Concrete' and represents the combination of high performance- or ultra-high performance concrete with micro reinforcement from steel wire meshes. The mesh wire reinforcement is uniformly stapled over the entire cross section, from the top- to bottom fiber of the building element to be cast. The mesh wire diameters vary, beginning from 1 mm, with axial distances from $5 - 35 \, mm$. The so achieved homogeneous set-up of the composite material has an almost linear gradient of stress distribution by approximation, allowing a linear elastic design procedure via *Van-Mises* stress analysis.

It is common that small reinforcement diameters and small axial distances are beneficial concerning the development of cracks: With constant reinforcement content, the number of cracks increases by decreasing crack sizes. Due to the fine mesh size of the micro reinforcement, the crack width can be reduced to values of $w < 0,1 \, mm$, qualifying the material as impervious, see [EVG+13, 5]. The material properties can be adjusted in a way to achieve an extremely high ductility with large plastic deformation prior failure. This leads to a high energy absorbing capacity, a key feature for building protection against earthquake, bullets and explosion. The micro reinforcement is prefabricated, with ranging contents of $1 - 10 \, Vol.-\%$ of the concrete volume, embedded and infiltrated with the concrete slurry. Depending on the composition of the reinforcement within the cross section,
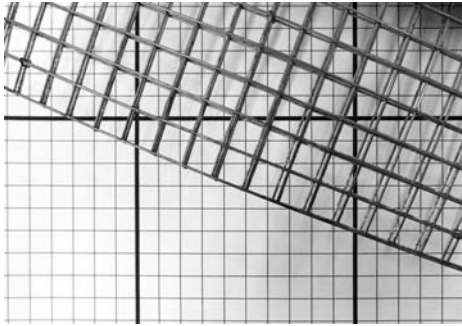
(a) Three layers of ready welded micro mesh reinforcement, here: diameter ø $= 1{,}2$ mm, axial distance $e = 12{,}5$ mm
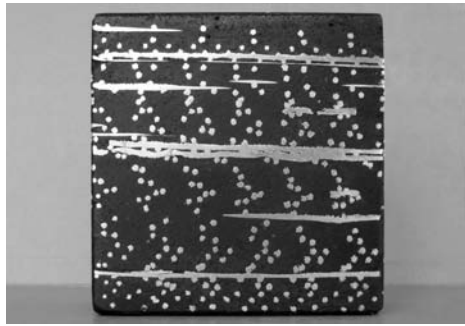
(b) Homogeneous set up of the reinforcement from top- to bottom fibers of the cross section [EVG+14a], ©*DUCON*

Figure 4.6 Micro mesh reinforcement as used for *DUCON* technology. Ready welded meshes are stapled layer-wise over the entire cross section

the material characteristics are programmable according to specific applications. The variation of reinforcement contents, diameters and strength characteristics, as well as partial enforcements and local interconnections, allow selective behaviour manipulations.

It may be noticed by the author, that for all investigations undertaken within this thesis, a micro mesh reinforced concrete according *DUCON* technology is applied.

Slump control with *Hägermann*-cones The application of mesh wire reinforcement mats leads to high requirements in the fluidity of the concrete to assure the concrete flows through the filaments of the mesh wires. The decision if the ready mixed concrete can be used is based on the size of the slump produced with a *Hägermann*-cone. This cone has the geometry of a frustum with the diameters of $D_t = 70$ mm at the top and $D_b = 100$ mm at the bottom and a height of $h = 60$ mm. This results in a predefined concrete volume of 345 cm^3.

The *Hägermann*-cone is placed onto a horizontal balanced plate with a plain steel surface. This surface is wet wiped before the cone is filled with the concrete to be tested. As soon as the cone is filled up to the top with concrete, the cone is lifted and rubbed clean. The concrete disperses to a slump, that is ideally a circle. As soon as the flowing stops, the diameters of the slump are measured in two directions. The achieved mean value of these diameters is the slump size.

4.1.3.4 Fiber reinforcement

Beneficial effects of fibers in massive building construction have already been known prior to the development of concrete. Ancient loam buildings were enhanced by the admixture of straw and fibrous parts of plants, to counteract immoderate development of cracks and to increase internal bonding of the brittle basic raw material. The unchanged principle is still state of the art for fiber reinforced, cementitious composites. The fibers applied are made of steel, plastic and glass. The admixture requires considerations in the concrete recipe, since the surface that has to be coated by the cement matrix, increases, see [P+13, 37].

Steel fibers   It is a tempting approach to replace steel reinforcement by a simple admixture of steel fibers, to achieve a tensile load carrying capacity. The placing of reinforcement is cost- and labour extensive and specific skills on site are required. However, the steel fiber reinforced concrete does not replace but enhance bar reinforcement in practice. As common practice, in the design of composite materials with concrete and steel, the design concept is based on the non-contribution of concrete for tensile stresses. Within crack openings, the crack bridging steel takes over the tension force. In case of steel fibers, the fiber has to connect the crack banks, with sufficient embedment length on both fiber ends. The sum of the fiber contributions define the tensile capacity after cracking. The main problems are uncertainties derived from production. Formation of clusters and gaps naturally have significant influence on the bearing behaviour. Especially when concrete elements are cast from two sides, cumulative fiber ends in the same section may occur. The random distribution, location and alignment of fibers are hardly controllable and appraised statistically, leading to the implementation of high safety factors. Naturally, fibers added to the ready mix concrete, are also located in areas of the section with no effect regarding structural enhancement, still affecting the costs. Thus the fibers constitute the major cost factor ($30-45\%$ of UHPFRC[1]) [LNK15, 12] of fiber reinforced concrete.
Fiber reinforced concrete has a maximum fiber content of 1,3 Vol.$-\%$, due to the workability. With this content almost no increase of tensile strength is gained. The fibers contribute in a crack distribution and ductility. Fiber contents in UHPFRC can be produced with fiber contents of about 2,5 Vol.$-\%$, leading to a hardening behaviour after initial crack formation [Rau10, 37].
After initial cracking, the fibers are activated. With the beginning of the activation phase,

---

[1]The terminology 'Ultra High Performance Fiber Reinforced Concrete' (UHPFRC) defines not a concrete but a composite, and it is also named 'Ultra High Performance Fiber Reinforced Cement-based Composite' [Brü16]

a bonding is given at the contact area of steel and concrete. In the delamination phase, the fiber separates from the concrete matrix, from the cracking bank towards the fiber end, and the load transfer in the delaminated zones is given by friction. In the pull-out phase, the complete fiber is delaminated. The design of the fiber is an optimization between delamination and bonding. The fibre length is slightly shorter than critical length to gain.

Although the contribution of the fibers, according to the design concept, is after cracking, investigations and practical experiences show a beneficial material behaviour and ductility gained by the admixture of fibers. As a backdrop, a possible tendency of the fibers to stick out of the concrete element may be mentioned, leading to the risk of injury in the serviceability.

Magnetic alignment   Current research investigations, undertaken at the *Institute of Structural Design* (ITE) of the *Technical University of Braunschweig*, are dealing with the magnetic alignment of fibers within the cementitious matrix. Motivated by the fact, that only one third of undirected steel fibers in UHPFRC members are contributing to the tensile strength, the goal is to provide and align fibers in zones where they are effectively needed in order to design UHPFRC members in a more effective, filigree and sustainable way.

With the help of robot-directed magnets, the alignment of fibers is manipulated according to predefined load paths. A desired micro overlapping of parallel oriented fibers is achieved by using different sets of magnets. Investigations in translucent concrete substitutes proofed repeatable and accurate results [LNK15].

Plastic and glass fibers   Plastic fibers consist of organic polymers with strengths characteristics, depending on the material composition and production processes. The application as structural reinforcement does not play a prominent role in the building industry. The typical usage is for sprayed concrete, screed and plaster. As described in section 4.1.2.3, polypropylene fibers are used for the fire protection of high strength concrete elements. Melted fibers, in the case of fire, build capillary tubes, allowing the discharging of internal vapour pressure, occurring in the heating of the concrete. The beneficial effect of plastic fibers is rather low, due to the low tensile strength and elastic modulus. Current research efforts are being undertaken, in order to achieve plastic fibers with increased performances [P+13, 38].

Alkaline resistant (AR) glass fibers, are commonly used in building construction. Glass fiber elements, due to a production company also known as *Eternit*, are produced in line

production from high strength cement and glass fibers and cut after hardening. The thin elements are durable, fire resistant and have a good workability and provide the possibility of drilling and screwing. A common use of glass fiber plates is the construction of facade- and roofing elements. Furthermore, as additive for sprayed applications, glass fibers are used, especially for fastening of multi-curved surfaces.

4.1.3.5 Textile reinforcement

Glass- and carbon fibers and filaments can be woven to rovings and cast in concrete. The so achieved textile netting is not an arrangement of randomly oriented fibers, but has a distinct and predictable amount of reinforcement, that can be considered in the structural design. Rovings consist of $100 - 1000$ filaments tailored to textile roving fabrics. Carbon fiber rovings have a tensile strength capacity up to ten times higher than steel reinforcement [Erh15].

A typical application of textile reinforced concrete (TRC) is the structural enhancement of existent structures, where the textiles are laminated or sprayed onto the existent concrete surface with cementitious mortar.

Restorations and enhancements with textile reinforcement satisfy with a high tensile capacity, fine crack distribution and a planar load introduction with no corrosion issues. A general technical approval allows an indoor application, limited to four textile layers, although with no consideration for sheer and fire resistance.

Special attention is paid to the casting process, when textile reinforcement is applied for ready mixed concrete, to avoid unwanted position delays. For a better handling, the filaments are treated with different coatings. The impregnation with styrol butadiene resin leads to a moderate rigidity of the net, whereas epoxy coatings lead to a high rigidity, necessary for the casting process [Mec16].

Whereas an increase of the filament rigidity leads to an easier handling of the production, it limits the field of applications for freeform structures. A pavilion, demonstrating the use of textile reinforcement, was designed by the *RWTH Aachen*, described in [SCH12]. Inspired by hyperbolic shells, designed in Mexico by *Félix Candela*, a pavilion of 2×2 identical prefabricated elements, made of textile reinforced concrete, was realized on the university campus. The shell has a thickness gradient of 60 mm at the edges and 310 mm at the clamping point in the middle. Due to the double curvature, a flexibility of the nets was necessary, and uncoated filaments were used. Twelve layers, equally spaced over the cross section, have a distance of 5 mm. To assure the location of the filaments,

and to avoid a shifting of the flexible net, sprayed concrete with a maximum grade size of 5 mm was sprayed layer-wise on the formwork, and the textiles were rolled on the wet matrix.

The structural design, based on experimental investigations, requires a consideration of the installation pattern in reference to the principal tensile stress direction of the structure. The optimal tensile activation of the textile filaments is a 0° direction. A shift of a deviation angle leads to a destruction of the outer filaments at the cracking banks.

An innovative approach, utilizing the material characteristics of textile reinforced concrete, is the spatial folding of initially plane structures according to origami methods, as described in [HHSC15, 2]. Flat elements are cast on the ground, with cavities in the folding and continuous textile reinforcement in the joints. After hardening, the prefabricated systems are installed with the help of vacuum caps, and the edges are grouted. During the assembly the textile reinforcement in the joints is flexible and behaves as a line hinge.

4.2 Formwork systems for double curved concrete faces

4.2.1 Specifications and history

Due to the manufacturing in a liquid state, concrete is able to adapt to any shape. All geometrical limits in the practicability of concrete constructions are caused by the form-work. The planning process of a concrete construction underlies the technical possibilities and the meticulous planning of formwork systems. As a casting mould and negative form, the formwork is the forthright image of the thereinafter concrete surface. Consequently, the desired surface quality of the exposed concrete, and concrete with aesthetic functions, influences the planning and manufacturing of the form, and is a cost determining factor accountable by regulated quality classifications.

Nowadays remarkable structures are viable in concrete, however the factor formwork has a major impact on the cost of the structural work, see [Gru09, 7]. As described by *Johnston* in [Naw08, 7.3], the impact of formwork on total cost of concrete structures can account up to 60 %.

Additional to aesthetic demands, the formwork requires a high stability to withstand impacts from the construction. Beside the self weight of the envisaged concrete object to be cast, and outer impacts like scaffolds and wind, the hydrostatic pressure of the ready mixed concrete is a major impact to deal with. The magnitude is dependent on the casting height and the configuration of the liquid concrete. The consistency, use of admixtures, shape and sizes of grains, but also concreting temperatures, have an influence to the density of the concrete. As a rule of thumb, the hydrostatic pressure results to $25-26\,\text{kN/m}^2$ per 1 m casting height. The impact on the formwork is even more intensified by the compact-ing process, where dynamic forces from the vibrating devices are added to the pressure impact. However, the ultimate strength of the structural formwork elements has to be de-signed. Furthermore, the deformations have to be limited, since formwork faces tend to bulge.

An important and design driving aspect of double curved formwork systems, is the preciseness of the concrete face achieved. The limited tolerances, defined in the building codes (refer to the graphs in fig. 4.7, showing the allowed deviations depending on the element sizes), are often not met for many freeform formwork techniques. This fact is one
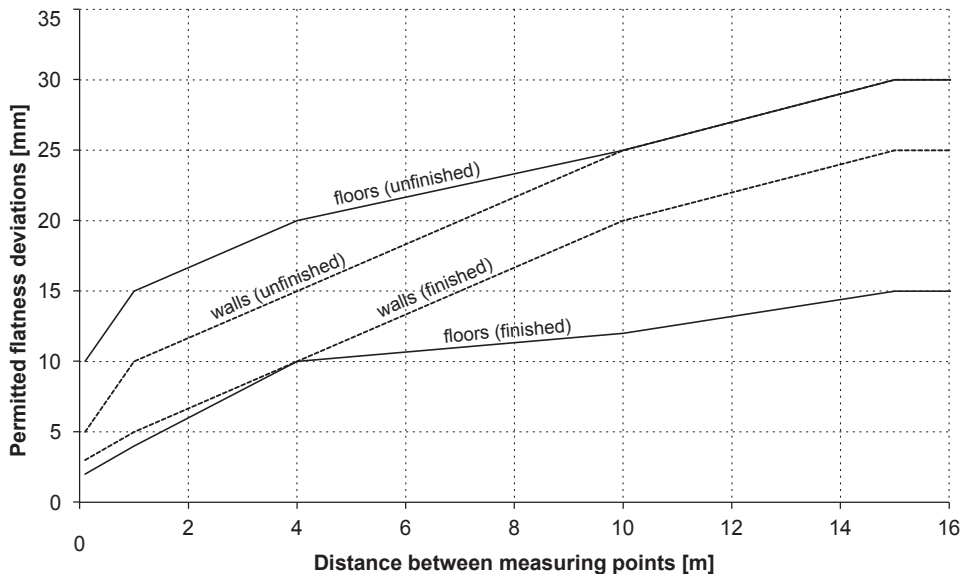
Figure 4.7 Acceptable tolerances in building construction defined by the building codes [DIN05, tab. 3]

reason for a large existing research field.

For many decades, the manufacturing of concrete formwork was in the field of duty of carpenters, a labor intensive practice, with high cost of material. The destructive time of the Second World War led to an intense reconstruction of the built environment, with great demands for providing accommodation. The building industry was exposed to tremendous tasks, complicated by the shortage of construction materials. Formwork structures occasionally were built with waste wood, old furniture or door leafs. In Ulm, Germany, as described by *Grupp* in [Gru09, 8], the young trainee *Fritz Leonhardt* (1909–1999), who later became an international formative engineer, implemented his idea to string scaffoldings with meshes to save wooden planks. Emphasized by increasing pricing pressure and rising labour fees, the development of more rational solutions and reusable system-formwork began.

plane formwork

single / double curved formwork
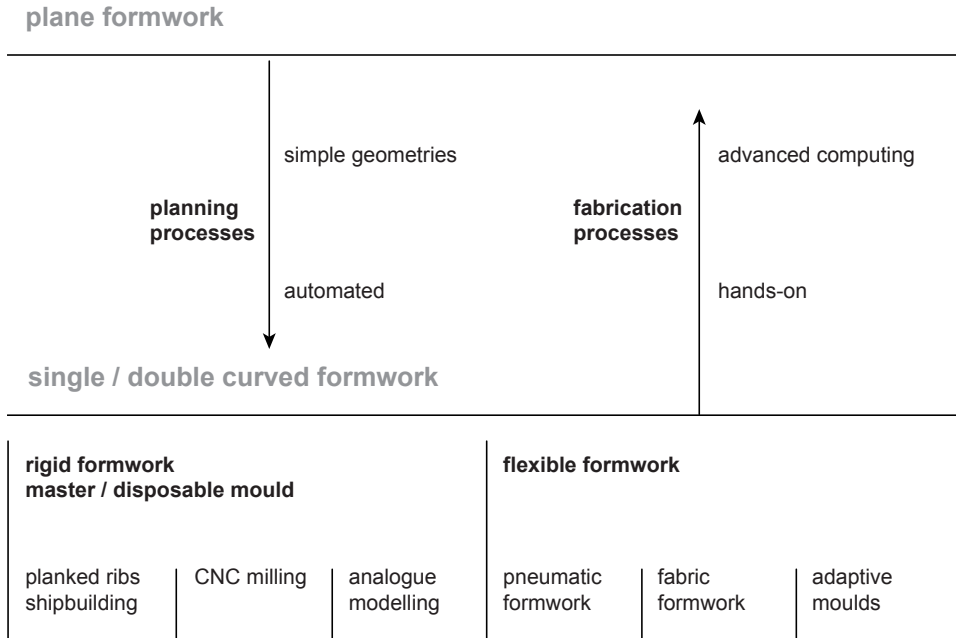
Figure 4.8   Overview of formwork techniques with single and double curved surfaces

4.2.2 Plane formwork faces

From the 1950s, panel and girder formwork, table forms as well as sliding and jacking formwork found their way into standardized construction procedures. The collateral development of prefabricated concrete elements, even allowed constructions independent from seasons, under labor friendly workshop conditions, with optimized in situ construction times for geometrical and straight lined concrete structures. As described by *Kind-Barkauskas* in [KBKPB02, 39], tower blocks of concrete elements rapidly became widely spread especially in the eastern blocs.

4.2.3 Single- and double curved formwork faces

The intense development of 3D software tools and computer capacities opened up possibilities to comprehend complex geometries and corresponding inter-dependencies from the architectural and structural point of view. Constraints, caused by geometry representation

Figure 4.9 Wooden formwork elements used for the double curved concrete shell of the *EPFL Rolex Learning Center* in Lausanne by *SANAA*, ©*B+G*

and unsolvable analysis problems, are repealed. Now the limitations are in the fabrication and implementation of freeform structures.

As opposed to planning processes, where complex shapes are generated with engineered software developments, the fabrication seems to be even more 'hands-on', the more sophisticated the shape becomes, whereas the fabrication of plane formwork is widely automated, as illustrated in the flow chart of fig. 4.8.

Production achievements of free form structures drag far behind computing developments. Until recently, freeform architecture, as described by *Schipper* et al. [SV10], originated in academic context or buildings with high budgets, designed by renowned architects.

Double curved formwork can be separated in rigid techniques, used for master moulds or disposable formwork, and the field of flexible and adaptive formwork systems (fig. 4.8). The latter in particular is the focus of many ongoing research efforts. Internationally, scientists try to develop techniques for reusable formwork systems, with diverse foci on manifold aspects, like environmental and economic acceptability, accuracy and level of geometric complexity.

4.2.4 Master moulds and disposable formwork

4.2.4.1 Planked ribs – shipbuilding

The most conventional production method of concrete formwork is the wooden formwork which is still the key aspect in the education of skilled concrete workers. The concrete facing panels, chosen according to the wanted concrete texture and quality, are fixed on a

structural substructure made of construction timber, scaffoldings or a combination of both. The building industry has developed manifold reusable systems, which are user-friendly and capable of being integrated in the planing process. However, the principle remains unchanged.

There are also various examples for curved concrete faces, produced with wooden formwork. Single curved formwork by now is even manifested in construction systems.

The fabrication of double curved concrete faces is often geared to the classic shipbuilding, where shape giving ribs serve as the substructures which are planked with the concrete facing panels. The substructure, integrated in the digital planning process, can be transferred in an automated production.

Beside wooden substructures, there are also attempts to use corrugated paper, as described by *Pawlofsky* [Sau08], who utilized the advantages of paper honeycomb structures. This low cost material can be folded apart and has a high stabilizing capacity in longitudinal direction.

The producibility of multi axial curvatures is highly dependent on the complexity of the desired geometry and the corresponding magnitude of radii. The thinner the formwork panels, the smaller the radii achieved by simultaneously rising demands to the substructure. With large curvature radii, as this is the case of the concrete shell structures of *EPFL Rolex Learning Center* in Lausanne by *Sanaa*, the curvature can be obtained by distorting the concrete facing panels, as shown in fig. 4.9.

A special case in conventional formwork construction, is the hyperbolic paraboloid, a geometry derived by straight lines. The formwork of the restaurant *Los Manantiales* built in 1958 in Mexico by *Félix Candela* (p. 24), could be manufactured by unbent wooden planks.

4.2.4.2 Digital controlled milling

For complex geometries with surfaces impossible to be realized with panels, milled formwork blocks can be utilized. This cost-intensive method generally is reserved for prestige building projects.

Computerized numerical control (CNC) technologies allow a digital transfer of geometrical information from design to production. In consequence, very low discrepancies can be obtained.

Almost solely limited by the construction of milling cutters available, any shape, including

(a) CNC-milling procedure, formwork of *Möbius-ban(k)d*, University of Kassel

(b) In situ concrete roof, extension of *Städel Museum*, Frankfurt by *Schneider + Schumacher*, ©*B+G*
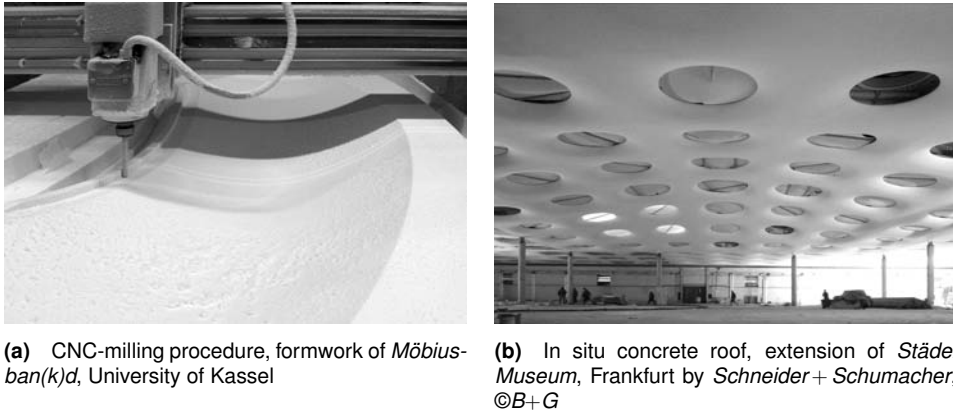
Figure 4.10 Foam formwork for double faced concrete surfaces fabricated with a subtractive (CNC-milling) method

edges and ridges, regardless of its complexity, can be realized, as long as the form has no undercuts restraining the stripping.

Typically polyurethane (PU) and polystyrene (PS) is used as basis material for milled formwork blocks. The lightweight foam is easy to handle in terms of fabrication, transportation and placing on site. Furthermore, it enables a quick and low-wearing milling progress.

A disadvantage from the fabrication point of view, is an elaborate surface treatment with lacquer or epoxy layers, since a casting directly on the milled foam surface is not possible due to the bonding. A further drawback is the environmental pollution. One part of the foam blocks is preliminary pulverized waste from the subtractive fabrication method. The remaining part is disposed of after casting. Although a multiple use is possible (depending on the coating), a one-way use is the usual practice, since the building industry is dominated by the realization of prototypes.

The formwork of the organic shaped concrete roof of the extension hall of *Städel Museum* in Frankfurt (fig. 4.10), is built with milled form blocks that have been used fourfold because of the double symmetry of the roof layout.

An innovative research project of the *Institute of Structural Design* (ITE) of the *Technical University of Braunschweig*, as described by *Mainka* et al. in [MKH14], is elaborating an environmentally friendly procedure of milling formwork with wax as basis material, that does not underlie a material mix, since no further coating is necessary and it is reusable by

simple melting.

As proposed by the author, the concept of wax formwork can also be applied as an additive 3D printing procedure that still needs to be investigated. Disadvantageous however, is the rather heavy weight of wax-formwork, affecting transportation and supporting efforts on site. Furthermore, the reshaping to a reusable wax block, requires again an energy input.

Research attempts of the *Institute of Building Structures and Structural Design* (itke) of the *University of Stuttgart*, are researching on freeform sandwich composite formwork. Filament windings, made of carbon fiber reinforced plastic (CFRP), are used for both, the lost formwork and the tensile reinforcement of the concrete. As described by *Waimer* et al. in [WK15], the shape is defined by a reusable winding core. Although this technique is promising as material based utilization, a drawback is the geometrical limitation to closed cross sections and synclastic components.

4.2.4.3 Analog shape modelling

A classical form generation of double- and multi-curved shapes of concrete surfaces, is an analog shaping, which is still state of the art, depending on the projects boundary conditions. Analog procedures are often hands-on and usually have a break between the planning and the fabrication processes. Especially in freeform construction, the deviations between desired and actual values are difficult to control. However, there are applications where geometrical lapses can be accepted.

The analog shaping of the negative mould can be differentiated from the direct modelling of the positive concrete object.

Conventional double curved formwork constructions, made of bent timber planks, as applied for many shell structures, realized in the middle of the 20th century, can be added to the analog modelling technique. Well known examples are the *National Congress* in Brasilia (fig. 4.11a), built in 1960 by *Oscar Niemeyer* and concrete shell structures conceived by *Heinz Isler* in Switzerland like the *Service area Deitingen* (p. 15), built in 1968. Analog formwork shapes can also be fabricated, applying principles of bell construction from the middle age.

A built example of a double-curved freeform shell is the *Teshima Art Museum* by *Ryue Nishizawa* and *Rai Naito*, as shown in fig. 4.11c, located on Teshima Island in Japan, opened in 2010. In analogy to dig-and-cast construction methods, an earthen formwork was molded as a form-giving negative.

The reinforcement was laid out, following the curved surface of the shell, and white concrete was poured in one step within twenty-two hours. Seven weeks after concreting, the

(a) *National Congress*, Brasilia by *Oscar Niemeyer*; built with formwork made of wooden planks.

(b) Hand-shaped concrete surface of skatepark *concrete jungle*, Frankfurt by *sinai*

(c) *Teshima Art Museum*, Japan by *Ryue Nishizawa* and *Rai Naito*; concrete shell cast on earthen formwork. Photo: *Iwan Baan*

Figure 4.11 Analog geometry shaping of the formwork- and concrete surfaces

soil below the shell was scraped out with heavy equipment and conveyor belts [JA+13]. The seamless shell of the open gallery space stretches over 40×60 m with a shell thickness of 25 cm. No further structural elements, like columns and edge beams, framing two elliptical openings, are disturbing the organic appearance [Ray10]. With a museum, opened to light, air and rain, the architects materialize their goal, to "*generate a fusion of the environment, art and architecture [...]*" [Jod12, 304].

An example of the above mentioned direct modelling of the positive concrete object, is the freeform concrete ground of the skatepark *Concrete Jungle* in Frankfurt, designed by *sinai*, shown in fig. 4.11b. Beside geometrical demands from the sport, skating bowls need highly smooth surfaces, since the small skateboard wheels react to smallest irregularities. The limitation of crack widths and avoidance of uneven settlements are major issues.
The concrete bowl in Frankfurt, opened to the public in 2012, is entirely realized with in-situ concrete for flat areas and shot concrete for steeper parts, and it has no expansion joints throughout the whole structure.
Reinforcement bars are placed on a subbase of blinding concrete, before the concrete is placed. The basic shape is achieved with gauges and rulers, whereas the final planing is done by hand with truing devices. This procedure of preparing concrete surfaces is fully handcrafted, requiring skills and experience of the concrete craftsperson.

4.2.5 Flexible and adaptive formwork

4.2.5.1 Pneumatic supported formwork

Pneumatic supported formwork techniques allow the realization of double curved concrete structures with lightweight-, and sometimes reusable substructures, that are commonly inflated with air as stabilizing medium. The thin and flexible membrane is utilized by tensile stresses only and builds a closed envelope under internal pressure. The such prestressed membrane adopts a specific form, see [Sob87, 7].
Although this technique has the advantage of a very low material input and a quick installation on site, the market remains a niche in building industry. There is a minor interest in research activities and only a few architects and engineers are applying this technology. The reason may be the low capability in form finding, the limitation in usability of the mostly circular arrangements and impreciseness in construction. As *Werner Sobek* states in [Sob90], the wide spectrum of possible shapes in pneumatic formwork is unutilized although there is the technology to realize free and 'ideal' shell structures for reasonable building costs. *Martin Bechthold* indicates that membrane-formed shells are starting on

the ground- and not on higher levels. This 'ground-hugging' is partly resulting from a lack of interest in pneumatic formwork, see [Bec08, 151].

The shapes mostly are partly rotationally symmetric such as cylinders and sphere segments. With additional shaped elements, the form can be manipulated and deformed, notches and ridges can be achieved with ropes, see [Sob87, 22,33]. The shapes of inflated structures have obvious similarities with shapes aspired for compression only shells as the ideal use to full capacity of concrete. However, the force vector of air pressure is orthogonal to the membrane, whereas the self weight follows the gravity direction, a fact that restricts this formwork technique as a form finding method.

The beginning of pneumatic formwork is presumably the pipeline construction in Italy in the 1930s. Vulcanized, air inflated fabric tubes, with an internal pressure of $21 - 35\,\text{kN/m}^2$, have been placed on a concrete subbase and fixed against uplift, before concreting the upper layer.

At the same time, *Wallace Neff* from California pioneered the use of inflatable domes as a formwork system for bubble houses, made of concrete. As a solution to the housing crisis in the 1940s, he presented the technique as a low cost and quickly erected construction technique, but also emphasized its aesthetic appeal and applied for a patent in 1941, see [VWB11, 170]. Since then, more than 1200 shells have been built after his invention [Sob87, 9].

Pneumatic formwork consists of tailored and welded prefabricated panels. On site the membrane has to be fastened and tightly sealed to the ground slab since the air-inflated structure tends to uplift. The reinforcement is placed onto the formwork with the difficulty of the smooth and double curved surface and complicated by the tendency of reinforcement and spacers deforming or damaging the skin.

The membrane of the formwork usually is a PVC coated fabric of polyester fibers, with a thickness of $1,2\,\text{mm}$ and a weight of $1,2\,\text{kg/m}^2$. Also rubber coatings find their application, but need to be multilayered for the same strength, resulting in a bigger weight. Both fabrics are non-sensitive for alkaline settings of concrete and are easy to separate after hardening. The smooth surface of the membrane leads to a smooth surface of the concrete. The supporting medium usually is air. Even large shells are inflated within a few hours, with speed-regulated fans. The internal pressure is neatly controlled; hermetically sealed formworks cannot be implemented. Pressure changes from concrete hydration and solar radiation lead to volume changes and form deformations that led to damages, especially at the beginning of the use of this technology, see [Sob90, 71].
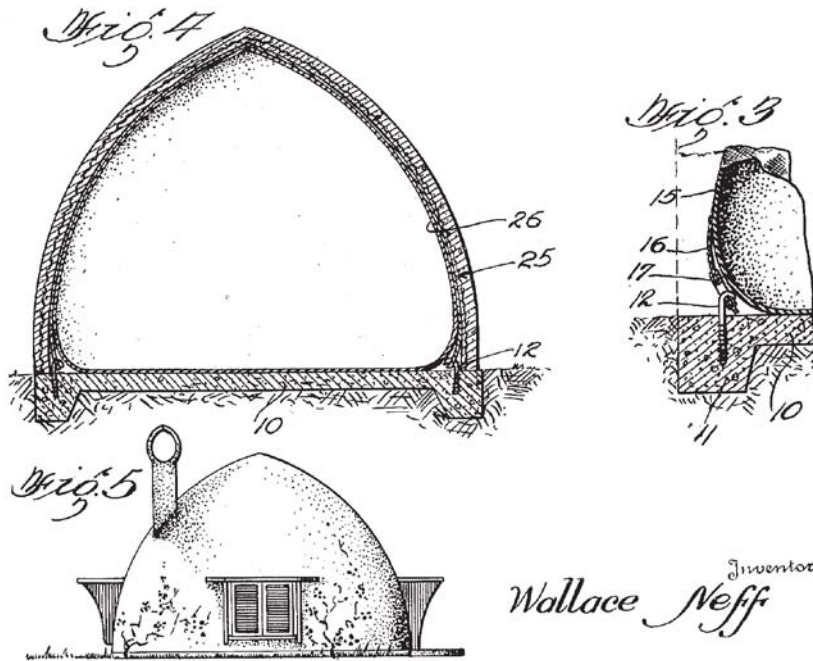
Figure 4.12 Sketches of pneumatically formed concrete shell taken from patent specification 1942 by *Wallace Neff*

Pneumatic prestressed membranes are appropriate structures for evenly distributed loads, with increasing capability when outer load vectors are converging with the direction of the internal pressure, acting on the membrane, utilizing compressed air as supporting medium. On the contrary, uneven distributed loads from the casting process and other local impacts like wind, cause comparable large deformations. The counteracting by raising the internal air pressure is a convenient action, already undertaken by *Neff*, when unwanted cracks and damages in his first domes occurred, accounted to an undersized internal air pressure, see [Sob87, 9]. It is a characteristic of the strength development of green concrete[2] that the strain to rupture reduces with increasing strength. When it approximates a minimum point, the concrete strength is still relatively low, also referred to as the critical phase.

There have been different approaches to reduce the deformation of the formwork during

---

[2]Green concrete is fresh concrete, already placed in situ, during its hardening process

the critical phase of the concrete, since the sole increase of internal pressure is limited, due to increasing membrane stresses and uplift forces at the foundation. The layer-wise spraying of the concrete is an early developed solution, leading to a successive stiffening of the formwork with successive increase of concrete self weight.

In 1965 *Dante Bini*, an Italian engineer, developed a distinguished method on the basis of pneumatic formwork. In addition to previous procedures, a second membrane is fixed on the concrete layer, which is cast in the flat state on the ground. The folded membrane, including the green concrete is lifted while inflating the membrane and concrete compaction is done with external vibrators. *Bini* developed a special reinforcement technique with elongating reinforcement bars, placed in steel spirals, to assure an all-over reinforcement of the concrete shell. From 1970–1990, about 1600 Binishells have been built, the largest one with a diameter of 100 m and a shell thickness of 20 cm in Australia in 1976, see [Zim07, 23].

There are techniques to stiffen the formwork itself, to minimize deformation impacts. The application of foaming synthetics from the inside (also the outside), is one approach for a pre-stiffening of the inflated membrane before concreting. The foam, combined with the membrane, has a stiffness-, insulation- and water-proofing function. Special hangers can be inserted within the foam, to hold the reinforcement network, before the concrete is sprayed on. Predominantly common in the US, shells with spanning lengths up to 105 m have been realized with this method. Short construction times are possible, with mainly indoor labour work, see [Sob90, 74].

Further methods to stiffen the membrane are utilizing the stiffness of the reinforcement and the imposing of bigger curvatures, with the help of cables nets, as investigated by *Jörg Schlaich*, *Fritz Bacher* and *Werner Sobek* in 1985 [Sob90, 72], for the construction of a rainwater overflow basin.

More recent investigations of pneumatically formed concrete grid shells, by *Gregor Zimmermann*, *University of Kassel* in 2007, integrate automated cutting- and welding techniques, as well as high performance fiber reinforced concrete (UHPFRC) technologies, with the technology of air supported membrane formwork. Two membrane layers are connected at predefined seam lines, creating a grid of interconnected tubes, which are inflated to achieve the global shape desired. Beginning at the bottom of the structure, the fiber concrete is pumped up to the top, and the air pressure is released after hardening of the concrete. Due to the fibers, no further reinforcement is needed and the membrane can remain as surface layer, see [Zim07, 242–243].

Johann Kollegger and *Benjamin Kromoser* from the *TU Vienna* invented a method of 'Pneumatic Forming of Hardened Concrete', also known as 'Pneumatic Wedge Method'.

Figure 4.13 Pneumatic forming of hardened concrete ©*TU Vienna*

Figure 4.14 Concrete canvas shelters [Con12]. Photo: *Concrete Canvas Ltd.*

The idea behind this construction technology is to build free form concrete shells, by casting the unwound surface as a plate on the planar membrane. After lifting the formwork, the final shape is fixed with additional post-tensioning cables and joints between the elements are filled with grout [KK15]. Similar to approaches by *Bini*, this method also avoids unwanted deformations of the membrane, damaging the concrete in its critical phase of strength development. A prototype of a 11×18 m free form shell, see fig. 4.13, was built in Vienna in 2014.

An advancement for the construction of deployable emergency shelter was developed by the British company *Concrete Canvas Ltd.*. These concrete shells are build of cement based composite fabrics, a similar practice to plaster bandages. On site, the pre-tailored and impregnated fabrics are unfolded, inflated and sprinkled with water to activate the hydration process. The shelters, as shown in fig. 4.14, are developed by two craftsperson in less than one hour and ready for occupancy within 24 hours.

4.2.5.2 Fabric formwork

Analog to the 'pneumatic supported formwork' described above, the whole topic on 'fabric formwork' is also based on the membrane action of the flexible formwork material. The shape is defined from a pneumatically prestressed membrane, with a shape giving tailoring. The difference of the two typologies is that the pneumatic pressure in 'fabric formwork' is generated by the concrete itself (from inside) and not from the supporting air. As *Diederik Veenendaal*, *Mark West* and *Philippe Block* state in [VWB11], the terminology 'fabric formwork' can be defined as "...*a formwork that uses a flexible membrane*

for the structural support of fresh concrete or rammed earth".

The technology is often marked as 'low-tech-production', based on the low material and labour input. Consequently, it is used amongst others in crisis regions. However, fabric formwork is also applied from an architectural background. Beside pillow-like shapes, diverse surface textures and excellent finishes with no air bubbles can be generated, depending on the permeability of the fabric. The textiles are economic, lightweight and reusable. That leads to benefits in material input, transport, storage and manufacturing. The main feature and restriction for all concrete surfaces, built with fabric formwork, is a convex bulging. Naturally, the freeform architecture is limited with this procedure. Furthermore, the prediction of the final shape and the corresponding translation to a membrane tailoring of the formwork, is very challenging, amplified by the massive self-weight of the fresh concrete. The prediction is highly dependent on the characteristics of the membrane but also on the consistence and compaction procedure of the concrete and the gradient of hydrostatic pressure over the height of the concrete element to be cast. Current research efforts are about shape determination, to emphasize applications in the building industry.

First approaches in the use of fabric formwork can be credited to *Gustav Lilienthal* (1849–1933), a German builder and architect, whose work took place after the Industrial Revolution in the late 18th- and the beginning of the 19th century. He invented a fabric-formed suspended floors system, patented in 1899. An impermeable layer of textile fabrics was placed on top of parallel wooden beams as a formwork system, before the concrete is cast [VWB11, 165]. A further key development was undertaken by the Irish engineer *James Hardress de Warenne Waller*, practising in Dublin, who transferred the technology of *Lilienthal* into spacial applications. Inspired by the ruins of the *Taq-e Kisra*-arch of the ancient city of Ctesiphon, he developed an innovative method to build concrete arch structures following catenary shaped cross sections, using fabric formwork, supported by reusable falsework. The Ctesiphon systems, initially without reinforcement for spans up to 12 m, was modified to reinforced systems, spanning up to 150 m. This specific system, with suspended fabrics from prefabricated trusses, was patented in 1955 [VWB11, 166]. The advancement of *Waller* in concrete shell construction and manufacturing has influenced architects and engineers during the 20th century, amongst others *Félix Candela*, who adopted his system in the first of his numerous works [Cia12].

The Spanish architect *Miguel Fisac* (1913–2006) pushed the technology of fabric formwork beyond the economic and construction efficient approaches. Constituting the aesthetic appearance of the texture of fabric formwork, he designed facade elements in 1969, for the *Centro de Rehabilitación para la MUPAG* in Madrid, using a formwork of polyethy-

lene lamina, hanging from a rigid substructure, see [VWB11, 167]. Hereupon a creation of a variety of new facade panel types followed.

Recent developments in architectural applications have been investigated by *Kenzo Unno* and *Mark West* from the 1990s, both working independently. *Unno*, a Japanese architect based in Tokyo, worked on fabric formwork systems for load-bearing walls. His concern, inspired by an earthquake in 1995, was to provide simple methods of construction, to enable people to build their own houses. He developed two basic methods of counteracting the loading of wet concrete. The 'frame method' subdivides the formwork membrane by outer linear frame elements as restraints, whereas the 'quilt-point method' is based on the fixation of the formwork membrane on the reinforcement in a defined pattern of quilt points [Wes08].

Mark West, founding director of the *Centre for Architectural Structures and Technology* (C.A.S.T), of the *University on Manitoba* in Canada, is an architect with a background as a builder. The research field of C.A.S.T[3] is construction culture, with fine art methods and architectural and engineering thinking. A large number of fabric formed concrete shapes, as column forms, walls, slabs, beams and shells have been investigated. The innovative fabrication of continuous beams, formed by rectangular and un-tailored sheets of fabric, are shaped bending-moment-orientated, saving 30 % of concrete (and thus self-weight) and 40 % of steel with unchanged structural performance. The restraint by *West*, to omit tailoring, makes the method applicable for everyone. Experiments with 'pull-buckles' and 'push-buckles' led to a material-based form-generation, providing structural efficiency. The corrugations arising by prestressing the fabrics of inverted hanging forms, for funicular compression vaults, provide buckling resistance due to a double curvature. Shapes generated by fabrics, strained in bent frames, can also be kept by spraying glass-fiber reinforced concrete onto the fabric, to achieve master moulds for multiple use.

The *Block Research Group* (BRG) of the *ETH Zurich* are investigating the so far analog and experimental form finding of fabric formwork from a computational point of view, as the reason for an insignificant tradition in building industry is a lack of understanding of this construction method, especially during early design stages [VB12], as well as unsatisfactory tolerances between digital and physical as-built geometries.

A current related research project of BRG is the design of *HiLo*, a two storey penthouse guest apartment as a research and innovation unit for *NEST* in Switzerland. The concrete roof shell structure is envisaged to be built with a reusable, light-weight, hybrid cable-net and fabric formwork system, allowing the construction of the thin shell roof within ac-

---

[3]C.A.S.T information taken from a lecture of *West* at the *ETH Zurich*, 2011 [Wes11]

Figure 4.15 Prototype of hybrid cable net and fabric formwork. Photo: *Block Research Group, ETH Zurich*

Figure 4.16 Fabric formwork in furniture scale. *Ambiguous Chair* by *Anne-Mette Manelius*. Photo: *Anne-Mette Manelius*

ceptable tolerances. The falsework for the fabric shuttering is created by a frame along the boundaries only, where the cable-net with the fabric on top is fixed. The falsework is heavily reduced and the access underneath remains undisturbed. With a predefined pre-tensioning, considering the load of the fresh concrete, particular anticlastic shapes can be obtained and constructed. Prototypes under laboratory conditions, refer to fig. 4.15, where the geometry deformations and spring forces are controlled, have been built with satisfactory tolerances, see [VBNB14]. In [Blo16], *Philippe Block* uses the term 'supercharging shell', meaning the reduction of energy use by implementing heating, cooling and insulation to the shell, as well as a thin-film of photovoltaic cells.

An interesting approach of the application of fabric formwork in furniture scale is the *Ambiguous Chair* by *Anne-Mette Manelius*, from the *Royal Danish Academy of Fine Arts* in Copenhagen, as shown in fig. 4.16.

4.2.5.3 Adaptive mould systems

Several research efforts are investigating the possibilities of flexible formwork as adaptive systems. The aim is to find an ideally digital controlled, free formable surface, that allows the exact production of complex shapes, fulfilling requirements from concreting, like tightness and sufficient stability, to withstand forces from concrete self-weight, hydrostatic pressure and compacting impacts.

The principal idea was formulated by *Renzo Piano* in the 1960s. His idea was a machine,

(a) Definition of double curved shape of sails with actuators

(b) Lamination process of the sail hydrofoil

Figure 4.17 Manufacturing of high performance sails with the technology of adaptive formwork. Photos: Images courtesy of *North Sails ©Outside Images*

where an architectural scale model is placed inside. The height of a point-network is then determined and electronically transferred to an up-scaled system of vertical pistons. The system enlarges the digital model a number of times and informs each piston with the corresponding height, see [dH08, 69]. Unfortunately the system has never been applied.

However, the principle remains unchanged for the application of adaptive formwork, with the description of the shape, with digitally informed and mechanically extendable pistons. This shape derivation can be described as 2½ D, a network of points in the field of x- and y-coordinates, each with a specific z-value. Still there are complex boundaries for the head points of the actuators. Not only the high and low points need to be precisely translated, but also the tangential angle of the desired surface, especially at the boundaries.

An industrial application of the adaptive formwork principle, was developed by the US sail manufacturer *North Sails*, for the production of high performance custom sails. The requirements to sail-shapes are similar to those of hydrofoils. The digital, double-curved shape, derived from computational fluid dynamics, is transferred to pneumatic actuators, spanning a system of longitudinal slats with a neoprene skin, describing the basic shape of the sail. The application of this system is shown in fig. 4.17. The technology for the sail manufacturing is possible, because of the low self weight of the sails in combination with large radii and thus small curvatures. Furthermore, no borders have to be implemented.

In concrete formwork construction, the distance between the pistons or actuators can vary up to zero. A skin on top of the actuators, describing the contact area of the concrete,

Figure 4.18 *Multihalle* in Mannheim 1975 by *Frei Otto*. A network of wooden strips has been pushed into shape and locked at the intersections
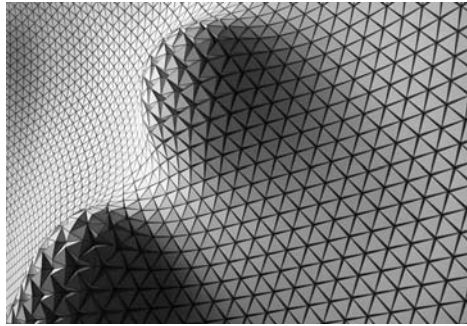
Figure 4.19 Adaptive folding structures are able to create rigid origami surfaces ©*Thomas Diewald*

interpolates the shape between the head points. The system of the actuators and the intermediating skin, needs to be well balanced and fine tuned. A too stiff layer interpolating the shape between the defined head points will lead to difficulties in adjusting the formwork into the desired curvature, whereas a layer with insufficient stiffness will deflect too much, especially when loaded with fresh concrete. Thus the choice of stiffness is dependent on both, the curvature, as well as the concreting load (shell thickness).

Most starting points of adaptive formwork in research applications, are found in the intermediate and shape-interpolating layer. Not only the required elasticity for the definition of the shape is conflicting with the required stiffness to withstand casting loads. A further limiting fact is the desired ability to change length in membrane direction (stretching), see [SJ11a, 7], since a double curvature cannot be generated by a plane surface. The research team around *Vollers* and *Rietbergen* from *TU Delft* recognized the proper choice of elasticity as a crucial factor to success, see [SJ11b]. The team of *Roel Schipper*, also from *TU Delft*, is investigating this layer analytically. The team of *Ulrich Knaack* from *TU Darmstadt* works with perforations of the concreting surface, to allow an in plane deformation.

A starting point of the author is based on the consideration that an adaptive form should be easy to arrange, before the shape is finally locked for the casting process, when the stiffness is required. A system like this is similar to the well known *Multihalle* in Mannheim, as shown in fig. 4.18, designed by *Frei Otto* for the German Federal Garden Show in 1975. A network of wooden strips has been arranged as a plane system on the ground, prior to forcing them into shape, by pushing them together. The final stiffness is given by the

post-locking at the points of intersection as well as by the enveloping membrane. This post-shape locking would not conflict with an unwanted stiffness.

Later ideas to build double curved rigid surfaces that can be informed by actuator systems, like fish scales and roofing shingles, have been further analysed by the *Department of Structural Design* of the *University of Kassel*. One approach is the 'Rigid Origami Tessellation', see [War15], shown in fig. 4.19, based on a triangulated pattern of a folded plane system, developed by *Ron Resch* in the 1990s. This system allows the creation of double curved surfaces that can be supported by pistons.

It may be noticed by the author, that a common unsolved issue of any kind of adaptive formwork is the realization of edges. Also the implementation of a closed formwork with a top layer is problematic. Most applications of adaptive formwork, even commercially supplied, as by the Danish company *ADAPA*, use the technique to cast the concrete, and to manipulate the desired shape afterwards.

4.3 Connection methods in concrete construction

4.3.1 Joining principals

Independently from the sole consideration of concrete constructions, the interconnection of elements to a technical formation can be categorized according their physical mechanisms. Solid state bodies have six degrees of freedom, three translational and three rotational, describing the mechanical connection to an adjacent element. Connections joints are restricting at least one movement of two or more connecting partners.

Figure 4.20 illustrates the separation of connection methods according the action principles in 'frictional bonding', 'adhesive bonding' and 'interlocking bonding'.

Connections can be reversible and irreversible, restricting a nondestructive disassembly. Examples of reversible connections are screwing, clamping and interlocking, whereas welding, gluing or grouting are valid as irreversible connections.

Frictional bonding   'Frictional bonding' or 'force fit' describes the connection of two adjacent partner elements, with a compression force, acting on the contact areas. The compression of the elements, which can be obtained by prestressed screws, leads to a frictional bonding. This bonding is kept, as long the friction is greater than the load transferred by the joint. Unwanted unwinding of screws is also restricted by frictional bonding, as well as the force transition of breaking and acceleration forces of wheels to the ground. The connection of knots in ropes is also given by frictional bonding.

Usually force fit-connections are reversible, as long as the frictional forces can be released like unscrewing. The use of rivets in steel constructions is such a connection, which is not possible to release.

Adhesive bonding   'Adhesive bonding' or 'molecular fit' describes a connection which is generally not reversible without destruction, since the connection partners are joined via a molecular bonding, gained by welding, vulcanisation or gluing. Also the grouting of two prefabricated concrete elements within the joint can be described as adhesive bonding.

Interlocking bonding   'Interlocking bonding' or 'form fit' describes the blocking of a movement in a distinct direction (one or more) of an element, given by the connecting partner. Under loading, the contact areas are under compression. If oppositional surfaces are existent, the movement in counter-direction is blocked as well. This means that for restricting degrees of freedom in transversal directions x, y and z, the movements in the

Connection methods of building elements in mechanics

frictional bonding	**adhesive bonding**	**interlocking bonding**
utilization of friction of connecting partner	welding, glueing, grouting non-dismountable	movement blocking of connecting partners

'force fit'   'molecular fit'   'form fit'
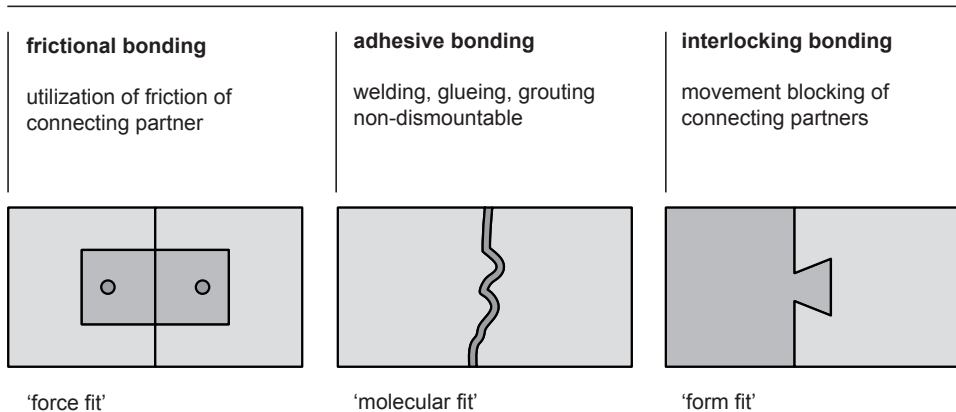
Figure 4.20   Diagrams of jointing techniques as connection methods

counter-directions $-x, -y$ and $-z$, have to be considered.

The connection of two plates with (non-prestressed) bolts, orthogonal to the load vector, is an interlocking bonding. Also *Gerber*-hinges or 'dovetail joints' in timber construction. 'Interlocking bonding' is generally reversible, as long as geometrical boundary conditions allow a disassembly.

4.3.2 Joining concrete elements

The problem of joining concrete elements usually arises for prefabricated elements. In system building construction, the benefits are on the site progress. The formwork and concrete casting is climate independent under workshop conditions and the required curing times can be scheduled independently from the site sequences, leading to shorter construction durations on site. However, this system excludes monolithic concrete buildings and the decision has to be taken at the beginning of the planning process, since the building has to be assembled from elements of deliverable sizes, and the focus is on the durability and structural feasibility of the joints.

Joints in system building construction   Most common joints in concrete system construction are 'interlocking bonding' connections, when elements are stapled onto each other. As long as the contact area is under compression, the system is stable. Uplift forces are usually not an issue and the inserting of bolts or grouting is for location security only. A combination of 'interlocking bonding' and 'frictional bonding' is given by joining prefabricated elements via prestressing. The entrance bridge to *MuCEM* in Marseille, shown in fig. 4.5 on page 57, has been assembled by UHPC section-elements 'threaded' on the prestressing cables. The prestressing leads to the pressure exceeding the bending tensile stress components. Here an interlocking bonding occurs. At the same time, the pressure gains the friction necessary for the shear transfer – a frictional bonding.

Connections by means of 'adhesive bonding' are mainly realized as grouted joints. A planned gap, located between prefabricated elements, provides a space for tolerances and is filled with concrete after final placing. Within this gap, continuous reinforcement is provided for a non-disruption of the load transfer of tensile forces. The width of the gab is designed according the required embedment length of the reinforcement. Columns and pylons, placed in sleeve foundations, are also tied in with the gap filled after final placement. The filling provides a continuous spacing and the adhesive bonding secures the system against pullout failure. A widespread system in slab construction is done with prefabricated filigree elements replacing the lower formwork, which are placed on site, with the topping cast afterwards.

Concrete gluing   Challenges of concrete gluing is the behaviour of adhesives over the time, one reason why glues are usually not approved in building construction. Furthermore, the capacity of glued connections is limited to the rather low tensile strength capacity of the concrete, directly at the surface. Usually, the location of failure is just next to the joint area. A major backdrop is the non-continuity of reinforcement. For glued connections in zones of tensile- or bending-tensile utilization, a brittle failure behaviour would be the consequence.

Feasible adhesives for the gluing of concrete are either adhesives based on epoxy resins (EP) or mineral compounds of reactive powder (RPC). Investigations, undertaken by the *Technical University of Munich*, showed that epoxy resins are faster hardening, whereas adhesives, based on reactive powder, have a higher strength capacity at the end. These investigations are based on roughening treatments via shot-blasting of the contact surfaces [Müh12, 228]. Further investigations were focused on the achievement of higher ductilities under consideration of the continuous reinforcement, that is also glued in. Short embedment lengths of only three times of the bar diameter lead to sufficient bonding in order

to achieve reinforcement steel failure. Whereas in the solely glued connections proofed to sudden failure, samples with glued reinforcement had a ductile behaviour and a load increase after cracking [Win13, 259].

The *Gärtnerplatzbrücke* in Kassel (fig. 4.4 on page 57) is a pilot project with UHPC construction elements, glued with epoxy resin.

5 Case studies

5.1 Parapluie

The construction and development of *Parapluie* has been published by the author as an article of *Beton- und Stahlbetonbau* [EVG+14a] and as a conference paper of the *International Association for Shell and Spatial Structures*, IASS [EVG+13]. As the winning paper of the 2013 *Tsuboi* Award it is republished in the 2014 IASS journal [EVG+14b].

5.1.1 Activating membrane effects

The construction project of *Parapluie* (French: umbrella) is an executed case study prototype, that verifies the increase of structural performance of shell structures with activated membrane effects.
The global bending load takedown of cantilevering systems is broken down to a reduced form dependent system with a negotiated force flow. The specification of the load paths naturally presumes an appropriate material, satisfying the structural demands and the engineering decoding of the force flow. The translation of forces in tensile and compressive stresses allows the construction of ultra slender concrete shells, where the thickness is derived from the utilization of the material properties.

The membrane system is designed to have a structural analogy to a sheet of paper with an imposed folding, as shown in fig. 5.1. Even though the material thickness compared to the span length is very small, the system is able to carry the self-weight and eventually extra loads. The gained static height from the top- to the bottom fibers shifts the system from an ineffective bending system to a membrane structure with tension stresses in the straight outer edges and compression at the bottom fibers, where the biggest curvature stabilizes the system against buckling [EVG+14b, 205].
Flipping the whole system, and inverting compression and tensile action, leads to an immediate buckling failure at the compressed edges with no curvature.

(a) Folding between fingers activates a structural height
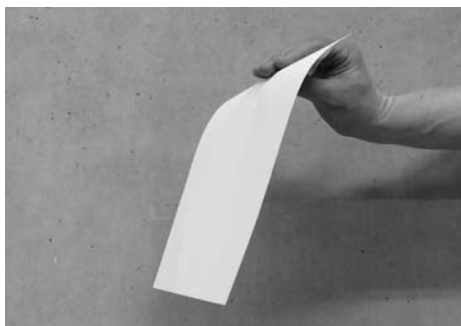
(b) Inverting the system leads to a collapse due to buckling failure at the edges

Figure 5.1 Structural analogy of a sheet of paper. Stability is given by the activation of membrane effects

However, even compression only structures have their boundary conditions that have to be considered in the design. The system of *Parapluie* is an intended hybrid structure, where the ratio of bending as well as tension and compression load transfer is balanced due to the material performance. Material enhancements from stress peaks of the fixing points are solved with a thickness gradient of the shell. A construction of the mounting joints has been developed, fulfilling the structural, architectural and functional demands, like water drainage.

5.1.2 Design intent roof shell

The conceptual assignment is the design of a roofing for a bus stop shelter, coming together with a glass windscreen and a seating construction, accommodating twelve waiting people.

The design is location-independent to enable a serial fabrication. To guarantee an unpretentious delivery and erection process, the aim is a roof shell with an adequate span length constructed as lightweight and thin as possible.

The result is a slender concrete shell, with no embedded steel items, allowing a multiple use of its formwork. It consists of two elements, the free form roof shell and the column with the shape of a hyperbolic paraboloid. The column is inclined, and the intersections of the head and base points are eccentric, that generates a dynamic form and allows a variation and combination of repeated *Parapluies*. The junction between roof and column is

(a) Top view

(b) Perspective view

(c) Side view

(d) Front view
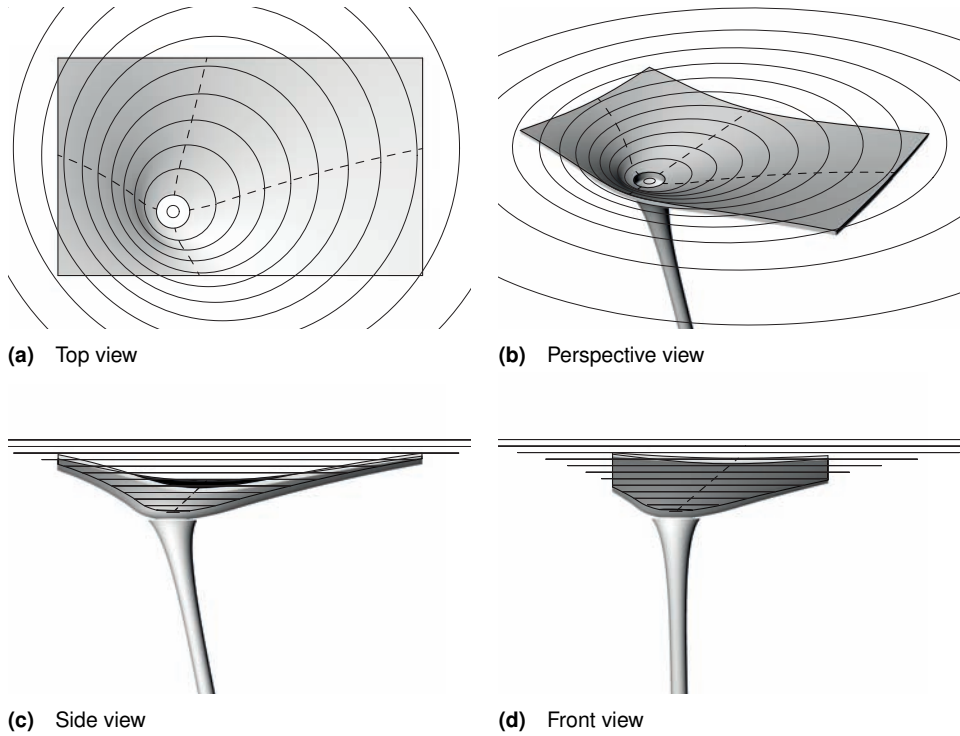
Figure 5.2 Parametric design process. The final shape is derived from an eccentric bowl in space, trimmed to a projected rectangle

the lowest point of the shell, so consequently the drainage is hidden inside the column. See [EVG$^+$14b, 201–202].

The development and realization of a prototype, as shown in appendix A.1, is a joint-venture of the architectural studio *schneider + schumacher*, the structural engineering company *Bollinger + Grohmann* and the material developer *DUCON*.

5.1.3 Schematic design

5.1.3.1 Parametric form finding

The architectural shape of the roof shell initially is derived from a large bowl-like form. A curve, defining the sectional geometry of the bowl, is generated with intersections, serving as boundary points for a number of circles with varying radii. The so achieved rotationally symmetric system is translated horizontally, to deform the shell to an asymmetric shape, intended for the design of *Parapluie*. The outer shape, rectangular in projected footprint, is punched out of the bowl, see [EVG+14b, 202]. The derivation of the shape is shown in fig. 5.2.

5.1.3.2 Structural information in the design process

A form investigation of the shell has been undertaken to optimize the geometry in consideration of architectural and structural demands. It may be noticed by the author, that this non-linear process and the exchange between form and structure, ideally is carried out with the architect and structural engineer working together in front of the same screen.
The parametric shape is modelled with *Grasshopper®* [Rut15], a graphical algorithm editor, integrated within the 3D NURBS modelling software *Rhinoceros* [McN15]. A series of input parameters, like inclination angles of the bowl boundaries, the position of the column and the eccentricity of the shape are released to a defined range. The structural behaviour, in the first instance the global material deformation, is monitored as a live analysis in *karamba* [Pre13], a finite element plug-in of the *Grasshopper* environment.
A further adjuster, next to the median surface model, is the gradient of the shell thickness, derived according to the load bearing capacity of the material; hence the compressive strength of the concrete, the tensile strength (dependent on the reinforcement ratio) and the bending-tensile strength capacity.

5.1.4 Structural system

5.1.4.1 System dimensions

The roof shell has a projected area of $1,70 \times 2,85$ m and a framing edge thickness ≤ 24 mm. The thickness has a gradient from $24 - 55$ mm from the edges to the clamping. The height of the column is $2,90$ m.
The cantilevering shell has a maximum cantilevering distance of $2,29$ m from the center of the clamping point to the furthermost corner. The shell is carrying vertical loads as a

membrane structure, however stress peaks at the column junction lead to local bending impacts, counteracted with a thickness increase at the fixed restraint.

The column, mainly exposed to bending impacts from the eccentric shell, is a composite section with a steel tube core cast in the hyperbolic concrete shape. The steel tube is both, a structural component providing bending strength and drainage pipe.

The footing is a raft foundation, countering the eccentricity of the structure with its self weight.

5.1.4.2 Loads and safety factors

The total self weight of *Parapluie* sums up to $\sim 9,6\,\text{kN}$ (960 kg). The live load considered, is snow impact only. Since a serial production is envisaged, the snow impact zone and the altitude of the building location are not known. During the design process the snow impact was limited to 'zone 2', according Eurocode 1 [Eur03], and the maximum altitude of Munich of about 520 m above sea level.
The characteristic snow load, see [EVG$^+$14b, 210], results to:

$$S_{\text{k}} = \mu \cdot s_{\text{k}} = 0,8 \cdot \left[0,25 + 1,91 \cdot \left(\frac{(520 + 140)}{760} \right)^2 \right] = 1,35\,\text{kN/m}^2$$

The snow load is considered as fully distributed on the roof shell and, on the safe side, on the cantilevering side only. It is mentioned by the author, that this load scenario is very conservative, since a snow block of that magnitude[1] will unlikely be able to accumulate, even partial, on a roof with present dimensions.
The safety factors considered, are $\gamma_G = 1,35$ for permanent loads and $\gamma_Q = 1,5$ for snow loads.

5.1.4.3 Materials

The material used for the roof shell, the most sophisticated element of *Parapluie*, is a micro mesh reinforced concrete, developed by the project collaborator and founder of DUCON. This composite material, as presented in section 4.1.3.3, consists of reinforcement layers, crosswise stapled over the entire shell section. The mesh reinforcement with diameters of $\emptyset = 1,2\,\text{mm}$ and an axial distances of $e = 12,5\,\text{mm}$ is infiltrated with a high performance

---

[1]For normal fresh-fallen snow this correlates with a snow depth of $1,5 - 2,5\,\text{m}$

(a) Qualitative distribution of principal normal stresses, n_1

(b) Qualitative distribution of in-plane bending moments, m_1

(c) Deflection in serviceability limit state $u_g + u_q = 43 \, \text{mm}$

(d) Stress utilization plot in ultimate limit state $\sigma_{v,max,d} = 19 \, \text{N/mm}^2$
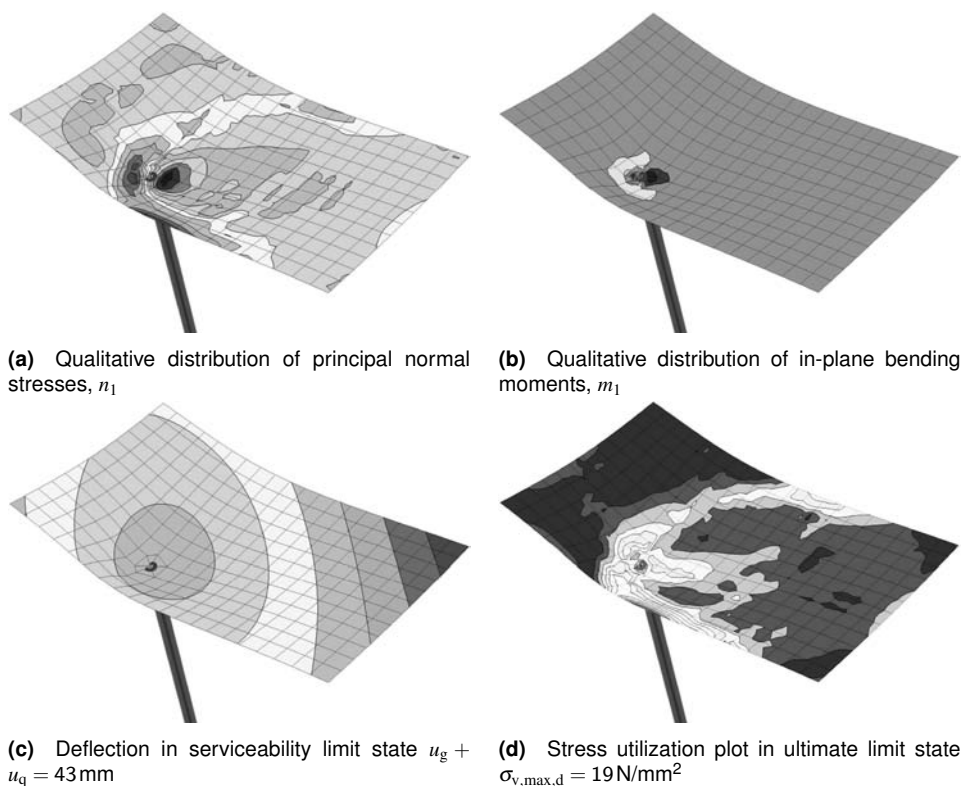
Figure 5.3 Member forces, deflections and shell stresses of *Parapluie*

concrete slurry, see [EVG$^+$14b, 206], with a strength capacity equivalent to C80/95.
The structural steel of the column has the steel grade 'S235JR', with a characteristic yield strength of $f_{y,k} = 235 \, \text{N/mm}^2$.
The raft footing is acting as a mass foundation with no remarkable demands to the strength capacity. The concrete grade C25/30 is chosen.

5.1.4.4 Load bearing behaviour and shell design

The analysis of the structure is taken out with a 3D model, within the structural analysis and design FE software *RFEM©* by *Dlubal Software GmbH* [Dlu15].
The qualitative distribution of axial shell stresses, refer to fig. 5.3a, and the in-pane bending

(a) Structure of the junction shell-column

(b) Structure of the junction column – foundation
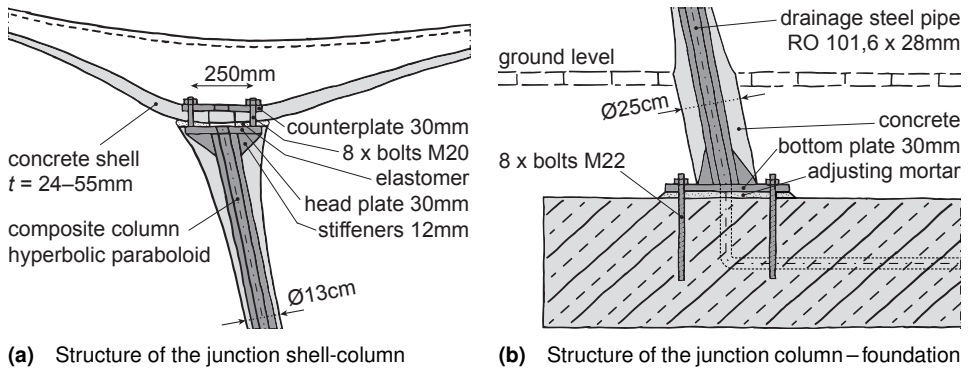
Figure 5.4 Construction details of the mounting joints of *Parapluie* as basis for the construction

moments, as shown in fig. 5.3b, verify the load bearing behaviour as a membrane system. The axial shell stresses are tension at the edges at the side and compression at the center, close to the fixing point, where the biggest curvature of the shell prevents the system from buckling. The in-plane bending moments are almost zero throughout the shell, apart from the intersection area with the column, where shell thickness has its maximum.

Since *Parapluie* is a freeform, with no adjacent structures or cladding, the deflection is of minor interest, but of course monitored. The self weight deformation of 16 mm is pre-cambered, and the possible live load deflection of 27 mm is not perceptible in the serviceability limit state, since the shape of the roof has no horizontal or vertical straight lines.

The steel wire reinforcement of the shell, distributed over the entire cross section, leads to a ductile material behaviour, with a crack allocation of numerous small cracks, well distributed over the length of the respective tension zone. The homogeneous material texture allows by approximation a linear elastic design via principle stress analysis, as shown in fig. 5.3d, see [EVG$^+$14b, 206]. The most utilized edges under tensile stresses are strengthened with extra reinforcement layers, bent around the free layer ends, to create a closed configuration of reinforcement. The maximum allowable design stress at the top and bottom fibers of the shell, according the manufacturer, are limited to $\sigma_{R,d} = 22\,\text{N/mm}^2$.

5.1.4.5 Mounting details

The connection of the column and the shell is a screwed connection, with eight circular arranged screws (fig. 5.4a). The shell has no embedded steel plates cast in the concrete.

The resistance against punching of the topmost counter plate is given be the concrete and the reinforcement only. The dry-fit connection method allows a quick assembly on site, without any curing times.

The foundation is a conventionally cast in situ, see [EVG+14b, 206], with embedded anchor bolts and drainage pipes (fig. 5.4b).

Generally, the contact faces of the prefabricated concrete elements have an interface to avoid stress peaks, an elastomer layer at the column head and a leveling course at the foot point.

5.1.5 Fabrication

5.1.5.1 Production of concrete elements

Concrete is the ideal appropriate material to create free form structures since it is able to transform from the initial fluid state to the solidified. However, the delicate and often cost driving part in the production of concrete free forms, is the formwork. The formwork surface is the mirror image of the exposed concrete and furthermore it has to be able to resist the hydrostatic concrete pressure.

In the project of *Parapluie*, the negative form is built in a subtractive CNC milling process from styrofoam blocks, as shown in fig. 5.5. To allow a multiple application, the contact faces are treated with a grounded FRP layer and a rubber coating. The edge transitions are formed as a tongue and groove interlocking, to guarantee an exact positioning and air tightening for the casting process.

The convex upper part of the formwork is used as a setting jig for the tailoring of the reinforcement layers. The closed and sealed formwork is provided with four exhausting holes, ensuring the inflow of the concrete slurry and the outflow of the air, see [EVG+14b, 209]. The holes are located at extremal points of the shell, to function also as control points, to check whether the formwork is completely filled with concrete.

The formwork of the column is fabricated in the same manner.

5.1.5.2 Installation on site

After an appropriate curing time, the prefabricated concrete elements are stripped and installed on site, to verify quick mounting in an installation situation.

As a fist step, the inclined column is installed and backfilled on the raft foundation. With the help of a crane (the threads for the crane hooks are the only embedded steel items within the shell structure) the roof shell is aligned to the column and the threads of the
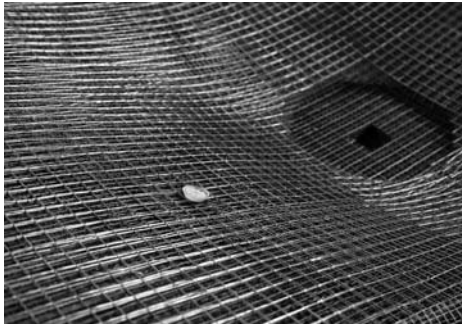
(a) Tailored reinforcement of the roof shell

(b) Airtight closing of upper and lower formwork

(c) Embedded steel pipe with screwed connection at the column head

(d) Composite column prior closing of formwork

Figure 5.5 Fabrication of concrete elements of *Parapluie*

column head are stuck through the respective openings. In the final position, as shown in fig. 5.6, the roof structure is fixed with the steel counter ring and screw end nuts from the top of the shell, see [EVG⁺14a, 58].

5.1.6 Utilization control

As a basis for the building permit of *Parapluie* as a bus stop shelter, the design team is asked to undertake a loading test. The magnitude of the test load is derived from the maximum snow load according to the snow impact zone and altitude limits as well as the safety
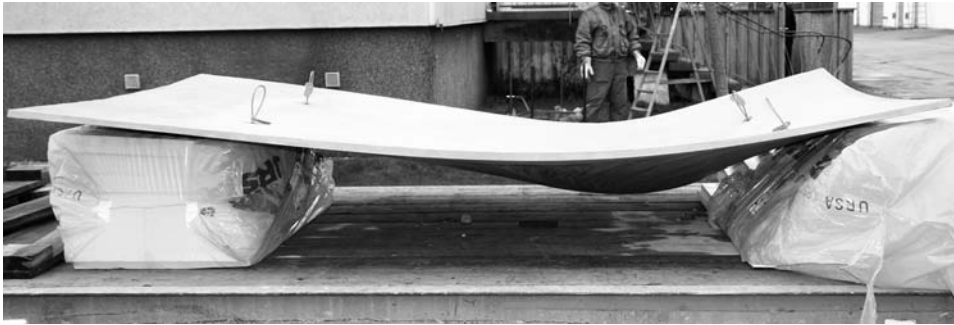
(a) Roof shell of *Parapluie* prior installation. Only embedded steel items are threads for crane hooks
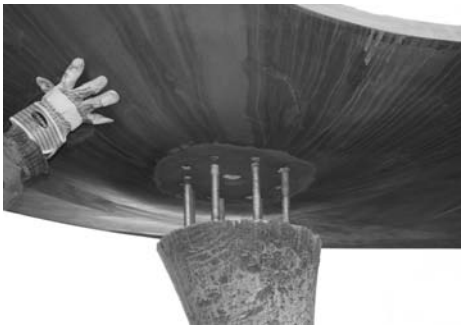
(b) Shell is aligned to the column-threads with the help of a crane...

(c) ...and fixed with screw end nuts from the top of water drain

Figure 5.6 Installation of *Parapluie* on site with an unpretentious screwed connection

factors on the loading and resistance side.

With a characteristic snow impact, as derived in section 5.1.4.2, of

$$S_k = 1{,}35\,\text{kN/m}^2$$

and a cantilevering projected footprint area of

$$A_{ref} = 1{,}95\,\text{m} \cdot 1{,}70\,\text{m} = 3{,}3\,\text{m}^2$$

the test loads without consideration of the safety concept is

$$F_k = 4{,}48\,\text{kN}.$$

Because of the homogeneous material texture and hence low strength variance, the safety factor on the resistance side, according to the material developer, is 1,07 to 1,17, rounded to $\gamma_M = 1{,}2$ on the conservative side [EVG$^+$14b, 210]. The safety factor on the impact side (snow) is $\gamma_Q = 1{,}5$.
The respective factor for the global safety concept is the product of the above as

$$\eta_{gl} = \gamma_Q \cdot \gamma_M = 1{,}8.$$

The resulting design test load magnitude, see [EVG$^+$14b, 210] is

$$F_d = 8{,}06\,\text{kN}\quad \text{(rounded to 850\,kg)}.$$

A pallet with sacks of de-icing salt and a weight of 850 kg (fig. 5.7) is offloaded all at once with a forklift truck, so that unwanted dynamic loads were unpreventable.
Nevertheless, no visible cracking or failure appearance occurred, as an evidence that the structure stayed within the elastic range of the material performance, see [EVG$^+$14b, 212].

Figure 5.7 Test loading of installed *Parapluie* prototype as verification of feasibility

5.2 Möbiusban(k)d

The development and construction of the *Möbiusban(k)d* has been published by the author as conference papers of the *International Association for Shell and Spatial Structures*, IASS, 'symposium on future visions', see [EGRH15] and [RGEH15].

5.2.1 Campus competition

In April 2014, a student project was tendered to design, to develop and to realize a slender concrete shell on the campus of the *University in Kassel*. The time frame for the project was limited to 14 weeks – the duration of the summer term. A group of 27 students of the school of architecture in their bachelor as well as master studies worked under the supervision of a mixed team of architects and structural engineers from the *Department of Structural Design*. The project *structural surface* aimed to evaluate the techniques to design and optimize freeform objects from high performance concrete.

To supervise a project to be realized in the end, leads to both, an educational and research attempt. The motivation in an accurate detailing for a realization project is naturally unlike enhanced, since unsolved details and errors cannot be just blurred or hidden. Although the amount of work rises[2], the identification with the project rises as well. Furthermore, the team work organisation and reliance is a valuable experience.

Two boundary conditions have been predefined, the site and the material.
The *University in Kassel* has given the construction permission and provided a prominent spot directly in front of the central canteen on a masonry platform, above a small stream and next to a willow tree. This platform, often used as a rest and lunch place, is located at the end of the axis of the main walkway on the university campus and thus clearly visible from all sides.
Predefined and decisive was the material. A big pack of high performance concrete, the appropriate admixtures as well as the mesh reinforcement has been sponsored by the industry partner *Ducon®*.

The participants were asked to react to the location with a design proposal, that pushes the limits of the material and to create an ultra thin and freely formed geometry. The program and the function have not been predefined. However, limitations of the size have

---

[2]the estimated sum of man-hours accumulated to ∼6000 h
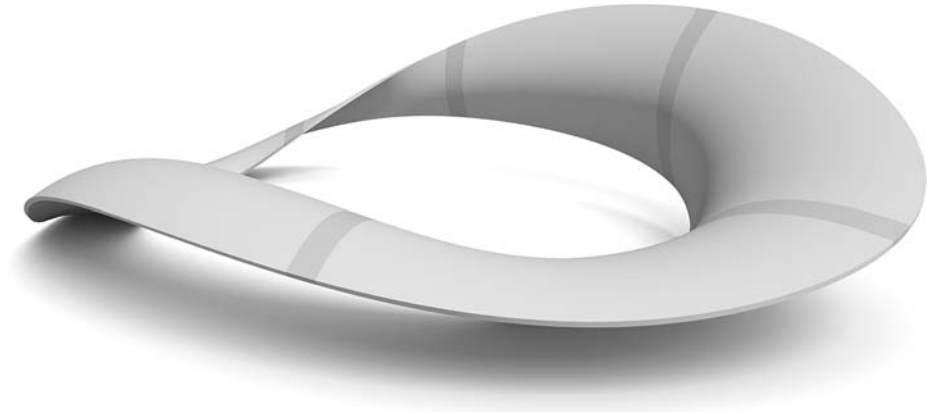
Figure 5.8 Visualisation of the winning contribution *Möbiusban(k)d*, illustrating the location of connection joints

been set: The maximum allowable surface area has been set to $15\,\text{m}^2$, in order to have a chance to realize the object.

In the first phase of four weeks, seven individual groups of three to five people worked together on their schematic proposals, to come up with a preliminary design. The proposals, covering sculptures, roofs, benches and seats were reviewed and judged by an external jury who selected one proposal for the following optimization and construction phases. The winning contribution is a public bench, describing the form of a *Möbius*-strip [EGRH15], [RGEH15]. A visualisation of the object is shown in fig. 5.8. All seven contributions of the competition phase are illustrated in appendix B.2 on page 251. In the second phase, for the duration of four consecutive weeks, all 27 participants grouped up in task forces and office-like structures, to elaborate the design, the detailing and the verification of construction principles of the chosen object to be realized.

The third phase, within the remaining four weeks of the summer term, was dedicated to the realization, in order to finish the *Möbiusban(k)d* to the end of semester exhibition of the school of architecture [RGEH15].

5.2.2 Schematic design

5.2.2.1 The *Möbius*-strip

In 1858 the mathematician *August Ferdinand Möbius* discovered the form of the infinite loop, later called *Möbius*-strip. The loop is defined as a surface, with only one edge and one face. Thus it has no distinct inner or outer face. If one starts to paint one apparent side, the whole strip will be covered at the end. A Möbius strip can easily be build: Taking a strip of paper, twisting one end 180° and sticking the ends together, leads to the intended result. Even cutting the entire strip along the middle of the strip does not lead to two strips – it remains one [EGRH15]. This procedure can be repeated arbitrarily.

5.2.2.2 Architectural function

The fundamental integrant is the geometric formulation of a sculptural element for the space next to the canteen, that up-values the local conditions and expands the possibilities of annexation. Due to the prominent and highly frequented situation, the object is intended to generate a place of encounter and communication.
The envisaged concept of the concrete bench reflects the omnipresence of science at the university. The sculpture has areas to sit on, to lie on or to lean against. Those areas are defined through the different heights of the bench. It opens up towards the canteen, to invite visitors to have lunch or to take a rest [EGRH15].

5.2.2.3 Form finding and optimization

The geometry of the concrete bench emerged from several boundaries like the site conditions and the limited size of $15\,\text{m}^2$. One major aspect is the intended usage as a seating-accommodation and hence ergonomic aspects. The desired form has different regions to either sit, where the sitting height (comfortable for at least three people) is predetermined, and to lean against, where a certain inclination of the surface area is a pre-condition. One important factor, determining the form, is the ground conditions. If it is possible to build mass foundations in the soil, the shape gets along with two supports, since the flipping-over capacity can be realized by a clamping into footings with a counterweight. If the sculpture stands on the ground only, in the case of plastered ground, at least three supports are required. In this case the site is a lawn, and the permission to cast mass foundations in given, thus the decision came up to have only two contact points at ground level.
The digital model of the sculpture is set up with the parametric software *Grasshopper®* [Rut15], a graphical algorithm editor, integrated within the 3D NURBS modelling software

Rhinoceros [McN15].

The derivation of the shape is illustrated in fig. 5.9. It starts with an ellipse around a center point on the ground, with radii in *x*- and *y*-direction, as informable parameters. This ellipse comprises twelve points in variable intervals; each point localizes a perpendicular curve, defined by three control points, at the beginning, in the middle and at the end. The translation of the control points defines the median surface shape of the object and the two rail curves along the edge of the *Möbius*-strip. Complementing the twelve curves with section profiles, with a shell thickness at the beginning, the middle and the end, leads to the volumetric shape of the concrete object [RGEH15].

The design chain from the initial shape modeled 'by hand', to an optimized structure, is compiled within one digital model, where all steps are within the same software environment. As described above, the parametric design is implemented in *Grasshopper*, a plug-in of *Rhinoceros*. A structural investigation is executed with *karamba* [Pre13], a finite element add-on, where the structural behaviour can be monitored as a live analysis in real time, while manipulating the input parameters. Utilizing the evolutionary solver *Galapagos* [Rut13], the geometry can be optimized in predicted ranges by the definition of fitness criteria; in this case the self-weight deflections.

The initial shape, satisfying all functional and aesthetical boundary conditions, is driven by the design, in order to achieve a convenient bench furniture, meeting the general necessities of site and location. The initial shape, modelled in *Grasshopper*, allows a direct forwarding to *karamba*: The surface meshes are converted to shells, which are not defined as volumes, but as shells with zero thickness. The nominal thicknesses are then defined in the analysis characters of the FEM software *karamba*. Further structural boundaries are defined: The supporting, together with the number and type of degrees of freedom activated, and thus the restrictions of translation and rotation in *x*, *y* and *z*-direction, the material characteristics and finally the loading conditions. In order to achieve a qualitative result from the optimization procedure, the only load considered within this design step is the computer-generated self-weight.

The output of *karamba* is both, graphical as well as numerical values, like deflection magnitudes, shell stresses, strains and utilization, support reactions etc. Any of these numerical values can be applied as fitness criteria for the evolutionary solver *Galapagos*, to get maximized or minimized. As *Rutton* describes in [Rut10], the variables are defined as genes, where a model with *n* genes, defines an *n*-dimensional solution space. The solver starts off with the random population of the fitness volume with genomes. These individuals are specific values for each gene. The solver breeds the best performing genomes of this

(a) Initial ellipse around center point with twelve section curves

(b) The three control points of each section curve are numerically translated

(c) Sections as profiles with adjusted thicknesses are swept along two rail curves

(d) 3D model of final shape
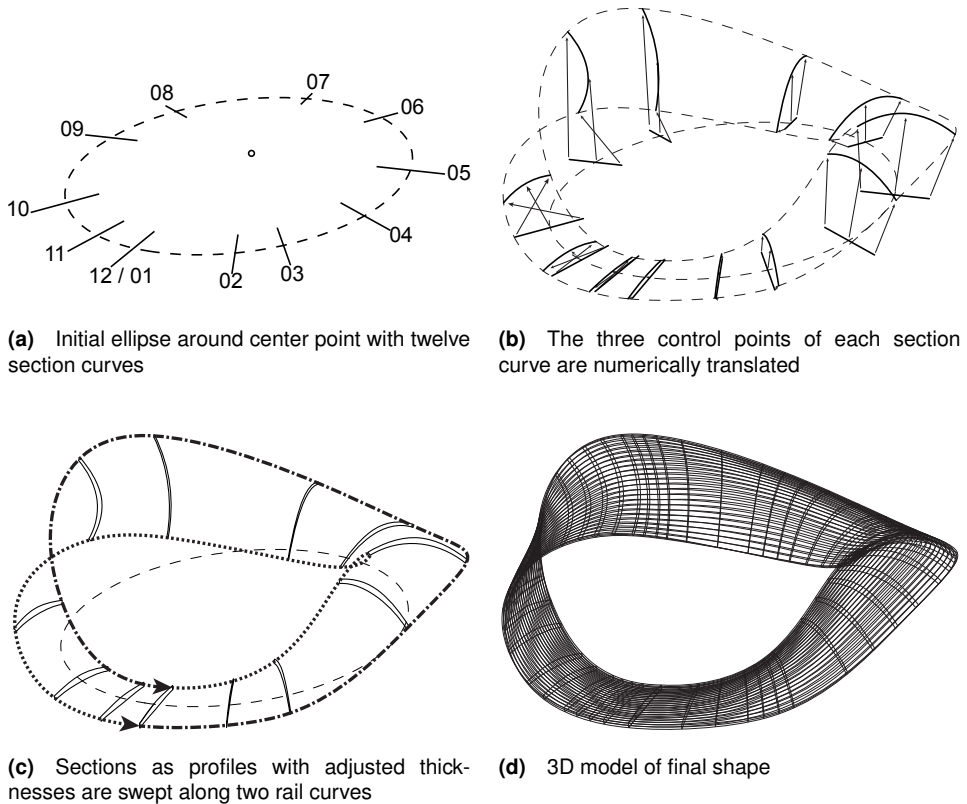
Figure 5.9 Shape derivation of the *Möbiusban(k)d*

first 'generation 0', against the fitness criterion to create a 'generation 1', which nature is no longer random. This iterative process leads to a solution, with the gabs scaled down successively.

In the current challenge to structurally optimize the *Möbiusban(k)d*, there are 72 parameters, describing the overall geometry (twelve section curves, with three control points each, and two translation directions, both in *z*, and along the initial orientational ellipse, gives $12 \times 3 \times 2 = 72$). These parameters serve as genes, feeding the evolutionary solver. The fitness criterion that seems suitable to represent the structural performance, is the

elastic self-weight deflection that counts to be minimized. In order to optimize the shape without a complete change of the design, it is necessary to determine the permitted range of change of the parameters during the optimisation iterations. It has been shown that providing a wide range leads to large improvements, thus large reductions of self-weight deflections. However, the achieved geometry turned out to be useless, because of a complete change of the initial desired smoothness of the shape. Finally, the range of the genes was restricted to ± 2 cm, leading to a performance improvement of 10 %. (A range of ± 20 cm led to an improvement of 200 % [RGEH15, 8].

A further application of optimization is not to manipulate the overall geometry but the distribution of cross section thicknesses. The major influence that enhances the need of material thickness is in plane bending moments. Thus the adaptation and verification of shell thicknesses leads to a more uniform stress distribution. However, due to numerical peaks of member forces within the FE analysis (unavoidable for free form objects, since the transition of two neighboring FE-elements does not reproduce the real object with all boundary conditions) the cross section optimization leads to abrupt changes of shell thicknesses that contradicts the desired smoothness of the Möbius strip.

In the report of *Rumpf* et al. [RGEH15, 5–9], a comprehensive display of the optimization process of the *Möbius*-bench is illustrated.

The optimizations described above are well applicable as form finding tools. Nonlinear material or geometrical effects like stiffness changes from concrete cracking or buckling, as well as second order analysis are not taken into account. The sole linear elastic material behaviour is considered, a problematic fact for the design of slender structures. However, the qualitative results, if carefully judged, are leading to reasonably improved results. Irregularities and uneven numerical peaks in the FE analysis do not enable an optimization, without further postprocessing of the results. It is important to note that an arbitrary geometry does not convert to a reasonable structure by the application of optimization tools – a fact underlined by the appropriate statement of *René Motro* (p. 38). Invariably the engineering intuition, primarily in the first design stages, is indispensable.

5.2.2.4 Construction progress strategy

From the beginning of the project, the absence of a crane is a driving design factor: The material sponsored by the industry partner *DUCON* has high requirements in the mixing and casting conditions of the environment. Minor changes of the surrounding air temperature, water temperature or changes in mixing time schedules may lead to deviations of
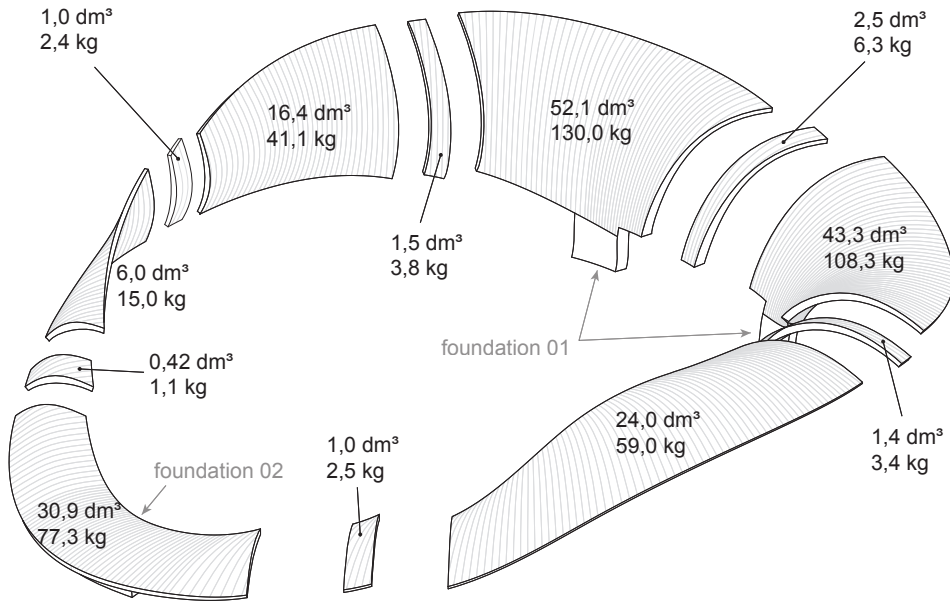
Figure 5.10   Segmentation of *Möbiusban(k)d*; $\sum = 180\,\mathrm{dm}^3 \mathrel{\hat{=}} 450{,}2\,\mathrm{kg}$

the viscosity of the ready mixed concrete and endanger the infiltration capability of the concrete through the mesh wires of the reinforcement. Furthermore, the concrete requires a compulsory mixer, therefore the concrete workmanship has to be done inside a concrete laboratory. Having no transport devices results in the fact that a segmentation of the object, and hence the development of a segmentation technique, is indispensable.
The segmentation layout, as illustrated in fig. 5.10, is arranged in a way, that four people are able to carry the single elements by hand, and the maximum weight is limited to 130 kg.

The envisaged construction sequence is intended to be reversed to conventional construction methods: The prefabricated elements are assembled on site and calibrated into position with the help of temporary substructures. After that, the gaps are closed with the casting of individual joint formworks. Finally, the two required foundations are produced, before removing the substructure. With the mounting order 'top to bottom', an expedient and load transferring application of prefabricated elements is ensured.

(a) Formworks of seams are installed on site

(b) Load bearing connection of prefabricated elements
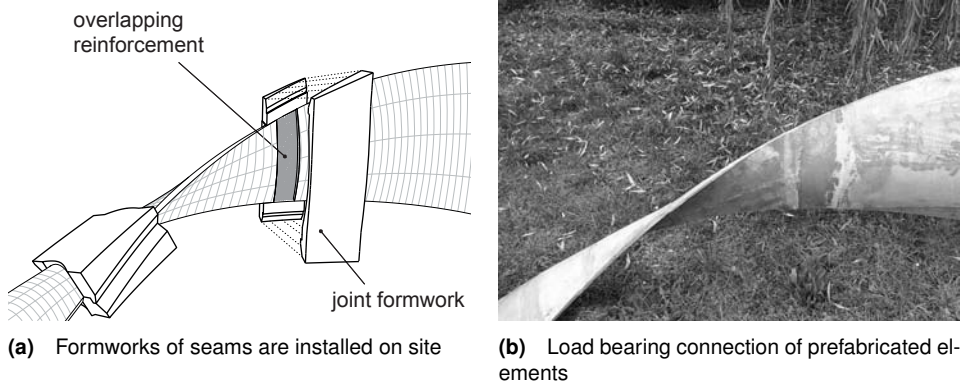
Figure 5.11 Joint connection concept of *Möbiusban(k)d* envisages the casting of the seams within a second step

5.2.2.5 Segmentation

A custom-made segmentation technique is developed, since the project is faced with the demand of fully load bearing joints, within a freeform slender shell. With that method, the joints have a width of 10 cm and are cast on site within a second casting step. To ensure the reinforcement is continuously running through the joint, it has to stick out of the formwork of the individual prefabricated elements. The stop-ends, thereby necessary, are realized with water soluble mortar, that seals the formwork within the joint section.

In chapter 6, a comprehensive report of the development of the construction technique for fully rigid joints, including the prototyping and testing-process, is illustrated.

The manufacturing of the prefabricated elements of the shell structure in all stages is driven by this segmentation concept. The formwork of the shell elements requires a separate mortar bed, and each joint has its individual joint formwork installed on site. Figure 5.11 illustrates the concept of setting up the formworks of the seams.

5.2.3 Structural System

5.2.3.1 System dimensions

The overall system dimensions of the concrete bench are summarized below. The distribution of shell thicknesses, as applied within the structural FE-analysis, is illustrated in fig. 5.12. These values are implemented for the preparation of the milled foam formwork.

overall length in plan	$l = 3{,}75\,\text{m}$
overall width in plan	$b = 2{,}49\,\text{m}$
overall height	$h = 1{,}05\,\text{m}$
shell area	$A_{\text{shell}} = 5{,}32\,\text{m}^2$
surface area (incl. edges)	$A_{\text{surf}} = 11{,}58\,\text{m}^2$
footprint area (over all)	$A_{\text{proj,all}} = 7{,}39\,\text{m}^2$
footprint area (shell)	$A_{\text{proj,shell}} = 3{,}85\,\text{m}^2$
average shell thickness	$t_{\overline{\text{M}}} = 33{,}8\,\text{mm}$ (range: $22 - 60\,\text{mm}$)
shell volume	$V_{\text{shell}} = 0{,}180\,\text{m}^3$
total self weight	$G_{\text{shell}} = 4{,}50\,\text{kN}$
foundation volume	$V_{\text{found}} = 0{,}13\,\text{m}^3 + 0{,}09\,\text{m}^3 = 0{,}220\,\text{m}^3$
foundation weight	$G_{\text{found}} = 3{,}25\,\text{kN} + 2{,}25\,\text{kN} = 5{,}50\,\text{kN}$

5.2.3.2 Material

The material chosen is *DUCON*, a micro mesh reinforced concrete, as presented in section 4.1.3.3. The material properties allocated for the design of the concrete shell structure, are equivalent to C80/95, with the elastic modulus of $E = 42\,300\,\text{N/mm}^2$, the shear modulus of $G = 17\,625\,\text{N/mm}^2$ and the appendant *Poisson*'s ratio of $\nu = 0{,}2$.
The crosswise allocated reinforcement bars have a diameter of $1{,}2\,\text{mm}$ and an axial distance of $e = 12{,}5\,\text{mm}$.

5.2.3.3 Loading and load combinations

The load cases implemented for the structural design are:

LC 1	g	self weight (computer generated)
LC 2	q_{l}	$2{,}5\,\text{kN/m}^2$ (live load 'left half')
LC 3	q_{r}	$2{,}5\,\text{kN/m}^2$ (live load 'right half')

(a) 22 mm   **(b)** 27 mm   **(c)** 32 mm

(d) 40 mm   **(e)** 50 mm   **(f)** 60 mm
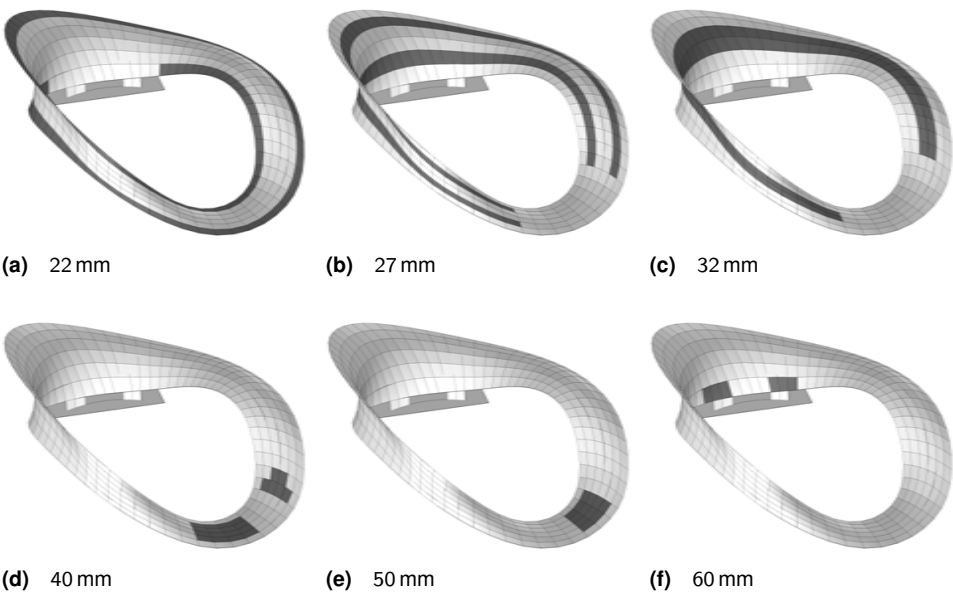
Figure 5.12 Calculative shell thicknesses applied for the shell structure of *Möbiusban(k)d*. Shaded areas referring to appropriate FEM areas

LC 11 imp^+ pos. imperfection (refer section 5.2.3.5)

LC 12 imp^- neg. imperfection (refer section 5.2.3.5)

The safety factors are $\gamma_G = 1,35$ for unfavourable dead loads, $\gamma_G = 0,9$ for favourable dead loads and $\gamma_Q = 1,5$ for live loads. The live loads have a magnitude of $2,50\,\text{kN/m}^2$, located on the projected surface area. An uneven distribution of the life loads is considered in the load combinations, refer table 5.1. It is separated in two halves; 'left side only', 'right side only' and 'fully loaded'. The dead load plus the fully loaded live load case is governing for the design of the shell structure, therefore the imperfections are introduced in those cases only; the partly live load is governing for the design of the foundation and the resistance against flipping over [EGRH15]. All load combinations are under consideration of second order analysis (assessment of the state of strain at the deformed geometry).

Table 5.1 Load combinations allocated for the structural design of *Möbiusban(k)d*

	load case	LC1	LC2	LC3	LC11	LC12
		g	q_l	q_r	imp^+	imp^-
	LG01	1,35	1,5	-	-	-
	LG02	1,35	-	1,5	-	-
	LG03	1,35	1,5	1,5	-	-
ULS	LG04	1,35	1,5	1,5	1,0	-
	LG05	1,35	1,5	1,5	-	1,0
	LG06	0,9	1,5	-	-	-
	LG07	0,9	-	1,5	-	-
	LG08	0,9	1,5	1,5	-	-
	LG11	1,0	1,0	-	-	-
SLS	LG12	1,0	-	1,0	-	-
	LG13	1,0	1,0	1,0	-	-

5.2.3.4 Assessment of state of stress

To determine necessary shell thicknesses and for the analysis of global stability, a structural design has been taken out at a 3D model, within the structural analysis and design FE-software *RFEM©* by *Dlubal Software GmbH* [Dlu15].

The shell is represented by nodes, which are an output of the median surface model of the bench. The *Möbius*-strip is divided into six sub-strips, again subdivided in segments of a length to height ratio, between one and four. The nodes, imported into the FE software, are connected by poly-lines (straight lines between the nodes). These poly-lines are the borders for 'quadrangle' areas. In *RFEM*, these areas are defined as quads, where the nodes are not mandatory in one plane; the boundaries may also be curves, allowing the modelling of shell structures. The software automatically generates an FE-mesh, obtaining the finite elements for the analysis. The sought lengths of the elements are defined to $l_{\mathrm{FE}} = 0,02\,\mathrm{m}$ ($<$ shell thickness).

The main focus of the analysis is the obtaining of a differentiation between a load transfer via in-plane bending versus membrane stresses. Having mainly membrane stresses, which is a load takedown with tensile and compressive forces only, the shell increments are designed by $\sigma = N/A$ with $A = b \cdot h$ (in the structural frame analogy), whereas the load transfer with in-plane bending moments is designed by $\sigma = M/W$ with $W = b \cdot h^2/6$ (again

in the structural frame analogy). The structural height h in this case is the shell thickness. For the load transfer with membrane forces, it is raised to the first power h^1, whereas for the in-plane bending system, it is raised to the third power h^3.

The diagrams, fig. 5.13b and fig. 5.13c, are showing the ultimate limit state (ULS) plots of the principal axial and the in-plane bending stresses respectively. The main axes '1' are in direction of the main load trajectories. It can be seen that the present system is a hybrid system of membrane- and bending action. The plot, showing the bending exposure, is an indicator where an increase of the shell thickness is expedient. In these sectors of the shell structure, the shell thickness t is amended to achieve the sufficient structural height [EGRH15]. By approximation, the final monitoring and design of the shell can be executed via the principal stress analysis (fig. 5.13d), as reported in section 4.1.3.3. The design stress resultant value, under worst load case scenario (fully loaded), is limited to $\sigma_{v,max} = 12 \, \text{N/mm}^2$ [EGRH15]. This restriction value does not consider peak values at geometric unsteady sections of the surface.

The serviceability limit state (SLS) is controlled by the linear elastic deflection behaviour, as shown in fig. 5.13a, with a maximum deflection value of $u_{max} = 4 \, \text{mm}$. Simplifying the unsupported flanks of the shell as a cantilever, with the overhanging length of $l = 130 \, \text{cm}$, the deflection results to a ratio of $l/324$.

5.2.3.5 Buckling analysis

Due to the slenderness of the concrete shell, the investigation of buckling is mandatory, since it might be a governing state of failure. The sections of interest are the outer edges under compressive membrane forces, where the shell has the smallest thickness and the smallest curvature. A nonlinear analysis has been executed to obtain the buckling shapes [EGRH15]. The governing failure shapes are simulated with an equivalent imperfection load, added to the load combination under consideration of effects second order, as listed in table 5.1.

In fig. 5.14a, the qualitative shape of the first eigen-mode is illustrated. It can be observed that the vulnerable section is the outer edge of one of the cantilevering flanks. The shapes of the second, third and fourth eigen-modes, have their peaks within the same regions, refer to the plots in fig. B.3. To consider the buckling failure shape, within the structural analysis, an equivalent load is implemented, leading to a deformation shape analog to the failure shape. The magnitude of the deflection to be achieved is $l_{comp}/200$, where l_{comp} describes the lengths along the compressed edge. Here $l_{comp} = 2,00 \, \text{m}$, thus the deflection $u_{imp} \geq 1,0 \, \text{cm}$. Since this approach leads to stresses coming from the imperfections itself,

(a)   Deformation, LG13 SLS; [mm]

(b)   Principal axial force, LG3 ULS; [kN/m]

(c)   Principal in-plane bending moments, LG3 ULS; [kNm/m]

(d)   Principal stress distribution, LG3 ULS; $\sigma_{v,max}$; $\left[kN/cm^2\right]$
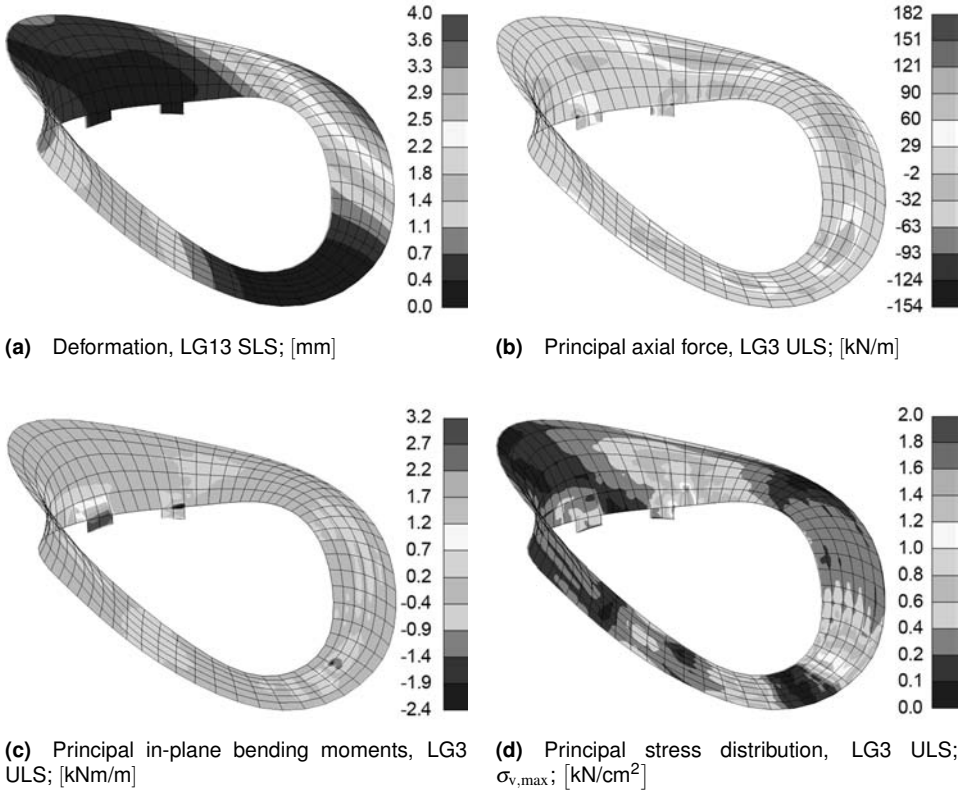
Figure 5.13   Deformations, member forces and shell stresses of *Möbiusban(k)d*

no increase of stresses due the buckling imperfection can be obtained. Comparing a pre-deformed shape, generated within the same approach with a deformed edge by $1{,}0\,cm$, enables the comparison of the ULS stresses. An increase factor of $1{,}018$ is identified, similar to and conservative to the results of the modal results of the eigen-value analysis, as in fig. 5.14a.

5.2.3.6 Foundation

The design of the *Möbiusban(k)d* envisages a foundation at two sections, located opposite to each other in regions where the loop touches the ground. Naturally, this design decision

(a) Eigen-mode 1
critical load factor $f = 84$ [-]
magnification factor $\alpha = 1,012$

(b) Deformation of the initial shape in analogy to
the failure shape; $u_{imp^{+-}} = 10\,\text{mm}$
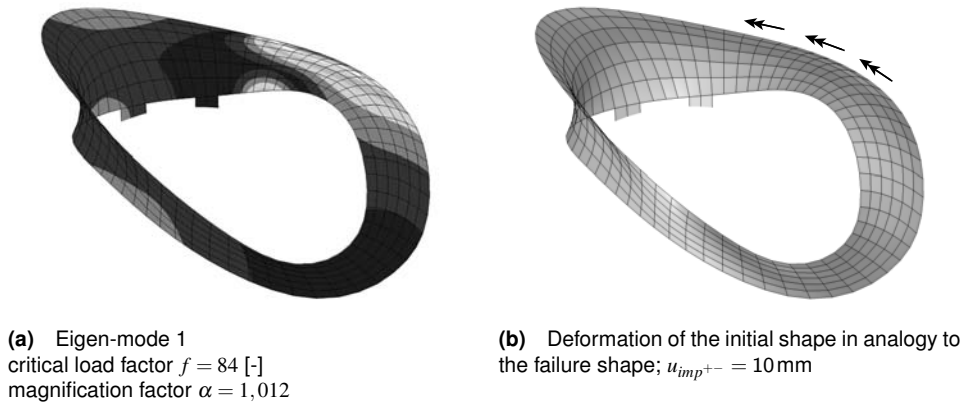
Figure 5.14 Buckling analysis of *Möbiusban(k)d*. The critical edge of the structure is pre-deformed analog to the failure shape from the eigen-mode analysis

eliminates the possibility to place the whole structure on the ground, because this would require at least three standing points. Here, a resistance against tilting or 'flipping over', has to be implemented by clamping the shell into a mass foundation, as shown in fig. 5.15. The mass foundation needs to be wide enough to provide a lever arm under ground, to withstand a flipping over, in case of the structure being loaded on one side only [EGRH15]. To design the size of the foundation, the load combinations LG11 and LG12 (table 5.1) are considered. These combinations cover the un-factored self-weight, together with the worst case scenarios for uneven live loads. An additional FE model is built, where the footing is idealized with two point supports for each foundation. This model cannot be used for the design of the shell, since point supports lead to a stress peak tampering. With this method discrete values of the support reactions in [kN] are gained. The size of the footing is designed in a way that the weight of the foundation exceeds uplift magnitudes of the support reactions. Figure 5.16 illustrates the concept of the reinforcement layout of the two foundations.

As a side note, the author likes to mention that the concept of a mass foundation is contrary to the approach of building lightweight structures: In this example, the total weight of the shell structure is 4,5 kN and the total weight of the foundations is 5,5 kN. This leads to the ratio mass ratio 'foundation over shell' $= 1, 22 : 1$.
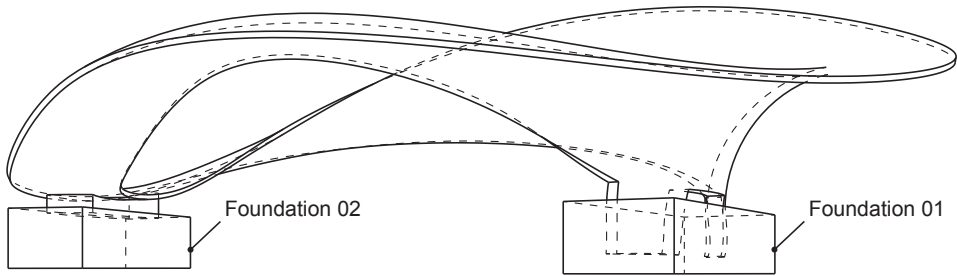
Figure 5.15 Positions of foundations; shell structure of *Möbiusban(k)d* clamped into mass foundations to prevent tilting over

(a) Foundation 01
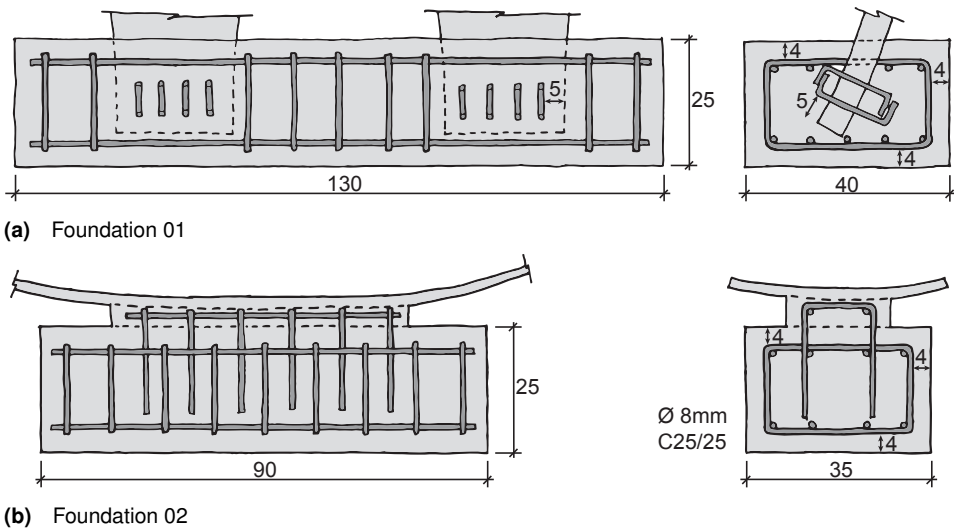
(b) Foundation 02

Figure 5.16 Foundation reinforcement concept of *Möbiusban(k)d*

5.2.4 Manufacturing

5.2.4.1 Formwork

The formwork is produced from a pressure resistant polyurethane foam, generally made for roof insulations. The raw blocks were cuneiform to define a drainage slope. The shell geometry and the negative shape, modelled in *Rhinoceros*, are transferred to a three-axis

computerized numerical control (CNC) milling machine, with the help of the computer aided manufacturing (CAM) software *RhinoCAM*. The CNC machine available is limited to a milling depth of $15-20$ cm, dependent on the milling cutter. Furthermore, the size of the raw foam blocks leads to the necessity to glue formwork segments together, prior and after milling the final shape, with a particular PU-glue. The bonding prior to milling results in a suitable surface quality, whereas the bonding after milling leads to a loss of geometrical precision, to be taken into account. Figure 5.17b shows glued sections before and after milling process. The joints of the formwork (glued after milling) are smoothed with a filling.

After the formwork is milled, three layers of a special lacquer, *Fratec®*, sponsored by the industry partner *Max Frank*, are coated on the PU-surface, to fill the pores. As a release agent, vaseline is used.

5.2.4.2 Reinforcement

The micro mesh reinforcement layers are stapled over the complete cross section. The bars have a diameter of $1,2$ mm and an axial distance of $e = 12,5$ mm. To realize the double curvature of the shell (both synclastic and anticlastic), the single layers have to be sliced and tailored, as shown in fig. 5.18. The aim of the tailoring procedure is to have as few cuts and hence weak points as possible and to spread the slices of the area of the shell. On the other hand, the reinforcement has to be smooth enough, and thus sliced, to fit in the formwork without being pressed into shape. Since the PU-foam of the formwork is locally weak, a cautious reinforcing process is required to avoid damage in the concrete contact areas. To prevent the outer meshes from corrosion, these layers are made of stainless steel, whereas for the inner layers, carbon steel wires are used.

Custom made spacers are used to assure a concrete cover of 3 mm. It has to be mentioned that it has been shown in the results that these spacers are considerably visible on the later concrete surface and result in the necessity of a design-wise post treatment.

5.2.4.3 Concreting shell elements

The concreting process has high requirements to the precision of the mixing procedure. To assure the concrete flows through the mesh wire filaments of the reinforcement, it needs a minimum fluidity which is controlled with the slump. The slump size achieved with a *Hägermann*-cone, see section 4.1.3.3, needs a minimum spreading diameter of $36-37$ cm. A smaller spreading size and hence a stiffer concrete, may result in a choking, which makes the formwork, as well as the reinforcement, no longer useable. It became apparent that the
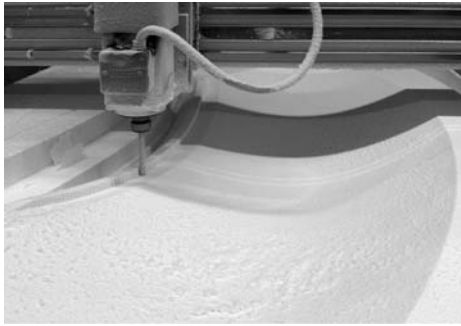
(a) CNC milling of the formwork foam blocks
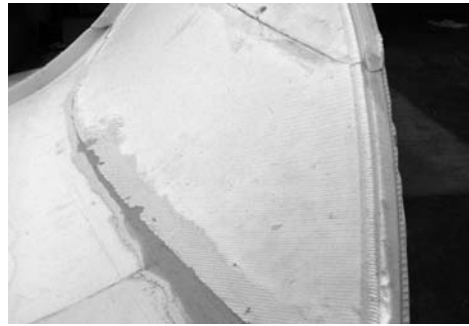
(b) Segmented formwork elements are glued together and smoothed with a filler

(c) Concrete contact areas are coated with a special lacquer and release agent
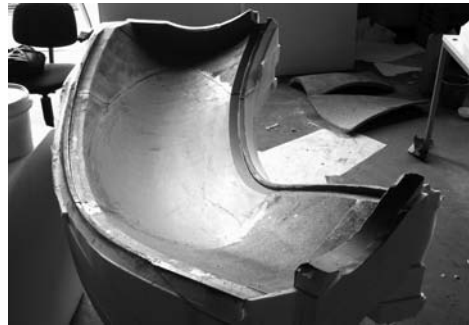
(d) Lower side of one formwork element ready for casting

Figure 5.17   Formwork manufacturing of *Möbiusban(k)d*

slump size achieved is not only dependent on the recipe, but also from the mixing time schedule. A constant ratio of the ingredients, shown in fig. 5.20a, the water over cement value and constant grading curves of the aggregates, still lead to different consistencies, for example by changing the mixing device. Furthermore, the plasticisers are developing the liquidation effect over the mixing time. Within a trial and error process, mixing time schedules were asserted for two different types of compulsory mixers, dependent on the quantity of concrete required. In fig. B.4 on page 254, sequence schedules for $15-20\,$L and $70-90\,$L are illustrated, leading to a sufficient concrete liquidity.

Figure 5.19 shows a closed and sealed formwork block of one shell element, just prior
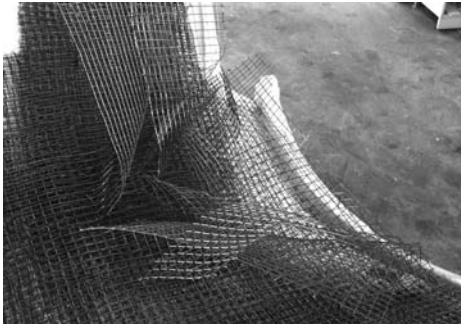
(a) Double curved shell requires slicing of reinforcement sheets...

(b) ...and tailoring to fit into the formwork without damaging foam surface
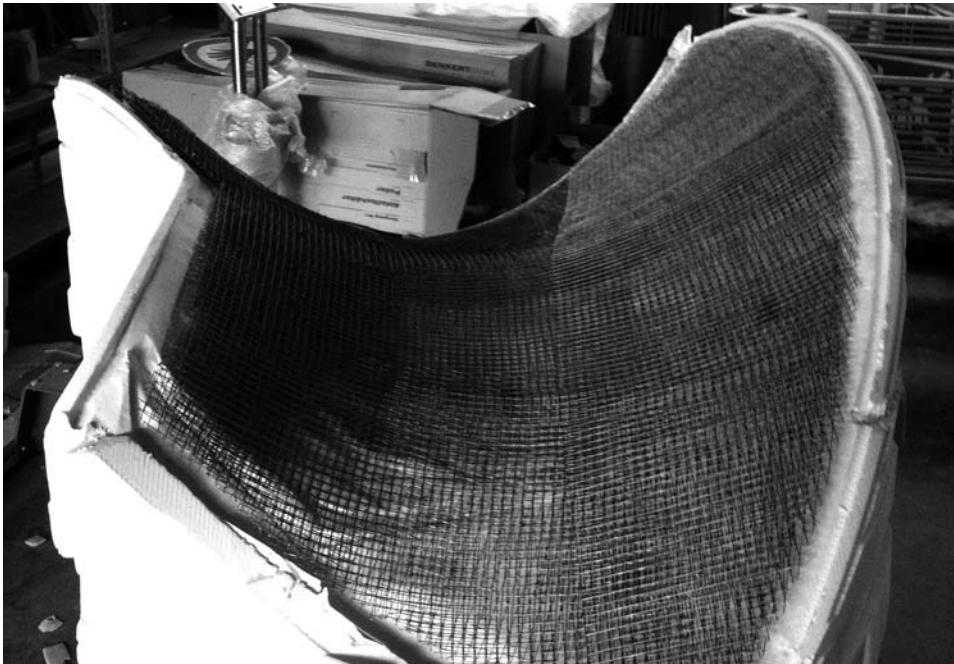
(c) Reinforcement package of one element ready for casting

Figure 5.18 Reinforcement manufacturing of *Möbiusban(k)d*

Figure 5.19   Closed formwork for one concrete element of *Möbiusban(k)d* ready for concreting

casting. The reinforcement sticking out on both ends, sealed with a lime mortar, can be recognized on that photograph. The hydrostatic pressure height reaches up to 70 cm. It has to be ensured that the formwork is absolutely watertight. Once the concrete leaks out of a small opening, it is hard to seal the gap while casting. Therefore the formwork joints are sealed with both, a sealing tape and a silicone seam. Furthermore, the upper and lower halves of the formwork blocks are pressed together with the help of tension belts.

The ability of the concrete to flow through the reinforcement filaments is not only dependent on the consistency of the ready mixed concrete, but also on the pressure, and to what extent it is pressed into the formwork. A gasketed infiltration pipe, as shown in fig. 5.20b and fig. 5.20c, gains the hydrostatic pressure directly at the infill openings. In addition to the infiltration openings, which are located at the lowest points of the concrete elements, there are air exhaust openings, located at the high points.

(a) Ingredients fltr: Aggregates $0-2,0\,$mm, $0-1,2\,$mm, cement *DUCON 1*, water, plasticiser
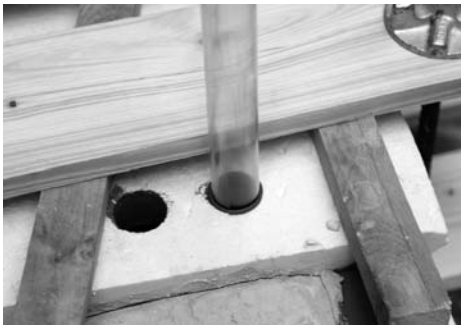
(b) Infiltration pipes are installed to gain hydro-static pressure for infiltration

(c) Flowable concrete that 'rains from the trowel' is required for casting process

Figure 5.20 Casting process of concrete elements

5.2.5 Assembly on site

5.2.5.1 Calibration and element positioning

As mentioned in section 5.2.2.4, the construction sequence of the shell is reverse with the casting of the foundation as the last step. The advantage of that sequence is the 'allowed' impreciseness for the digging of the footing pits, which is the first step on site. The calibration is done with the help of reference points, located in the surrounding environment.

The prefabricated elements, with the retracted formwork and the connective reinforcement bent up, are placed into the exact position, with custom made scaffolding made of wood, as shown in fig. 5.23. The scaffolding is made of oriented strand boards (OSB), a
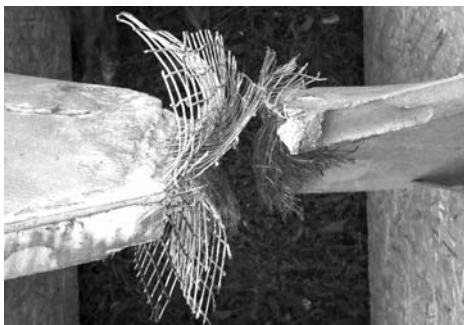
(a) Reinforcement inside joint section bent up...
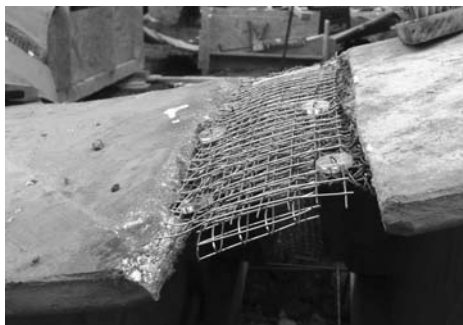
(b) ...and interweaved after final positioning

(c) Assembly and positioning of prefabricated concrete elements

Figure 5.21 Prefabricated concrete elements of *Möbiusban(k)d* are positioned and joint reinforcement is interweaved

Figure 5.22   All connection joints of the shell structure in their formwork, just after concreting

glued wooden sheet material, deployable in outdoor areas. The geometry of the panels is CNC-milled and stuck together to scaffolds, similar to guitar racks.

5.2.5.2 Seams

As soon as the elements are in their final position and the reinforcement is interweaved properly to fulfil the requirements to perform as a fully rigid joint, the formwork of the seams can be installed. Each joint itself has a width of 10 cm. To assure the seam is properly covered with the formwork, and the formwork is able to be closed with some pressure, an overlapping width of another 10 cm on each side is chosen, thus the custom made joint formworks have a width of 30 cm with the length, dependent on the length of the joint. Here again, each formwork has to be completely tight, and the foam blocks are utilized with infiltration as well as air exhaust holes.
In contrast to the casting of the prefabricated elements, the joints cannot be cast in the

Figure 5.23   Building of the foundation as the final construction step

concrete laboratory under constant environment conditions. In this case, the site is close
to the required facilities, for which reason the concrete could get mixed under laboratory
conditions and carried with buckets on site. The processing has to be as quick as possible,
to avoid a fatal reduction of liquidity. Figure 5.22 shows all planked joins of the shell
structure, shortly after casting.

As the last casting step, before removing the wooden scaffolding, the foundations have to
be produced, by simply pouring concrete inside the excavation, where the reinforcement,
as shown in fig. 5.23, is prepared and the connection reinforcement is positioned. The
foundations do not have any formwork; the concrete is poured against the soil.

5.2.6 Ready for service...

Finally after the removal of the scaffolding and cleaning up the site, the concrete bench
has undergone some postprocessing. Lacquer remains of the coating are removed with
electrical scrubbers and air blisters are smoothed with concrete filler. Furthermore, the
concrete shell is coated with a hydrophobicity paint to protect the surface from environ-
mental impacts and moisture.

After the repair of the lawn, the concrete bench *Möbiusban(k)d* is handed over to the pub-
lic. It is well accepted, people have their lunch there and it functions as a meeting point.
Leftovers from pleasant summer's evenings can be taken as an evidence of its comfort.

Figure 5.24   Finished concrete bench after handing over to the public

5.3 Concrete mobile

The development and construction of the concrete mobile *Stable Equilibrium* has been published by the author as a conference papers of the *International Association for Shell and Spatial Structures*, IASS, 'symposium on future visions', see [GERH15].

5.3.1 IASS symposium contest

The organisation committee of the *International Association for Shell and Spatial Structures*, IASS, set up an international contest and exhibition of structurally innovative pavilions. The competition was tendered to architects, engineers and scientists from all over the world to realize demonstrators of their research context.
The expected standard was described in the tendering document: *"...The pavilions have to give a future vision on structural design and innovation and have to be the outcome of excellent structural research."* [Int15].

The exhibition venue is the foyer of the *Muziekgebouw aan 't IJ* in Amsterdam, a concert building located in the city center at the south waterfront of the *IJ* and the port entrance of *IJhaven*. The building contains large voids and balconies, encased by the roof and a free spanning facade, that enable a visibility from multiple perspectives from inside and outside, especially for pavilions suspended from the roof.
The exhibition was opened to the public from June to August 2015.

With the permission from the IASS organisation jury to realize the pavilion, the project was set up within the team of the *Department of Structural Design*. The participants and sponsors are listed in appendix C.1.

5.3.2 Constraints evolve design concept

To equalize the contest conditions for all participants, there were restrictions in size and weight for both, the exhibits and the packaging, in order to enable a transportation by an airplane.
The maximum size of a box was limited to $100 \times 75 \times 65$ cm and the weight to 32 kg per box. The total weight was limited to 192 kg. The provided volume for the pavilions, suspended at the entrance facade, was $8,0 \times 4,0 \times 4,0$ m.
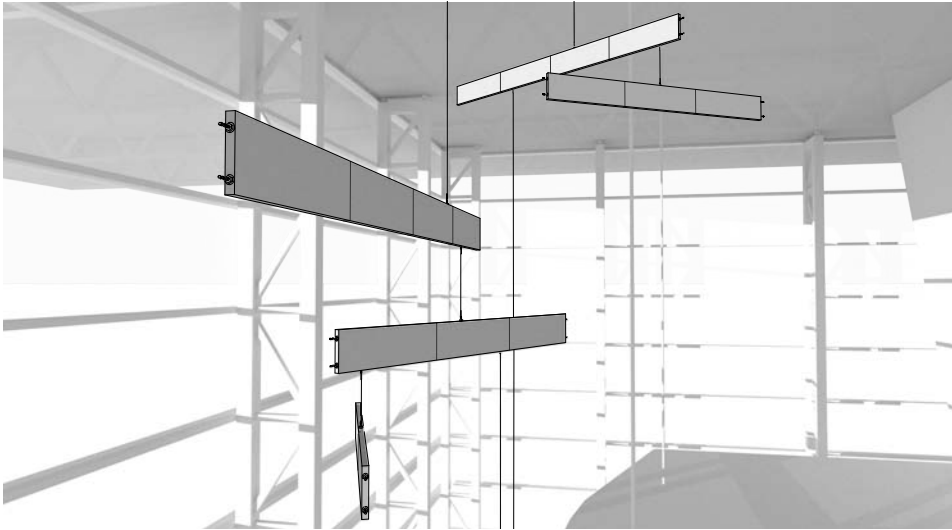
Figure 5.25 Visualisation of the concrete mobile *Stable Equilibrium*, the contribution for symposium contest *IASS Expo*, 2015 in Amsterdam

Special demands were made on the construction and deconstruction times on site. To keep the daily routine of the concert venue, the construction and deconstruction had to be finished within one day each, for all participants. This led to a narrow time schedule for the teams and a design driving boundary condition: Constructions, requiring complicated assembly or materials, necessitating curing times (e.g. concrete without dry-fit connections) had to be excluded.

The research interest of the team involved is focused on the design and processing of slender concrete constructions. Thus the material was predefined, encouraged by the availability of a big pack of high performance concrete *DUCON®*, the appropriate admixtures and mesh reinforcement.

The ambition of the design process was to treat the given rules of the contest as a design criteria, rather than a restriction and incorporate them as conceptual advantages in the design, instead of splitting a project into packaging pieces in the end [GERH15, 3]. Architectural and sustainability demands legitimate research efforts in lightweight concrete structures. The development in increasing the strength performance of concrete and

reinforcement materials has successfully moved forward. A collateral demand with the development of high performance materials is the necessity to manufacture under laboratory conditions with special mixing devices and predefined environmental conditions like air and water temperatures. Furthermore, shorter life cycles of the building environment promote the prefabrication of concrete elements to enable not only a quick assembly, but also a de- and reconstruction of structures. See introduction of [GERH15, 2].

The boundaries, derived from the setting of the symposium contest, led to similar demands, however in an exhibition context. The design intent pursued is a suspended concrete structure, made of prefabricated concrete elements, assembled with a dry-fit connection method.
The proposal submitted is a concrete mobile named *Stable Equilibrium*, as illustrated in fig. 5.25. The structure has a modularization, fulfilling the packaging and transportation requirements. All elements have the exact same geometry, with load bearing connections from prestressing devices. The result is a light and floating structure from an initial heavy material, that allows a quick and easy assembly on site, with an open end spanner as the only tool required [GERH15, 1].

5.3.3 Schematic design

The design of the installation is based on two basic conceptual design intents, the structural approach of a concrete structure, connected with a prestressing method, and the fascination of a mobile in its delicate equilibrium condition, with the aim to create a certain level of confusion, based on the paradox of the lightness of the floating structure and the heaviness of concrete, see [GERH15, 3–4]. Chapter 7 illustrates a comprehensive investigation of the prestressing connection technique.

All in all, the mobile consists of seven suspended beams, assembled by 23 prefabricated elements. Each element is rectangular, with the dimensions $480 \times 150 \times 22\,\text{mm}$. The unpretentious and repetitive shape is intended for both, the focus on the basic essentials of a mobile as well as the simplifying of the fabrication effort.

The state of equilibrium can be expressed with the global moment equilibrium, which can be formed at an arbitrary horizontal point as $M_\text{i} = F_\text{i} \cdot r_\text{i}$ and $M_\text{R} = F_\text{R} \cdot r_\text{R}$, with $F_\text{R} = \sum F_\text{i}$. R is the resultant of all individual force components F_i, as shown in fig. 5.26.
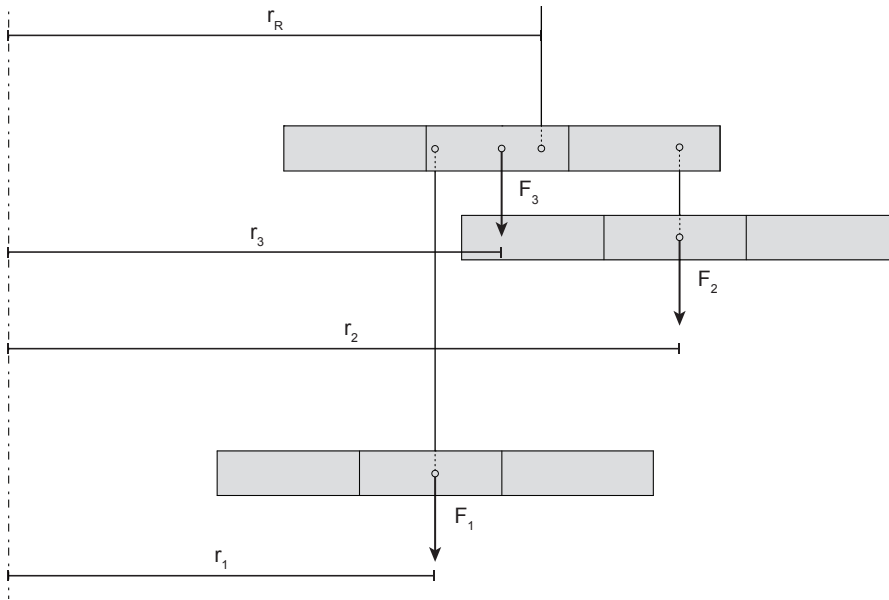
Figure 5.26 State of equilibrium of a mobile. With constant dimension and density in longitudinal direction of the elements the equilibrium can be formed geometrically

Due to the fact that the thickness, the height and the density ($\rho = 25\,\text{kN/m}^3$) are constant within the whole system, the state of equilibrium can be solved geometrically.
With the software *Grasshopper®* [Rut15], a graphical algorithm editor integrated within the 3D NURBS modelling software *Rhinoceros* [McN15], the whole system can be modelled parametric, so that the layout, size and number of elements can be controlled in a playful approach, with the possibility of a monitoring of total weight and possible collision of mounting parts.
Every element is defined by its point of origin, adjustable directly in *Rhinoceros*, and the dimensions based on numeric parameters. The length is not controlled continuously, but in $2-5$ increments of $l = 480\,\text{mm}$, each to enable the modular set-up wanted. The mobile is designed from 'bottom to top'. The lowest beams (three times existent) are independent from the above located elements and the location of the weight resultant is identical with the location of the suspension. All other elements are informed by the system below [GERH15, 5].
A variety of proportions are tested until a final system is chosen that fulfills the architec-

tural aesthetics and the demands of fabrication (distance between suspension points and element joints $\leq 20\,$mm) and the exhibition requirements.

5.3.4 Structural system

5.3.4.1 System dimensions

The dimension of the mobile can be taken from fig. 5.27. Generally, there are four types of beams assembled with different numbers of elements:

$$(1\times) \quad \text{2-fold} \quad l = 96\,\text{cm}$$

$$(4\times) \quad \text{3-fold} \quad l = 144\,\text{cm}$$

$$(1\times) \quad \text{4-fold} \quad l = 192\,\text{cm}$$

$$(1\times) \quad \text{5-fold} \quad l = 240\,\text{cm}$$

he enveloping space is a cylindrical volume with a height of 450 cm and a rotational diameter of 313 cm.

Each element has the same dimensions of $l = 480\,$mm, $h = 150\,$mm and the thickness $t = 22\,$mm. Two PVC hulls with an axial distance of $e = 75\,$mm are cast centric in the concrete. The hulls have an inner diameter of $\varnothing = 8\,$mm.

The lengths of the suspension cables are designed to satisfy aesthetic and collision requirements, but have no impact to the equilibrium system.

5.3.4.2 Materials

The following materials and characteristics respectively, see [GERH15], are used for the structure of the mobile.

Concrete and reinforcement   The concrete used is a micro mesh reinforced concrete, sponsored by *DUCON*, with a concrete grade equivalent to a C80/95 as used for the concrete bench *Möbiusban(k)d*, described in section 5.2. For specific information of the material, refer to section 4.1.3.3.

Also the crosswise allocated reinforcement bars have a diameter of $\varnothing = 1{,}2\,$mm and an axial distance of $e = 12{,}5\,$mm.
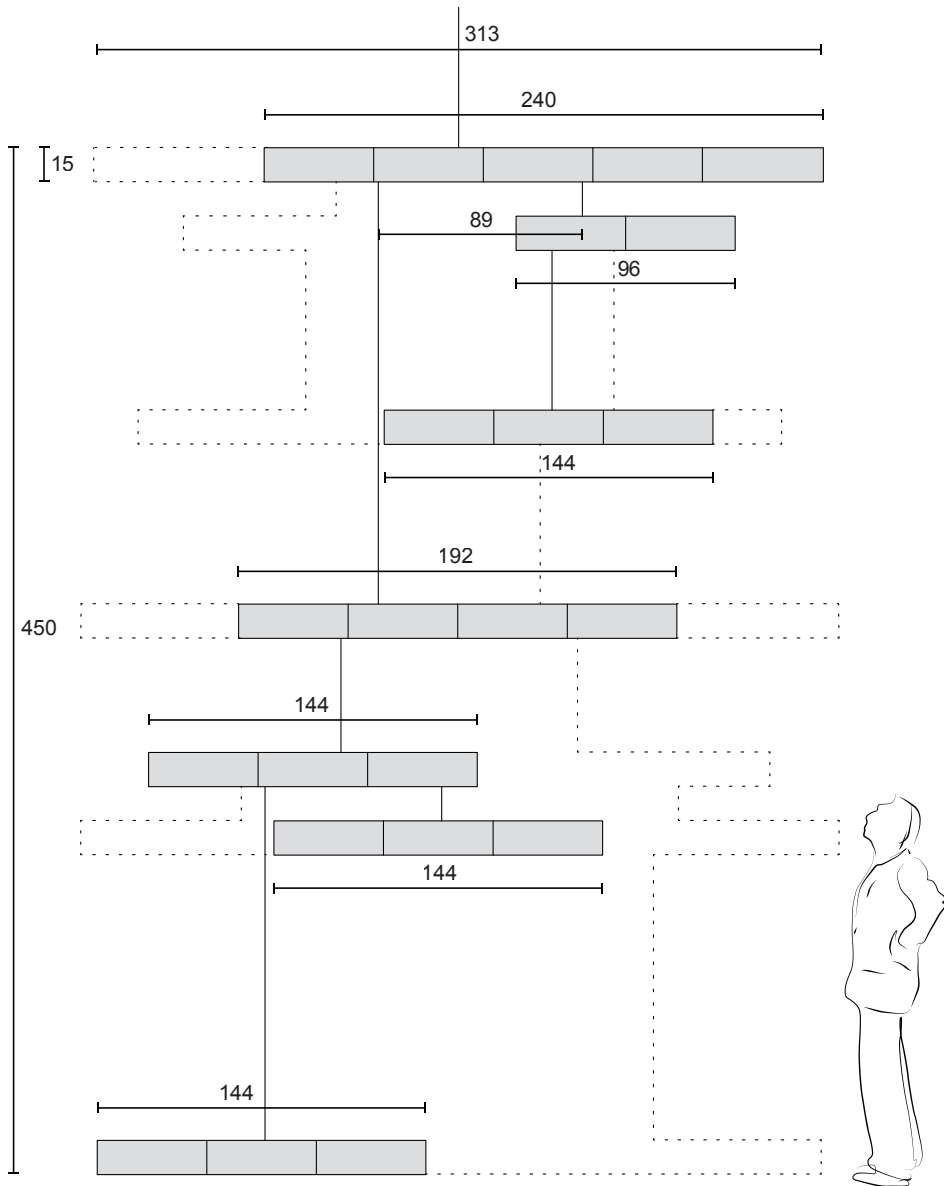
Figure 5.27 Dimensions of the final layout of concrete mobile *Stable Equilibrium*; dashed lines are framing the enveloped space filled [cm]

Prestressing media and screw nuts   The concrete elements are connected with a dry-fit connection method, here a prestressing, to avoid the necessity of a concreting on site. The prestressing is applied with threaded bars $\emptyset = 6\,\text{mm}$. The grade of the bars is 4.6. According Eurocode 3 [Eur05, tab. 3.4], the tension resistance of each bar is $F_{t,Rd} = 5,8\,\text{kN}$, refer to eq. (7.1) on page 204.

Initially the usage of confected steel cables was envisaged as a prestressing medium. Tests have shown that these cables are not feasible for this application, as comprehensive illustrated in section 7.5.

To assure that the thrusts are not damaged and slipping during the installation, long nuts are used, with a length of $2 \times 9\,\text{mm}$ on the countering end and $1 \times 20\,\text{mm}$ on the opposite end.

Embedded steel items   The connection points of the suspension cables into the concrete are causing concentrated loads that have to be introduced. The designated embedded steel items manufactured, have a steel grade of 'S235JR', with a characteristic yield strength of $f_{y,k} = 235\,\text{N/mm}^2$. The welded sections are produced with steel plates $t = 2\,\text{mm}$.

Suspension tension elements   For the suspension of the mobile, steel cables are pre-tailored. The wires used are taken from the series *TECHNOCABLES* from *CarlStahl*®. The nominated outer diameter is 2,5 mm and the tensile strength $f_y = 1570\,\text{N/mm}^2$. The minimum breaking load, according to the manufacturer is $N = 5150\,\text{N}$, see [Car15, 16].

Both ends of the cables, sponsored by the manufacturer *CarlStahl*, have swaged terminals with screw threads M6 with a length of 50 mm. These terminals are causing a calculative reduction of the strength capacity of 40 %.

The author likes to mention that for the exhibition in the *Muziekgebouw* in Amsterdam, these cables have not been used. Instead free-climbing ropes with an eye-catching colour were installed to emphasize the contrast between the concrete and the suspension.

Joint spacers   To avoid stress peaks in the joint area between two elements, spacers are interjacent. 3 mm lasered MDF boards, as shown in fig. 5.32b, compensate any roughness of the concrete faces and distribute the compression forces from the prestressing and outer load into the concrete.

5.3.4.3 Loads and safety factors

The only load considered for the structural design is the dead load of the concrete elements. Naturally the mobile will 'float' out of shape, once it is loaded with live or serviceability loads. Furthermore, the installation of the lowest point of the system is 3,5 m above the ground and therefore out of reach of the public. Thus any dynamic loads from touching are excluded.

Generally the safety factor of $\gamma_G = 1,35$ for unfavourable dead loads is applied. However, the organizing committee requested a global safety of 10, since the installations are accessible for public. For all elements, exposed to a failure with no deformation failure indication, this global safety factor is applied.
The governing areas for the structure are the suspensions, with the corresponding load introduction points.
It is mentioned, that due to this fact, the structure has been split in two independent systems, suspended from two points in the roof. For the documentation later in the *Portikus* in Frankfurt, the complete structure is installed. The documentation illustrated in this chapter is given for the complete mobile, as shown in fig. 5.27.

5.3.4.4 Member forces

The force gradients of the complete structure N, M and V are given in appendix C.2 on page 256. The governing forces are naturally in the topmost beam, not only because of the accumulation of the weight, but also because of the greatest distance between two suspenders, causing the bending moment in the beam.
Each element has a concrete volume of $V_c = 2,2 \times 15 \times 48\,\mathrm{cm} = 1584\,\mathrm{cm}^3$. This corresponds to a weight of 39,6 N. The total gravity load of the 23 elements of the mobile sums up to 0,91 kN (91 kg).

The governing characteristic member forces, all in the top beam, are:

axial force $\qquad\qquad N_{\mathrm{k,max}} = 911\,\mathrm{N}$

bending moment $\quad\ \ M_{\mathrm{yk,max}} = 210\,\mathrm{Nm}$

shear force $\qquad\quad\ \ V_{\mathrm{zk,max}} = 585\,\mathrm{N}$
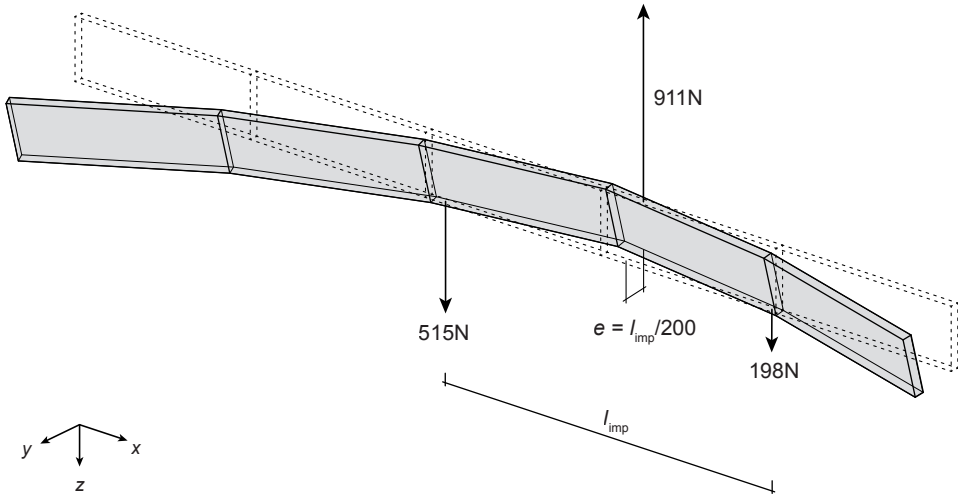
Figure 5.28 Buckling shape of topmost beam of *Stable Equilibrium* with the governing compressive zone of the segmented system

5.3.4.5 Buckling

The main failure criterion is given by buckling effects in the topmost beam of the concrete mobile. Within the section, between the two loads from the adjacent mobiles below, a bending zone arises, with the tension zone in the top half and a compression zone in the bottom half of the section. The compressed area of the lower part of the section is exposed to a deflection out of plane. The qualitative buckling shape is illustrated in fig. 5.28. In order to consider this buckling effect, within the design of the components, a calculative eccentric shape is analyzed, where the magnitude of the eccentricity is taken as $e = l_{imp}/200$. With $l_{imp} = 89$ cm, the eccentricity gives $e = 4{,}5$ mm.

According to the bowden cable principle (more comprehensive illustrated in section 7.2.1), the prestressing procedure does not cause any stability failure. Buckling effects are caused by outer loads only.

The mean compressive stress, causing stability failure of the bottom part of the section, is dependent on the outer load and the inner lever arm of the section, taken as $h_{i,z} = 9{,}4$ cm. With the maximum outer bending moment of $M_{yk,max} = 210$ Nm, the resultant inner forces result to $D_k = Z_k = M_{yk,max}/h_{i,z} = 2234$ N.

This compressive inner force, with a calculative eccentricity derived from the buckling

shape, causes a bending moment in direction of the narrow axis of the section, resulting to $M_{zk,max} = D_k \cdot e = 9,94\,\mathrm{Nm}$. The inner lever arm, available in the narrow direction, is considered with $h_{i,y} = 7\,\mathrm{mm}$. The corresponding characteristic equivalent buckling force, to be bore by the threaded bar in the compression zone, results to $D_{k,imp} = Z_{k,imp} = 1420\,\mathrm{N}$. Considering the safety factor of $\gamma_G = 1,35$, the design value is $D_{d,imp} = Z_{d,imp} = 1917\,\mathrm{N}$.

5.3.4.6 Details

To introduce concentrated loads from the suspenders into the concrete, embedded items are produced. All items are planned to provide M6 screw threads, to allow a quick installation, where the swaged terminals of the suspension cables are simply screwed in. The layout of the items separates between the hangers and the suspenders. To allow adjustments on site, the items housing the hangers are within a sliding device. Generally the complete structure is viewed from below, consequently the anchor points on the bottom side, housing the suspenders, are as unobtrusive as possible. The items provided with a sliding support for the hangers are on the top side of the elements. An isometric illustration of both types of embedded items is given in fig. 5.29.

Detailed dimensions as well as the ultimate stress analysis are illustrated in appendix C.3 on page 260.

The concept of the items is the transfer of concentrated loads through the concrete sections to the respective opposite face. Thus the load paths have to cross the hulls of the prestressing cables. With two welded butt straps, the force is guided on both sides of the hulls to obtain the slenderness of the section. At the end of the butt straps, the load is transferred into the concrete with blank steel bolts, pushed through holes in the steel plates. The position of the bolts prior concreting is secured by the double side formwork.

5.3.5 Fabrication

5.3.5.1 Formwork

The structure as an exhibition object demands a high-grade surface quality. Naturally every concrete object requires an infiltration opening or an open face of the formwork. Supplemental to the decision, to locate the sliding devices on the upper side of the elements, is the layout of the formwork with the open side up. This also leads to a higher precision of the edge between two connecting faces. The element edges become absolutely rectangular. Consequently, the concrete needs to be cast inside a vertical orientated formwork, inside
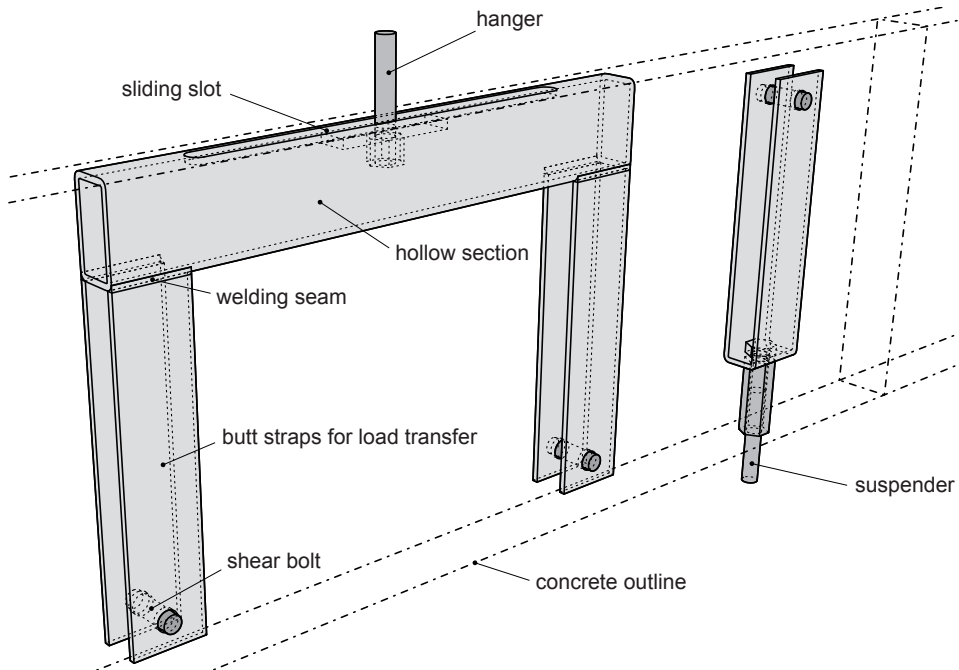
Figure 5.29 Embedded steel items for the concrete mobile, to transfer concentrated loads around prestressing hulls

the narrow side.

Since each element has identical dimensions with no curvature, medium density fibre-boards (MDF) were used for the formwork. The raw material is highly water absorbing. Therefore all sides facing the concrete are covered with a synthetic adhesive foil with a slick surface, to achieve a concrete surface as shiny as possible. The narrow formwork faces are both, the edge surface, as well as spacers, in order to achieve the desired thickness of 22 mm.

5.3.5.2 Reinforcement configuration

The planned layout of the mobile requires an accurate configuration of the embedded items, the hulls and the shear studs of the joint areas. All of these items are exactly positioned, according to shop drawings and fixed at the formwork with bolts, plunged in the

(a) embedded item suspender

(b) sliding device hanger
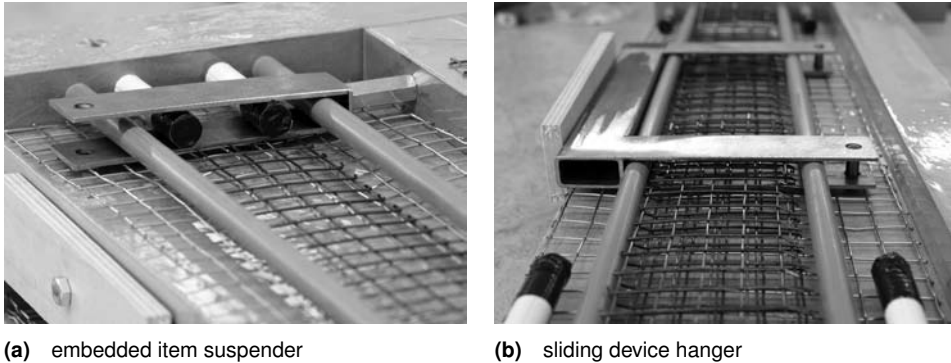
Figure 5.30   Configuration of embedded items screwed onto the formwork and enclosing prestressing hulls

formwork spacers. In order to keep the track of the system, the elements are numbered in the pattern of the global layout, *A–G* for the seven beams in the vertical sequence, and *1–5* for the horizontal progression of each element.

The high slenderness of the concrete elements and the embedded items are somehow conflicting, since the steel flanges disturb the continuity of the longitudinal reinforcement to a certain degree. Every element has one continuous sheet of micro mesh reinforcement on each outer side of the element, regardless of the presence of embedded items. Within the centroid of the elements, additional three continuous reinforcement layers are located in between the hulls, as shown on the photographs in fig. 5.30. The so achieved ratio of reinforcement, mainly required for shear resistance, is sufficient for the maximum loads occurring.

5.3.5.3 Concreting

One benefit of the fact that each element of the concrete mobile has identical dimensions, is the possibility to reuse the formwork. However, caused by logistical simplifications, the whole structure is cast within one single attempt, leading to the compulsion that no casting errors occur, to guarantee that the concrete properly flows in all areas of the formworks, passing the hulls. A neat observation of the slump size determines the casting process here.

(a) Open faces for concrete casting from the top **(b)** Casting process undertaken in three steps
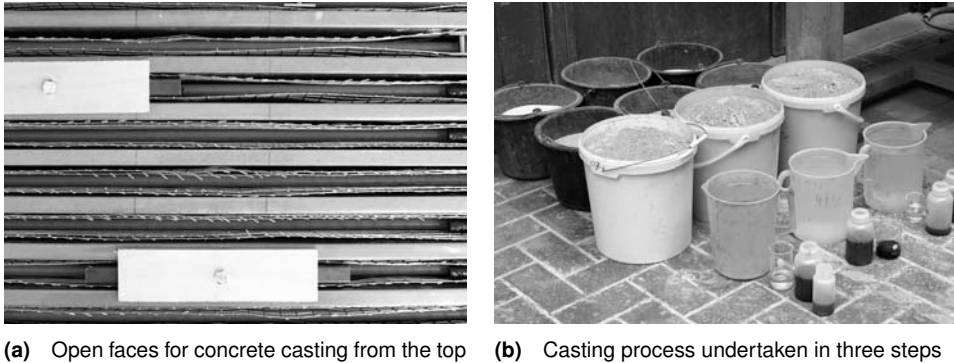
Figure 5.31 Concreting of the mobile elements

5.3.6 In exhibition

For eight weeks the concrete mobile was presented to the public in the *Muziekgebouw* in Amsterdam. The installation happened within the short given time frame. Preassembled on the third floor west balcony, as shown in fig. 5.32, the structure is lifted by a team of riggers and fixed with clamps on the steel structure of the theatre roof. The mobile in exhibition is shown in fig. 5.33. Due to the high self weight of the elements, the floating of the beams is very slow, comparable with hands of a clock. The slow transformation, caused by the gentle indoor airflow, led to the desired confusion, based on the paradox of lightness and concrete.

The non-destructive removal of the structure at the end of the exhibition, went as quick as the rigging. Therefore the re-assembly of the structure in a different venue was possible without any fabrication demands.

The structure hanging in the *Portikus* in Frankfurt is shown in fig. 5.34.
The main difference in the representation are the different suspensions: Colorful climbing ropes in Amsterdam and thin confected steel cables in Frankfurt. Although the concept of the mobile is identical, the impression is completely different.

The concrete mobile serves as a proof of concept for joining prefabricated concrete elements in a dry-fit connection method. The use of prestressing devices allows an assembly of extremely slender concrete objects. With the help of embedded items, concentrated
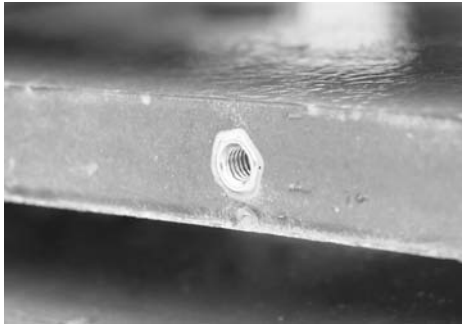
(a) Suspension points visible from below as un-remarkable are possible
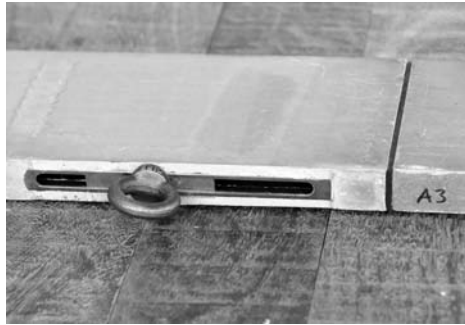
(b) MDF-spacers between to concrete elements to avoid stress peaks in joints

(c) Sliding device with ropes as suspension

(d) Prestressing threads and countering nuts

Figure 5.32 Close-up details of the concrete mobile prior to lifting

loads can be introduced, enabling the slender elements to be part of a superior structural system that can also be de- and reconstructed.
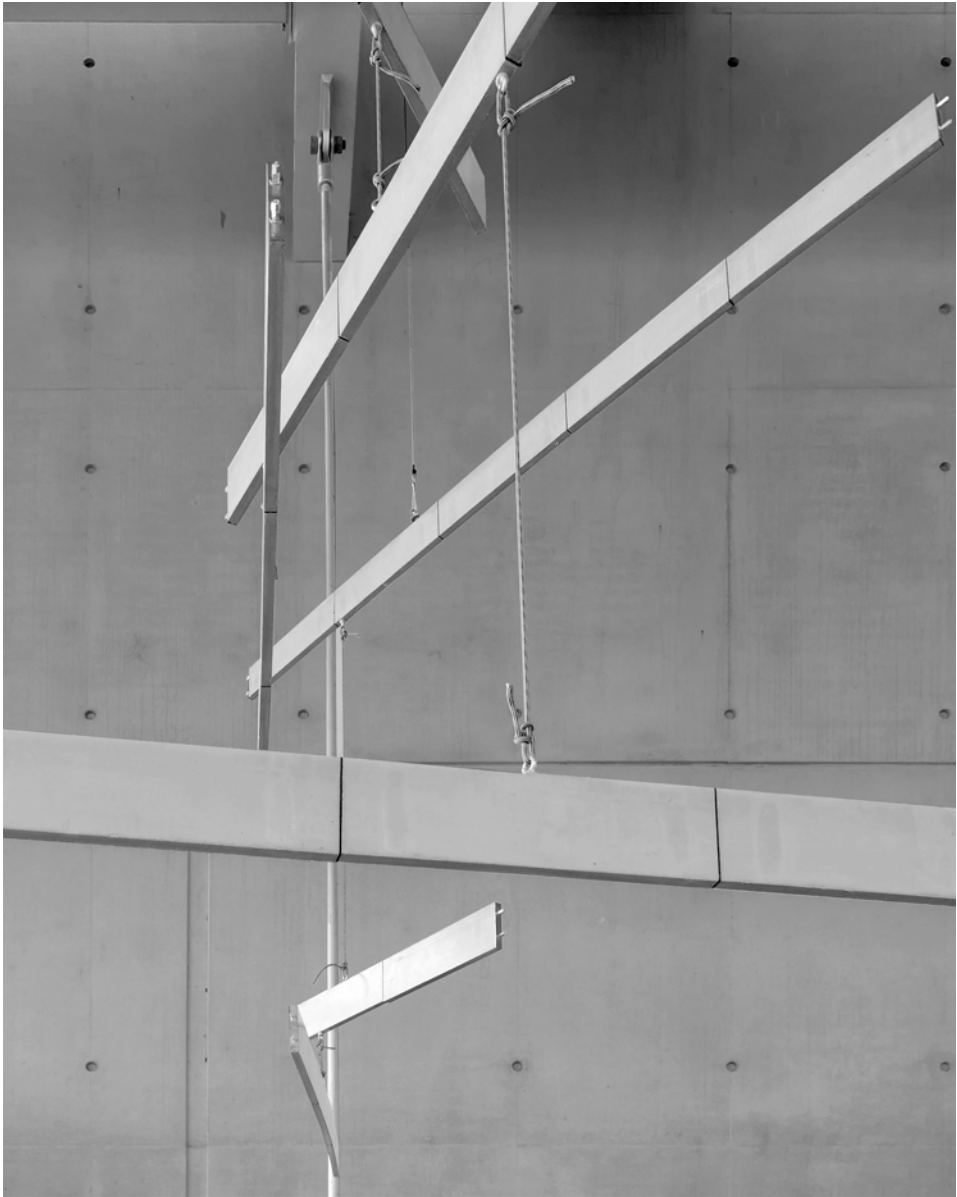
Figure 5.33 *Stable Equilibrium* in exhibition in the *Muziekgebouw* in Amsterdam

Figure 5.34 *Stable Equilibrium* hung up in the *Portikus* in Frankfurt ©*Stefanie Pretnar*
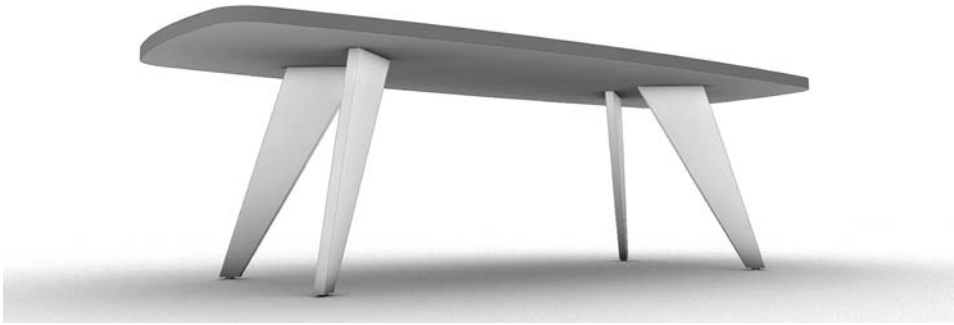
Figure 5.35   Visualisation of the dining table with inclined concrete legs

5.4 Concrete table substructure

5.4.1 Motivation

In chapter 7, the constructive capabilities of micro prestressing connection techniques are discussed. The load bearing sequence of prefabricated elements is realized with a pre-compression of the respective joint areas.

This concept can be pursued as a technique to attach prefabricated concrete elements onto existing structures. The prestressing wires have now to be fixed from one side only, with a well countered and ideally hidden screw end nut.

The dialogue with the industrial designer *Robert Cristinetti*, founder of *Cristinetti – Studio for Planning and Design*, led to the request to redesign an existing conference desk. The table ought to serve as a dining table with the transformation of the solid wooden table legs, to a relieved arrangement of inclined table legs made of concrete.

5.4.2 Design intent

The starting point of the design is the authenticity of the selected materials. This is the warm surface quality of the wooden tabletop on the one hand and the resilient appearance of the concrete as a substructure on the other hand. The appropriateness of the materiality is emphasized with the self-conscious tolerating of the natural wood structure and the effort to accomplish a surface of artificial stone, as evenly as possible.
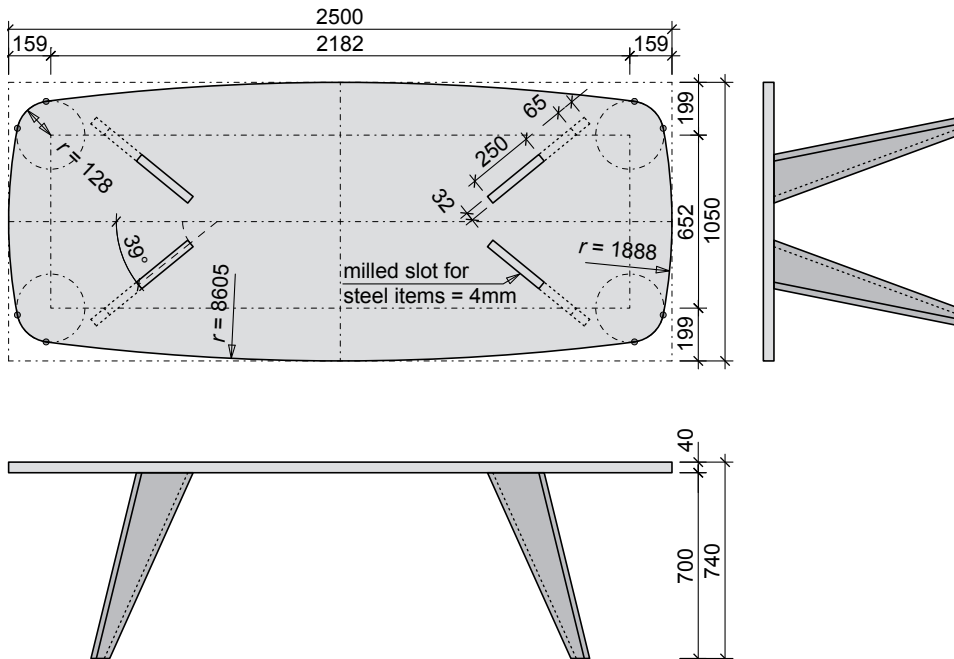
Figure 5.36 Dimensions of dining table with concrete substructure; [mm]

The verifying and appliance of construction techniques in a furniture scale, is simplification and difficulty at the same time. Naturally the handling of elements is possible without cranes and construction stages are of minor priority. However, the demands on indepth designed details and surface qualities are the fundament of a building construction, serving as a piece of furniture.

As a design specification, an invisible structure is requested, also for the worms-eye view. Thus a clear transition of the concrete and the wooden table board with no visible screws or plates is taken as a boundary condition of the construction design.

The result is a substructure of four individual cantilevering flat concrete elements. The bracing of the structure is given by the geometrical arrangement, with two points of intersection of the respective shell centerlines and hence a minor load impact around the weak axis of the elements. The inclined shape of the legs emphasizes the structural necessity of tension resistant fixings, oppositional to common trestles, standing by themselves.
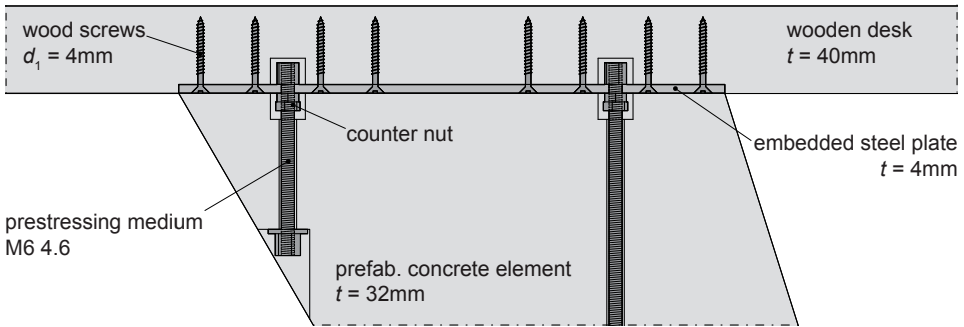
Figure 5.37   Concept of prestressing connection hidden inside the concrete and wood desk

The envisaged material of the table top is a solid plate of continuous bonded oak timber bars.

The substructure made of slender concrete shells acts as a designwise counterpart. All structural mounting parts at the fixing points are hidden inside the architectural elements. Figure 5.36 shows the dimensions of the envisaged dining table with the concrete substructure.

5.4.3 Structure

5.4.3.1 Loads and safety factors

The table desk has a length of 250 cm and a width of 105 cm. The shape is derived with an allocation of different construction radii, as shown in the top view of fig. 5.36. The surface area results to 2,44 m². With a thickness of 40 mm and a weight density of $\rho_{oak} = 8,4$ kN/m³, the characteristic gravity load of the desk is $G_{desk,k} = 0,82$ kN. The surface area on one concrete leg is 0,11 m². With a concrete thickness of 32 mm, the characteristic load of the complete substructure is $G_{legs,k} = 0,35$ kN. Thus the total self weight of the table results to $G_{tot,k} = 1,17$ kN.

The life load is considered with $Q_{tot,k} = 4,0$ kN, the equivalent load of four people sitting simultaneously on each corner of the table.

Multiplying with the safety factors, considered as $\gamma_G = 1,35$ and $\gamma_Q = 1,5$, the total design load is $G_d + Q_d = 7,6$ kN and thus a reaction force of 1,9 kN per leg.

(a) Open formwork with reinforcement and pre-stressing hulls

(b) Close-up detail of the prestressing appliance in the formwork
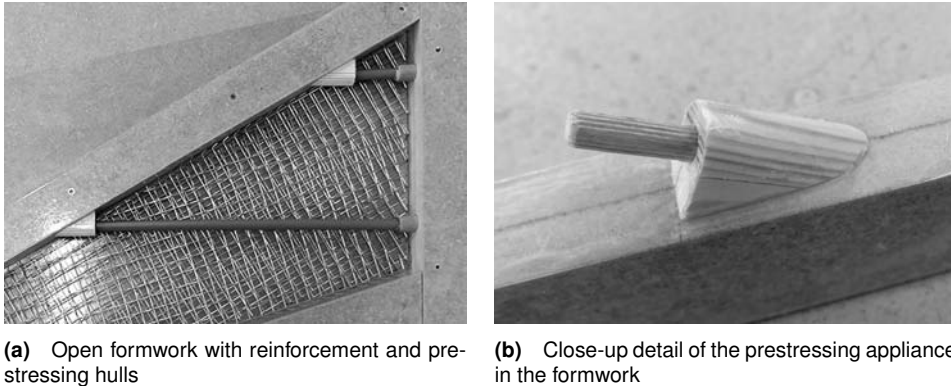
Figure 5.38 Fabrication of the table legs formwork and reinforcement with high attention to surface quality and formwork tightness

5.4.3.2 Materials and detailing

The high performance concrete, the micro mesh wire reinforcement, prestressing threads and embedded steel items used for the table substructure, are identical with the materials used for the concrete mobile. The respective material characteristics and resistant forces can be taken from section 5.3.4.2. The resistance of the wood screws against pulling out of the table board as well as the tensile strength of the prestressing media, are given in appendix D.2. The type of wood, chosen for the table top, is oak, with the structural advantage of a relatively high density and hence a high resistance against pulling out of tensile stressed wood-screws.

The outer lever arm (the horizontal distance from the reaction force to the fulcrum of the cantilever) and the inner lever arm (the distance from the fulcrum to the anchor points, facing inside the table) are almost identical and constitute the equilibrium of the joint restraint. Accordingly, the force of the inner threaded bars, induced by outer loads, is identical with the reaction force. Due to the consistent force direction, the outer bars are not contributing to the load transfer and serve as a location fixation.

Figure 5.37 illustrates the mounting concept with the prestressing items, hidden inside the wooden desk, and the prefabricated concrete elements.
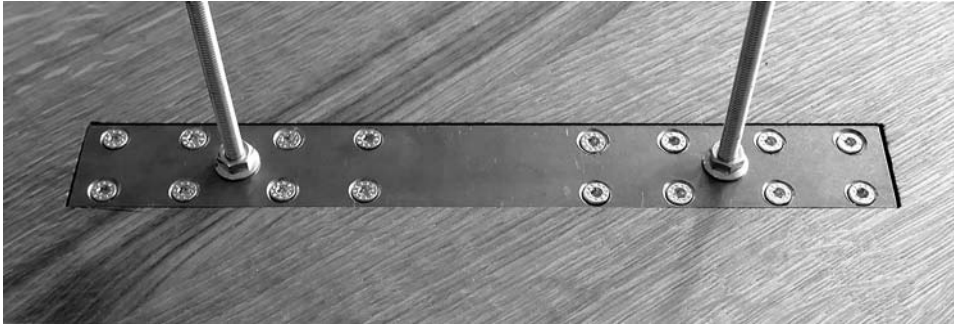
(a)   Embedded steel items screwed into the timber with threaded bars for mounting

(b)   transition from timber to concrete with no visible structure

(c)   Threaded bar end and mounting nut

Figure 5.39   Close-up details of the load bearing connections of the table substructure

5.4.4 Fabrication

The basic material of the formwork is medium density fibreboards (MDF). The side faces, also serving as spacers, are assembled with two boards 16 mm each, to achieve the desired diaphragm thickness of 32 mm. All areas facing the concrete, are covered with a synthetic adhesive foil to achieve a shiny concrete surface, analog to the formwork technique of the concrete mobile. However, a new aspect led to the necessity to produce the entire concrete substructure twice: The envisaged concrete openings chosen are the narrow faces of the soles, facing the ground, the only non-visible faces in the serviceability state. Thus the elements have to cast upside down, leading to a concrete pressure height of 70 cm, in

comparison to the 15 cm of the concrete mobile, an increase factor of almost five. This results in a water drainage of the ready mixed concrete, with unwanted discoloring at the edges. Consequently, the formwork of the second trial is sealed with a twin-sided adhesive sealing, made of a special cellular foam, squeezable to almost zero thickness. The initial application of this foam, *DuploCOLL®*, is the sealing of fridge elements.

Special consideration is given to the recessing of the end screw nuts of the fixation, located in the inner-facing inclined flanks. Also resulting from the experience of the first trial, the remaining edges are delicate for breaking and therefore formed rounded and as small as allowed by the plain washers, as shown in fig. 5.38.

Although the four elements are identical, the concrete casting is carried out in one step, to avoid gradients in the coloring of the concrete.

5.4.5 Ready for dinner...

The oak bars are glued together, planed and cut out by a carpenter. The surface is given a wax finish. The assembly of the prefabricated elements and the desk is unpretentious and requires a screw driver and an open end spanner only (fig. 5.39).

The table in service fulfills the designwise requirement to have a delicate substructure, emphasizing the longitudinal orientated wooden desk, as shown in fig. 5.40. The light grey-shiny colouring of the exposed concrete faces seem to be lacquered, although the concrete is untreated.

Figure 5.40   Finished dining table ready for service

6 Seamless rigid connections for prefabricated shell elements

6.1 Segmentations in concrete construction

Segmentations in reinforced concrete elements are applied in a standardized way in building construction. Concrete buildings are naturally not cast in one monolithic piece, but rather in a number of sections, divided by joints. The casting segments are usually planned accurately, thus the design is motivated either by the construction progress, or joints are arranged due to constructive and structural reasons. Typical applications for construction joints are:

Construction stages Dependent on the size of the building element to be cast on site, different construction sequences may be necessary. Geometrical issues may cause the necessity of one cast element to support its adjacent element. A typical example is the transition between a concrete wall and a floor slab, where the floor slab carries the formwork of the wall. Also time lapse issues of the construction process may lead to the application of segmentations.

Contraction joints During the curing process of ready-mixed concrete, shrinkage occurs. Shrinkage terms the shortening, respectively the reduction of the concrete volume over the time, caused by the release of water during the drying phase and microstructural transformations from the hardening process. It is independent from loading conditions. Shrinkage end-values $\varepsilon_{cs,\infty}$ can account for up to $-0,6\,\mathrm{mm/m}$ under adverse boundary conditions. Due to restraints and support conditions, shrinkage leads to tensile stresses in the concrete, which are abolished by the cracking of the concrete. These shrinkage crackwidths are limited to certain values, for aesthetical reasons, as well as to reduce the water permeability and the carbonation depth of concrete, in order to prevent corrosion of the reinforcement. Crack sizes can be limited by the amount of reinforcement, the mixture

(a) Formwork stop-end prior casting   **(b)** Formwork stop-end after casting
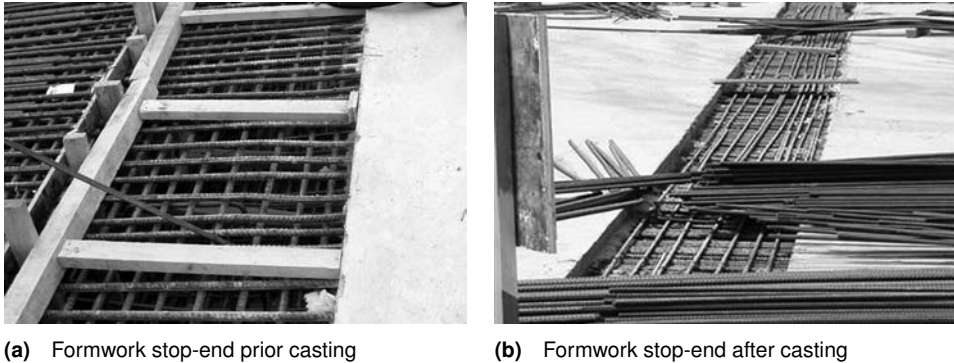
Figure 6.1   Wooden hand crafted stop-end for a settlement joint in a raft foundation, where the holes for the rebars are drilled through

recipe and the post processing of the concrete. To avoid excessive restraints, the concrete elements can be built smaller and thus segmented.

Settlement joints   Restraints are not necessarily caused by shrinkage, but also by un-even settlements. A typical example is given by the construction of foundations of highrise buildings, together with adjacent buildings. When both parts of the foundation (the high loaded part of the highrise and the less loaded part of the adjacent building) are combined, due to user demands or requirements to water tightness, stresses occur, caused by different settlements, and movements have to be temporized. This can be solved with temporary joints, where the reinforcement is running continuously through. After erection of the buildings, when major parts of the settlements are occurred, the joints are cast and closed. Such a joint on site is shown is fig. 6.1.

Predetermined breaking joints   Construction with reinforced concrete implies the handling with cracks, since it is a construction method, based on the formation of cracks to activate the tension capacity of the reinforcement in the first place. Furthermore, due to the shrinkage effects mentioned above, cracks in concrete constructions are unavoidable. However, there are techniques to guide the cracks by inventing a systematic weakening of the cross section. This can be achieved by using separating ties, retarding parts of the concrete bonding. These techniques are also applicable for non-structural concrete elements, like industrial floors.

Mounting joints   There are manifold reasons to design with prefabricated concrete elements. The main advantages are logistical issues, since the curing phases can be scheduled independently from the building erection processes. The formwork and casting can be done under factory or even laboratory conditions, without considering weather and seasonal characteristics. This leads to more accurate results that are even considered in the building codes. Nevertheless, the design with precast concrete components has a major influence on the complexity of the building and requires high planning efforts to the design of the (mostly load bearing) connections of the components.

Whatever the motivation is based on to design with segmented concrete components, an evaluation of the demands of the load bearing capacity needs to be undertaken. A fully or even partly rigid, and thus load bearing connection, leads to the requirement of a continuous reinforcement running through, that has to be considered, when the individual segments are built. The challenge here is to build a formwork that is tight enough to withstand the hydrostatic pressure of the ready mixed concrete, but still allows the reinforcement to stick out on at least one surface of the building element.

6.2 Stop-end techniques as formwork banks

6.2.1 Stop-ends in building industry

The term 'stop-end techniques' describes solutions of the building industry to achieve formwork systems for concrete surfaces that will have adjacent concrete elements in the finished state. It generally implies a required reinforcement, running through the joint, to achieve a load bearing connection.

As a traditional solution, stop-end formworks are made of timber, with drilled holes for the longitudinal reinforcement to stick through, as shown in fig. 6.1. This technique can be time consuming, since it has to be built manually. With the removal of the formwork, prior casting the adjacent bay, an additional working step is required.

The removal of the formwork can be omitted by using permanent or lost formwork, like galvanized expanded metal. In this case, the reinforcement is simply punched through, or attached, as shown in fig. 6.2. Depending on the product used, the expanded metal fulfills requirements of the roughness of the joint to also provide a shear force capacity. However, attention has to be paid concerning the problem of concrete bleeding. The expanded metal

(a)   Formwork stop-end prior casting   **(b)**   Formwork stop-end after casting
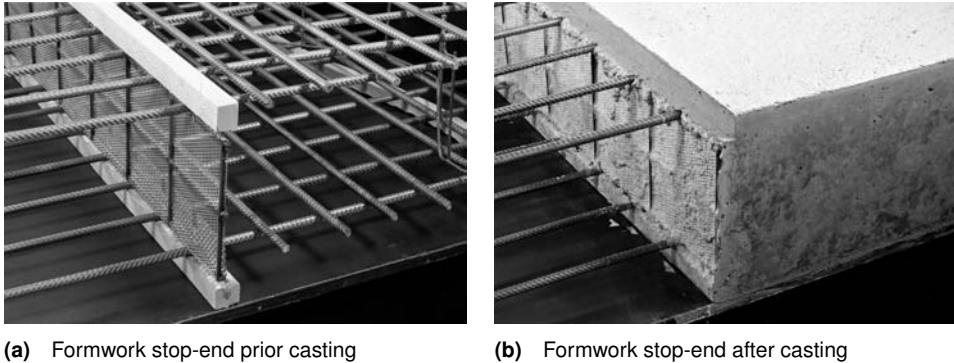
Figure 6.2   Expanded metal prefabricated stop-end *Stremaform®* as permanent formwork

has a certain percentage of openings, therefore it is not watertight. During the casting process, these openings are blinded by the aggregates, after a certain amount of the cement slurry has flowed out already, with the consequence of a changed microstructure of the concrete mixture. The consequences of the bleeding are increasing, the more fluid the concrete and the smaller the aggregates of the grading curve.

Cast-in starter bar solutions may speed up the processes of forming construction joints. Reinforcement boxes are simply nailed on the inner face of the formwork surface and cast in the concrete element. These boxes are containing reinforcement bars to be bent into position after removal of the formwork, as shown in fig. 6.3. These continuity strips help to avoid damage of concrete and reinforcement bars, in contrast to traditional timber solutions, although the straightening of the rebars naturally disturbs the microstructure of the steel. This technique therefore is limited to a diameter size of 16 mm [Ben02, 116]. The typical application is the connection of staircase runs and slabs with walls.

6.2.2 Stop-ends for mesh wire reinforcements

6.2.2.1 Problem statement of crosswise reinforcement

The construction concept of the *Möbiusban(k)d*, described in section 5.2, envisaged a fully rigid concrete shell, withstanding membrane as well as bending forces. Consequently, the connections of prefabricated elements have to be load bearing, with the longitudinal and transversal reinforcement running continuously through the joints. The applied material

(a) Box on the outer concrete face

(b) Starter bars prior to straightening
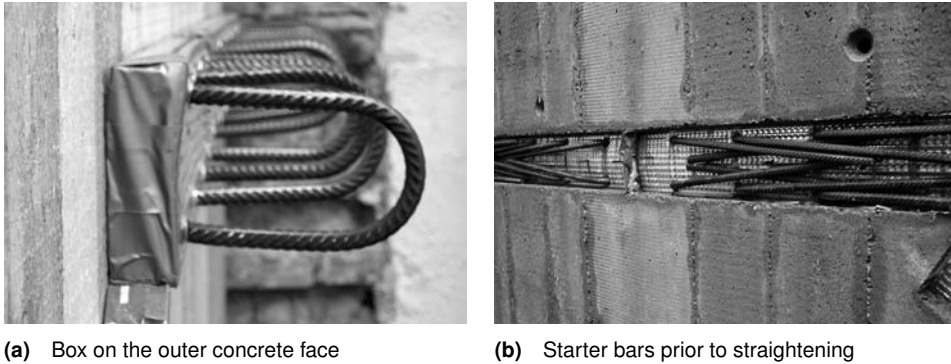
Figure 6.3   Cast-in starter bars, transition of a staircase-run to the adjacent concrete wall
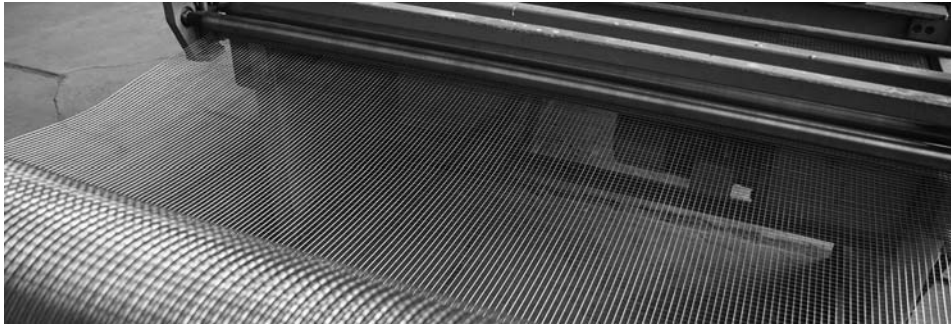
Figure 6.4   Micro mesh reinforcement mats *MicroMat*, to be stapled over the entire cross section of the concrete element

for the shell is a high performance concrete, reinforced with layers of micro mesh reinforcement. This material, developed by *DUCON*, is further described in section 4.1. The mesh-wire reinforcement is shown in fig. 6.4

Each prefabricated segment of the *Möbius*-strip naturally has two neighboring elements, therefore two faces of the formwork have the requirement, both, the reinforcement meshes to stick out and the formwork to be watertight. These two requirements, combined with the fact that the faces are underlying a double curvature, forecloses the implementation of a traditional stop-end technique, anticipated in section 6.2.

6.2.2.2 Demands of double curved formwork sealing

The minimum demands on possible formwork ends for mesh reinforcements, are as listed below:

> *Tightness*: Since the concrete needs a high flow ability to ensure it runs through the reinforcement meshes, the formwork needs to be completely sealed. Otherwise the concrete would quickly pour out of its formwork.

> *Pressure resistance*: The hydrostatic pressure of the ready mixed concrete (due to its self-weight of $2,5\times$ the water pressure) is the most crucial issue to consider for the formwork construction. The most extreme shell element, envisaged for the *Möbiusban(k)d*, reached a formwork height up to $70\,\mathrm{cm}$, leading to a hydrostatic pressure of $\sim 18\,\mathrm{kN/m^2}$.

> *Mouldability*: The faces are double curved and the formwork material of the stop ends has to fill in between the reinforcement mesh wires. Thus the material used needs to be moldable, with a grain size not bigger than the one applied for the concrete.

> *Removability*: The process of sealing the formwork needs to be complete reversible. The removal of the filling material needs to be undertaken without damaging the reinforcement meshes. Furthermore, no residues should be left on the steel wires, which may lead to a possible reduction of the concrete bonding.

6.2.2.3 Options for double curved formwork sealing

The options for possible formwork ends, considered in the following paragraphs, have to fulfill the requirements listed above.

Loose sand One method for the construction of a formwork stop-ends for mesh wire reinforcements, is the usage of loose sand. A procedure for the casting of industry floors, reinforced with 3D mesh-wires, is developed by *DUCON*: The joint lines can be positioned with a small embankment of sand. With the usage of self compacting concrete, the sand is not pushed away. After the concrete is cured, the sand embankment can be removed with a vacuum devise. The application of this method requires the consideration of the effect that the water – cement ratio might be disturbed near the joint area.
Naturally, this method is only relevant for systems with almost no hydrostatic concrete pressure.

Wax sealing   There are already existing formwork systems made of wax, as described in section 4.2. Wax is moldable, watertight and removable (although not completely) with the usage of heat. However, it might require big containers, depending on the formwork geometry, to dip the formwork edges into the wax, that excludes that material for further considerations.

Modelling kneading material   Tightening of the formwork edges with kneading materials might lead to a tight and pressure resistant formwork, but similar to the usage of wax, the complete removal is complicated. Thus there is a risk of not achieving the full bonding between concrete and steel reinforcement.

Construction foam   Polyurethane (PU) foams are widely used in construction, especially for the fitting of window frames and door cases, but also for sealing issues. It can be spread by spraying and easily finished by cutting, sawing or grinding. However, the removal without damaging the reinforcement is almost impossible and the foam has a high bonding itself, therefore remnants will persist on the reinforcement steel.

Silicone   Similar to the construction foam mentioned above, sealing materials from silicones are not applicable as stop-end materials, due to the difficult removability from the reinforcement bars.

Mortar   A promising material to use for the stop-ends is mortar, since it has a similar consistence and structure as concrete. It is easy moldable, depending on the viscosity adjusted, and it is tight and pressure resistant. The only issue is obviously the removability, when cured. One solution is the build-up of a permanent sealing, using a mortar with the same compressive strength as the concrete, which is difficult to achieve. Another option is the usage of a mortar that does not harden with a cement based binder, but with a water soluble medium. As a result, the mortar used for the formwork sealing can be washed off.

Here the option of using water soluble mortar is the option chosen for the further investigations.

6.3 Formwork sealing concept with dissoluble mortar

6.3.1 Schemed construction process for rigid joints

The joint connection concept of the *Möbius*-sculpture envisaged a fully rigid connection of single shell segments. The reinforcement is supposed to be fully utilized and hence has to run through continuously. The joint therefore needs a certain width to ensure sufficient embedment and lap splice lengths.

The construction sequence consists of three general steps:

(1) The casting of single segments, with the reinforcement sticking out (fig. 6.5a)

(2) The exact placing and setting of the segments to each other. This step includes the overlapping reinforcement within the joint area. The width of the joint is set to 10 cm to provide enough space for the reinforcement embedment (fig. 6.5b)

(3) The casting of the joint area (fig. 6.5c).

6.3.2 Building lime – a water soluble mortar

Building lime or lime hydrate is a bonding agent applied in the building industry. It is used for the production of lime mortar as masonry mortar and plaster material. Air hardening limes are non-hydraulic and usually used in combination with hydraulic binders, like cement, to enhance the compressive strength properties.

Building lime mortars are a composition of building lime (one part) and sand (three and a half parts) and widely used as plaster materials. The reason is a higher elasticity of lime mortars, compared to cement mortars, thus it is less susceptible to cracks in plastered facades. Minor movements of the building, from temperature or environmental changes or settlements, can be graduated. Because of the solubility of the lime, fine cracks in these facades are able to 'heal', when surfaces are exposed to humidity.

One application of lime mortar, discovered by the author, are temporary wall structures, especially in masonry training workshops. The consistency of the mortar is the same as hydraulic mortars and the compressive strength is sufficient for horizontal joint beds. For masonry training workshops and examinations, the walls have to be de-constructed and materials have to be separated for multiple use. In this specific case, the mortar is simply scratched and washed off the bricks.

concreting opening   exhaust
                                                        mortar sealing

                                                        mesh reinforcement

upper formwork

                                                        lower formwork

(a) Casting of the single shell segments

reinforcement overlapping

100 mm

(b) Arrangement of segments and adjustment of reinforcement

concreting opening

joint formwork

(c) Casting of the joint
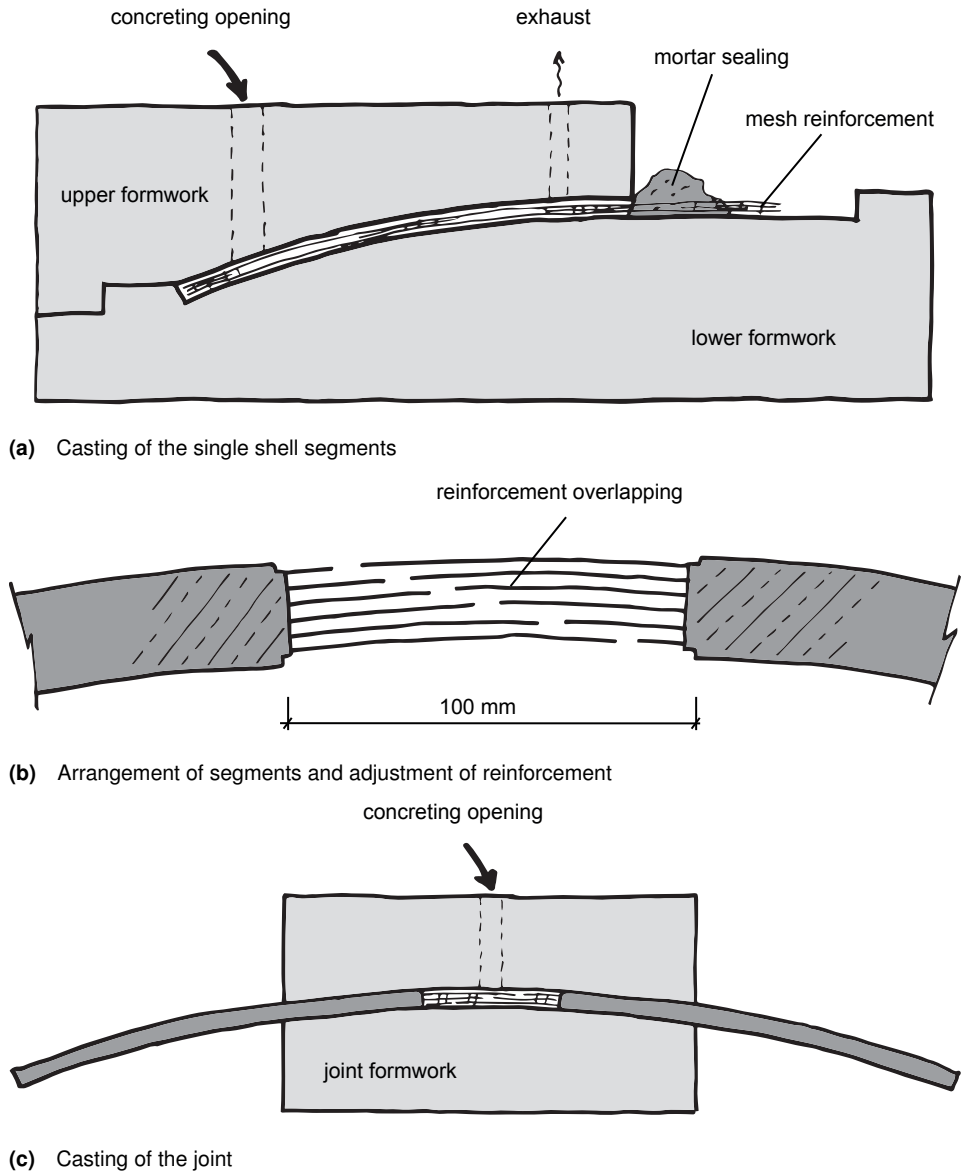
Figure 6.5 Construction sequence of the rigid joint connection concept

These prerequisites seemed to meet all requirements for the application as a formwork sealing for stop-ends, since it is easy moldable, reasonable water tight and compression resistant, as well as thoroughly removable by the use of water, without affecting the reinforcement.

6.3.3 Rigid joint prototypes

Rigid joint prototype – trial #01   To start off the procedure of verifying the joint connection concept, a random shape for a concrete shell has been designed. A free form shape with a constant thickness of 20 mm was chosen. Each segment size has a projected area of 30×40 cm. One face of the shell has the reinforcement sticking out for the connection with the adjacent element. The width of the joint is 10 cm. Parallel, a complete flat element was designed, with the same projected area, to be able to cast the shell without an upper formwork.

The formwork is milled foam, coated with lacquer, to assure the concrete is not bounding on the foam surface. The formwork edges provide an interlocking boundary for a precise closing of the formwork that needs to be complete watertight. The boundary faces, with the reinforcement sticking out, are sealed with water soluble mortar.

The reinforcement consists of six layers of mesh wires.

The concrete used has a mixing recipe recommended by the industry partner *DUCON* and envisaged a grain curve layout with a grain size of $0 – 1{,}2$ mm.

Generally, the reinforcement technique with mesh wires has high requirements on the consistency of the concrete. The size of the slump has to be controlled throughout the whole mixing and casting process. The slump controlling is done with a *Hägermann*-cone (refer to section 4.1.3.3). The experience of several trials of mixtures shows the sensitivity of the concrete texture: The boundary conditions, like the water temperature, air temperature and type of mixing lorries, have to be predefined. Also the time schedule of the mixing and casting process has to be controlled throughout the whole process.

The casting of the first prototype lead to failure, since the concrete did not flow into the formwork and soon plugged the concreting opening. This failure was due to major mistakes. Firstly the slump size was too small. Instead of the $36 – 38$ cm, recommended by the supplier, it achieved 32 cm only. Adding more water did not result in a bigger slump, but in a bleeding of the concrete, as shown in fig. 6.6. Secondly, no air exhaust was provided in the formwork. Thus, the displaced volume of the concrete was not able to escape. The failed test pieces are shown in fig. 6.7.

(a) The slump dispersion width of 32,3 cm is to small for the concrete to flow through the mesh wires

(b) Bleeding of the concrete because of adding too much water
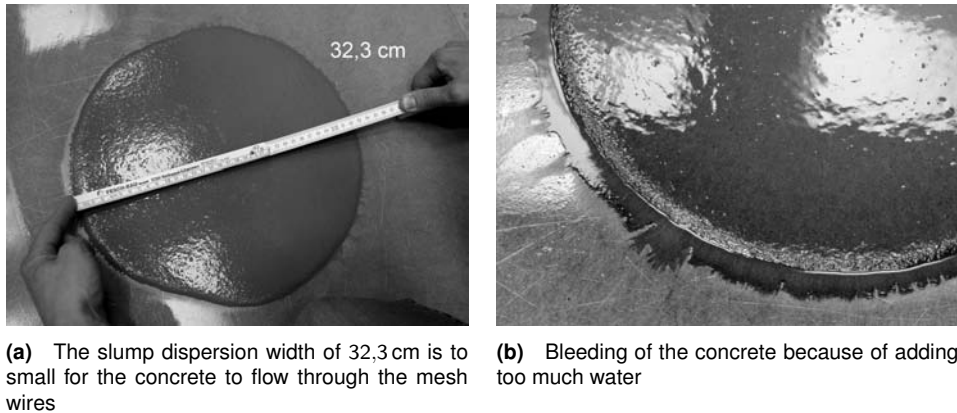
Figure 6.6 Control of concrete slump; an extreme water cement value leads to concrete bleeding

(a) Formwork of one segment. The joint face is sealed with mortar – an air exhaust is missing

(b) The concrete did not flow through the mesh wires – the concreting opening is plugged
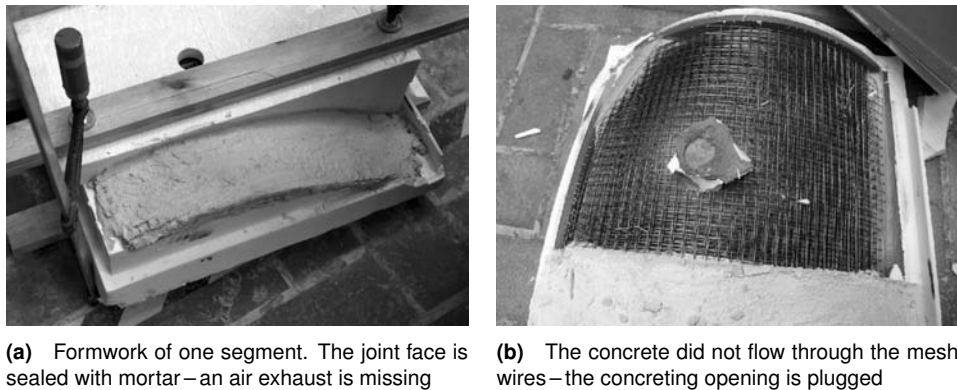
Figure 6.7 Failure result of the first joint connection prototype

Rigid joint prototype – trial #02 Since the first trial lead to failure, the errors were identified and changes were implemented for the second approach. The overall surface geometry was kept. The improvements were the following:

> *Increase of slump size*: As the most urgent improvement, the necessary increase of the slump size was identified. Simply adding water leads to a bleeding of the concrete and thus to a reduction of the compressive strength. Similar effects occur by adding more flow agent. The only adjusting left is the change of the grain

curve. The maximum grain size here is increased from 1,2 mm to 2,0 mm. The increasing of the grain size leads to a reduction of the overall surface area of the grains that have to be moistened during the mixing process. Therefore the fluidity can be increased without affecting the delicate water–cement ratio w/c. A mixing trial led to a slump size of 36 cm, which was set as a minimum value.

Increase of of shell thickness: To allow the concrete to flow through the mesh wire filaments, the shell thickness was increased from 20 mm to 35 mm, without increasing the number of reinforcement layers. Narrow spacers between the reinforcement and the formwork were implemented.

Adaptation of formwork borders: The formwork was adapted with more stable borders to be able to attach the upper and the lower formwork with outer pressure, without destruction of the weak foam material.

Presetting of the infiltration path: To avoid a plugging of the concreting opening, the location of the infiltration hole was located at the deepest point of the shell, with a corresponding exhaust at the high point. Furthermore, a pipe was installed at the infiltration hole to increase the pressure height. With this pipe, the concrete is squeezed into the formwork. The streaming of the concrete out of the air exhaust is the evidence of the formwork being filled up properly.

Coating of formwork surface: Although the formwork was lacquered to fill the pore cells of the foam, the concrete was bonding with the formwork, and the lacquer remained on the concrete surface and had to be scrubbed off. To achieve a separation layer, the formwork was additionally coated with vaseline.

The second approach of concreting succeeded, especially the stop-ends with the sealed mortar. The mortar was washed off and the reinforcement was exposed without major damage. However, the thickness of the shell missed the favoured elegance. Furthermore, the concrete slightly leaks out of the formwork, resulting from the joint formwork not fitting perfectly with the flanges.

Rigid joint prototype – trial #03   For the third approach, the geometry tested is directly taken from an extract of the *Möbiusban(k)d* geometry. The projected dimensions of the segments are 40×54 cm and 40×24 cm. The width of the joint remained 10 cm. Additionally, the stop-end system with mortar sealing was applied on both ends, complicating the handling of the formwork. Thus that approach, as shown in fig. 6.8, could be treated as
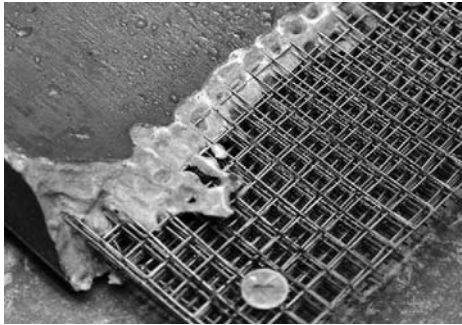
(a) The continuity reinforcement is exposed from the mortar sealing

(b) The concrete of the joint casting leaks slightly out of the formwork

Figure 6.8   Successful approach of stop-end mortar technique

rehearsal for the construction of the *Möbius*-strip, where naturally every segment has two adjacent elements.

The thickness was now reduced to 22 mm – the desired thickness of the concrete bench.

To gain a more accurate transition between the concrete of the segments and the joints, a small ridge of 3 mm is implemented in the formwork, as shown in fig. 6.9c. The proceedings of the construction of the final prototype are shown on the photographs in fig. 6.9.
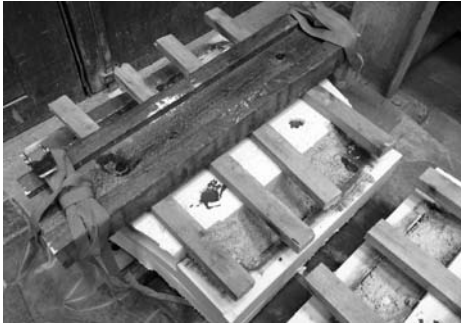
(a)　Milled formwork for the individual segments; the stop-ends are sealed with mortar
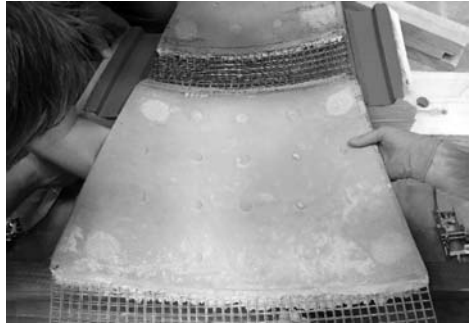
(b)　Exact positioning of the segments on a foam substructure

(c)　Overlapping reinforcement in the joint; implemented ridges at the border of the segments

(d)　Closed formwork for the casting of the joint
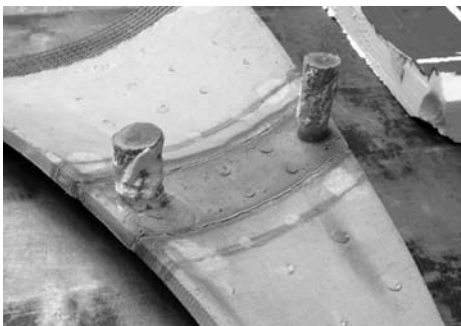
(e)　The casting nozzles of the joint (one for casting, one for exhaust) still have to be cut off

(f)　Finished prototype, upper side. The dots on the surface are resulting from spacers

Figure 6.9　Construction process of the joint prototype consists of two casting steps

6.4 Experimental investigation of load bearing capacity

6.4.1 Experiment set-up

The prototypes of the rigid joints, described above, validate the construction procedure, using lime mortar as a formwork sealing to create stop-ends. Applying that technique, certainly lime remains are left at the direct transition of the concrete and mortar, even after washing off the temporary sealing. To discover if the concrete texture in the transition area is disturbed, and if so, if this has an impact to the load bearing capacity of the joint, an experimental investigation is carried out.

The focus is on the bending capacity, thus a constant bending moment throughout the whole joint area is required. This is achieved by carrying out 'four point bending' tests, where the maximum bending moment is a constant over a certain predefined length. Since the width of the joint is set to 100 mm, the length of the constant bending moment maximum, is chosen to 200 mm to assure the joint being completely covered within that value. The applied test force is separated with a rocker to $2 \cdot F/2$.
The spanning length of the machine is positioned to 400 mm, that is why the length of the whole specimen is chosen to $l = 500$ mm. The width is set to $b = 150$ mm; the thickness is taken from the envisaged design of the concrete bench *Möbiusban(k)d* with $t = 22$ mm, as illustrated in fig. 6.10.
To achieve most accurate results, in terms of the tensile bending capacity, the test specimens produced, are flat without any curvature.

There are two different ways to apply the testing load: 'Driven over the force', where the force is increased within predetermined time steps and the corresponding displacement is recorded, and 'driven over the way', where a way in force-direction is applied, within predetermined time steps, and the corresponding force is recorded. In this case, the tests are driven over the way, to achieve the magnitudes of the remaining load bearing capacity after failure [EGRH15]. Since a high ductility is expected, this method is the most appropriate.

The four point bending tests are carried out for twenty-four samples, with the testing machine *Zwick-150 kN* of the *Amtliche Materialprüfanstalt für das Bauwesen* (AMPA),
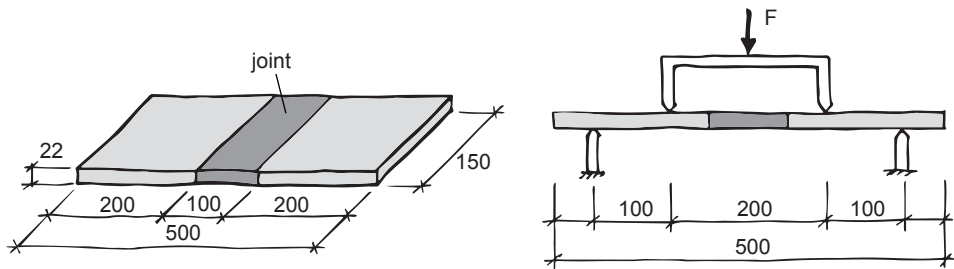
Figure 6.10   Envisaged four point bending loading test set-up

University of Kassel. It has a maximum load range up to 500 kN and a precision of $\sim 1\%$. The width of the specimens is limited to the length of the rockers to 250 mm.

6.4.2 Reinforcement arrangements

The aim of the experimental investigation is to verify, whether the joint developed is fully load bearing and if the joint transition, between mortar and cast concrete, disturbs the concrete texture. Naturally, the concept is based on the fact that the complete continuous reinforcement is overlapping within the joint zone. Therefore both effects are investigated: The disturbance of the concrete texture on one hand, and the influence of different reinforcement allocations on the other hand. Therefore a number of different reinforcement alignments have to be proven, covering a range from 'no reinforcement' at all, to a 'fully continuous reinforcement' alignment. The intermediate steps are situations, with the rebar layers overlapping in different steps of capability.
To examine the distinct effect of the joint casting procedure, all tests are executed twice:

(1) The joint cast in one step (monolithic), in the following termed '*MO*' (fig. 6.11a).

(2) Separated with a temporary mortar stop-end within the joint area, in the following termed '*FU*' (fig. 6.11b).

To cover the mean variation of the results, at least three samples of each identical specimen are produced.
The number of reinforcement layers is taken as a constant $n = 6$, derived from the thickness of the shell specimen of 22 mm. Each layer has two orthogonal filament wires, with a diameter of 1 mm each. Providing 3 mm of concrete cover on the upper and lower surface

(a) Specimen monolithic cast in one stage *MO*

(b) Specimen with the joints cast in a second stage *FU*
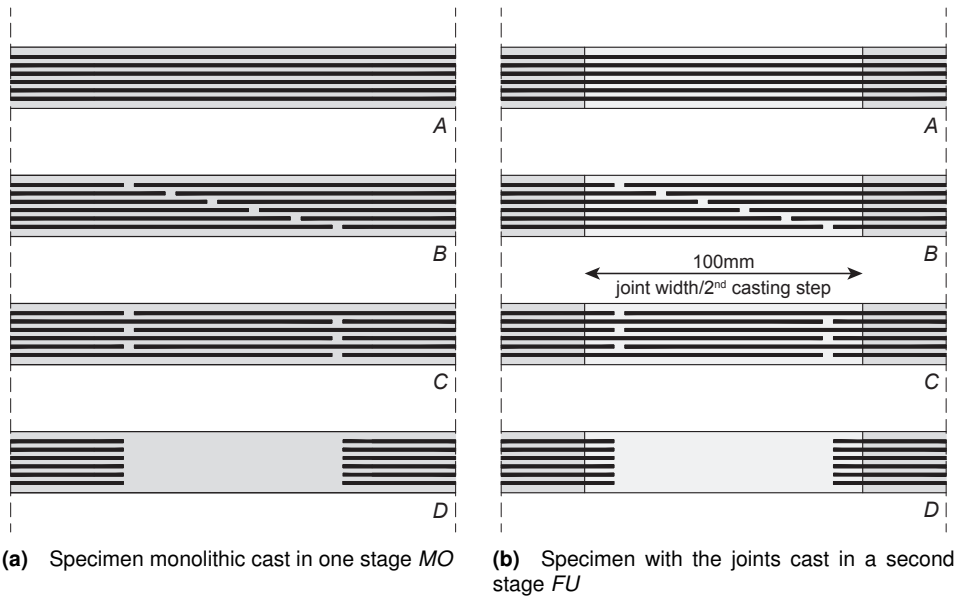
Figure 6.11 Four reinforcement allocations are investigated, from top to bottom the sample types *A*, *B*, *C* and *D*

leads to a remaining reinforcement depth of 16 mm. Having six layers, each layer has an available space of 2,7 mm, which satisfies a space buffer of 33 %.

The reinforcement layout, arranged with micro mesh reinforcement, has the following geometrical data:

rebar diameter:	$\varnothing = 1\,\text{mm}$
rebar distance:	$e = 12{,}5\,\text{mm}$ (80 wires/m)
rebar layers:	$n = 6$
steel area:	$A_s = \pi \cdot (1\,\text{mm})^2/4 \cdot 80/\text{m} \cdot 6 = 377\,\text{mm}^2/\text{m}$
concrete area (brutto):	$A_{c,\text{brutto}} = 1000\,\text{mm/m} \cdot 22\,\text{mm} = 22\,000\,\text{mm}^2/\text{m}$
concrete area (netto):	$A_{c,\text{netto}} = A_{c,\text{brutto}} - A_s = 21\,623\,\text{mm}^2/\text{m}$
reinforcement ratio:	$A_s/A_{c,\text{brutto}} = 1{,}71\,\text{Vol.–\%}$ per direction

There are four reinforcement layouts investigated, as illustrated in fig. 6.11: 'Type *A*' – continuously in the section; 'type *B*' – overlapping with thrusts distributed equally over the width of the joint; 'type *C*' – overlapping with two locations of the thrusts within the

joint; 'type *D*' – no reinforcement within the joint. These four reinforcement layouts are respectively tested in two different casting situations: 'Type *FU*' – the flanges are cast first with the water soluble mortar joint and the joint itself is cast one day later, after washing off the mortar; 'type *MO*' – the samples are cast monolithic in one piece. For each version, three samples are tested. This leads to $4\,(A, B, C, D) \times 2\,(FU, MO) \times 3 = 24$ samples [EGRH15].

The syntax of the specimen numbering is as follows:

{*casting situation*}_{*reinforcement allocation*}_{*number of specimen*}_{*casting date*}

with:

{*casting situation*}	*MO*	'Monolithic', specimen cast in one stage
	FU	'Fuge', specimen cast in two stages; first the flanges, secondly the joints
{*reinforcement allocation*}	*A*	continuous throughout the joint
	B	overlapping thrusts distributed equally over the width of the joint
	C	overlapping thrusts at two locations within the joint
	D	no reinforcement within the joint area
{*number of specimen*}	*1,2,3*	consecutive numbering of specimen
{*casting date, YYMMDD*}	*140805*	casting of all *MO* and flanges of *FU*
	140806	casting of joints of *FU*

e.g. MO_B_1_140805

6.4.3 Fabrication of test specimens

Concrete test cubes   The concrete compressive strength is evaluated with concrete test cubes, according to DIN/EN 12 390-3. The strength capacity is listed in table 6.1. The boundary conditions of the testing procedure are as follows:

number of specimens:	3
cube dimensions:	$15\,\text{cm} \times 15\,\text{cm} \times 15\,\text{cm}$
concrete age:	7 days
post-treating:	water storage $20\,°\text{C}$
testing machine:	*Toni-4000 kN*

Table 6.1   Concrete compressive strength investigated with concrete test cubes

no.	length [mm]	width [mm]	height [mm]	mass [kg]	density [kg/m^3]	area [mm^2]	$F_{\max}$ [kN]	$F_{c,\,cube}$ [N/mm^2]
cube 01	150,0	149,4	150,0	7,677	2 283	22 416	1 932,8	86,2
cube 02	150,3	151,3	150,0	7,776	2 280	22 727	1 863,7	82,0
cube 03	149,8	152,4	150,0	7,767	2 267	22 828	1 989,2	87,1
$\overline{x}$	150,0	151,0	150,0	7,740	2 277	22 657	1 928,5	**85,1**
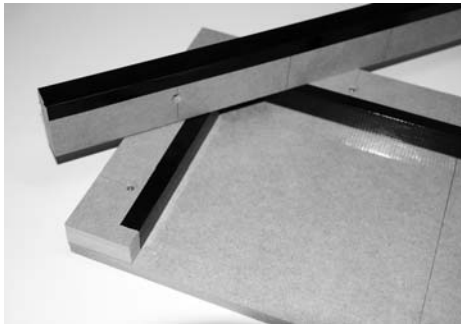
(a)   Side borders are defining the sample thickness of 22 mm
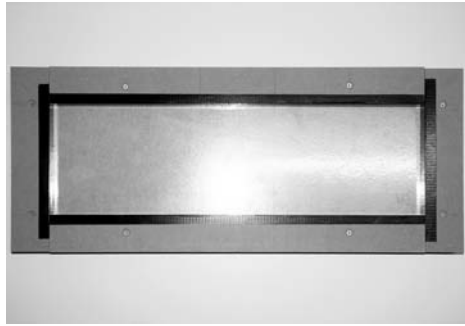
(b)   Formwork surface are laminated with synthetic adhesive foil

Figure 6.12   Open formwork for the flat specimen made of medium density fiber boards

testing method: driven over the force
testing speed: 0,5 N/mm^{2}sec
compressive strength: 85,1 N/mm^2

Formwork   The formwork for the test specimens is built from medium density fiber boards (MDF). These boards are made of fine frayed timber fibers that are compressed and glued together. The material texture is rather homogeneous and easy to process. The raw material is delivered in boards of several thicknesses, amongst others in 22 mm, the desired thickness of the concrete samples. Borders of this distinct thickness have been screwed on a base-plate from the same material. One (in this case negative) characteristic of the fibreboard material is the fact that it is highly water absorbing. As a direct contact area of a formwork it would influence the water–cement ratio of the concrete. To avoid
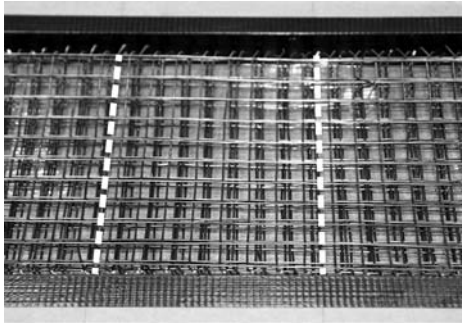
(a) Reinforcement 'type *A*' – reinforcement is running continuously through the joint
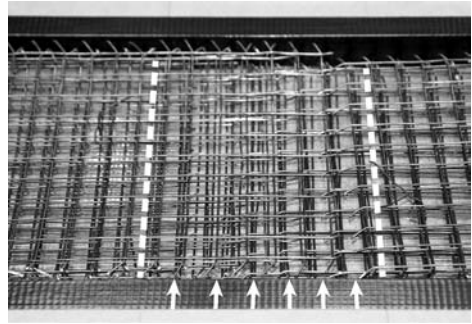
(b) Reinforcement 'type *B*' – overlapping with thrusts distributed equally over the joint width
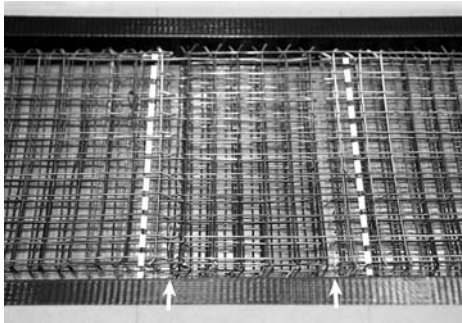
(c) Reinforcement 'type *C*' – overlapping with two locations of thrusts with the joint area
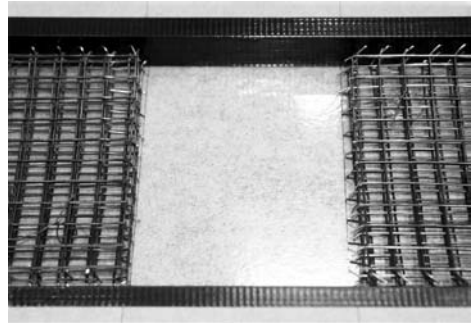
(d) Reinforcement 'type *D*' – no reinforcement in the joint area

Figure 6.13 The reinforcement of the investigated specimen. Dashed lines are indicating the position of the joints (width = 100 mm), arrows are pointing to the location of thrusts

that, the surfaces are laminated with a synthetic adhesive foil and duct tape, as illustrated in fig. 6.12. Since there are no aesthetic demands of the concrete surface to be achieved, the formwork boxes where constructed open, for horizontal casting.

Reinforcement The mesh wire reinforcement is delivered by the meter on a reel. It can be cut (ideally orthogonal), with wire cutting machines, pliers or angle grinders. The meshes are tailored and stapled on top of each other. To stabilize the arrangement, the wires are interconnected with filament straps. For wider shells, the borders can be re-
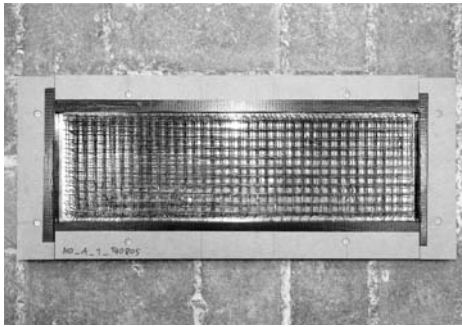
(a) Preparation of specimen to be cast in one stage *MO*
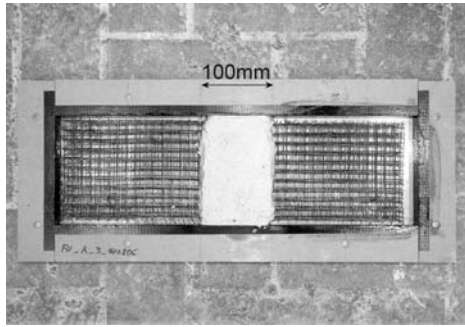
(b) Preparation of the stop-ends with mortar for specimen to be cast in two stages *FU*

(c) First casting stage – casting of the segments

(d) Washing off the mortar sealing
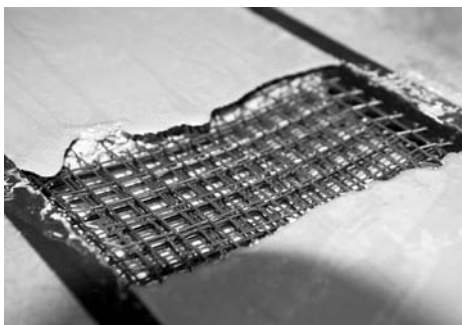
(e) Exposed joint section

(f) Second casting stage – casting of the joints

Figure 6.14 Preparation and casting of the specimens to be investigated

Table 6.2 Time schedule for concreting and testing of concrete specimens

work step	series	date
concreting	complete specimen *MO*	05.08.2014
	segments series *FU*	05.08.2014
	joints series *FU*	06.08.2014
		time gap: 28 days
testing	series *MO*	02.09.2014
	series *FU*	03.09.2014

inforced by enveloping one layer around the staple, to enhance the surroundings. That has been refused here, since the bearing capacity of the plane shell with a unit width is wanted.

To meet the concrete cover of 3 mm, distance holders were produced as buttons from lasered plastic sheets. The specimens were reinforced neatly under consideration of the desired reinforcement layouts *A*, *B*, *C* and *D*, as shown in fig. 6.13. After reinforcing and labelling, the mortar joints have been plastered for the samples to be cast in two stages, see fig. 6.14b, and left for 48 hours to harden.

Casting time schedule   The casting process is based on a definite casting sequence. The nominated characteristic concrete strength, according to the codes, corresponds to a concrete age of 28 days. Therefore the order of producing the specimen is the same as the one for testing, with a time gap of 28 days. The first casting stage covers the segments of the series *FU* as well as the complete specimen of the series *MO*. The second casting stage, accordingly 24 hours later, covers the joints of the series *FU* only. The casting and testing procedures have been executed, as listed in table 6.2.

6.4.4 Four point bending load capacity tests

The testing sequence is following the order of the casting schedule. The series of specimens investigated, are illustrated in table 6.3. To set up the deflection depth of the testing machine, one extra specimen is cast as a dummy. The specific number of that one is *MO_A_1_140805*. In account of this, the starting number of the series *MO* and *A* starts with '2' whereas all other series are starting with '1'.

The testing speed of the testing machine *Zwick-150 kN* is set to

(a) Specimen cast in one stage *MO*
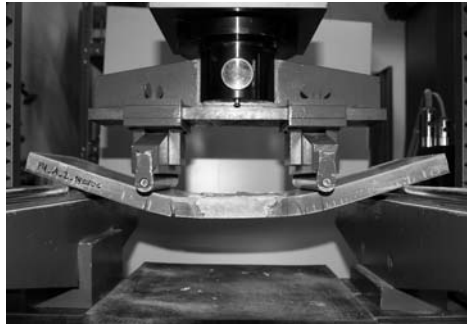
(b) Specimen cast in two stages *FU*

Figure 6.15 Four point bending loading test execution. Image shows specimens shortly before failure

0 – 5 mm:	0,02 mm/sec
5 – 40 mm:	0,10 mm/sec.

The sample in the testing machine, as shown in fig. 6.15, illustrates the ductile behaviour of the micro mesh reinforced concrete.

Table 6.3 Series of specimens investigated with four point bending tests

reinfocement layout	cast in one stage	cast in two stages
A	MO_A_2_140805 MO_A_3_140805 MO_A_4_140805	FU_A_1_140806 FU_A_2_140806 FU_A_3_140806
B	MO_B_1_140805 MO_B_2_140805 MO_B_3_140805	FU_B_1_140806 FU_B_2_140806 FU_B_3_140806
C	MO_C_1_140805 MO_C_2_140805 MO_C_3_140805	FU_C_1_140806 FU_C_2_140806 FU_C_3_140806
D	MO_D_1_140805 MO_D_2_140805 MO_D_3_140805	FU_D_1_140806 FU_D_2_140806 FU_D_3_140806

6.5 Evaluation of experimental results

6.5.1 Qualitative evaluation of crack behaviour

As a result of the investigations, naturally the absolute values of the failure load is of major interest, since this leads to the design magnitudes of the load bearing behaviour. However, the qualitative cracking pattern is also significant, to appraise the mechanical failure model. The destructed specimens after testing are shown in fig. 6.16 for the monolithic cast samples and in fig. 6.17 for the samples cast in two stages. It can be seen clearly that the main influence of the crack-layout is not given by the fact, whether the specimens are cast in one stage or two, but by the allocation of the reinforcement. The ductile behaviour is one advantage of the micro mesh reinforced concrete and a driver of a material decision. The high load-bearing capacity after cross section failure is facilitated in the ductility and thus in the crack distribution over the length of a building element. The deliberate pattern is with a multitude of small cracks, well distributed over the entire tension zone, with small distances, instead of fewer wider cracks.

 This 'well tempered' cracking behaviour is given in areas where the reinforcement is allocated continuously without any thrusts, as shown in fig. 6.16a. As soon there is a thrust (especially in the outer tension layer), an initial crack occurs, as visible in fig. 6.16b and
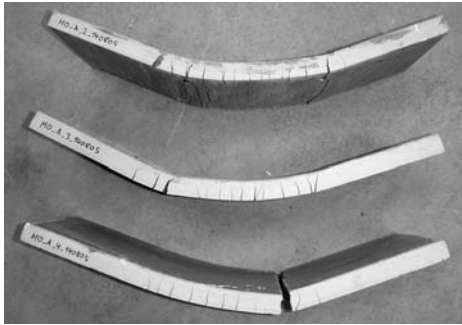
(a) Crack pattern series *MO*, *A*: Cracks are well distributed over the length of the tension zone
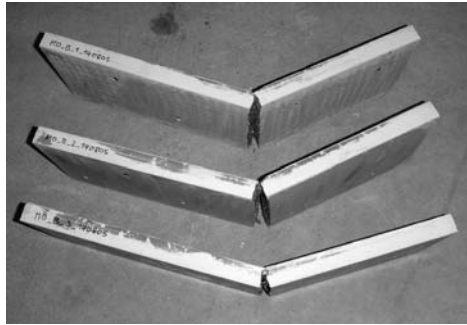
(b) Crack pattern series *MO*, *B*: Initial cracking at thrust position; here one in tension zone
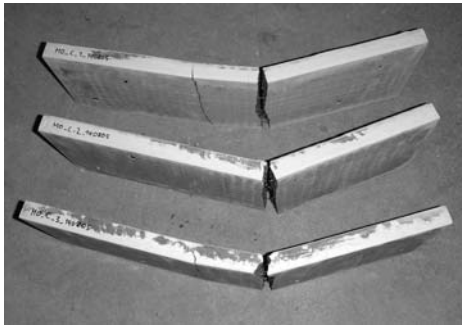
(c) Crack pattern series *MO*, *C*: Initial cracking at thrust positions; here two in tension zone

(d) Crack pattern series *MO*, *D*: Abrupt failure with no previous crack formation

Figure 6.16 Crack distribution of all specimens from series *MO*

fig. 6.16c, for the crack pattern series *MO, B* and *MO, C*, where the reinforcement layers are overlapping. On closer inspection, it can be detected, that for the series *MO, C* two initial cracks are visible. The reason for this is that the reinforcement here has two distinct locations of thrusts, whereas the thrusts of series *MO, B* are distributed along the length of the joints. Therefore the initial cracking of series *MO, C* consists of one distinct and one smaller crack. However, it can be seen that the effect of the thrust allocation is of minor influence.

Naturally an abrupt failure with no ductility and no crack development occurs when there is no reinforcement at all within the joint area, as in fig. 6.16d. The location of breaking
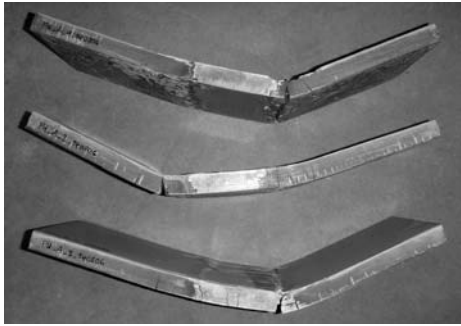
(a) Crack pattern series *FU*, *A*
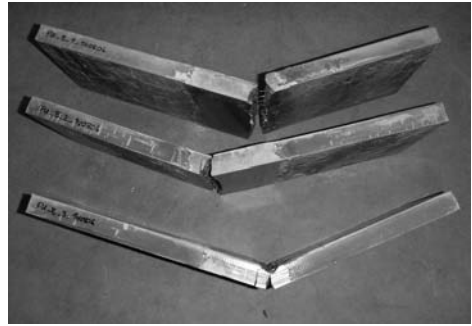
(b) Crack pattern series *FU*, *B*

(c) Crack pattern series *FU*, *C*
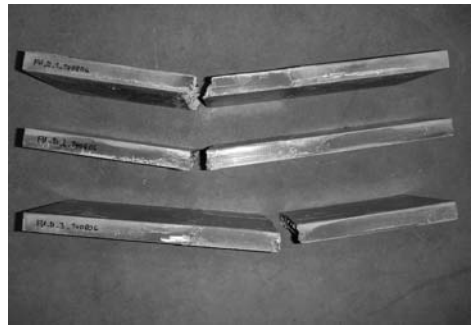
(d) Crack pattern series *FU*, *D*

Figure 6.17   Crack distribution of all specimens from series *FU*

is either located on the left or the right edge, where the reinforcement filaments are ending.

Generally the cracking and failure behaviour of the specimens cast in two stages *FU*, are similar to the monolithic ones, which is the result searched for. The effect of the joint area cast at a different time than the elements to be connected, definitely has an influence in the texture of the concrete in the transition zone. Inspecting series *FU, A*, with the reinforcement continuously placed, the joints seem to be even more steady than the connecting elements: The cracks are still well distributed over the length of the tension zone but the joint areas are not as much deformed as the adjacent parts. Nevertheless, the location of failure is independent from the joint location, as shown in fig. 6.17a.
The series *FU, B* and *FU, C* are behaving in a similar way to the monolithic samples, with

(a) Specimens cast in one stage *MO*: The transition zone shows the teared steel filaments

(b) Specimens cast in two stages *FU*: Lime remains in the transition zone causing low concrete tensile strength
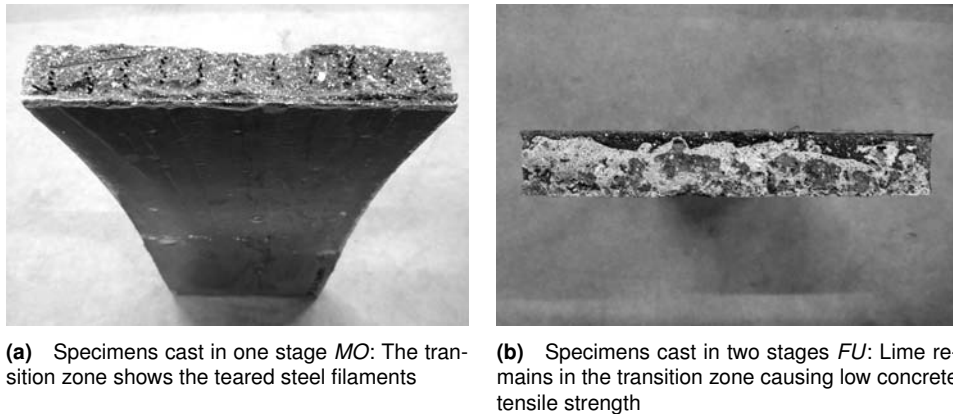
Figure 6.18 Concrete texture in the transition zone between joint and adjacent elements

the location of the failure at the points, where the overlapping thrusts of the reinforcement are located. Here also the joints seem to be stiffer than the adjacent parts and in contrast with the monolithic samples, the series *MO, C* have no smaller cracking at the second thrust, which is constituted in the stiffer joint area. Nevertheless, the failure is independent from the transition between the concrete steps, but in consequence of the reinforcement layout. Figure 6.17b and fig. 6.17c are showing the position of failure even within the joint zone.

Even more distinct is the failure noticed for the samples *FU, D*. The location of the breaking location is exactly at the either left or right edge of the joint and not, as for the monolithic samples, at the location where the filaments are ending, as shown in fig. 6.19. Resulting from a disturbance of the concrete texture in that zone, the tensile strength of the concrete is very low without reinforcement. The investigation of the cross sections of the broken specimens *FU, D*, where the break occurs, shows that there are still lime remains in the casting separation area, as shown in fig. 6.18b.

6.5.2 Numerical evaluation of experimental results

6.5.2.1 Absolute failure loads

The test equipment machine records the force and displacement data, as well as the corresponding time steps over the entire testing period. The tests are controlled over the displacement way and the maximum peak load is equivalent to the failure load. From the

(a) Specimens cast in one stage *MO*   (b) Specimens cast in two stages *FU*
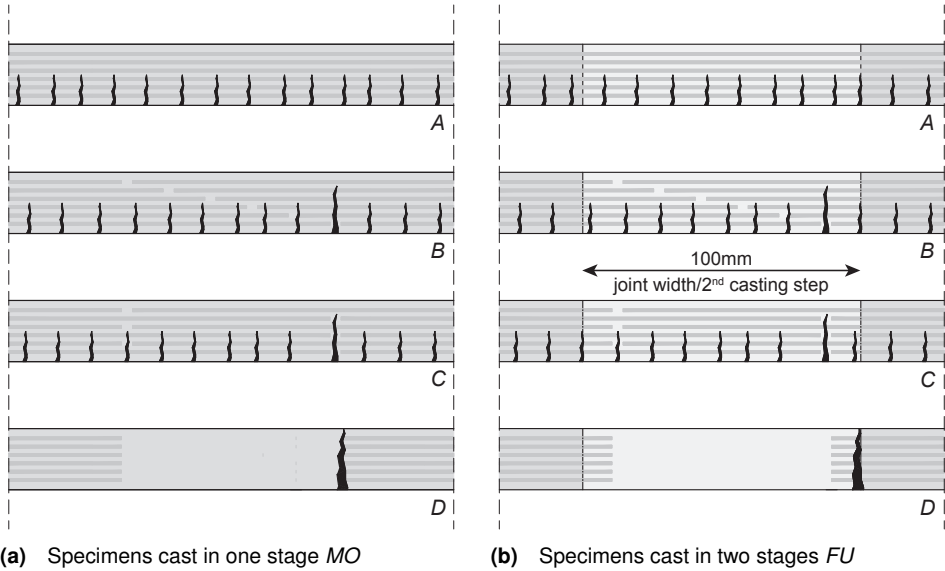
Figure 6.19 Diagrammatic illustration of crack distribution, from top to bottom the sample types *A*, *B*, *C* and *D*. The crack formation is not dependent on concreting sequence

maximum force, the maximum bending moment can be derived as $M_{\max} = F/2 \cdot 100\,\mathrm{mm}$ [N mm]. With the section modulus $W = b \cdot h^2/6$ $\left[\mathrm{mm}^3\right]$ the maximum bending tensile stress capacity results to $\sigma = M/W$ $\left[\mathrm{N/mm}^2\right]$ [EGRH15].

The results are summarized in table 6.4. The magnitudes of these values are illustrated as arithmetic mean values β_{BT} of three identical samples in each case. The all-encompassing results of the four point bending tests are listed in appendix E.2.

Because of the manufacturing impreciseness, the specimens have slightly different dimensions. Therefore the failure load $F_{\max}$ is not the appropriate value to consider for comparison issues. In contrast, the values of the bending tensile stress β_{BT} are considering geometrical differences, due to the derivation with the section modulus.

The capacities of the monolithic cast samples, with continuous reinforcement scheme *A*, are $10-15\,\%$ higher, compared to the ones cast in two stages. This results from the disturbance of the concrete texture, but may also be a matter of a general mean variation. However, this reinforcement allocation has no practical benefit, because the investigation is about the seamless mounting, where a undisturbed continuity of the filaments is impos-

Table 6.4 Bending tensile strength investigated with four point bending tests, samples *MO, FU*

Series	No.	width [mm]	height [mm]	F_{max} [kN]	M_{max} [Nm]	W_y [mm^3]	β_{BT} [N/mm^2]
MO	$\overline{A}$	151,2	22,6	4,3	217,1	12 927	**16,8**
	$\overline{B}$	151,6	23,1	2,7	136,8	13 505	**10,1**
	$\overline{C}$	151,7	23,2	2,9	145,7	13 569	**10,7**
	$\overline{D}$	151,3	23,8	2,4	119,7	14 309	**8,4**
FU	$\overline{A}$	151,7	23,8	4,2	211,8	14 345	**14,8**
	$\overline{B}$	151,7	24,4	3,3	166,5	14 996	**11,1**
	$\overline{C}$	151,7	24,5	2,9	144,8	15 110	**9,6**
	$\overline{D}$	151,6	24,6	0,9	43,0	15 285	**2,8**

sible.

The specimens, interesting for practical purposes because of a considered reinforcement overlapping, are the ones with the wire alignments *B*, with the thrusts distributed over the joint length and *C*, with the thrusts located in two positions within the joint. The deviation of the failure loads for all of these samples is within a range of 12 %, comparing the casting sequence series. It is noteworthy as a matter of fact, that the value of *MO, C* is even slightly higher than *MO, B* against the expected outcome.

The most distinct difference between the series *MO* and *FU* is for the specimens with no reinforcement at all inside the joint. In this case, the complete tension capacity is provided by the concrete. The disruption of the concrete texture and the lime-remains on the casting stop-ends have the biggest influence. However, the cut out of reinforcement is naturally not of a practical purpose.

6.5.2.2 Load displacement gradients

The material characteristics can be evaluated by plotting the load – displacement paths. The diagrams (fig. 6.20 and fig. 6.21) are illustrating the compensating curves, obtained from the arithmetic mean values of specimens identical in construction. The circumstantial illustration of every single load – displacement plot is given in appendix E.2.

The starting of the curve gradients is similar to all specimens, describing the linear elastic region. From that point, the plastic range and the point of failure are hit. The following region describes the remaining load capacity and is an indicator of the ductility. The more 'bulgy' the gradient, the displacement is possible at a constant load level. As expected,

not only the highest failure load, but also the biggest ductility is given for an undisturbed reinforcement allocation (*A*), especially for the specimens cast monolithic. The curves of the specimens, with the reinforcement overlapping within the joint, are showing a similar trend. The difference, whether the casting sequence is in one step or two, or if the reinforcement thrusts are well distributed over the joint (*B*) or at two locations (*C*), has insignificant influence. The shape of the curves, as well as the peak magnitudes, are in a similar range, with a similar behaviour of the remaining load capacity after failure.

As expected, the curves of the samples having no reinforcement at all (*D*), are showing an abrupt dropping after failure. These samples have a completely non-ductile material behaviour.
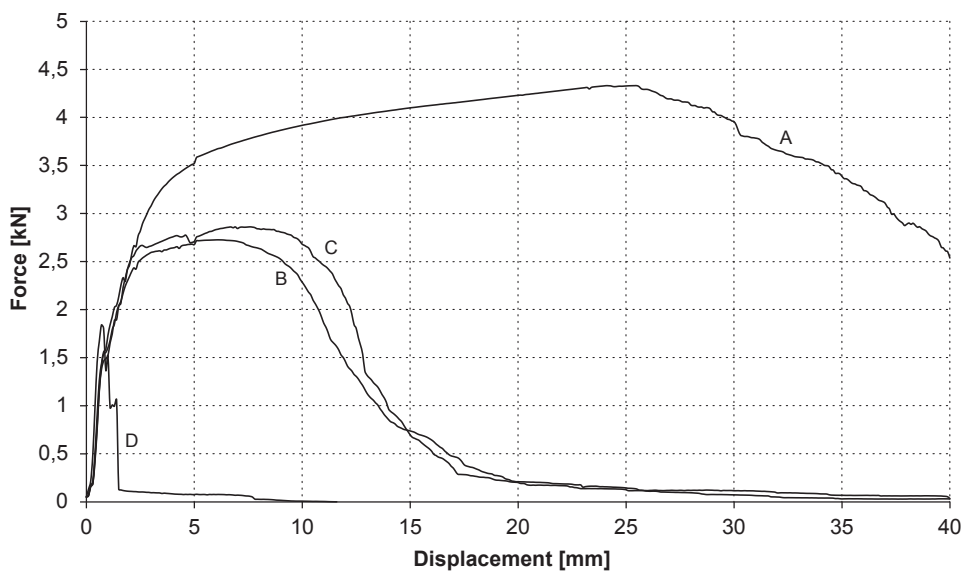
Figure 6.20 Load – displacement plots *MO* (cast in one stage), mean value graphs of specimens $\overline{1,2,3}$
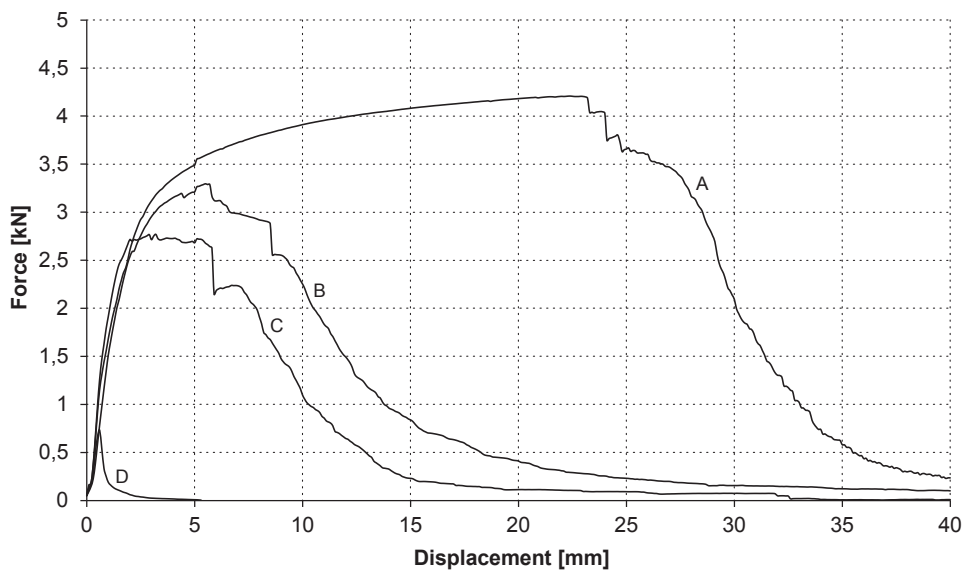
Figure 6.21 Load – displacement plots *FU* (cast in two stages), mean value graphs of specimens $\overline{1,2,3}$

6.6 Outcome – 'seamless rigid connections'

The results of the investigations are verifying the introduced method of creating stop-ends with water soluble mortar for micro mesh reinforced concrete. A direct comparison of the test result is given in fig. 6.22, where the mean value curves of all tested specimens are overlayed in one diagram; both the monolithic-cast and those cast in two stages. It can be noticed that three major groups of material behaviour are emerging:

(1) The samples with a continuous reinforcement *A* are naturally performing best, with a distinct ductile behaviour after failure. The starting of the curve, in the linear elastic as well as in the plastic region, until the point of failure, are almost identical for the series cast monolithic *MO* and in two casting stages *FU*. The remaining curve is exposed to a larger deviation, mainly affecting the after-failure behaviour.

(2) The gradients of the specimens *B* and *C* are within a narrow range, regardless of the fact, whether the samples are cast in one or two steps. The presence and respective absence of lime remains within the transition zone of the concrete elements and the joints have minor influence.

(3) The non-reinforced specimens *D* are underlying an abrupt fracture behaviour with no ductility. In this case, the difference between *MO* and *FU*, and hence the casting sequence is crucial, because the complete tension capacity is provided by the concrete.

The grouping, described above, shows that the main influence in the load bearing capacity is coming from the reinforcement layout and not from the fact whether the sample is cast in one or two pieces. This counts especially for the samples *B* and *C*, where the reinforcement is overlapping. These two reinforcement allocations are those of a practical significance and applied for the *Möbiusban(k)d*, described in section 5.2. The overlayed load – displacement diagram shows that there is almost no influence of the disruption in concrete texture [EGRH15].

The values of the flexural strength capacity are up to $\beta_{BT} = 16,8 \, \text{N/mm}^2$. These values still can be raised by increasing the amount of reinforcement. The material supplier *DUCON* specifies the range of the flexural strength with $20 - 75 \, \text{N/mm}^2$ [DUC15, 3]. Therefore the present investigation should not be appraised as an effort to enhance the absolute failure values of this material, but to research this specific method of mounting concrete elements with rigid joints. However, it has been noticed that there is still potential
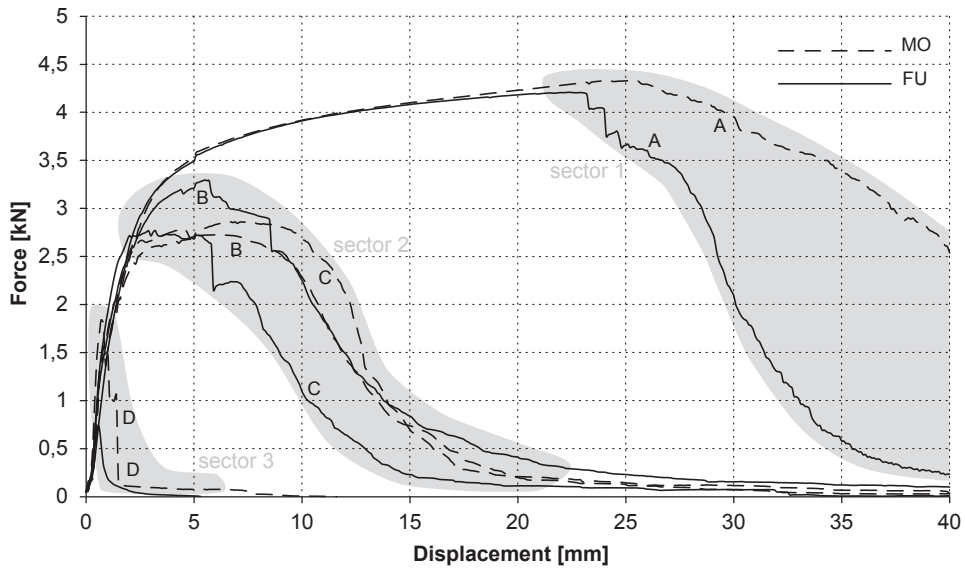
Figure 6.22 Load-displacement plots of all series *MO* (dashed line) and *FU* (solid line) with reinforcement arrangements *A*,*B*,*C* and *D*; plots are showing the mean value graphs of specimens $\overline{1,2,3}$

to increase the amount of reinforcement within the section. Investigating the photographs of the cross sections after testing (fig. 6.18a) reveals that the reinforcement filaments are all ruptured, combined with a negligible compression failure of the concrete.

7 Micro prestressing connections of prefabricated shell elements

7.1 Prestressing in concrete construction

7.1.1 Prestressing fundamentals and applications

The terms 'prestressing', 'pre-tensioning' and 'post-tensioning' are sometimes misunderstood because of the prefix 'pre'. Prestressed concrete has internal compressive stresses, as inherent stress conditions, to counteract tensile stresses imposed from outer loads when corresponding elements are in service. Prestressing is either achieved by 'pre-tensioning' or 'post-tensioning' the concrete element. In pre-tensioning, the tension items are strained prior to casting, whereas in post-tensioning, hulls are cast inside the concrete, where the tension items are threaded.

Although this section is about a connection technique, based on a post-tensioning, the mechanical principle is still described with the generic term 'prestressing'.

Principle of prestressing   Concrete as a construction material is able to carry high compression loads, but comparable low tensile loads. The mean tensile strength capacity accounts 5 – 13 % of the compressive strength capacity for standard concrete grades. For the concrete grade C80/95, the mean tensile strength capacity, according to Eurocode 2, is $f_{ctm} = 4,8\,\text{N/mm}^2$, whereas the compressive strength capacity is $f_{ck} = 80\,\text{N/mm}^2$ [Eur04, sec. 3.1.3]. That leads to a ratio of 6,0 %[1].

The idea of prestressing systems suggests itself to construct concrete elements which are exposed to external loading, ideally in way that occurring tensile stresses are zero or as low as possible. This can be achieved by generating compressive stresses up-front, in areas of

---

[1]In the case of the usage of prestressing as a connection technique, the tensile strength capacity in the joint is naturally zero

expected tensile stresses from service loads. The so gained 'stock' of compressive stresses has to be dissipated within the service state before the structure (concrete) is exposed to tensile stresses.

"... Prestressing is a means to an end, to artificially transfer a given structure into such a permanent state of basic stress, by loading it with elasto-static energy, so that all constructional elements are utilized within their natural sector of their resistance, regardless their asymmetric conditions of rigidity, even under the exposure of all expected combined service loads." [Hos13, 161, own translation].

To achieve the artificially activation of an inherent stress condition, prior to exposing to external service loads, the structure is loaded with elasto-static energy. The necessary work is generated by mechanical appliances. An expedient application of prestressing is given, when the structure has unutilized reserves, present in the non-prestressed state.

Applications of prestressing in concrete construction In reinforced concrete constructions, the reinforcement is located in the tension zone of the building element. Exposed to service loads, the concrete sections transfers to its cracked state 'state II'. The concept here is based on the cracking of the concrete section. From that moment on, the tensile stresses are taken over by the reinforcement, so that the system is still under force equilibrium with the inner lever arms. The load bearing capacity can be increased by increasing the amount of reinforcement up to a certain level. With a reinforcement ratio greater than 2 %, the steel does not reach its yield limit and the concrete strength capacity governs the failure of the section. An increase of reinforcement hardly leads to an increase in the load bearing capacity. Furthermore, large amounts cannot be placed within the concrete section, see [SH03, 1–2], and the reinforced concrete system becomes uneconomic. Especially for structures with large span lengths and/or structures with limited cross section dimensions, the prestressing of the concrete is a favored technique, where the influence of the self-weight increases disproportionately with increasing span length. Deflections (particularly from physical non-linear effects, like cracking, creep and shrinkage) as well as the crack sizes can be significantly reduced by the pre-compression of the premeditated tension zone.

Applications of prestressing in building industry The terminology 'prestressing' in construction is usually linked with the techniques of prestressing concrete, as described above. Nevertheless, the concept is used in further domains of construction.

Screws in steel construction can be tightened under a defined torque, to press steel plates against each other. A transfer of tensile forces in a girder joint is possible without the opening of the gap of the end-plates. Also a certain friction is gained, allowing a transfer of shear forces. The same effect is achieved with rivet joints. Brought in and closed hot glowing, the contraction from cooling down, generates the friction between the plates [SB08, 5].

Tempered glass is widely used, because of its fine fracture behaviour. Due to the notch sensitivity, the tensile strength is much lower than the compressive strength [WSF13]. However, bending and thus flexural tension often occurs in glass construction. A significant increase of bending capacity of glass is reached by thermal prestressing: During the production, the glass is heated up and quickly cooled down with blown air. The surfaces are cooling down and solidify more quickly than the inner core and inner stresses are built up. During the relaxation process, when the section wants to shrink, the outer surfaces are hardened already and get compressed [Fra15].

Further well known examples of prestressing applications in construction are inflated structures or pneus, where (analog to tyres) the stressing medium is air. Furthermore, the concepts of cable networks and spoke structures are based on the methodical precompression of building elements with stress reserves.

7.1.2 Historical outline of prestressed concrete construction

The overview of the history of prestressed concrete, enables an understanding of the problems, trials and errors, documented by the pioneers with the aim to avoid occurred mistakes.

The development of this construction technique was not driven by the demand of building wide spanning structures, but rather from the economic situation after World Wars One and Two. The lack of construction timber, as an example, led to the development of concrete tiles by *Karl Wettstein* in 1919, as a replacement for roof boards. He concrete-casted prestressed piano strings, as a first approach of the application of high strength steel, without clear knowledge of the mechanics. In the years after the Second World War, the motivation of prestressing was the saving of steel reinforcement [Rom05, 14].

The first approaches of prestressing[2] are done by *P.H. Jackson* (San Francisco, USA), who had a patent for prestressed anchors, tensioned by screws, to take over horizontal shear forces of vault structures [AG05, 11].

---

[2]apart from Egyptians who prestressed the hulks of their open sea vessels already 2700 years before Christ [Leo73, 625]

The de facto birth of prestressed concrete, as the technique carried out today, is based on investigations of *Eugene Freyssinet*. In 1928 he applied for a patent for the use of high strength steel bars, pre-tensioned prior to concreting. In addition to the approaches of *Wettstein*, he developed the understanding of the different tasks of the material components and discovered the influence of short- and log term deformations. His main participation in the development of prestressed concrete, is his long term investigation over more than fifteen years about the creep behaviour of concrete, since the long term deformation has a major influence in the execution of prestressed concrete [Leo73].

The first prestressed concrete bridge was built during 1936–1937 in Aue, Saxony in Germany, according to the design of *Franz Dischinger*. The first affiliation in the building codes (DIN 4227) was in 1943. These codes, as a guideline for the design and construction of prestressing concrete, were a basis of numerous prestressed structures in Germany and promoted this construction technique [Leo73, 634].

7.1.3 Prestressing methods in practice

The following selected prestressing techniques are common in the building industry.

'Pre-tensioning' – prestressing with immediate bonding   The stressing medium is tensioned in a frame, external to the concrete member, before casting. After curing of the concrete and developing sufficient strength, the tendons are cut off the surface of the concrete element. From that point, the tension force, over a certain transfer length of the tendon, is released to the concrete. The transfer length is dependent on the steel diameter and the surface properties. Usually this method is used for prefabricated concrete elements. The gradient of the tendons is straight.

'Unbounded post-tensioning' – prestressing without bonding   In this method, the concrete element is cast first with embedded hulls or ducts. After concrete curing, the tendons are tensioned and anchored. The load is introduced at the ends of the concrete element, where the anchors are located. Not only this, but applying post-tensioning allows a curved layout of the tendons over the whole lengths. For bending elements, the gradient chosen often is affined to the bending moment diagram, located on the tension side. The curvature of the gradient leads to a deviation of the force vector. The deviation force, perpendicular to the tension force in the tendon, is used as an internal force, counteracting the external loads.

'Post-tensioning' – prestressing with subsequent bonding Similar to prestressing without bonding is the method of the post-tensioning. Here also ducts are cast in the concrete and a curved layout of the tendons is possible. After the concrete is hardened, the tendons are tensioned and anchored. After that, the ducts are additionally grouted with a mortar injection and a bonding is established. For that method, special hulls with a toothed surfaces are required, allowing an interlocking of the grout and the concrete element.

Other There are other types and variations of prestressing, like external prestressing, where tendons are unbound and located outside the cross section. There are also methods without any tendons, where constraints are gained, for example with external presses.

Corrosion protection For all kinds of prestressing, the corrosion protection has to be assured for corrosion-sensitive elements. In case of a direct bonding with the concrete, the protection is given due to the alkaline concrete environment. In case of unbounded post-tensioning, the cables can be surrounded by grease.

Stressing media As *Schlaich* describes in [SB08, 7], every prestressed system needs both, a 'stressed object' and a 'stressing medium'. The stressed object is the element affected by prestressing, whereas the stressing medium describes the energy store to produce and to preserve the tension force. The stressing can be induced externally by tendons, air, or as a residual stress, for example in the case of tempered glass.

The first approaches in prestressing were undertaken by tensioning reinforcement-steel bars. Every stress medium is exposed to the deformation of its surrounding environment, also, or above all, the self-originated deformation, that directly affects the magnitude of the tension force. The summation of elastic and long term deformation from creep and shrinkage are 'consuming' the elastic strain of the tendon. It has been shown, that the use of standard reinforcement is inefficient for prestressing, since the prestressing (depending on the system) almost disappears after all deformation has occurred.

High yield tendons, that are bearing high stresses and respectively large strains are suited for prestressing to minimize losses of the tension force.

It may be concluded, that in this case of using prestressing as a connection technique, the loss of tension force by creep and shrinkage can be re-established by simply re-tightening the end screw-nuts.

(a) Bowden cables (here on a bicycle) are able to guide magnitudes and directions of force vectors. Although hulls are under compression they never underlie buckling failure

(b) Confected steel wire inside hull for concrete-casting. Both, flexible cable and hull allow curved layout in concrete section
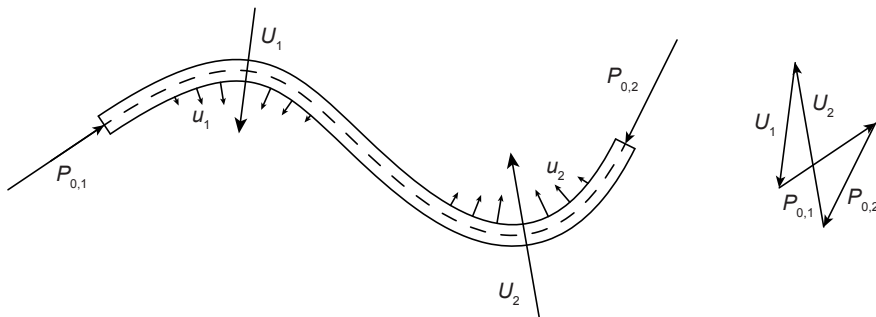
(c) Cable and deviation forces from prestressing, acting on a bowden cable. All forces arising, build a closed equilibrium system, see [Hos13, 166]

Figure 7.1   Construction principle of prestressing connection technique with bowden cables

7.2 Micro prestressing concept

7.2.1 The bowden cable principle

The bowden cable is named after the inventor *Ernest Monnington Bowden* (1859–1904), who had a patent in 1896 *"(...) Mechanism for Transition of Power"* [IPE15]. It is a flexible and portable combination of a steel cable together with a hull, stable in longitudinal direction. The bowden cable is able to transfer mechanical movements and/or tension

forces. The hull has to be compression resistant and functions as a slider for the flexible tendons.

The Bowden cable principle enables a precise decomposition of structural systems into tension and compression. Magnitudes and directions of force vectors can be guided to any point of interest. A well known application of bowden cables are brake cables for bicycles (fig. 7.1a). Figure 7.1b shows confected steel cables inside flexible hulls, with threads pressed on, as used for load bearing tests described later.

At both ends of a post-tensioning system, the cables release their force as a compression force on the prestressing object. Although the bowden cable (hull) is a slender compression element, is does not tend to buckle. As soon as the hull swerves orthogonal to its longitudinal axis, deviation forces arise, acting as a counter force. As long as the material strength of the hulls is not exceeded, the shape of the system is stable and self calibrating. In the common example of bike brakes, the non-buckling behaviour can be observed. An increase of the braking effort on the brake system, and thus an increase of the prestressing, leads to an increase of stiffness, and the cable systems turns to be 'harder'. The bowden cable analogy can be projected to pearl chains: A thread running through a number of pearls, leads to a stable system, as soon as the thread gets pulled. Here again the system does not tend to buckle.

The bowden cable principle is a promising starting point for the idea of prestressing slender concrete elements. The benefits of these objects, including the high compressive strength, are used to full capacity, whereas the disadvantages, the low tensile strength, buckling sensitivity and small inner lever arm around the weak axis, are retreated.

7.2.2 Rescaling prestressing systems

In the following sections, the concept of prestressing slender concrete elements is introduced as a 'dry-fit' connection technique. The concrete material used for the stressed objects is based on the technology of DUCON (section 4.1.3.3), a reinforced concrete with micro meshes as reinforcement. Simplified, the mechanical behaviour is analog to conventional reinforced concrete as treated in building codes: A high performance concrete is responsible for the occurring compression, whereas the tension within the section is bore by steel wires which are stapled crosswise over the entire cross section. The placing of the meshes over the complete section guarantees that the tension zones, wherever located, are reinforced. All components of a reinforced concrete section are qualitatively scaled down by a crude factor around 10, depending on the system considered, see table 7.1.

Table 7.1 Dimensions of components in conventional vs. micro mesh reinforced concrete are scaled by a crude factor around ~ 10

	conventional reinforced concrete[a]	**micro mesh reinforced concrete**[b]
section height	$h = 220\,\text{mm}$	$h = 22\,\text{mm}$
rebar diameter	$\varnothing = 10\,\text{mm}$	$\varnothing = 1\,\text{mm}$
rebar spacing	$e = 150\,\text{mm}$	$e = 12{,}5\,\text{mm}$
concrete cover	$c = 25\,\text{mm}$	$c = 3\,\text{mm}$
aggregate sizes	$0-16\,\text{mm}$	$0-2\,\text{mm}$

[a] random but typical reinforced concrete section, i.e. floor slab
[b] component dimensions as used for concrete mobile, refer section 5.3 on page 126

 It is a convenient concept, to dispose a respective scaling for a potential prestressing of the micro-mesh reinforced concrete section: Simplified, this method stands for an operation with 'small' prestressing media with corresponding narrow axial distances. The tension members, and rather their ducts, must be small enough to fit inside the narrow concrete sections, with space left for some extra reinforcement and concrete cover on both faces. In the field of slender concrete sections, with section heights around $20-30\,\text{mm}$, it can be eliminated to change the position of the tension members inside the section. This is not only because of the limited height, but also because of the fact that the mesh reinforcement is cross wise. The change of the position between the layers would result in a slicing of the reinforcement mats which would not be workable.

Thus the placing of the prestressing media is envisaged to be centric, in the middle of the concrete section. However, the layout in plane of course can be curved, as long as the tension members are flexible, enabling a prestressing of freeform objects. In the following sections, as well as for the construction of the concrete mobile *Stable Equilibrium*, see section 5.3, threaded rods were used as prestressing media. The type of prestressing method is unbound post-tensioning.

7.3 Dry-fit connection methods

7.3.1 Construction principle

A 'dry-fit connection' describes a method of connecting prefabricated elements without embedded items or grouting components. In some cases, the connection can be realized by sticking elements together; in others a mechanical fixing is necessary, for example with

Figure 7.2 Construction principle of prestressing connection technique demonstrated on a toy giraffe

screws, bolts or prestressing.

The simple toy, as shown in fig. 7.2, illustrates demonstratively the construction principle: A spiral spring, in the pedestal of the toy giraffe, tensions a rope, going through the longitudinal centroid of each member and is fixed inside of head and tail. The rope, tensioned by the work of the spring, induces a compression in each member, just high enough to withstand the outer forces from self weight, with the result that the toy is standing erected. Releasing the spring, immediately leads to a collapse of the structural system.

This technique, applied in a simple toy, is based on the bowden cable principle. The system is stable and a closed equilibrium system. Although the arrangement of the construction elements, similar to a pearl catenary, builds a hinged chain, the system never underlies buckling or stability failure.

7.3.2 Application in construction

The practice of using prefabricated concrete elements, is marginally younger than the developments of reinforced concrete. The casino building in Biarritz, France, designed in 1891 by the structural engineer *Edmond Coignet* (1856–1915), is presumed to be the first construction, assembled with concrete elements, prefabricated in a field manufactory [BDEN13, 64].

The benefit of using prefabricated elements is an optimization of the construction time schedule, since the concrete curing time can be brought forward. Furthermore, the effort of formwork construction can be reduced by shifting it in workshop or laboratory conditions, usually located indoor.

With the application of high- and ultra high performance concrete, it becomes a necessity

to cast concrete under laboratory conditions, because of its sensitivity on mixing conditions. To reach a specific slump size, distinct climate conditions, water temperature and mixing devices need to be predefined. Furthermore, the time between mixing and casting processes needs to be in a specific frame to guarantee the necessary fluidity of the concrete. These facts complicate an application of high performance concrete on site.

A further use of dry-fit connection methods can be motivated by the use and the circumstances of a construction. Not only a quick assembly may be requested, but also a possible de-assembly or re-assembly, presuming a non-destructive retreat working. In the case of the exhibition object *Stable Equilibrium*, presented in section 5.3, it was manifested in the tender, that the installation has to happen within a few hours only, eliminating the option of a concrete casting on site. The same boundary conditions may be for any temporary structures, exhibition structures, or structures with short life cycles.

The *Institute of Building Materials, Concrete Construction and Fire Protection* (iBMB) together with the *Institute of Structural Design* (ITE) of the *Technical University of Braunschweig* are undertaking investigations with non-standard concrete joints, made of ultra high performance fibre reinforced concrete (UHPFRC). Motivated from the request to consolidate high-tech materials and digital design and production tools in an economic way, the development of non-metallic dry-fit connections are described in *Mainka* et al. [MLBK13]. They investigated that the assembly on site is a big challenge, often leading to uninspired node details. The application of steel embedded items in enlarged dimensions, in areas where forces are transferred, is the consequence. Their approach of non-standard joints is the design of complex, individual joints, which are able to transfer shear and compression forces. The fabrication of the member-ends requires an exact CNC produced formwork. In the report of *Lehmberg* et al. [LLW+15], these results are pursued to surface structures, with the example of a coffered ceiling, assembled from individual pieces. The outlook is to create prestressed dome structures, with the combination of dry-fit pipe members and shear resistant surface elements.

The construction techniques, based on the non-standard joints, require complex node-ends to be able to also transfer shear forces additional to the compressive contact stresses. These complex nodes require a steel fibre reinforcement, since a mesh reinforcement is not applicable in small complex geometries. Furthermore, digital controlled production tools for the formwork are compulsory.

The following investigations are motivated to create a dry-fit connection for non-complex node geometries. The slender concrete surface elements are reinforced with a micro mesh

reinforcement, with the aim to develop a prestressed jointing system, that enables the design of hybrid structures. A low-tech fabrication of the transition parts with wooden formwork elements is envisaged.

7.4 Validation of construction principle 'concrete mobile'

7.4.1 Specimen dimensions

The dimensions of the elements tested are primarily derived from architectural issues from the construction of the concrete mobile *Stable Equilibrium*. At any time of the planning phase, the feasibility of the production has to be considered to assure the manufacturing of the formwork, the placing of the reinforcement and prestressing media, as well as the concrete casting. Furthermore, it has to be guaranteed that the samples fit inside the testing machines. All specimens have identical dimensions, allowing a multiple use of the formwork.

Only the length of specimens changed from $l = 500$ mm to $l = 480$ mm, between first and second approach described below, because a prestressing, amongst others with threaded bars, is envisaged. The length of delivery of these bars is in increments of 50 cm. The deviation of 20 mm for each element allows the construction of screw-nuts outside the elements.

The width of the specimens is $b = 150$ mm. The specimens incorporate two prestressing hulls, coming up to an axial distance to each other of $e = 75$ mm. The width, again, is derived from the design of the concrete mobile. The cast-in threads for the suspension points, require a certain embedment length of cast-in steel items, to introduce tension forces.

The specimen thickness is $t = 22$ mm. This size is a deliverable thickness of MDF boards, used for the construction of the formwork. The prestressing hulls have an outer diameter of 10 mm, thus a remaining thickness on each side is 6 mm, just enough to fit two layers of mesh reinforcement in between, still assuring the flow of concrete.

Summarized the dimensions are:

$$l = 500 \, \text{mm (approach}\,{}^{\#}01) \qquad l = 480 \, \text{mm (approach}\,{}^{\#}02)$$

$$b = 150 \, \text{mm}$$

$$t = 22 \, \text{mm}$$

To allow the use of threaded rods as a prestressing medium, the geometry chosen for the testing has no curvature, since the bending flexibility of the bars is limited. Also the structural mobile (the reason to undertake the investigations) is built of straight elements.

7.4.2 Fabrication details and quality defects – approach [#]01

A major motivation to undertake the investigations of prestressing connection techniques, is the verification of the construction principles and to proof whether the production, as well as the serviceability, are feasible.

The production of the specimens resulted in two consecutive approaches, where the knowledge gained in the first approach is corrected and improved in the second approach. It may be noticed that the elements described in the second approach are the ones used for the concrete mobile *Stable Equilibrium*, presented in section 5.3.

The build-up of the specimen in the first approach is shown in the series of fig. 7.3. Generally the layout of the cross section is double symmetric and has two prestressing hulls between two layers of reinforcement. The concreting is envisaged to be horizontal, which makes it easier for casting, but results in two different concrete surface textures.

Quality defects – approach [#]01   During the construction process, formwork stripping and load bearing investigations, several quality defects and impracticabilities have been detected and approved in the subsequent following approach [#]02, as there were:

> *Surface quality and thickness preciseness*: A horizontal concrete casting simplifies the casting process significantly. Nevertheless, it results in an imprecise upper concrete surface and a non-exact element thickness, as shown in fig. 7.4a. Also reinforcement ends are sticking out, or slightly uneven layers of mesh reinforcement cause problems in reaching a reasonable surface quality. In the second approach, the elements were cast vertical. That results in the necessity that the concrete needs to be able to flow between prestressing hulls and formwork surfaces.

> *Flexible steel hulls*: Flexible steel hulls (refer to fig. 7.1b) are generally useful for curved cable layouts. Since the cables are produced with winded steel spirals, it is not possible to cut the cables with an accurate cut. There are sharp ends, comprising not only injury risks, but also a destructive rubbing on the prestressing cables. Furthermore, the hull thickness is rather thick, a contra productive fact, in order to create slender shells, since the space is needed for concreting. The compression, induced from tensioning the prestressing media in the end, is bore
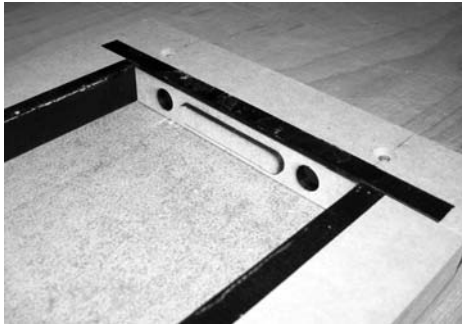
(a) Formwork made of laminated MDF boards. The element ends are formed as tongue and groove transitions, to bear shear forces
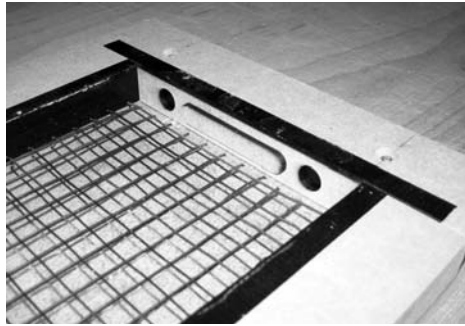
(b) Two layers of mesh wire reinforcement on each face of element
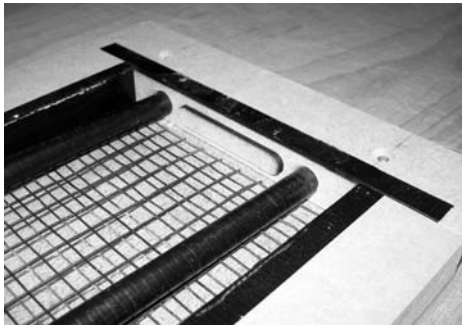
(c) Flexible hulls for prestressing. The ends are stuck inside the formwork to assure centric positioning
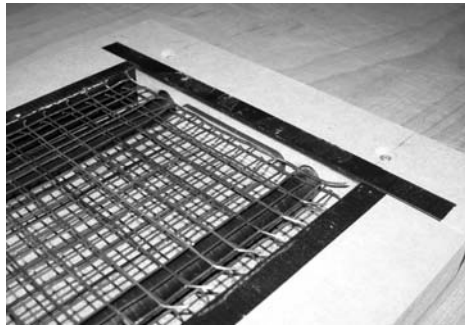
(d) Element ready for horizontal casting. The two faces will have different concrete surface textures

Figure 7.3 Build-up of testing specimen (approach $^\#$01) prior to casting and prestressing

by the concrete and not by the hull itself. Thus a load bearing hull is not necessary. In the second approach, thin-walled PVC hulls were used. It may be noticed, that for curved sections, a simple rubber tube can be used, as long as the correct positioning is ensured.

Shear studs: The tongue and groove ends, as shown in fig. 7.4b, are meant to transfer shear forces. As visible in the photograph, the edges tend to crumble. Furthermore, the formwork of these ends requires an accuracy that cannot be en-

(a) Horizontal concrete casting leads to un-precise surface textures

(b) Tongue and groove transitions tend to crumb at the edges
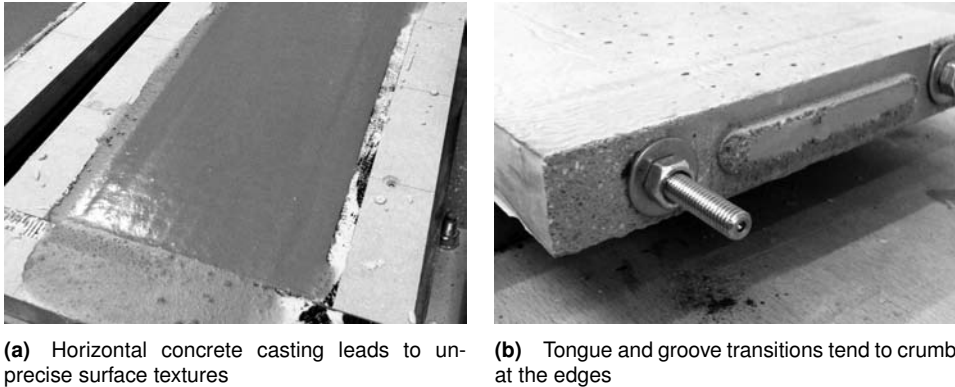
Figure 7.4 Quality defects of approach [#]01 led to a revision of the fabrication approach

sured. In the second approach, the tongue and groove transitions are replaced by steel shear studs, simply stuck into a hole, recessed with a small piece of PVC-tubes. Generally the shear forces are a minor issue of the load bearing concept. As soon as the system is prestressed, the shear is bore by the friction, gained within the transition zone. The bigger the prestressing, the bigger the shear force capacity gained from the friction. However, the studs are indispensable as a location fixation during assembly.

Counter ability of screw nuts: It has been investigated that screw nuts need a countering during the tensioning process. It may happen that the screw, when turned, does not turn around the thread, but twists the threaded bar instead. That makes a tensioning impossible, since the torsion flips back, when releasing the open end spanner. Furthermore, it has been proven that in some cases the threads are damaged, prior reaching the envisaged tension force. In the second approach, longer nuts of 9 mm instead of 4 mm are used and the torsion of the threaded bars is restricted with the help of two compressed counter nuts.

7.4.3 Fabrication details – approach [#]02

Figure 7.5 shows the fabricated specimen approach [#]02, where the findings of the first trial are incorporated. A comprehensive report of the fabrication of the concrete elements, used for the concrete mobile *Stable Equilibrium*, is given in section 5.3.
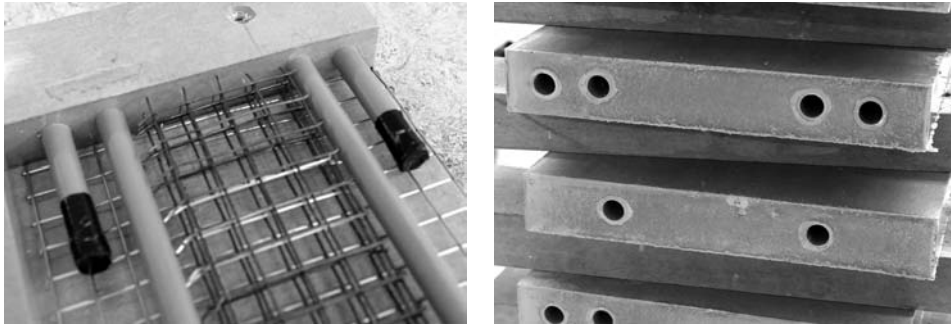
(a) Open specimen formwork of approach #02 shows the recess hulls for the shear studs as well as the PVC hull for prestressing media

(b) Eliminated tongue and groove transition ends, exact thickness of specimen because of closed formwork cast vertical

Figure 7.5 Concrete elements of approach #02 as used for concrete mobile *Stable Equilibrium*

7.5 Experimental investigation – approach #01 / low tensioning

7.5.1 Experiment set-up – 'vertical'

The experiments of approach #01 are primarily meant for verification of the envisaged structure of the structural mobile *Stable Equilibrium*, described in section 5.3. The longest cantilever includes three connected elements, and the maximum characteristic bending moment of the entire structure is $M_k = 210\,\mathrm{N\,m}$. To assure a sufficient global safety factor, the investigations with the concept, illustrated in fig. 7.6, are undertaken.

The investigations are separated in the categories 'vertical', bending around the strong axis, and 'horizontal', bending around narrow axis, as shown in the investigation concepts, illustrated in fig. 7.7.
The specimens tested vertical, are applied with a load, inducing a bending around the strong axis, the main impact of the concrete mobile in service. The motivation, to undertake the vertical test approach, is to achieve a valuation of the load bearing behaviour if the system is loaded beyond the ultimate limit state. Generally the system, regardless if described as a cantilever or a single span system, underlies the exposure to stability failure, since one narrow end is naturally under compression.

approach #01
verification of concrete mobile

{ appr01 }

---

bending around strong axis (elements vertical)		**bending around narrow axis** (elements horizontal)
{ _vert }		*{ _hor }*
cantilever beam point load at cantilever end increased to design state	**simply supported beam** point load at midspan increased until failure	**four point bending** load increased until failure
{ _1a }	*{ _1b }*	*{ _2 }*

Figure 7.6 Approach #01, investigation procedure and syntax of specimen numbering for the experiments with focus on the verification of concrete mobile *Stable Equilibrium*

The dimensions of the experiments chosen are taken from the concrete mobile *Stable Equilibrium*, with:

> Test 1 a) – the maximum cantilever, loaded with self weight only, with a span length of three elements

> Test 1 b) – the maximum single-span system, with a span length of also three elements, but loaded by the adjacent (lower) parts of the mobile.

The experiments undertaken are set up with unpretentious testing devices. An analog scale is used as a force meter and the deflections are observed with the help of a metering rule, with an accuracy of $1 - 2$ mm. The testing force is applied with the help of tension belts.
 The testing of the cantilever, experiment *{ appr01_vert_1a }*, as shown in fig. 7.8, is driven up to a weight of 143 kg, shown on the force meter. According to equilibrium conditions, that corresponds to an applied force of $\sim 16{,}5$ kg and a maximum bending moment around the strong axis of $M_{\max} = 370$ N m, thus a loading with a force factor of 3,85, compared to the self weight loading. The tested specimen did not fail and no visible cracking occurred.
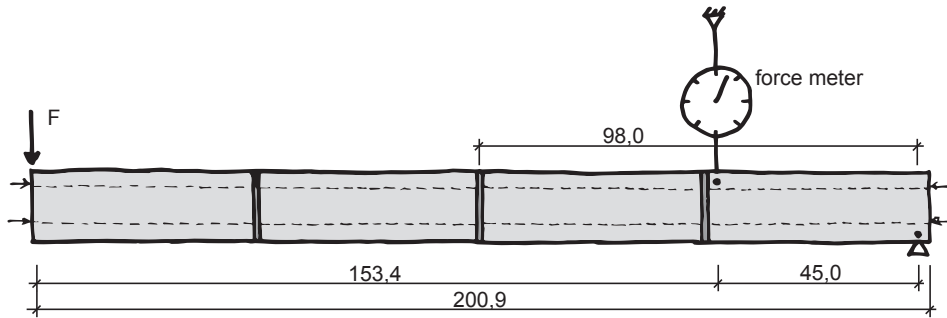
(a) *{ appr01_vert_1a }*; dimensions of cantilevering system of connected elements as present in *Stable Equilibrium* [cm]
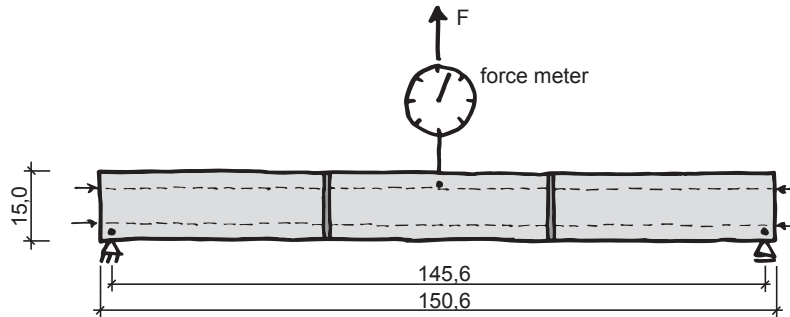
(b) *{ appr01_vert_1b }*; system to apply a bending moment induced by outer loading [cm]

Figure 7.7   Approach #01, test set-up 'vertical' – bending around strong axis
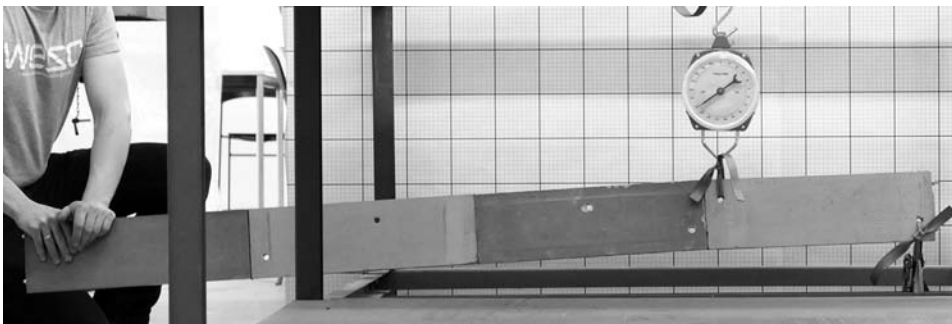
Figure 7.8   Load testing of cantilever *{ appr01_vert_1a }*. A load that resulted in a bending moment of $M_{\max} = 370\,\mathrm{N\,m}$ $(3,85 \times M_{\mathrm{selfweight}})$ was implemented, not leading to failure

(a) front view

(b) side view
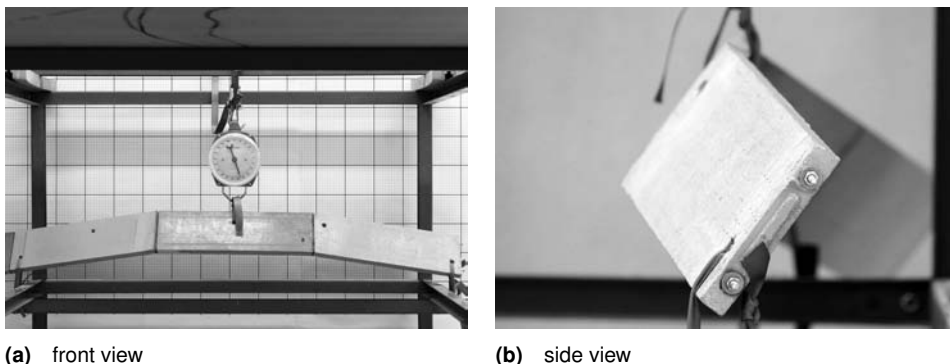
Figure 7.9   Load testing of a simply supported beam *{ appr01_vert_1b }* assembled with prefab elements. Displacement figure of the connected system is bending out of plane, thus stability failure

The experiment *{ appr01_vert_1b }*, as shown in fig. 7.7b, has the same applied impact, bending around the strong axis. In this case, the structural system chosen is a simply supported beam, with a point load at midspan. Within the experiment, the load is increased until failure.

The photographs in fig. 7.9 are documenting the investigations after testing. It can be observed that the failure is not a linear behaviour, where the collapse is defined by the material strength. In this case, the failure is driven by the global stability, where a (sudden) bending out of plane occurs from a distinct loading level.

Outlining the applied bending moment versus the displacements of the single span system, a distinct behaviour becomes apparent, as shown in fig. 7.10. Up to a certain level, the system is in a linear elastic range. Once the system starts to deflect out of plane, the inner lever arm drastically shrinks. Within the following loading (displacement) increments, this effect is amplified and the load bearing capacity is given by bending out of plane. As soon as this capacity is also 'consumed', the remaining load bearing is only given by a system, comparable with a catenary, provided by the tension elements.

As mentioned above, the maximum characteristic bending moment, occurring in the system of the concrete mobile *Stable Equilibrium*, is $M_k = 210 \, \mathrm{N\,m}$. The maximum characteristic bending moment on the resistance side, within the linear elastic range, is $M_{R,k} = 564 \, \mathrm{N\,m}$, as established within the experiments, refer table F.1. The corresponding global safety factor is $\sim 2{,}7$.

It may be noticed that a failure, although it is described as a stability failure, would not
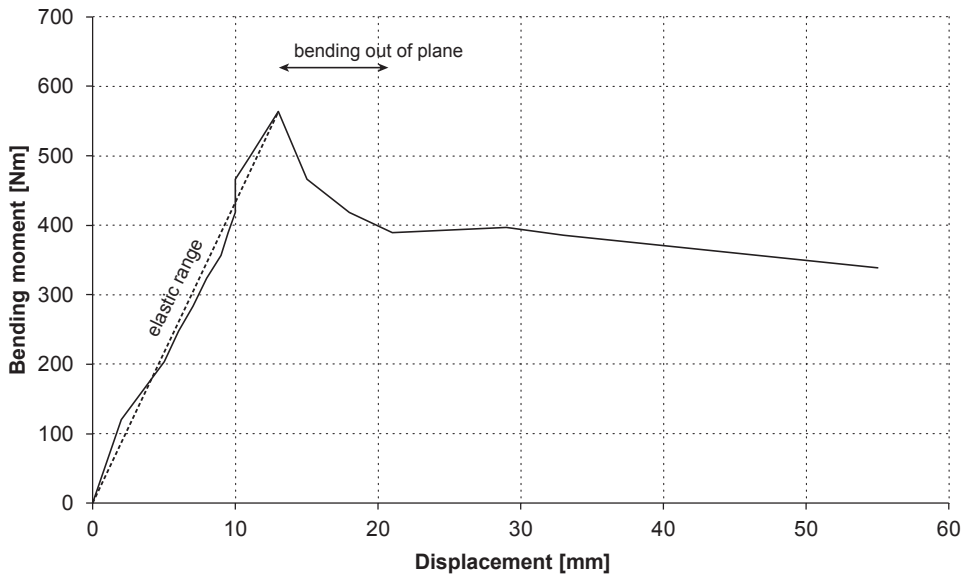
Figure 7.10 Load–displacement curve of vertical test set-up *{ appr01_vert_1b }*, a simply supported beam assembled with prefab elements. The path describes a distinct elastic range before the structure underlies stability failure out of plane

lead to a 'falling-down' of the sculpture, since a catenary system builds up, after the out-of-plane capacity is exceeded.

Representative photographs of the load bearing test, showing the significant points of the load – displacement curves, as well as the single values of the curves, investigated during the testing, are given in appendix F.1.1.

7.5.2 Experiment set-up – 'horizontal'

The experiments of the vertical set-up are illustrating the necessity of a load bearing capacity in the direction out-of-plane, although this type of loading is not envisaged for the structure in service.

Figure 7.11 shows the concept of a further experiment *{ appr01_hor_2 }*, where the focus is on the out-of-plane load bearing capacity, thus the bending around the narrow axis. Naturally, this loading type is contrary to the motivation, to realize concrete sections, as
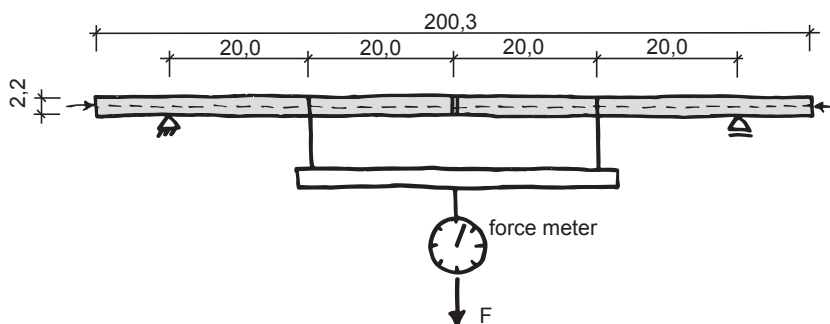
Figure 7.11 Approach [#]01, four point bending test set-up 'horizontal' *{appr01_hor_2}* – bending around narrow axis is the loading that has to be born if narrow system deflects out of plane [cm]

slender as possible. Nevertheless, it is a failure model, which is not negligible, also for the structure of the concrete mobile. The experiment envisages an investigation of the bending moment capacity around the narrow axis M_z. Two concrete elements are connected by a prestressing, induced by two threaded bars $\varnothing = 6\,mm$. The structural system is a simply supported beam, where two point loads are applied. In this four point bending test set-up, the force again is applied with the help of tension belts and separated in two forces of $F/2$, each by separating the force with a rigid bar.

In the photograph fig. 7.12, the experiment is shown, just before initial cracking of the concrete occurs. It can be noticed that the failure behaviour of the experiment is dominated by large deformations which are strongly visible even prior to failure, making the system (as a flat system) unserviceable. However, in this case, the bending around the narrow side provides a buckling resistance according the analytical buckling model. The maximum characteristic bending moment, from the analytical buckling model of the concrete mobile, is $M_{z,d} = 9{,}6\,N\,m$, as further documented in section 5.3.

Regardless of the consequences of large deformations, the system has a distinct load bearing behaviour. The applied load, versus the deformations observed, are plotted on a graph, shown in fig. 7.13. It can be noticed that there is an approximately linear elastic range at the beginning of the experiment, before an initial cracking occurs at a load impact of $M_z = 86\,N\,m$, which is a global safety factor of almost 9. As soon as the first visible cracking starts in the compression zone of the contact area within the joint, the deformation curve of the graph becomes more flat, and a plastic post-failure behaviour still allows
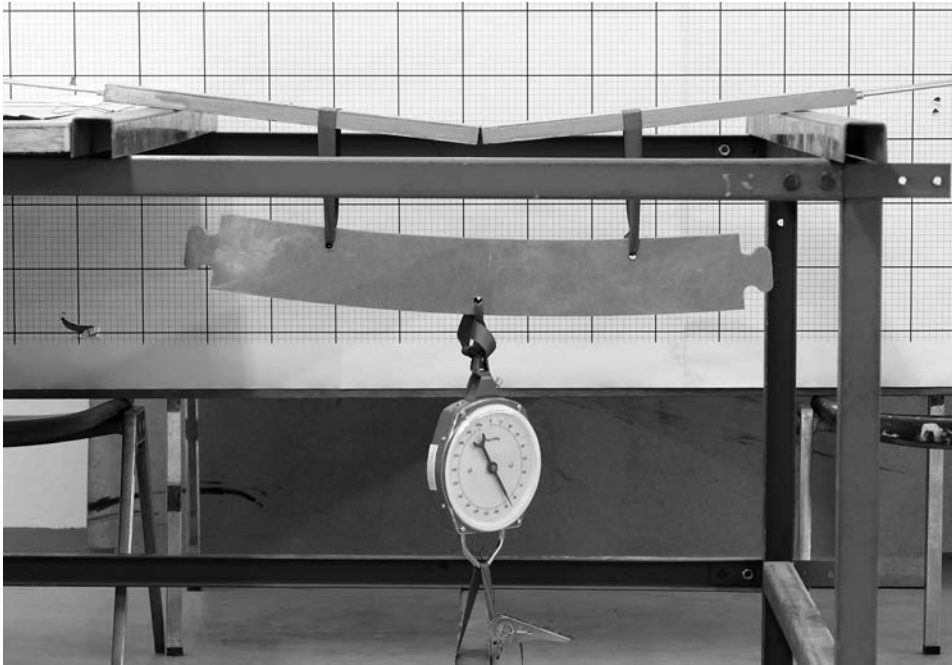
Figure 7.12 Experiment *{ appr01_hor_2 }*; specimens just before initial cracking occurs ($M_z = 86\,\mathrm{N\,m}$). Failure model shows that experiment is dominated by (unserviceable) large deformations

an increase of the loading, before the system completely fails at the point of collapse, indicated on the graph.

7.5.3 Intermediary outcome

The results of the experiments undertaken verify the buildability of the concrete mobile *Stable Equilibrium*, described in section 5.3. It has been observed that it is compulsory to provide a buckling resistance for a bending out of plane, induced by the imperfection of the loaded system.

Within the experiments of approach #01, the magnitude of the prestressing is hardly controlled; the screws of the threaded bars are hand-tightened only. Especially the visible large deformations of the horizontal four point bending test, shown in fig. 7.12, give the assumption that the magnitude of the prestressing may be a major criterion with a potential
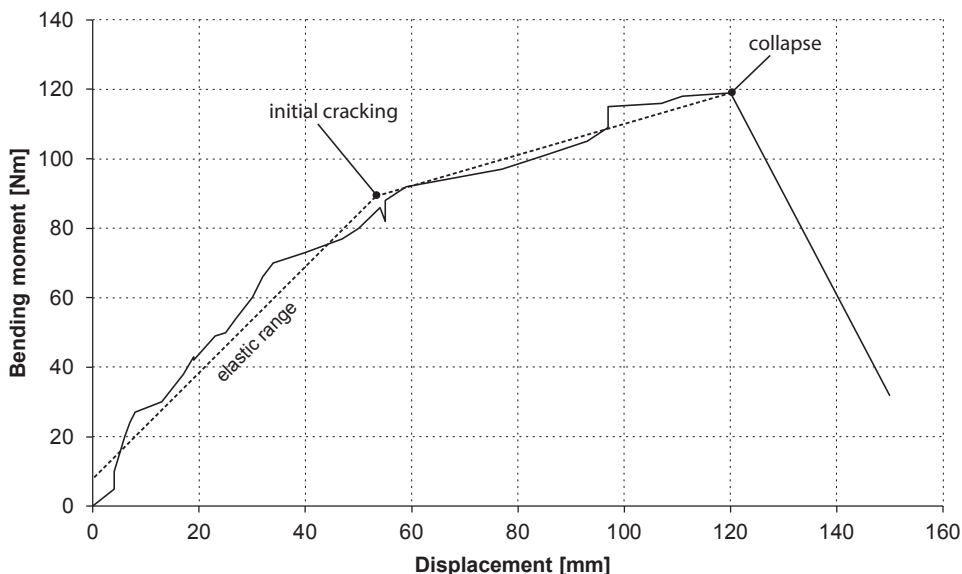
Figure 7.13   Load−displacement curve of horizontal test set-up *{ appr01_hor_2 }*

capability to increase the load bearing resistance if a counter inner moment, induced by prestressing, is achieved.

A further intermediary result has been observed within the choice of the prestressing media. The hulls, cast in the concrete, have an inner diameter of 8 mm, whereas the tendons are threaded bars $\varnothing = 6$ mm. Once the system deflects, the threaded bar shifts to the upper side of the inner diameter. In consequence, the inner lever arm downsizes, since the centroid of the bar shifts towards the compression zone. It may be mentioned that approaches using the same hulls, but flexible tension cables, magnify this effect, since the delta of the cable and the hull diameter increases.

According to Eurocode 3 [Eur05, tab. 3.4], the tension resistance of a threaded bar is calculated as:

$$F_{t,Rd} = \frac{k_2 \cdot f_{ub} \cdot A_s}{\gamma_{M2}} \tag{7.1}$$

With $k_2 = 0,9$; $f_{ub} = 400\,\text{N/mm}^2$; $A_s = 20,1\,\text{mm}^2$ and $\gamma_{M2} = 1,25$, a threaded bar $\varnothing = 6\,\text{mm}$ with the steel grade 4.6 has a tension capacity of $F_{t,Rd} = 5,8\,\text{kN}$.

In contrast, the full compression resistance of the concrete section can be calculated:

$$N_{c,Rd} = f_{cd} \cdot A_{netto} \tag{7.2}$$

With $f_{cd} = 45,3\,\text{N/mm}^2$ and $A_{netto} = 150\,\text{mm} \cdot 22\,\text{mm} - 2\,\varnothing\,10\,\text{mm} = 3143\,\text{mm}^2$, the full compression resistance force of the netto concrete section is $N_{c,Rd} = 142\,\text{kN}$.

Although the concrete compression capacity is given for the complete utilized concrete section, there is a large delta, between $2 \times 6\,\text{kN}$ for the tendons, and $142\,\text{kN}$ for the concrete. Between these two capacities is a difference factor of ~ 12.

In other words, it is expected that the capacity for a bending around the narrow axis can be increased substantially by increasing the tensioning magnitude.

The following issues are focused for an improvement of the capacities in the second approach:

> *Increase of steel grade:* To be able to increase the prestressing of the concrete, the enhancement of the steel grade is one effective proceeding.

> *Utilizing the space within the hulls:* The increase of both, the tensile stress area and the tensioning magnitude, ensures that the centroid does not shift towards the compression zone.

> *Predicting and control of tensioning magnitude:* In order to fully utilize the prestressing medium, a method needs to be evaluated to calibrate the tension force as accurately as possible.

7.6 Experimental investigation – approach #02 / high tensioning

7.6.1 Experiment set-up

It has been discovered within the previous approach that the load bearing capacity of prefabricated elements, connected with the help of a prestressing, is to a large extent dependent on the bending strength around the narrow axis. Due to stability deflections, orthogonal to the outer force direction, the joint connection tends to bend open. An inner

(a) Approach $^\#$02; test set-up

(b) Approach $^\#$02; envisaged specimen build up
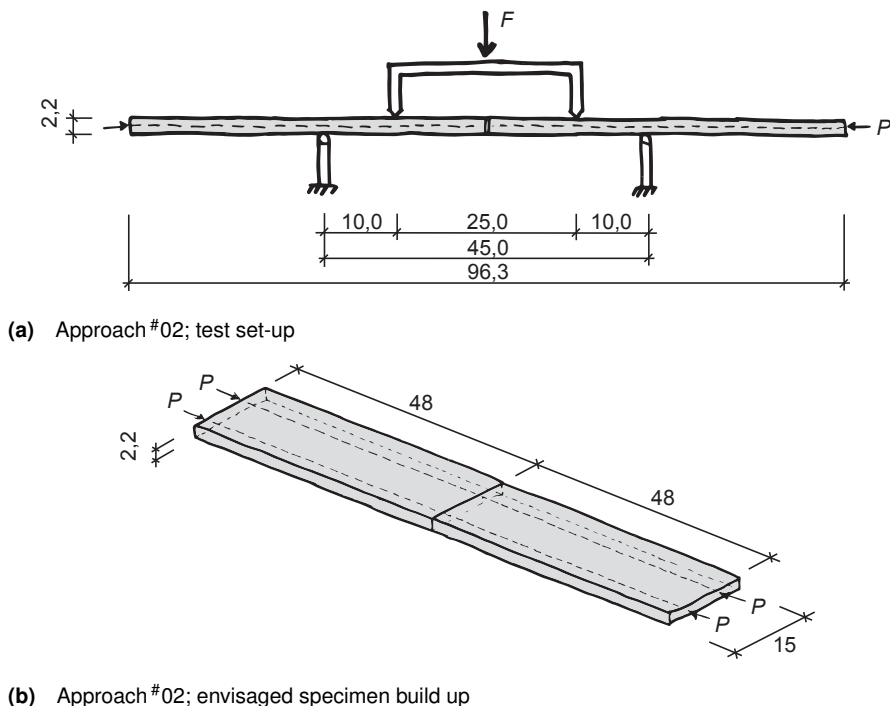
Figure 7.14   Approach $^\#$02; test set-up for prestressed connection [cm]

back turning moment, induced by the prestressing, has to be established to prevent a deformation of the joint. Naturally, the stability resistance increases with an increase of the prestressing, and thus of the activated back turning inner moment, within the joint.

To set up further experiments, investigating the bending capacity around the narrow axis, four point bending tests are envisaged, as illustrated in the concept shown in fig. 7.14. The prefabricated elements are directly taken from the concrete mobile *Stable Equilibrium*, with the dimensions $l = 480\,mm$, $b = 150\,mm$ and $h = 22\,mm$. To avoid a direct contact of the two adjacent concrete faces and respective unwanted stress peaks, an MDF plate with the thickness $t = 3\,mm$ is fitted inside the joint. In order not to falsify the results, the shear studs, as used for the concrete mobile, have been relinquished, since the joint is in the zero-crossing zone of the shear force distribution diagram.

  The utilization variation of the prestressing media and the investigation agenda are il-

approach #02
utilizing prestressing

{ appr02 }

prestressed section		**prestressed joint**		
{ _PS }		*{ _PJ }*		
stressing media: none - -	stressing media: threaded bars Ø 8mm grade 12.9	stressing media: threaded bars Ø 8mm grade 8.8	stressing media: threaded bars Ø 8mm grade 12.9	stressing media: steel wires Ø 2mm grade 1570
{ _0_0 }	*{ _M8_12.9 }*	*{ _M8_8.8 }*	*{ _M8_12.9 }*	*{ _D2_1570 }*
no. of specimen *{ _1 }* *{ _2 }* *{ _3 }*	*no. of specimen* *{ _1 }* *{ _2 }* *{ _3 }*	*no. of specimen* *{ _1 }* *{ _2 }* *{ _3 }*	*no. of specimen* *{ _1 }* *{ _2 }* *{ _3 }*	*no. of specimen* *{ _1 }* *{ _2 }* *{ _3 }*

Figure 7.15   Approach #02, investigation procedure and syntax of specimen numbering for the experiments with focus on utilizing prestressing

lustrated in the chart of fig. 7.15. To determine the influence of the actual joint, the investigations have been taken out for both, the undisturbed concrete section as well as the connected joined section. The series of tests started off with the concrete sections without a connection joint. First the 'pure' reinforced concrete section, without any prestressing and empty prestressing hulls, followed by a test series, with a prestressed concrete section, but without a joint. These series are indicated as 'prestressed section' *{ PS }*.
The following series are treating connected elements, build up with varying types and grades of the prestressing media. These series are indicated as 'prestressed joint' *{ PJ }*.
Each experiment set-up is carried out for three specimens *{ 1, 2 and 3 }* each.

7.6.2 Calibration of micro prestressing

7.6.2.1 Prestressing media investigated

Threaded bars and screws   The specimens investigated are completely without any curvature. Therefore there are no demands on a flexibility of the prestressing media. Threaded screw bars $\varnothing = 8\,\text{mm}$ were used in order to utilize the space available in the hull as well as to ensure a non-relocatable position of the centroid of the bar within the concrete section.

Two different steel grades have been used; 'grade 8.8' as the highest grade available with a zinc-coating and 'grade 12.9'. According to Eurocode 3 [Eur05, tab. 3.1], the yield strength f_{yb} and the ultimate tensile strength f_{ub} are covered up to 'grade 10.9'. Although 'grade 12.9', as used, is even higher, the values used for the pretension are kept within the range of the Eurocode.

With eq. (7.1) the tensile strength capacities for a utilized threaded bars can be calculated as follows:

$$F_{\text{t,Rd}}(\text{M8}, 8.8) = \frac{0{,}9 \cdot 800\,\text{N/mm}^2 \cdot 36{,}6\,\text{mm}^2}{1{,}25} = 21\,082\,\text{N} \tag{7.3}$$

$$F_{\text{t,Rd}}(\text{M8}, 12.9) = \frac{0{,}9 \cdot 1000\,\text{N/mm}^2 \cdot 36{,}6\,\text{mm}^2}{1{,}25} = 26\,352\,\text{N} \tag{7.4}$$

The elastic modulus of the threaded bars is independent from the steel grade:

$$E_{\text{b}} = 210\,000\,\text{N/mm}^2$$

Figure 7.16 shows a prestressed section end, where threaded bars grade 12.9 are used. The characteristic black colour of the high strength steel is noticeable.

Flexible strands   In order to investigate the possibility to transfer the connection technique to curved or free form concrete sections, a further experiment is envisaged, using flexible wires, as shown in fig. 7.1b.

The wires used are the series *TECHNOCABLES* from *CarlStahl®*. The product is a stainless steel strand construction 1×19 (nineteen wires in one strand) with material characteristics
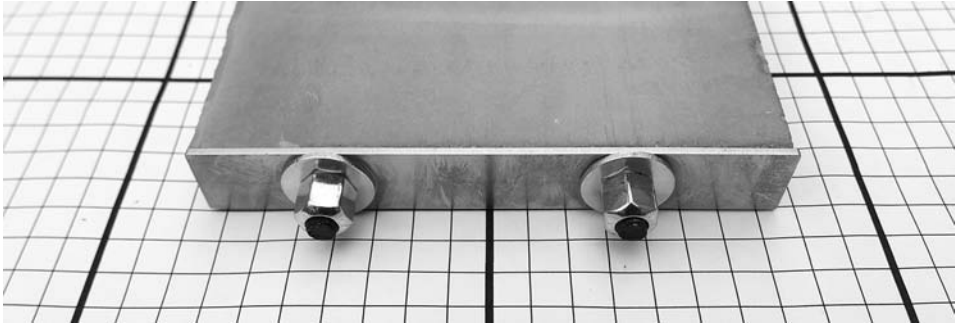
Figure 7.16 Jointed section, prestressed with two M8, grade 12.9; the black color of high strength threaded bars is noticeable

taken from the specifications of the manufacturer, see [Car15, 16]:

tensile strength: $f_y = 1570\,\text{N/mm}^2$

nominated outer diameter: $2\,\text{mm}$

area of singe wire: $A_i = 0{,}1106\,\text{mm}^2$

area of complete strand: $\sum\limits_{i=1}^{19} A_i = 2{,}102\,\text{mm}^2$

min. breaking load: $N = 3300\,\text{N}$

The tensile strength capacity for the flexible strand is calculated to:

$$F_{t,Rd}(D2, 1570) = \frac{0{,}8^{*)} \cdot 3300\,\text{N}}{1{,}25} = 2112\,\text{N} \qquad (7.5)$$

*) 20 % loss from the swaged terminal.

The elastic modulus of the strand, under consideration of the helical twisting of the wires, is taken as:

$$E_p = 195\,000\,\text{N/mm}^2.$$

7.6.2.2 Control of prestressing magnitude

In concrete prestressing concepts, the prestressing medium can be tensioned until its maximum capacity. Although it appears curious, the magnitude of the tension force does not increase by applying the outer service loads, because these loads are consuming the compressive stresses introduced in the concrete. The correlations of the strains are constant, apart from the deformations, induced by the outer loading. For the experiments undertaken here, the tension force magnitude applied, is utilized until the limit of the elastic range of the prestressing media, not until the ultimate breaking limit, which would be within the plastic range.

It seems obvious that the control of the prestressing magnitude is essential for the realization of the experiments. A prestressing too low will not satisfy the expectations of the load bearing capacity and a prestressing too high would endanger the tendons to shift into the plastic range, since these are already fully utilized.
There are different methods to monitor the tension force applied. A selection is given below.

Strain gauges: With stripes stuck onto a specimen, even small strains can be recorded. With the linear relationship between the measured strain and the stress magnitude as a result, the use of stress gauges is a reliable and common method of monitoring stresses and forces.
In this case, the tendons are inside the concrete section, complicating the installing of the stripes with the corresponding electrical leads.
An existing method, relinquishing the necessity of accessibility, is the installing of the stress gauge through the center axis from the end of the screw. Disregarding the extensive effort, this method weakens the effective stress area of the tension rods.

Control of torque friction: The friction between the screw head and the adjacent area, stressed by the screw, increases with an increasing tensioning of the screw or screw nut respectively. A constant friction allows inferences between the magnitude of the torque moment, while tightening the screw nut and the force applied in the screw. Torque spanners, measuring the torque moment, are widely used to prevent off-shearing of screw heads.
As mentioned, this method requires a constant friction of the contact areas. This coefficient is dependent on a multitude of boundary conditions, diminishing the accuracy of this method.

Control of deviation way: Similar to the application of stress gauges, the control of the extension way is based on the linear elastic relationship between stress and strain of the material. The challenge of the measuring are the small values that have to be determined. For the experiments described, the deviation is $\Delta l = 1 - 4$ mm. A measuring with the help of common metering rules can be excluded, because of the missing accuracy.

However, every standardized thread has a distinct inclination of the grooves. Unified screw threads have a flank angle of $\alpha = 30°$. The pitch P is the double distance from root to crest of the threads, and defines the distance of a screw-nut moving with one turn of $\vartheta = 360°$. Standard metric screw threads, as used here, have the following pitches:

$$P(\text{M6}) = 1,00\,\text{mm}$$

$$P(\text{M8}) = 1,25\,\text{mm}$$

During the tightening of the screws, the angle of rotation can be controlled by 'counting' the increments of rotation. Since the screw heads have the geometry of a hexagon, the counting can be done with the accuracy of a half increment of the screw (flange or edge up). Thus a rotational angle of a twelfth part of a circle ($\vartheta = 30°$) can be twisted accurately. That equates an elongation (and respectively an accuracy) of $\Delta l = 1,25\,\text{mm}/12 \approx 0,10\,\text{mm}$ that can be reached.

The method of controlling the deviation way, with the help of the rotation angle of the screw heads, is chosen for the experiments here.

7.6.2.3 Prestressing arrangements

All prestressing media of the specimens, prepared for the four point bending tests, are utilized to the limit of the respective elastic range. To apply the prestressing force of the tendons, the screw heads are tightened and the extension way Δl is controlled by the rotation of the hexagonal screw heads. Since all prestressing processes are carried out within the linear-elastic range, the calculation of the necessitated way is done with *Hooke*'s law of elasticity, describing the proportional relationship between the elastic deformation, and impact forces with the proportionality factor E:

$$\sigma_\text{x} = \frac{N_\text{x}}{A} \tag{7.6}$$

$$\varepsilon_x = \frac{\Delta l}{l_0} \tag{7.7}$$

$$\sigma_x = E \cdot \varepsilon_x \tag{7.8}$$

Converting and inserting the equations above gives the necessary extension way, separated for each material:

$$\Delta l_i = \frac{N_x \cdot l_{0,i}}{E_i \cdot A_i}$$

The input values for the calculations are as summarized below.

Elastic moduli E_i:

elastic modulus concrete C80/95: $E_{cm} = 42\,000\,\text{N/mm}^2$

elastic modulus MDF plates: $E_{c,1} = 3100\,\text{N/mm}^2$ [DIN01a]

elastic modulus threaded bars: $E_b = 210\,000\,\text{N/mm}^2$

elastic modulus steel strands: $E_p = 195\,000\,\text{N/mm}^2$

Stress areas A_i:

area of brutto concrete section: $A_{brutto} = 150\,\text{mm} \cdot 22\,\text{mm} = 3300\,\text{mm}^2$

area of netto concrete section: $A_{netto} = A_{brutto} - 2\,\text{Ø}\,10\,\text{mm} = 3143\,\text{mm}^2$

effective stress area M8: $A_s\,(M8) = 36{,}6\,\text{mm}^2$

Initial lengths $l_{0,i}$:

length of concrete element: $l_{0,c} = 480\,\text{mm}$

length of MDF spacers: $l_{0,MDF} = 3\,\text{mm}$

length of end steel plates: $l_{0,s} = 4\,\text{mm}$

Table 7.2 Prestressing deviation lengths and respective screw rotations for prestressed specimen

deviation			prestr. section	prestressed joint		
			PS_M8_12.9	PJ_M8_8.8	PJ_M8_12.9	PJ_D2_1570
force per tendon		[N]	26 352	21 082	26 352	2 112
force on section		[N]	52 704	42 164	52 704	4 224
elastic	Δl_c	[mm]	0,19	0,31	0,38	0,03
	Δl_{MDF}	[mm]	-	0,01	0,02	0,00
	Δl_p	[mm]	1,67	2,66	3,33	5,17
	$\sum \Delta l_{el}$	[mm]	**1,86**	**2,98**	**3,73**	**5,2**
	ϑ_{el}	[°]	537	859	1074	1872
	rot'ns	[-]	1,49	2,39	2,98	5,2
creep	Δl_{cc}	[mm]	**0,05**	**0,08**	**0,10**	**0,01**
	ϑ_c	[°]	14	23	28	3
	rot'ns	[-]	0,04	0,06	0,08	0,01

Within the time frame, between tightening the screws and the actual testing, the concrete sections underlie a creep deformation, thus a plastic shortening in load direction. This effect is taken into account by re-adjusting the screws, just before testing, about the value of creep deformation. The creep shortening of the concrete $\varepsilon_{c,c}$ is calculated as:

$$\varepsilon_{cc} = \varphi(t,t_0) \cdot \varepsilon_{c,el} \tag{7.9}$$

with

$$\varphi(t,t_0) = 0,2566$$

The determination of the coefficient of creep $\varphi(t,t_0)$ for constant stress levels, according to DAfStb, issue 525 [DAf10, 60], is given in appendix F.2 on page 294.

Table 7.2 sums up the prestressing deviation lengths for the experiment series undertaken. It is separated between the elastic deviation and deviation from creep.

Table 7.3 Series of specimens investigated with four point bending tests

prestressing media	concrete sections only *PS*	prestressed joints *PJ*	prestressing [kN]
no prestressing device	PS_0_0_1	-	0
	PS_0_0_2	-	0
	PS_0_0_3	-	0
threaded bars 'M8, 12.9'	PS_M8_12.9_1	-	52,7
	PS_M8_12.9_2	-	52,7
	PS_M8_12.9_3	-	52,7
threaded bars 'M8, 12.9'	-	PJ_M8_12.9_1	42,2
	-	PJ_M8_12.9_2	42,2
	-	PJ_M8_12.9_3	42,2
threaded bars 'M8, 8.8'	-	PJ_M8_8.8_1	52,7
	-	PJ_M8_8.8_2	52,7
	-	PJ_M8_8.8_3	52,7
steel wires 'D2, 1570'	-	PJ_D2_1570_1	4,2
	-	PJ_D2_1570_2	4,2
	-	PJ_D2_1570_3	4,2

7.6.3 Four point bending load capacity tests

The load bearing capacity tests are carried out as four point bending tests, where a constant bending moment is gained in the zone of the prestressed connections. The experiments are carried out with the testing machine *ToniTrol-250 kN* of the *Amtliche Materialprüfanstalt für das Bauwesen* AMPA, *University of Kassel*.

The load tests are 'driven over the way', where the way in force-directions is applied, and the corresponding force is recorded. The testing speed is set to 0,1 mm/sec. The order of the fifteen samples investigated is listed in table 7.3.

7.6.4 Evaluation of experimental results

7.6.4.1 Qualitative evaluation of failure behaviour

The four point bending test started with undisturbed concrete sections with no prestressing, to achieve a contrast level for a comparison with the prestressed specimen. As already

known from the seamless arrangements in section 6.5.1, these specimens show a ductile behaviour with a large post failure load bearing capacity. The occurring cracks are well distributed over the length of the maximum bending moment, as shown in fig. 7.17a.
The following experiment is also an undisturbed concrete section, but prestressed with two M8 grade 12.6 and a prestressing load of 52,7 kN. This experiment, obviously with the highest expected load bearing capacity, is tested within the same boundary conditions of the set-up. Since the loading machine is driven over the way, the time duration is similar, but it is noticeable that the corresponding force is increased rapidly[3]. Until the abrupt failure at the end of the elastic range, no visible cracking occurs because of the compressed section. The failure is accompanied with an acoustic bang, caused by concrete failure, and a sudden drop of the force recorded.

The capacity after failure is still existing, similar to non-prestressed concrete sections. The failed system catches up after the prestressing is released from the ultimate failure.
It can be noticed from the elements after testing, shown in fig. 7.17b, that the cracks are not well distributed over the entire stress zone. The section fails explosively, with a horizontal splitting failure from an initial cracking point, which is located randomly within the zone of the maximum bending moment. Thus the failure can be described from both, a compressive failure of the concrete section at an initial point as well as the subsequent splitting failure from this initial crack, until the load introduction point at the end of the section.

The failure of the connected elements is similar to the prestressed undisturbed section, see fig. 7.18. The main difference in the qualitative failure behaviour is that the location of the initial cracking point is (foreseeable) in the middle, at the thrust of the two connected elements. Also the deflection figure is rather triangular and not parabolic. This can be explained with the MDF joint inlay that allows a small rotation in the transition zone. Comprehensive photographs of the elements during the testing are shown in appendix F.2.2.
An exemption, and thus an investigation with no continuative results, is the experiment with the connected elements, prestressed with flexible steel cables. Loaded from the bending machine, the elements deflect up to the bottom of the testing machine. Since the machine used (*ToniTrol-250 kN*) needs a minimum testing force level of $\sim 2 \times 0,5$ kN, no force could be recorded, because the resistance stiffness of the specimen is too low. Re-

---

[3]obviously astonishing the executing staff-member of the concrete laboratory
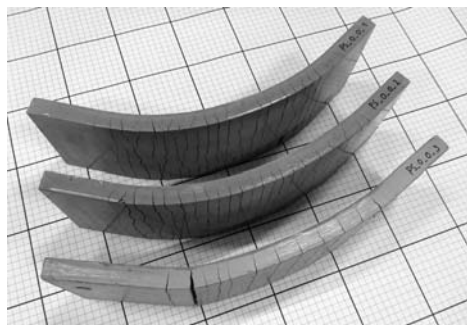
(a) Crack patten of specimen without prestressing; {PS_0_0_1,2,3}
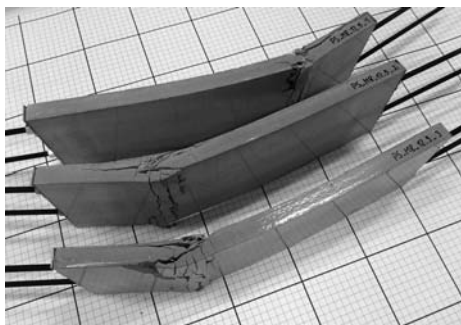
(b) Crack patten of specimen prestressed with 52,7 kN; {PS_M8_12.9_1,2,3}

Figure 7.17 Crack pattern of non-connected concrete sections after load bearing test

Table 7.4 Resultant stresses from outer- and inner (prestressing) loads

Series	P [kN]	$M_{k,max}$ [Nm]	$M_{k,max,\overline{123}}$ [Nm]	$\sigma_p{}^a$ [N/mm^2]	$\sigma_{k,b}{}^b$ [N/mm^2]	$\sigma_{tot,t}$ [N/mm^2]	$\sigma_{tot,b}$ [N/mm^2]
PS_0_0_1	0	240,0					
PS_0_0_2	0	229,9	**202,3**	0	16,7	−16,7	16,7
PS_0_0_3	0	137,0					
PS_M8_12.9_1	52,7	805,0					
PS_M8_12.9_2	52,7	843,0	**794,8**	−16,0	65,7	−81,7	49,7
PS_M8_12.9_3	52,7	736,5					
PJ_M8_12.9_1	52,7	462,5					
PJ_M8_12.9_2	52,7	511,0	**489,5**	−16,0	40,5	−56,4	24,5
PJ_M8_12.9_3	52,7	495,0					
PJ_M8_8.8_1	42,1	406,5					
PJ_M8_8.8_2	42,1	391,5	**404,2**	−12,8	33,4	−46,2	20,6
PJ_M8_8.8_3	42,1	414,5					

with $W_y = b \cdot h^2/6 = 12\,100\,\text{mm}^3$; '+' tension; '−' compression
[a] from prestressing (inner) load
[b] from outer load; $\sigma_{k,t} = -\sigma_{k,b}$
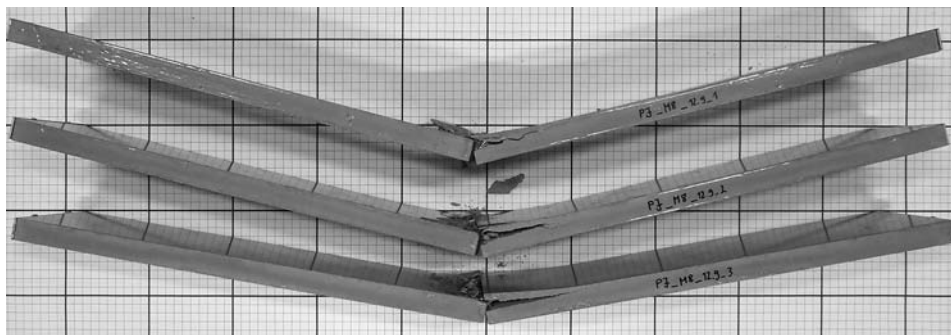
(a) Crack patten of specimen prestressed with 52,7 kN; { PJ_M8_12.9 $\overline{1,2,3}$ }
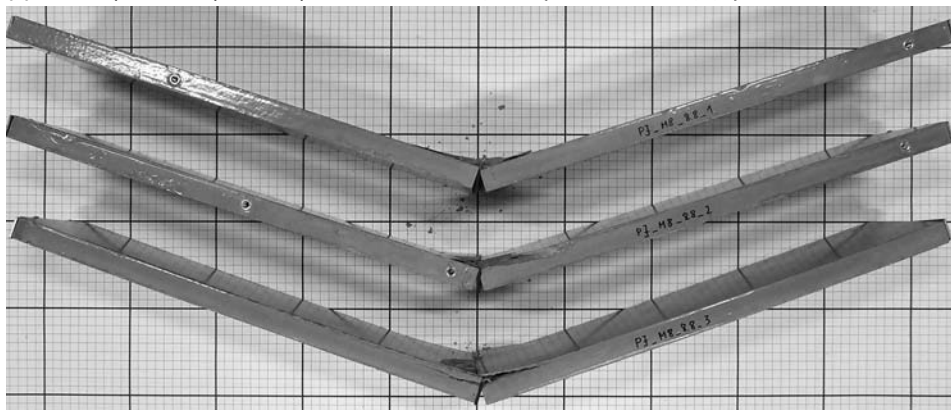
(b) Crack patten of specimen prestressed with 42,2 kN; { PJ_M8_8.8 $\overline{1,2,3}$ }
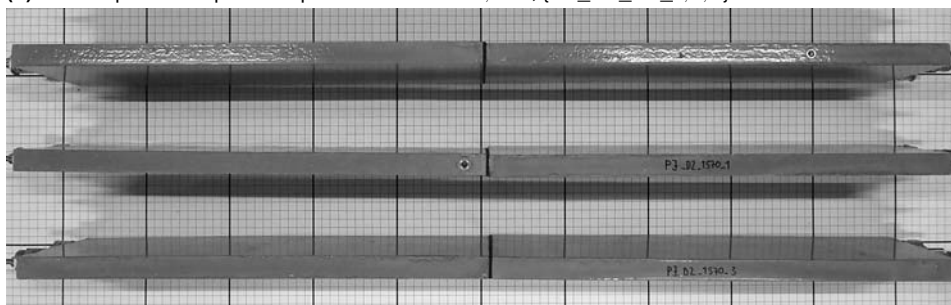
(c) Crack patten of specimen prestressed with 4,2 kN; { PJ_D2_1570_$\overline{1,2,3}$ }, no material failure

Figure 7.18 Crack pattern of connected concrete sections after four point bending tests. The higher the prestressing, the smaller the deformation prior to failure; prestressing with cables is not feasible, as shown in fig. 7.18c

leasing the test load leads to a spring-back of the elements to the initial position, with no failure in both, the concrete elements and the prestressing cables.

7.6.4.2 Numerical evaluation of failure behaviour

The magnitudes of the load bearing capacities are listed in table 7.4. Significant values are the resistant outer loads, the bending moments, applied with the four point bending test set-up. The deviations of the capacities are directly dependent on the level of the inner prestressing. Furthermore, an explicit cohesion can be observed, whether the sections are connected or undisturbed concrete sections. Not self-evident at all is the fact that the capacities of the prestressed and connected elements are significantly higher (factor $f > 2$) than the non-prestressed concrete only sections.

The load – displacement plots in fig. 7.19 are illustrating the difference in the resistances of the experiments undertaken. The gradients are determined as median gradients from three samples $\overline{1, 2, 3}$, investigated for each experiment. It may be noticed that the gap in the gradients, directly after failure, resulted in the averaging of three individual curves. A large deviation can be recognized within the linear elastic range, up to the point of ultimate failure M_{max}. Within the post failure behaviour, all samples are behaving similarly and, to a certain grade, unpredictably.

As the basis material, a micro mesh reinforced concrete, *DUCON*, as described in section 4.1.3.3, is used. It is furthermore mentioned that the high ductility of this material is not utilized within the prestressing connection method, apart from the post failure capacity, which is much lower than the resistance within the elastic range.

The total stresses σ_{tot} inside the section in the zone of the maximum loading, can be decomposed in two partitions; the stress from the prestressing σ_{p} and the stress from the outer loading σ_{k}. Ideally the sections are fully compressed to avoid a gap in the joined area. Table 7.4 gives the superposed total stresses on the top side $\sigma_{\mathrm{tot,t}}$ and the the bottom side $\sigma_{\mathrm{tot,b}}$ respectively. The resultant stresses on the bottom side are tensile stresses, causing a gaping of the joint. This is the reason why the prestressed samples with the undisturbed concrete sections, are gaining the highest capacities. To assimilate the connected and unconnected elements would require an even greater prestressing.

A comprehensive illustration of the individual load – displacement gradients is given in appendix F.2.2.
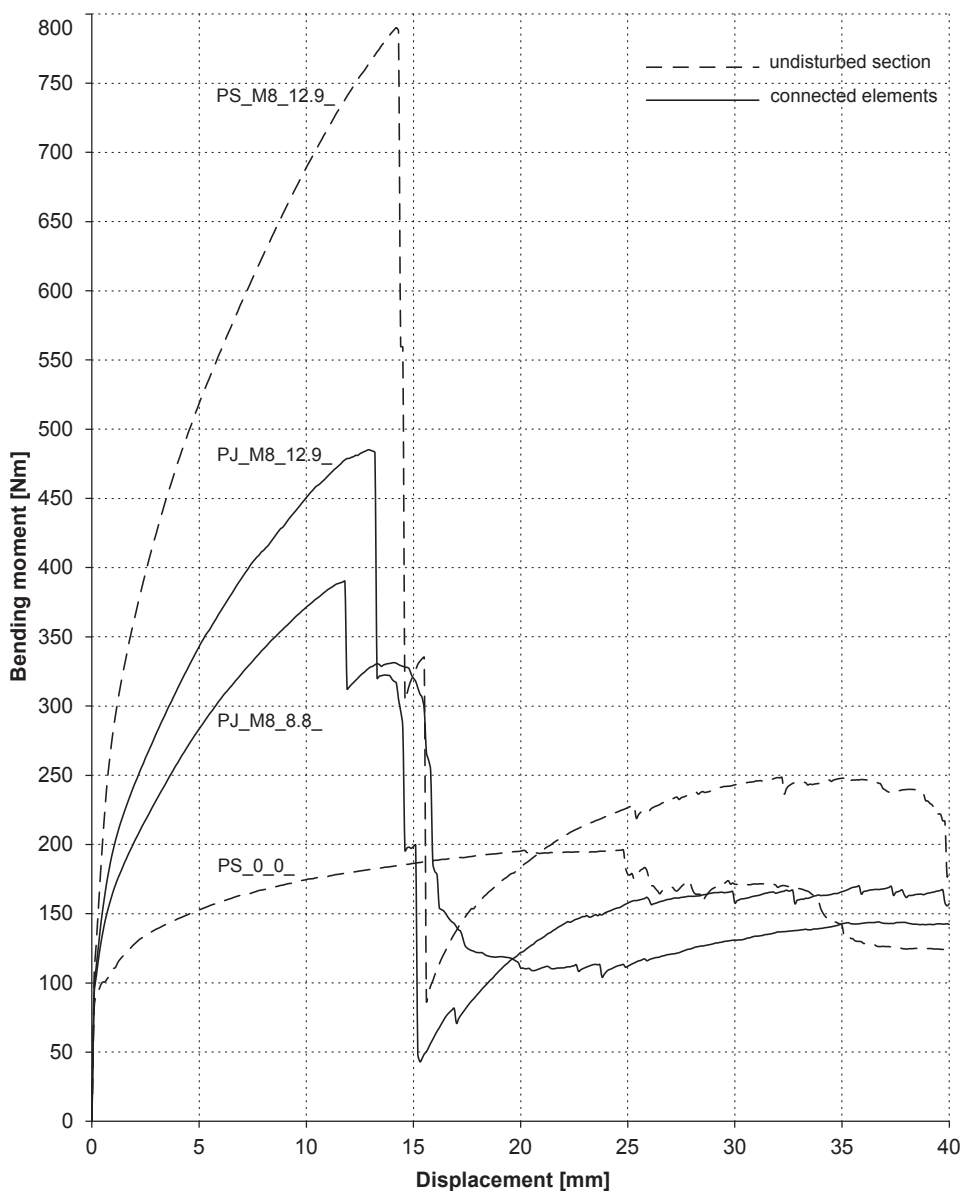
Figure 7.19 Load – displacement plots for non-connected concrete sections (dashed line) and connected elements (solid line), plots are showing the mean value graphs of specimen $\overline{1, 2, 3}$
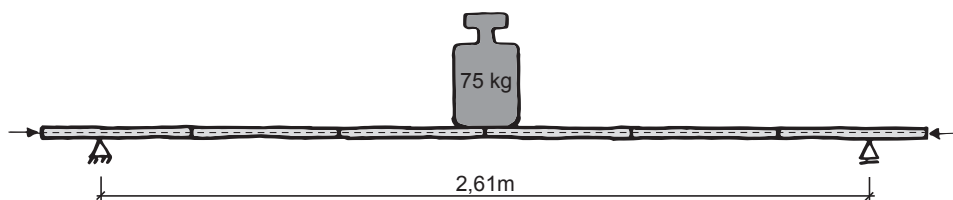
Figure 7.20 Illustration of gained capability: Equivalent structural system assembled with prefabricated elements, with the same bending moment applied as for prestressing connection investigations

7.7 Outcome – 'prestressing connection technique'

A method has been developed to assemble prefabricated slender concrete elements as a dry-fit connection method. The results exceed the demands, given by the concrete mobile *Stable Equilibrium*, by far. It has been shown that the load bearing capacity of the connected elements is even higher than the one from a monolithic cast reinforced concrete section with no prestressing.

The median characteristic bending moment, accomplished for a prestressed concrete section, with a thickness of $h = 22\,\text{mm}$, is $M_k = 489{,}5\,\text{N m}$. That equates with a simply supported beam, loaded by an average person, with the span length of $l > 2{,}6\,\text{m}$, as illustrated in fig. 7.20. However, such a system would require a pre-cambering, to counteract the elastic deflections.

The system still has potential to increase the load bearing capacity, by further advancing the prestressing magnitude. As soon as the lower face of the specimen is under tension, the joint is gaping. The subsequent effect is a decrease of the contact zone and thus a smaller inner lever arm.

A preliminary outlook is to increase the prestressing by adding tendons, although a spacing distance of $e = 75\,\text{mm}$ is already dense. A further option would be to increase the steel grade of the threaded bars.

One (however negative) outcome is the non-feasibility of the flexible cables. A cable strand with swaged terminals requires too much space for the threads at the end of the cables. Furthermore, these cables have to be tailored, which is a disadvantage according to the planning effort. A prestressing device needs to be developed with no loss of space within the flexible hulls and a tightening system that allows the monitoring of the force applied.

8 Conclusion

8.1 Results and achieved objectives

Material-optimized structures are to a great extend relevant in architecture and the building industry. Not only because of aesthetic appearances and design, but also in the context of resource shortages and rising standards in sustainable design.

Concrete, as an artificial stone with high strength characteristics, producible in almost arbitrary shapes, is an appropriate construction material for these postulated objectives.

Slenderness and reduced cross-section dimensions of structures, and particular concrete shells, are achieved by two measures: The increase of stiffness and strength characteristics, as well as the directed allocation of material within the design space, in order to create form-dependent structures with consistent stress fields.

On the material side, latest research developments led to high- and ultra-high performance concretes, with extremely high compressive strength capacities, closing up with properties of steel. Such concrete has workable consistencies, is self-compacting and characterized by a high density and durability. In combination with reinforcement strategies, suitable for the respective boundary conditions, tensile- and bending-tensile strengths as well as a ductile material behaviour is achieved.

With respect to the design, diverse form finding and optimization tools have been developed, facilitating the design of structurally efficient geometries, under consideration of multiple boundary conditions and load combinations. The creation, capturing and handling of digital models is enabled by advanced processing and storage capacities. Standardized formats and interchanges allow the transfer of data from design to manufacturing, minimizing sources of error.

Within this thesis, possible form finding methods of experimental and numerical nature, as well as optimization and design strategies are presented. The implementation, including the specialties of double-curved formwork and material options are comprehensively illustrated and discussed.

The necessity of prefabrication under laboratory conditions is outlined, in order to fulfill

the environmental requirements of sensitive mixing and casting processes as well as the conditions of post treatment.

The problem statement that consequently rises, of how to create load bearing connections of thin-walled concrete elements, is picked up. The contradiction of the possibility to reduce cross-section dimensions on one hand, and the thereby originating complexity of discontinued homogeneity on the other hand, is argued.

In order to develop strategies of connection techniques, in the first instance, mechanical principles are revealed and categorized, according to their respective effects.

Validated at realized structures as practical examples, connection techniques for slender, prefabricated concrete elements are proven. These case studies serve for both, problem identification as well as demonstration medium for applied solutions. All of the selected objects are in service and/or presented to the public. A therefore required accuracy, safety and high quality finish is invariably given for all projects presented.

Two developed techniques, 'seamless rigid connections' and 'micro prestressing connections' are investigated elaborately. The application range is determined, and the capability of either method is verified by means of experimental surveys.

With the development of 'seamless rigid connections', the focus is on the creation of stop-ends inside the formwork, allowing mesh wire reinforcement to stick out, in order to enable an overlapping in a joint area. The formwork sealing with water soluble lime mortar has been proven feasible. Investigations, considering several reinforcement allocations, confirmed the minor influence of the concrete texture, disturbed by the temporary mortar joint. The outcome of that survey is given, supplementing the feasibility of this joint technique on site and verifying the construction method of the concrete bench *Möbiusban(k)d*.

The invented technique of 'micro prestressing connections' is an implementation of a concept, which scales system dimensions of reinforced and prestressed concrete. The theorem of a non-existent buckling sensitivity, due to an internal, self-levelling force-equilibrium, is revealed. A comprehensive detailing of prestressing media, the control of deviation-measures, as well as the integration and embedment inside the narrow concrete sections, is executed. Experimental investigations prove a gained capacity, as outlined in the outcome of that survey. The load bearing capacity considerably exceeds the intended purposes of the exhibited concrete mobile *Stable Equilibrium*.

In context of this thesis, connection techniques as construction principles for prefabricated elements, with minimized cross-section dimensions, have been developed. The

range of application for the implementation of slender concrete shells in architecture has been expanded.

The techniques developed are applicable for any geometry and scale, offering new opportunities in processing contemporary concrete shell structures for architects and engineers.

8.2 Future prospects

The investigations, concepts and developed fundamentals of this research thesis raise subsequent questions, tasks and potentials for further research efforts, in order to transfer the techniques investigated to serial production.

A potentially promising approach is seen in the expansion of micro prestressing to curved- and double-curved concrete sections. Whereas threaded (straight) bars have been used within this survey, the development of applicable, flexible prestressing media could be one issue to be investigated. This includes the construction of the tendon-ends, the application and monitoring of tensioning and the discussion whether a re-tensioning should be enabled to counteract creep and shrinkage effects.

The transfer of connection techniques, from planar to freeform shapes, includes a neat examination of the joint geometry. As discovered within student research projects, which are not presented in this thesis, the design procedure of joints is geometrically challenging. Postulating intermediate layers[1] of constant thickness, the intersections of the joints are inconsistent, or joints are respectively twisted . A technical construction and automated implementation is another research prospect.

Also the elaboration of construction stages, the sequence of element assembly and falsework design, is a design task that requires further considerations.

A research field of great relevance, however less related to this thesis, is the concept development of adaptive and flexible formwork. The debate of increasing sustainability in building construction, postulates the consideration of formwork fabrication, accounting to a mass and emission balance. A rethinking of design procedures can be one approach, where the realization of a desired shape, with an appropriate formwork, is inverted to a determination of possible shapes, convertible with a predefined, reusable and sustainable shuttering concept.

---

[1]The intermediate layer inhibits the formation of stress peaks, occurring by the pressing two adjacent faces, made of concrete as a brittle material, similar to mortar joints in masonry construction

List of Figures

List of Tables

Bibliography

[ABVW14]   Sigrid Adriaenssens, Philippe Block, Diederik Veenendaal, and Chris Williams. *Shell Structures for Architecture: Form Finding and Optimization*. Taylor & Francis - Routledge, 2014.

[ACF$^+$14]   Shahram Abbasian, Leon Charlet, Harun Faizi, Jessica Froese, Adrian Golab, Christoph Herlitze, Denitsa Koleva, Michael Korn, Jannik Kratzenberg, Svenja Krieg, Nils Kuehn, Jakob Leppin, Nora Levsen, Alexander Lischke, Yiyang Liu, Henrik Neusuess, Laura Nolte, Richard Pfeiffer, Tim Reichert, Florian Reichmann, Jan Niklas Rieckmann, Aliaksei Rybalchanka, Julia-Yvonne Scharf, Witali Suchan, Andreas Steffen, Serge Well, and Cynthia Ward. *Concrete Structural Surface Shell; Structural Surface-Hochleistungstragwerke aus duktilem Beton*. Reader: Dokumentation Projektarbeit Sommersemester, 2014.

[Add14]   Bill Addis. Physical modelling and form finding. *Shell Structures for Architecture: Form Finding and Optimization, Chapter 4 (eds S. Adriaenssens, P. Block, D. Veenendaal and C. Williams)*, pages 32–43, 2014.

[AG05]   Ralf Avak and Ronny Glaser. *Spannbetonbau Theorie Praxis Berechnungsbeispiele*. Bauwerk Verlag Berlin, 2005.

[And04]   Matthias Andres. *Zum Stabilitätsnachweis von Schalentragwerken aus Hochleistungsbeton*. PhD thesis, Bergische Universität Wuppertal, 2004.

[BBF$^+$08]   Hubert Bachmann, Martin Benz, Horst Falkner, Dominique Gerritzen, and Hans Wlodkowski. Das neue Bewehrungssystem; Druckglieder mit hochfestem Betonstahl SAS 670/800. *Beton-und Stahlbetonbau*, 103(8):530–540, 2008.

[BDEN13]   Henning Baurmann, Jan Dilling, Claudia Euler, and Julius Niederwöhrmeier. *Scale – Tragen und Materialisieren : Stützen, Wände, Decken*. De Gruyter Basel, 2013.

[Bec08]   Martin Bechthold. *Innovative surface structures: Technologies and applications*, volume 1. Taylor & Francis New York, 2008.

[Ben02]   David Bennett. *Innovations in concrete*. Thomas Telforf Publishing. Thomas Telforf Ltd, 1 Heron Quay, London, 2002.

[Bil14]   David Billington. *Der Turm und die Brücke – Die neue Kunst des Ingenieurbaus*. John Wiley & Sons, 2014.

[Blo16]   Philippe Block. Parametricisms structural congeniality. *AD Architectural Design*, 86(2):68–75, March/April 2016. Special issue P. Schumacher (Ed.) – Parametricism 2.0: Rethinking Architectures Agenda for the 21st Century.

[BLR14]   Philippe Block, Lorenz Lachauer, and Matthias Rippmann. Thrust network analysis – design of a cut-stone masonry vault. *Shell Structures for Architecture: Form Finding and Optimization, Chapter 7 (eds S. Adriaenssens, P. Block, D. Veenendaal and C. Williams)*, pages 70–87, 2014.

[Bor62]   Joachim Born. *Schalen, Faltwerke, Rippenkuppeln und Hängedächer in Stahlbeton und Spannbeton – Band 1 Doppelt gekrümmte Schalen*. Werner, 1962.

[Brü16]   Eugen Brühwiler. Strengthening and sustainability of RC-slabs using UHPFRC – concept and applications. 4th International Symposium on Ultra-High Performance Concrete and High Performance Construction Materials, HiPerMat, Kassel, 2016. Session C6 speech: 2016-03-10.

[BVB14]   Shajay Bhooshan, Diederik Veenendaal, and Philippe Block. Particle-spring systems – Design of a cantilevering concrete shell. *Shell Structures for Architecture: Form Finding and Optimization, Chapter 9 (eds S. Adriaenssens, P. Block, D. Veenendaal and C. Williams)*, pages 102–113, 2014.

[Car15]   Carl Stahl GmbH. Carl Stahl[®] Technocables Edition No.6. `http://www.carlstahl-technocables.de/fileadmin/files/katalog-carl-stahl-technocables.pdf`, 2015. Accessed: 2015-12-23.

[Chi00]   John Chilton. *Heinz Isler – The engineer's Contribution to Contemporary Architecture*. Thomas Telford Ltd, 2000.

[Cia12]   Ciaran Conlon.   James Waller: Economy in Concrete.   `http://wallerconcrete.blogspot.de/`, 2012. Accessed: 2016-03-29.

[Con12]   Concrete Canvas Ltd. Concrete Canvas Shelters – Rapidly deployable concrete shelters. `www.concretecanvas.co.uk`, 2012. Accessed: 2016-03-24.

[DAf10]   DAfStb. Erlaeuterungen zu din 1045-1. *Schriftreihe des Deutschen Ausschuss fuer Stahlbeton*, (525), 2010.

[dH08]   Eline den Hartog. Prefabrication of concrete shells. *Masterthesis, Delft University of Technology, Faculty of Civil Engineering and Geosciences*, 2008.

[Dic13]   Cengiz Dicleli. Ulrich finsterwalder 1897–1988. *Beton-und Stahlbetonbau*, 108(9):662–673, 2013.

[DIN01a]   DIN EN 12369-1. *Wood-based panels – Characteristic values for structural design*. Part 1: OSB, particleboards and fibreboards. DIN Deutsches Institut fuer Normung e.V., April 2001.

[DIN01b]   DIN EN 206-1. *Festlegung, Eigenschaften, Herstellung und Konformität*. Teil 1: Beton. Deutsches Institut für Normung e. V., Juli 2001.

[DIN05]   DIN 18202. *Tolerances in building construction – Buildings*. DIN Deutsches Institut fuer Normung e.V., October 2005.

[Dis28]   Franz Dischinger. Schalen und Rippenkuppeln. *Handbuch für den Eisenbetonbau. VI Bd., 2. Teil, Ernst und Sohn, Berlin*, 1928.

[Dlu15]   Dlubal Software GmbH.   Rfem 5.xx structural analysis and design software. `https://www.dlubal.com/en/rfem-5xx.aspx`, 2015. Accessed: 2015-10-19.

[DUC15]   DUCON Europe GmbH & Co. KG. DUCON® An Innovative Metamorphosis of Form and Function, Technical Data Design. `http://en.ducon.eu/file_download/9/ducon-design-2015_en.pdf`, 2015. Accessed: 2015-10-08.

[Dud16]   Duden. Schale, die. `http://www.duden.de/rechtschreibung/Schale`, 2016. Accessed: 2016-07-21.

[EGRH15]   Philipp Eisenbach, Manfred Grohmann, Moritz Rumpf, and Stephan Hauser. Seamless rigid connections of thin concrete shells – a novel stop-end construction technique for prefab elements. *Proceedings of the IASS2015 Annual International Symposium on Future Visions*, August 2015.

[Erh15]   Erich Erhard. Textilbeton – Neuer Meilenstein der Bautechnik in der Bauwerkserhaltung. *CiA – Composites in Architecture, 6. Internationales Symposium Leipzig, Germany*, December 2015.

[Eur03]   Eurocode 1. *Actions on structures, eglish version*. Part 1-3: General actions - Snow loads. The European Union Per Regulation, July 2003.

[Eur04]   Eurocode 2. *Design of concrete structures, english version*. Part 1-1: General rules and rules for buildings. The European Union Per Regulation, April 2004.

[Eur05]   Eurocode 3. *Design of steel structures, english version*. Part 1-8: Design of joints. The European Union Per Regulation, May 2005.

[EVG+13]   Philipp Eisenbach, Ragunath Vasudevan, Manfred Grohmann, Klaus Bollinger, and Stephan Hauser. Parapluie – ultra thin concrete shell made of uhpc by activating membrane effects. *Proceedings of the IASS2013 Annual International Symposium "Beyond the Limits of Men"*, September 2013.

[EVG+14a]   Philipp Eisenbach, Ragunath Vasudevan, Manfred Grohmann, Klaus Bollinger, and Stephan Hauser. Parapluie – Realisierung einer ultraschlanken Betonschale durch Aktivierung einer Membrantragwirkung. *Beton- und Stahlbetonbau*, 109(1):53–59, 2014.

[EVG+14b]   Philipp Eisenbach, Ragunath Vasudevan, Manfred Grohmann, Klaus Bollinger, and Stephan Hauser. Parapluie – Ultra Thin Concrete Shell Made of UHPC by Activating Membrane Effects; Winning paper of the 2013 Tsuboi Award for the outstanding paper published in the proceedings of the annual IASS Symposium: "Beyond the Limits of Men", held in September 2013 in Wroclaw, Poland. *Journal of the International Association for Shell and Spatial Structures: J.IASS*, 55(4):201–212, 2014.

[For13]   Adrian Forty. *Concrete and culture: a material history*. Reaktion Books, 2013.

[Fra15]   Johannes Franz. *Investigation of the residual load-bearing behaviour of fractured glazing*. PhD thesis, Technische Universitaet Darmstadt (TUD), Institute of Structural Mechanics and Design, 2015.

[FSW⁺13]   Ekkehard Fehling, Michael Schmidt, Joost Walraven, Torsten Leutbecher, and Susanne Fröhlich. Ultrahochfester Beton UHPC. *Beton-Kalender 2013: Lebensdauer und Instandsetzung-Brandschutz, Chapter IX (eds K. Bergmeister, F. Fingerloos and J.-D. Wörner)*, pages 117–239, 2013.

[FSW⁺14]   Ekkehard Fehling, Michael Schmidt, Joost Walraven, Torsten Leutbecher, and Susanne Fröhlich. *Ultra-high Performance Concrete UHPC – Fundamentals, Design, Examples*. John Wiley & Sons, 2014.

[GB09]   Maria E. Moreyra Garlock and David P. Billington. Felix candela's legacy. *Proceedings of the International Association for Shell and Spatial Structures (IASS) Symposium 2009, Valencia. Evolution and Trends in Design, Analysis and Construction of Shell and Spatial Structures*, September 2009.

[GB14]   Maria E. Moreyra Garlock and David P. Billington. Felix Candela and Heinz Isler. *Shell Structures for Architecture: Form Finding and Optimization, Chapter 3 (eds S. Adriaenssens, P. Block, D. Veenendaal and C. Williams)*, pages 246–257, 2014.

[GERH15]   Manfred Grohmann, Philipp Eisenbach, Moritz Rumpf, and Magdalena Hellmann. Stable equilibrium – on-site mounting technique of lightweight concrete structures. *Proceedings of the IASS2015 Annual International Symposium on Future Visions*, August 2015.

[GERW16]   Manfred Grohmann, Philipp Eisenbach, Moritz Rumpf, and Cynthia Ward. Hinged folded festival pavilion – membrane bearing in lightweight dismountable structures. *Proceedings of the IASS Annual International Symposium 2016 "Spatial Structures in the 21st Century"*, September 2016.

[Gru06]   Friedrich Gruttmann. *Schalentragwerke*. Vorlesungssskript. Institut fuer Statik, Technische Universität Darmstadt (TUD), 2006.

[Gru09]   Peter Grupp. *Schalungsatlas – Schalungssysteme und Einsatz in der Praxis*. Verlag Bau + Technik, 2009.

[Hae64]   Gustav Haegermann. Teil A – Vom Caementum zum Zement. *Vom Caementum zum Spannbeton (Huberti G. (ed.)). Bauverlag, Wiesbaden and Berlin, Germany*, 1:1–72, 1964.

[HHSC15]   J Hegger, M Herbrand, A Stark, and M Claßen. Betonbau der zukunft: leicht, filigran und nachhaltig. *Bauingenieur*, 90(7/8):337–344, 2015.

[Hos13]   Heinz Hossdorf. *Das Erlebnis Ingenieur zu sein*. Springer-Verlag, 2013.

[Hub64]   Günther Huberti. Teil B – Die erneuerte Bauweise. *Vom Caementum zum Spannbeton (Huberti G (ed.)). Bauverlag, Wiesbaden and Berlin, Germany*, 1:1–198, 1964.

[Int15]   International Association for Shell and Spatial Structures, IASS. 2015 IASS SYMPOSIUM CONTEST and ART EXPO. `http://www.iass2015.org/ExpoIASS2015.pdf`, 2015. Accessed: 2016-01-07.

[IPE15]   IPEXL Intellectual Property EXchange Limited. New or improved mechanism for transmission of power. united kingdom patent 189625325-a. `http://patent.ipexl.com/GB/189625325-a.html`, 2015. Accessed: 2015-11-28.

[JA+13]   JA+U Japan Architecture + Urbanism. Teshima Art Museum. `https://vimeo.com/66543296`, 2013. Accessed: 2016-03-18.

[Jod12]   Philip Jodidio. *Architecture now! Architektur heute: 8*. Taschen, 2012.

[Joe62]   Jürgen Joedicke. *Schalenbau – Konstruktion und Gestaltung*. Karl Krämer Verlag, Stuttgart, 1962.

[Jür00]   Thomas Jürges. *Die Entwicklung der Biege- Schub- und Verformungsbemessung im Stahlbetonbau und ihre Anwendung in der Tragwerklehre*. PhD thesis, Rheinisch-Westfälische Technische Hochschule Aachen, Fakultät für Architektur, 2000.

[KBKPB02]   Friedbert Kind-Barkauskas, Bruno Kauhsen, Stefan Polonyi, and Jörg Brandt. *Beton Atlas: Entwerfen mit Stahlbeton im Hochbau*. Basel: Birkhäuser Verlag, 2002.

[KK15]   Benjamin Kromoser and Johann Kollegger. Building shells from initially flat
              hardened concrete plates. *Proceedings of the IASS2015 Annual International
              Symposium on Future Visions*, August 2015.

[Kno15]   Charlotte Knoll.   MOEBIUSBAN(K)D – Entwicklung durch Evolution.
              Competition, issue 11, April-June, pages 26–27, 2015.

[Lam93]   Heinz-Otto Lamprecht. *Opus caementitium: Bautechnik der Römer*. Beton-
              Verlag, 1993.

[Leo73]   Fritz Leonhardt. *Spannbeton für die Praxis*. Wilhelm Ernst & Sohn, 1973.

[Lin14]   Klaus Linkwitz. Force density method – design of a timber shell. *Shell Struc-
              tures for Architecture: Form Finding and Optimization, Chapter 6 (eds S.
              Adriaenssens, P. Block, D. Veenendaal and C. Williams)*, pages 58–69, 2014.

[Lip07]   Andreas Lipka. *Verbesserter Materialeinsatz innovativer Werkstoffe durch
              die Topologieoptimierung*. PhD thesis, Universität Stuttgart, Institut für
              Baustatik und Baudynamik, 2007.

[LLW$^+$15]   Sven Lehmberg, Lukas Ledderose, Franz Wirth, Harald Budelmann, and
              Harald Kloft. From jointing systems to light-weight structures: Hybrid, dry-
              fit beam, surface and spatial structures made of uhpfrc. *Proceedings of the
              IASS2015 Annual International Symposium on Future Visions*, August 2015.

[LNK15]   Lukas Ledderose, Stefan Neudecker, and Harald Kloft. Robot-controlled
              magnetic arrangement of steel fibres in uhpfrc. *Proceedings of the IASS2015
              Annual International Symposium on Future Visions*, August 2015.

[Luc14]   Lucerne University of Applied Sciences and Arts.   Struktur – System
              Hennebique.   `blog.hslu.ch/beton2014/files/2014/04/`
              `4-System-Hennebique.pdf`, 2014. Accessed: 2016-06-03.

[Lug02]   Matthias Lugenheim. *The Correlation of the Architectural Form and the
              Structural Form in Dome Architecture and its Influence on the Art of Civil
              Engineering – Represented by the Example of the Dresden Church of Our
              Lady*. PhD thesis, Technische Universität Dresden, 2002.

[Mau98]   Kurt Maute. *Topologie- und Formoptimierung von dünnwandingen Tragw-
              erken*. PhD thesis, Universität Stuttgart, Institut für Baustatik, 1998.

[Max14]   Max Frank GmbH & Co. KG.   Stremanform® Abstellelemente.
          http://www.maxfrank.de/media/dokumente/produkte/
          intl-de/broschueren/010-Frank-Stremaform-BR.pdf,
          2014. Accessed: 2015-10-08.

[McN15]   Robert McNeel. Rhinoceros; design, model, present, analyze, realize...
          https://www.rhino3d.com, 2015. Accessed: 2015-10-09.

[Mec16]   Viktor Mechtcherine.   Deformation, cracking and failure behaviour of
          UHPC – challenges and solutions. 4th International Symposium on Ultra-
          High Performance Concrete and High Performance Construction Materials,
          HiPerMat, Kassel, 2016. Plenary speech: 2016-03-10.

[MKH14]   Jeldrik Mainka, Harald Kloft, and Tim Heinemann. A novel recyclable wax
          formwork-system for high-precision free-form uhpc members and joints.
          *Proceedings of the IASS-SLTE 2014 Symposium "Shells, Membranes and
          Spatial Structures: Footprints", Brasilia, Brazil*, September 2014.

[MLBK13] Jeldrik Mainka, Sven Lehmberg, Harald Budelmann, and Harald Kloft.
          Non-Standard Fügeprinzipien für leichte Bauteile aus UHPFRC. *Beton-und
          Stahlbetonbau*, 108(11):763–773, 2013.

[Müh12]   Christian Mühlbauer.   *Fügen von Bauteilen aus ultrahochfestem Beton
          (UHPC) durch Verkleben*. PhD thesis, Technische Universität München,
          Lehrstuhl für Massivbau, 2012.

[NA14]   Laurent Ney and Sigrid Adriaenssens. Shaping forces. *Shell Structures
          for Architecture: Form Finding and Optimization, Chapter 2 (eds S. Adri-
          aenssens, P. Block, D. Veenendaal and C. Williams)*, pages 14–19, 2014.

[Naw08]   Edward G Nawy. *Concrete construction engineering handbook*. CRC press,
          2008.

[Nef42]   Wallace Neff. Building construction. *US Patent 2,270,229*, 1942.

[OB14]   John Ochsendorf and Philippe Block. Exploring shell forms. *Shell Struc-
          tures for Architecture: Form Finding and Optimization, Chapter 1 (eds S.
          Adriaenssens, P. Block, D. Veenendaal and C. Williams)*, pages 6–12, 2014.

[P$^+$13]   Martin Peck et al. Atlas Moderner Betonbau. *Konstruktion, Material, Nach-haltigkeit. München: Institut für internationale Architektur-Dokumentation*, 2013.

[Pes09]   Horst Peseke. The Grossmarkthalle – an experimental building. *Martin Elsaesser and the New Frankfurt (eds T. Elsaesser, C. Gräve, J. Schilling and P. C. Schmal)*, pages 166–171, 2009.

[PHF10]   Hartmut Pasternak, Hans-Ullrich Hoch, and Dieter Füg. *Stahltragwerke im Industriebau*. John Wiley & Sons, 2010.

[Pol48]   Giovanni Poleni. *Memorie istoriche della Gran Cupola del Tempio Vaticano*. 1748.

[Pol09]   Polonyi, Stefan and Walochnik, Wolfgang. Heinz Isler 1926-2009. db deutsche bauzeitung 09-2009 `www.db-bauzeitung.de/allgemein/heinz-isler-1926-2009`, 2009. Accessed: 2016-07-31.

[Pre13]   Clemens Preisinger. Linking structure and parametric geometry. *Architectural Design Special Issue. Computation Works: The Building of Algorithmic Thought, 83(2)*, pages 110–113, 2013.

[PRGB15]   Horst Peseke, Raül Vinyes Raso, Manfred Grohmann, and Klaus Bollinger. Reflection about the first dome of jena. *Proceedings of the IASS2015 Annual International Symposium on Future Visions*, August 2015.

[Rae01]   Ingo Raecke. *Flächentragwerke I/II*. Vorlesungssskript. Institut fuer Mechanik, Otto-von-Guerkicke-Universität Magdeburg, 2001.

[Rau10]   Marion Rauch. *Tragwerke aus ultrahochfestem Beton*. PhD thesis, Technische Universitaet Hamburg Harburg (TUHH), Institut für Massivbau, 2010.

[Ray10]   Raymund Ryan. Teshima Art Museum. `http://www.domusweb.it/en/architecture/2010/12/09/teshima-art-museum.html`, 2010. Accessed: 2016-03-18.

[RGEH15]   Moritz Rumpf, Manfred Grohmann, Philipp Eisenbach, and Stephan Hauser. Structural surface – a multi parameter structural optimization of a thin high performance concrete object. *Proceedings of the IASS2015 Annual International Symposium on Future Visions*, August 2015.

[Rom05]   Günter Rombach. *Spannbetonbau*. Ernst & Sohn, 2005.

[Rut10]   David Rutton.   Evolutionary principles applied to problem solv-
           ing.   `http://www.grasshopper3d.com/profiles/blogs/`
           `evolutionary-principles`, 2010. Accessed: 2015-10-12.

[Rut13]   David Rutton. On the logic and limitations of generic solvers. *Architec-*
           tural Design Special Issue. Computation Works: The Building of Algorith-
           mic Thought, 83(2), pages 132–135, 2013.

[Rut15]   David Rutton.   Grasshopper; algorithmic modeling for rhino.   `www.`
           `grasshopper3d.com`, 2015. Accessed: 2015-10-08.

[Sau08]   Marion Sauter. *Computergestützte Produktion von Freiformen in der Ar-*
           chitektur. Imhof, 2008.

[SB08]   Mike Schlaich and Achim Bleicher. *Konstruktiver Ingenieurbau II*. Vor-
           lesungssskript. Fachgebiet Massivbau, Technische Universitaet Berlin (TU –
           Berlin), Juli 2008.

[Sch11]   Clifford W. Schwinger. ASTM A615 Grade 75 Reinforcing Steel – When,
           Why & How to Use It. *STUCTURE magazine*, August:34–35, 2011.

[SCH12]   Alexander Scholzen, Rostislav Chudoba, and Josef Hegger. Dünnwandi-
           ges schalentragwerk aus textilbewehrtem beton. *Beton-und Stahlbetonbau*,
           107(11):767–776, 2012.

[Sch14]   Patrick Schumacher. The congeniality of architecture and engineering – The
           future potential and relevance of shell structures in architecture. *Shell Struc-*
           tures for Architecture: Form Finding and Optimization, Chapter 3 (eds S.
           Adriaenssens, P. Block, D. Veenendaal and C. Williams), pages 271–273,
           2014.

[SH03]   Martina Schnellenbach-Held. *Grundlagen des Spannbetonbaus*.   Vor-
           lesungssskript. Institut fuer Massivbau, Technische Universitaet Darmstadt
           (TUD), Februar 2003.

[SJ11a]   Roel Schipper and Bas Janssen. Manufacturing double-curved elements in
           precast concrete using a flexible mould – first experimental results. 2011.

[SJ11b]   Roel Schipper and Bas Janssen. Manufacturing double curved precast concrete panels. *Concrete Plant International*, 4:32–38, 2011.

[SK07]   Werner Sobek and Martin Kobler. Form und Gestaltung von Betonschalen. *Beton-Kalender 2007: Schwerpunkte: Verkehrsbauten, Flächentragwerke*, pages 1–18, 2007.

[Sob87]   Werner Sobek. *Auf pneumatisch gestützten Schalungen hergestellte Betonschalen*. PhD thesis, Universität Stuttgart, Institut für Massivbau, 1987.

[Sob90]   Werner Sobek. Pneu und Schale – Betonschalen und pneumatisch vorgespannte Membranen. *Deutsche Bauzeitung*, 124(7):66–74, 1990.

[SPA13]   SPAX®. *Hinweise zur Bemessung von tragenden SPAX-Verbindungen*. SPAX International GmbH & Co. KG, January 2013.

[SV10]   Roel Schipper and Jan Vambersky. A flexible mold for double curved precast concrete elements. *BFT International,(8), 2010*, 2010.

[Tue16]   Nguyen Viet Tue. Application oriented Development in UHPC. 4th International Symposium on Ultra-High Performance Concrete and High Performance Construction Materials, HiPerMat, Kassel, 2016. Plenary speech: 2016-03-09.

[VB12]   Diederik Veenendaal and Philippe Block. Computational form finding for fabric formworks: an overview and discussion. *Proceedings of the 2nd international conference on flexible formwork, Bath, UK*, June 2012.

[VBNB14]   Diederik Veenendaal, Mile Bezbradica, Davis Novak, and Philippe Block. Controlling the geometry and forces of hybrid cable-net and fabric formworks. *Proceedings of the IASS-SLTE 2014 Symposium, Brasilia, Brazil*, September 2014.

[vdH15]   Marion von der Heyde. *Gestalten mit Beton – Planungshilfen Details Beispiele*. Verlagsgesellschaft Rudolf Müller GmbH & Co. KG, Köln, 2015.

[VWB11]   Diederik Veenendaal, Mark West, and Philippe Block. History and overview of fabric formwork: using fabrics for concrete casting. *Structural Concrete*, 12(3):164–177, 2011.

[Wal11]   Alexander Frederic Walser. Formfindung von Schalen mit numerischen Hängemodellen. *Diplomathesis, University of Stuttgart, Institute for Structural Mechanics*, 2011.

[Wal13]   Tobias Walliser. Digitale Entwurfs- und Fabrikationsmethoden. *Atlas Moderner Betonbau – Konstruktion, Material, Nachhaltigkeit*, pages 106–113, 2013.

[War15]   Cynthia Ward. Flexible Schalungssysteme – Entwicklung einer flexiblen Schalhaut auf Grundlage der Rigid-Origami-Tessellation. *Bachelorthesis, University of Kassel, Department of Structural Systems, ASL*, 2015.

[Way16]   Wayss & Freytag Ingenieurbau AG. Wayss & Freytag – History. `www.wf-ib.de/en/about-us/history`, 2016. Accessed: 2016-06-01.

[Wes08]   Mark West. Kenzo unno, fabric formed walls. *Winnipeg, University of Manitoba*, 2008.

[Wes11]   Mark West. Heavy Light – Fabric-Formed Concrete Structures. `http://youtu.be/36gOx3dguWs`, 2011. Accessed: 2016-03-29.

[Wil14]   Chris Williams. What is a shell? *Shell Structures for Architecture: Form Finding and Optimization, Chapter 3 (eds S. Adriaenssens, P. Block, D. Veenendaal and C. Williams)*, pages 20–31, 2014.

[Win13]   Daniel Rudolf Wingenfeld. *Fügetechnische Konstruktionslösungen für Bauteile aus ultrahochfestem Beton (UHPC)*. PhD thesis, Technische Universität München, Lehrstuhl für Massivbau, 2013.

[WK15]   Frederic Waimer and Jan Knippers. A novel hybrid composite construction for complex concrete shells in architecture. *Proceedings of the IASS2015 Annual International Symposium on Future Visions*, August 2015.

[WSF13]   Johann-Dietrich Wörner, Jens Schneider, and Andreas Fink. *Glasbau: Grundlagen, Berechnung, Konstruktion*. Springer-Verlag, 2013.

[Zas05]   Bernd Zastrau. *Schalentragwerke*. Vorlesungssskript. Institut fuer Mechanik und Flächentragwerke, Technische Universität Dresden, 2005.

[Zim07]   Gregor Zimmermann. *Membran Beton Gitterschalen Tragwerke – Entwicklung und Vorbemessung*. PhD thesis, Universität Kassel, Fachbereich 6 Architektur, Stadtplanung und Landschaftsplanung, 2007.

A Parapluie – making of

A.1 Involved parties

Design concept

schneider + schumacher Planungsgesellschaft mbH
Till Schneider
Prof. Michael Schumacher
Ragunath Vasudevan

B+G Ingenieure Bollinger und Grohmann GmbH
Prof. Dr. Klaus Bollinger
Prof. Manfred Grohmann
Philipp Eisenbach

Contractor

Ducon Europe GmbH & Co.KG
Dr. Stephan Hauser

B Möbiusban(k)d – making of

B.1 Involved parties

Organisators

University of Kassel / FB 06 – School of Architecture Urban Planning and Landscape Architecture; Department of Structural Design
Prof. Manfred Grohmann
Philipp Eisenbach
Moritz Rumpf

University of Kassel / FB 06 – School of Architecture Urban Planning and Landscape Architecture; Department of Digital Design Techniques
Ragunath Vasudevan

Partners

University of Kassel / FB 14 – School of Civil Engineering; Department of Concrete Constructions
Prof. Dr. Ekkehard Fehling

University of Kassel / FB 14 – School of Civil Engineering; Department of Construction Materials and Chemistry
Prof. Dr. Bernhard Middendorf

DUCON Europe GmbH & Co.KG
Dr. Stephan Hauser

University of Kassel / Real estate management
Norbert Krempel

Sponsors

DUCON Europe GmbH & Co.KG
Dr. Stephan Hauser

Max Frank GmbH & Co.KG
Dr. Max Frank

Paul Bauder GmbH & Co.KG

karamba3d.com

Pfeiffer trust of the University of Kassel

Participating students

The following students (alphabetical order) have built the team for the project *structural surface*:
Shahram Abbasian, *Leon Charlet*, *Harun Faizi*, *Jessica Fröse*, *Adrian Golab*, *Christoph Herlitze*, *Denitsa Koleva*, *Michael Korn*, *Jannik Kratzenberg*, *Svenja Krieg*, *Nils Kühn*, *Jakob Leppin*, *Nora Levsen*, *Alexander Lischke*, *Yiyang Liu*, *Henrik Neusüß*, *Laura Nolte*, *Richard Pfeiffer*, *Tim Reichert*, *Florian Reichmann*, *Jan Niklas Rieckmann*, *Aliaksei Rybalchanka*, *Julia-Yvonne Scharf*, *Witali Suchan*, *Andreas Steffen*, *Serge Well*, *Cynthia Ward*.

The project team of *structural surface* is the winner of the award *competition campus 2015* announced by *Competitionline Wettbewerbe und Architektur Verlags GmbH* in Berlin. The annotation of the jury:
"...from the beginning to the end a well deliberated and excellently implemented solution... Material understood, converted into a shape and put into practice"
[Kno15, own translation].

B.2 Competition contributions

Seven groups of students submitted their proposals of the campus competition *Structural Surface*, as shown in fig. B.2. The winning contribution, chosen by an external jury is the infinity loop, later termed *Möbiusban(k)d*, shown in fig. B.1.
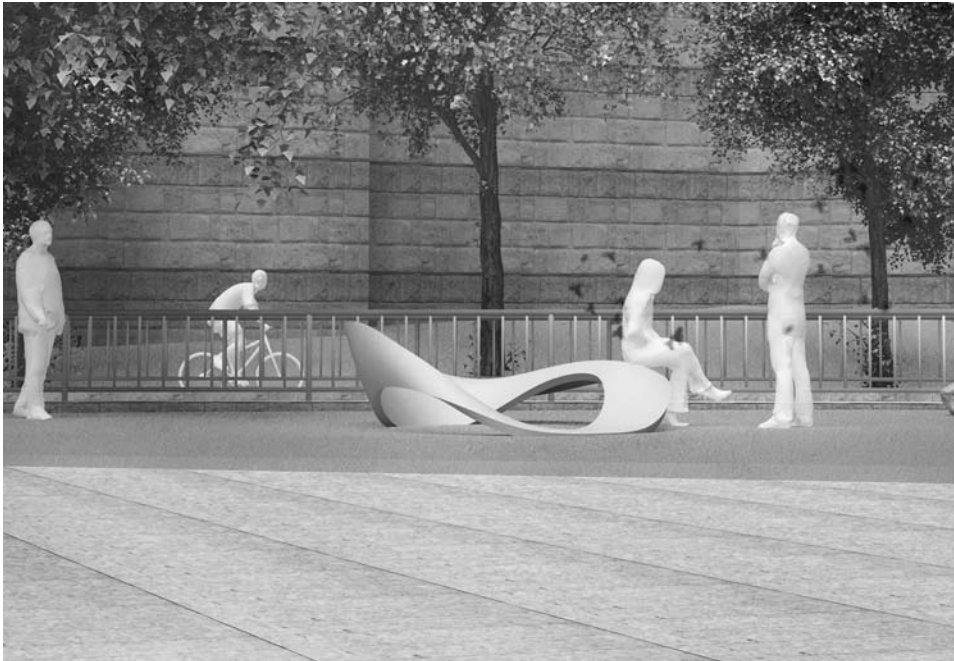
Figure B.1 Winning contribution of the campus competition *Structural Surface*: 'Endless' by *D. Koleva*, *J. Kratzenberg*, *S. Krieg*, *C. Ward*

(a) 'Diversity Curvature' by *C. Herlitze*, *J. Leppin*, *T.Reichert*, *A. Rybalchanka*, *J.-Y. Scharf*, *J. Leppin*

(b) 'Twisted Frames' by *L. Charlet*, *H. Faizi*, *N. Kühn*

(c) 'Aerocon' by *A. Golab*, *F. Reichmann*, *W. Suchan*
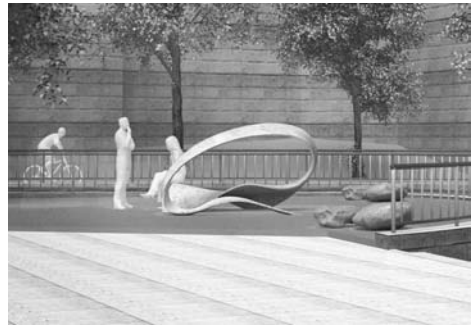
(d) 'Windwirbel' by *J. Froese*, *N. Rieckmann*, *Y. Liu*, *A. Steffen*

(e) 'Kante zu Kante' by *S. Abbasian*, *N. Levsen*, *H. Neusüß*, *R. Pfeiffer*

(f) 'Leaf a Trace' by *M. Korn*, *A. Lischke*, *L. Nolte*, *S. Well*

Figure B.2   Contributions of the campus competition *Structural Surface*

B.3 Structural analysis

In addition to the report of the buckling analysis in section 5.2.3.5 the buckling eigen-mode shapes 2, 3 and 4 are shown in fig. B.3.

The governing eigen-mode 1, as used for the buckling design of the concrete bench is given in fig. 5.14 on page 115.

(a) Eigen-mode 2
critical load factor $f = 91$ [-]
magnification factor $\alpha = 1,1\%$

(b) Eigen-mode 3
critical load factor $f = 99$ [-]
magnification factor $\alpha = 1,0\%$

(c) Eigen-mode 4
critical load factor $f = 106$ [-]
magnification factor $\alpha = 1,0\%$
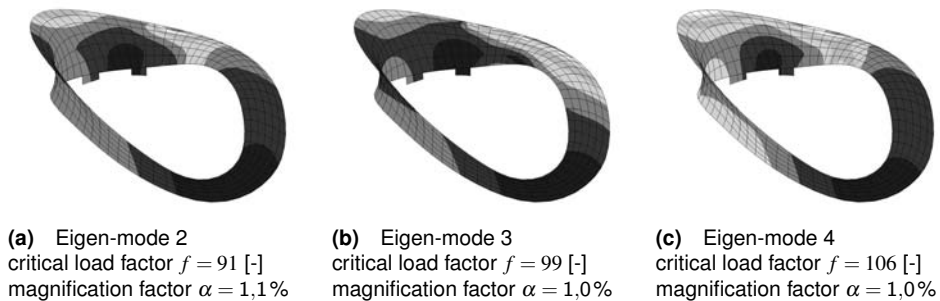
Figure B.3 Buckling eigen-mode shapes 2, 3 and 4 of *Möbiusban(k)d*. All buckling peaks are within the same region of the 'smaller' cantilevering flank

B.4 Concrete mixing schedules

The following mixing schedule, shown in fig. B.4, has been established empirically. It leads to a sufficient slump size measured with a *Hägermann*-cone.
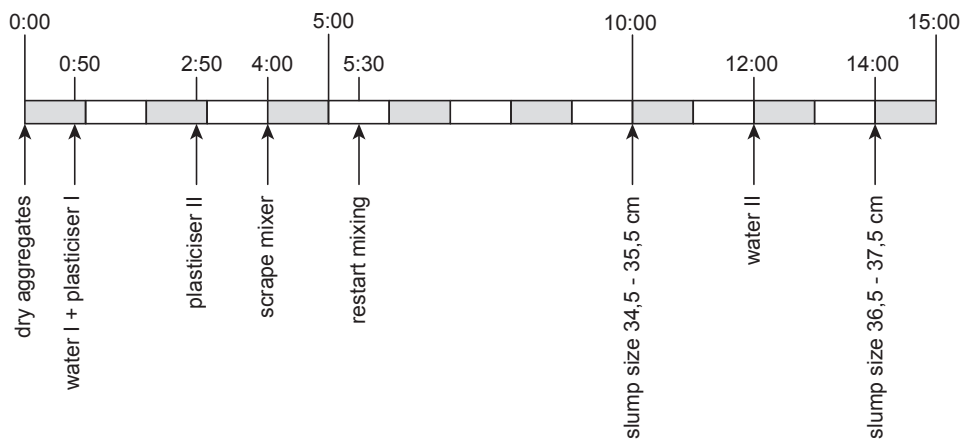
(a) Mixing time schedule for mixtures 15 – 20 L
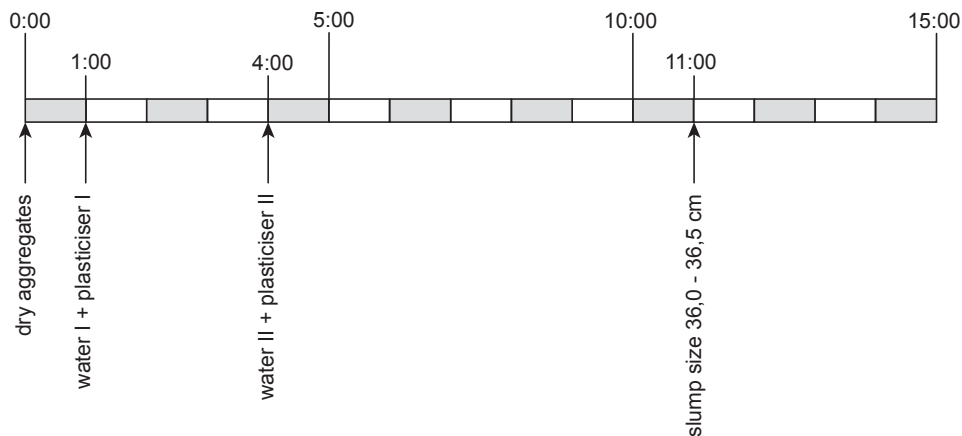
(b) Mixing time schedule for mixtures 70 – 90 L

Figure B.4   Concrete mixing time schedules established that lead to sufficient fluidity; [min:sec]

C Concrete mobile – making of

C.1 Involved parties

The concrete mobile has been exhibited in the *Muziekgebouw aan 't IJ* in Amsterdam from June to August 2015. The curation and arrangement of the international contest and the following exhibition has been organized by the *International Association for Shell and Spatial Structures*, IASS.

Design concept

University of Kassel / FB 06 – School of Architecture Urban Planning and Landscape Architecture; Department of Structural Design
Prof. Manfred Grohmann
Philipp Eisenbach
Moritz Rumpf

Architecture student involved
Magdalena Hellmann

Partners

University of Kassel / FB 14 – School of Civil Engineering; Department of Construction Materials and Chemistry
Prof. Dr. Bernhard Middendorf and *AMPA*-team

DUCON Europe GmbH & Co.KG
Dr. Stephan Hauser

Sponsors

DUCON Europe GmbH & Co.KG
Generous financial support

Arnold AG
Fabrication of embedded steel items

Carl Stahl GmbH
Confection of steel cables, hulls and suspenders

Portikus Institution for Contemporary Art, Frankfurt am Main
Providing of exhibition space for documentation

C.2 Force gradients

The following force gradients of the concrete mobile *Stable Equilibrium* have been used
for the structural design. The maximum axial force in the topmost suspension member is
$N_{max,k} = 911\,N$, as shown in fig. C.1. The highest bending moment in the topmost beam
results to $M_{max,k} = 210\,N\,m$, see fig. C.2. The absolute value of the highest shear force,
again in the topmost beam, fig. C.3, is $V_{max,k} = 585\,N$.
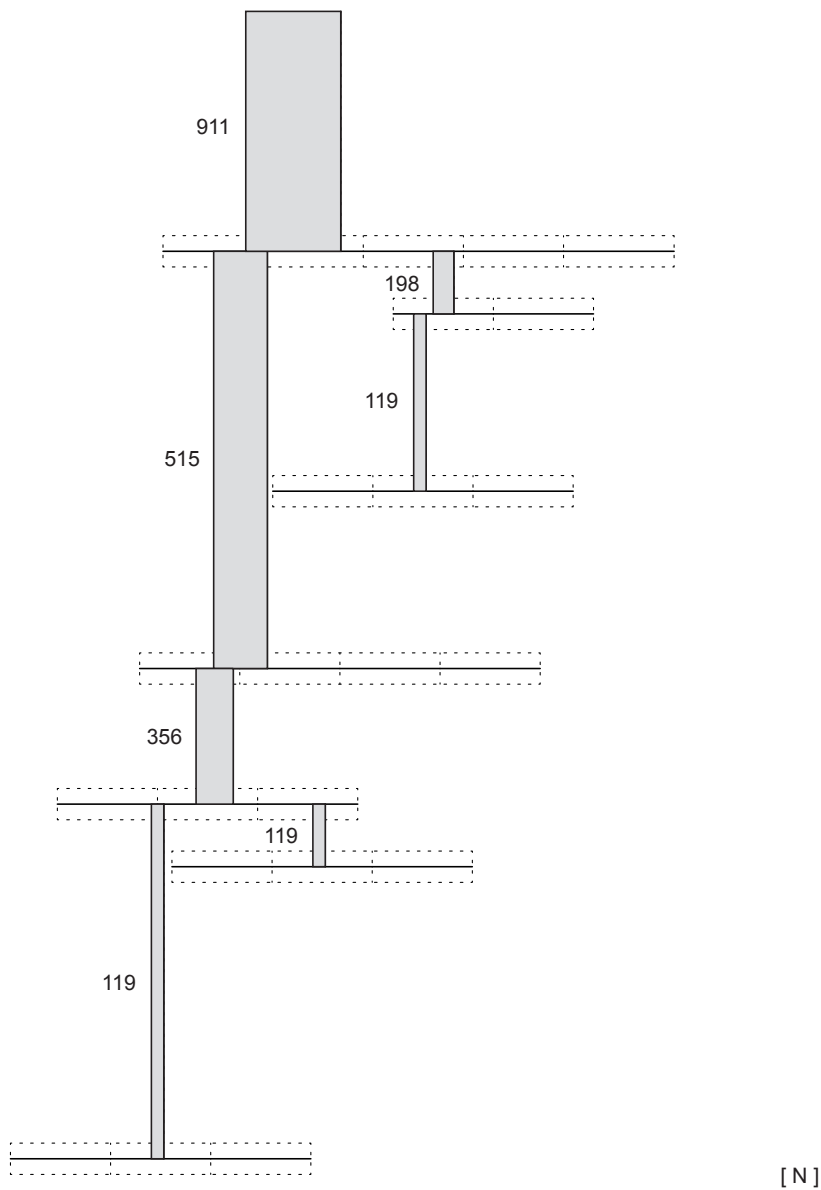
Figure C.1 Axial force diagram of concrete mobile *Stable Equilibrium*; $N_{max,k} = 911\,\text{N}$
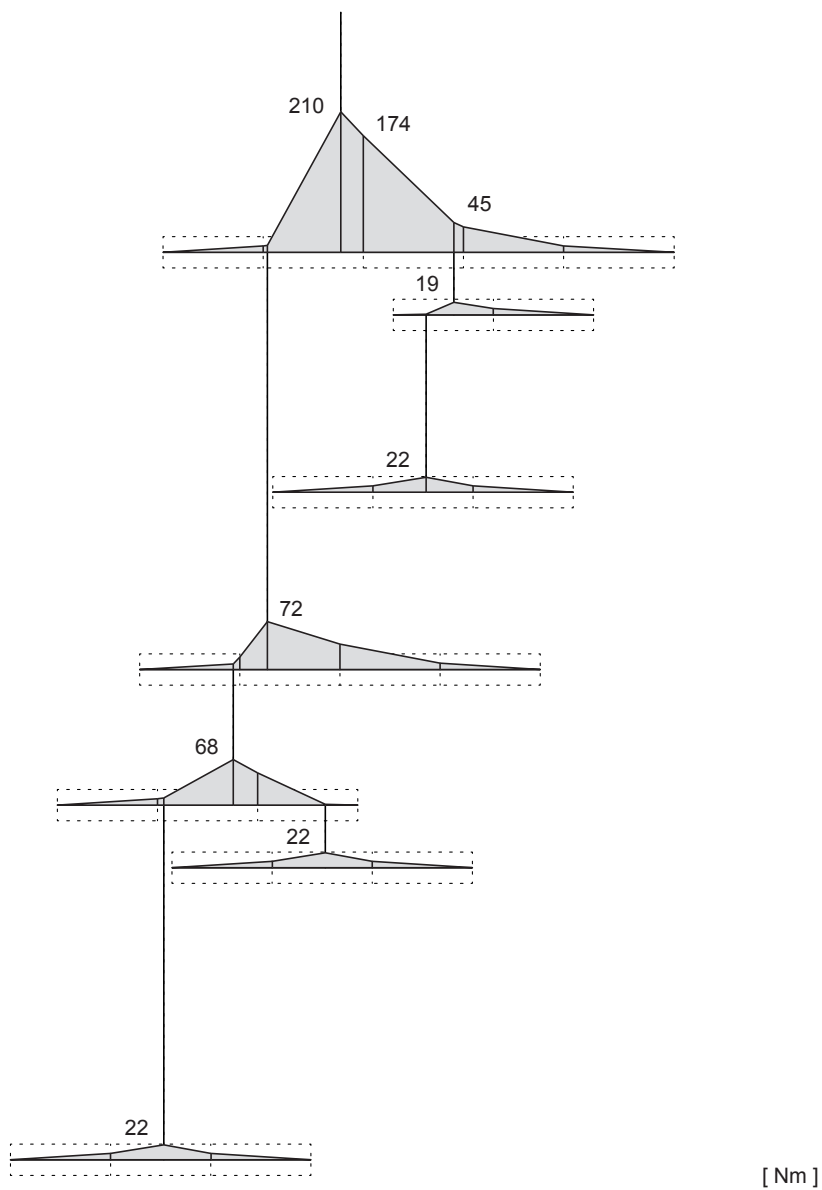
Figure C.2   Bending moment diagram of concrete mobile *Stable Equilibrium*; $M_{\mathrm{max,k}} = 210\,\mathrm{N\,m}$
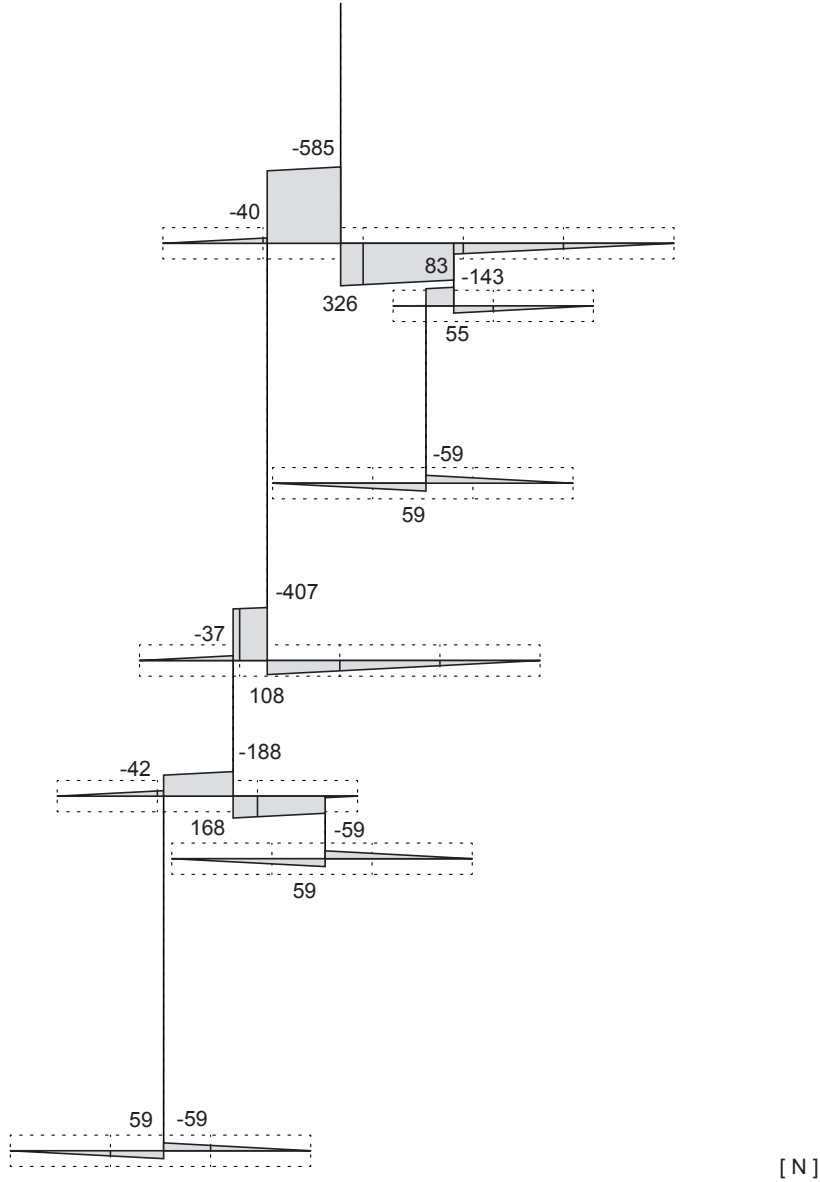
Figure C.3   Shear force diagram of concrete mobile *Stable Equilibrium*; $V_{max,k} = 585\,\text{N}$, $V_{min,k} = 326\,\text{N}$

C.3 Details

The embedded items of the concrete mobile need to be small enough to fit inside the section with the thickness of $t = 22\,\text{mm}$. The structural design is executed with the finite element software *RFEM©* by *Dlubal Software GmbH* [Dlu15].
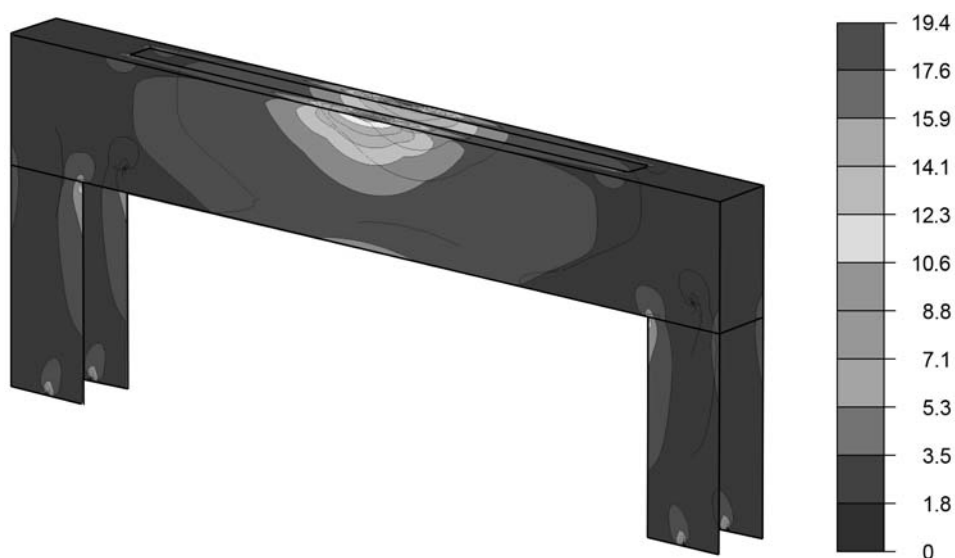
Figure C.4 Principal stress distribution $\sigma_{\text{v,max}}$ of the embedded items in the ultimate limit state; $\left[\text{kN/cm}^2\right]$
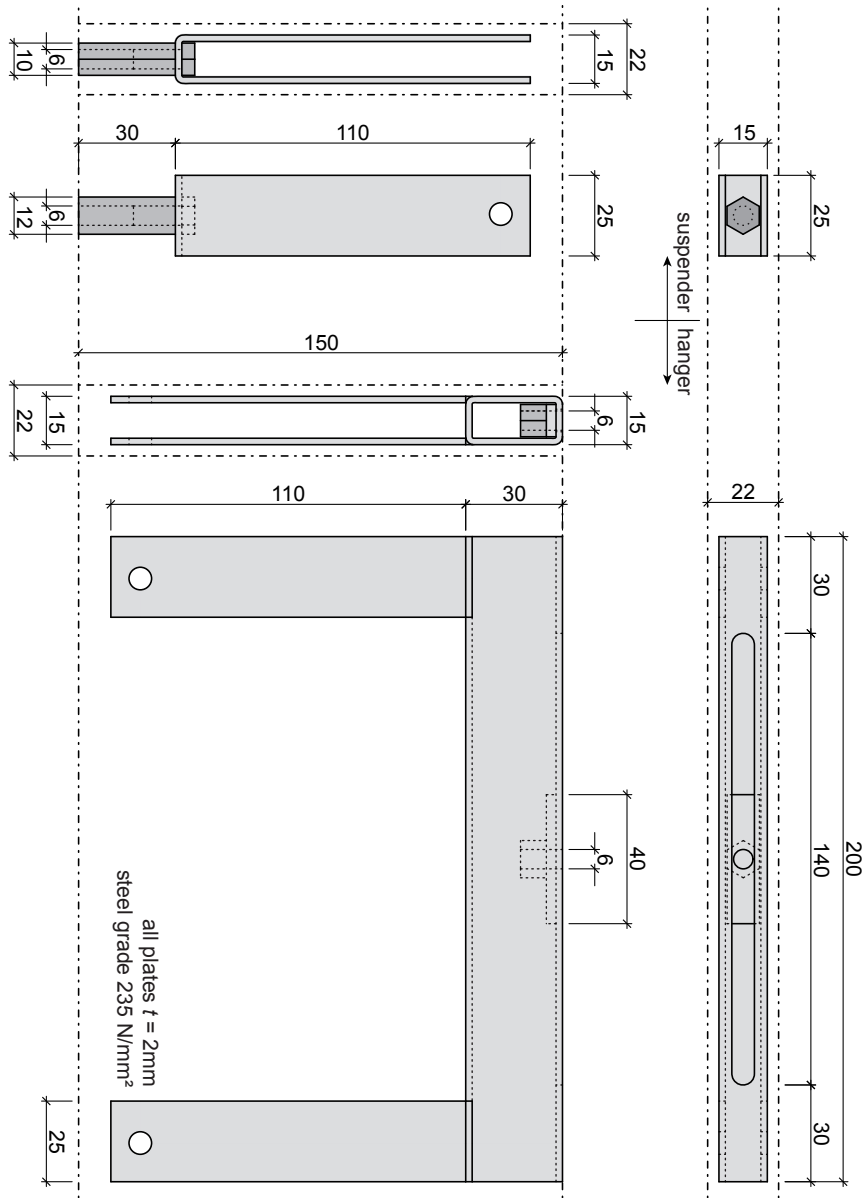
Figure C.5 Dimensions of the embedded items of concrete mobile; [mm]

D Concrete table substructure – making of

D.1 Involved parties

Design concept

University of Kassel / FB 06 – School of Architecture Urban Planning and Landscape Architecture; Department of Structural Design
Prof. Manfred Grohmann
Philipp Eisenbach

Cristinetti – Studio for Planning and Design
Robert Cristinetti

Sponsors

Ducon Europe GmbH & Co.KG
Concrete ingredients and reinforcement

Arnold AG
Fabrication of embedded steel items

Lohmann GmbH & Co.KG
Adhesive cellular sealing

D.2 Joint detailing

The wood screws, eight screws per prestressing thread, are connecting the embedded items with the table board. These screws are transferring tension forces only. The resistance according to the screw manufacturer *Spax®*[SPA13, 14] is the minimum of the steel resistance and the resistance against pulling out:

$$
R_{\text{ax,d}} = \min \begin{cases} R_{\text{ax,d}} = \frac{k_{\text{mod}} \cdot R_{\text{ax,k}}}{\gamma_M} & \text{pulling thread out of timber} \\[2mm] R_{\text{t,u,d}} = \frac{R_{\text{t,u,k}}}{\gamma_M} & \text{screw steel strength} \\[2mm] R_{\text{ax,d}} & \text{punching screw head (not relevant)} \end{cases} \tag{D.1}
$$

With the input parameters:

$d_1 = 4\,\text{mm}$ outer diameter of thread

$l = 35\,\text{mm}$ screw length

$l_{\text{ef}} = 25\,\text{mm}$ thread length

GL36h   nominated strength category

the design resistance capacity per screw (one out of eight) results to

$$
R_{\text{ax,d}} = \min \begin{cases} R_{\text{ax,d}} = \frac{0.8 \cdot 1620\,\text{N}}{1.3} = 997\,\text{N} \\[2mm] R_{\text{t,u,d}} = \frac{3800\,\text{N}}{1.3} = 2923\,\text{N} \end{cases} = 997\,\text{N}
$$

The tensile resistance of the prestressing media M6 grade 4.6, as shown in eq. (7.1) on page 204, is $F_{\text{t,Rd}} = 5.8\,\text{kN}$.

E Evaluation of rigid joint investigation

E.1 Procedure of four point bending tests

The following photographs are illustrating the testing procedures of the four point bending tests undertaken and the respective failure behaviour of the samples.

The images are arranged starting with the specimen cast in one stage *MO* (pages 265–271), followed by the specimen cast in two stages *FU* (pages 272–277).
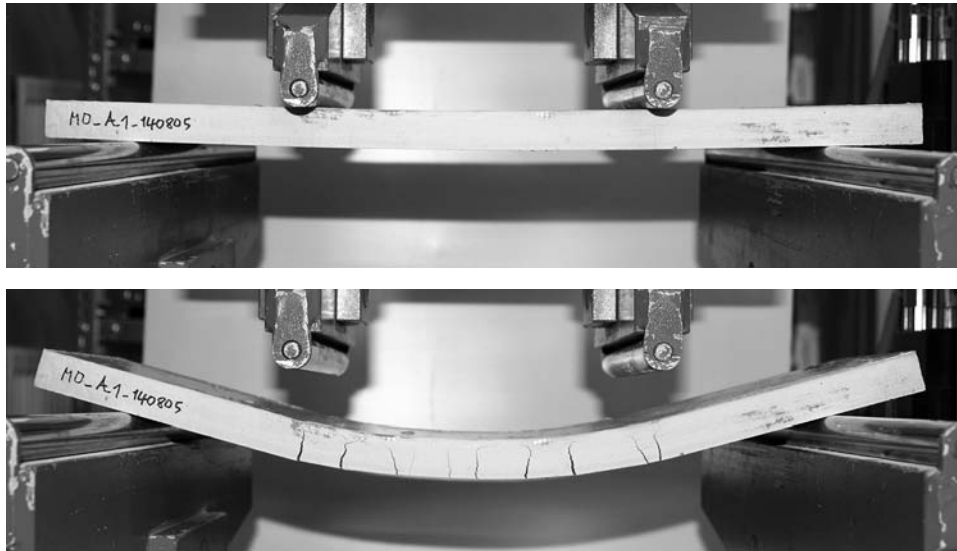
Figure E.1   Testing of specimen MO_A_01
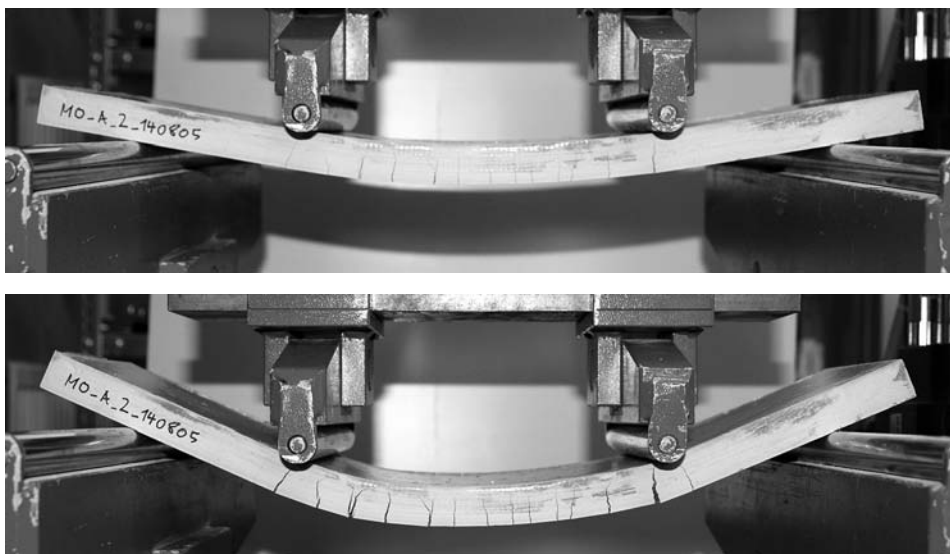
Figure E.2   Testing of specimen MO_A_02
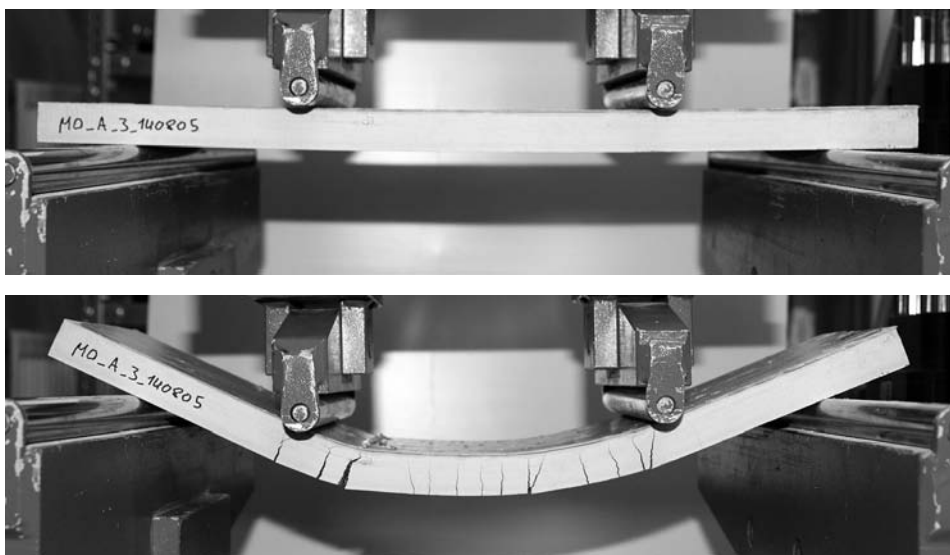
Figure E.3   Testing of specimen MO_A_03
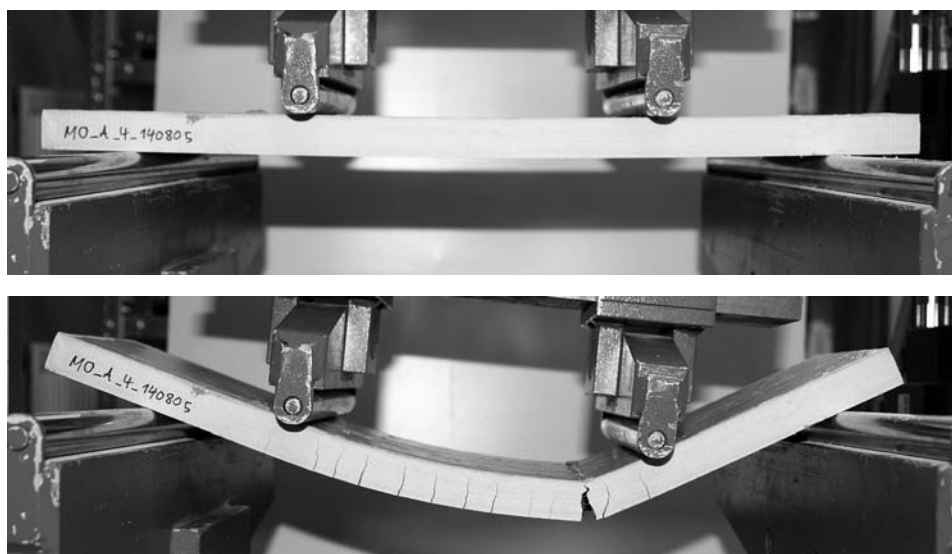
Figure E.4   Testing of specimen MO_A_04
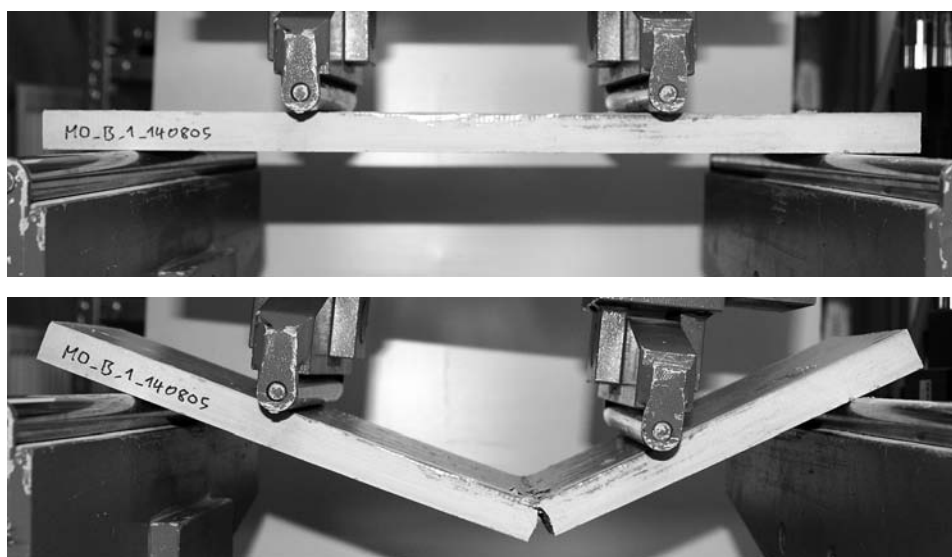
Figure E.5   Testing of specimen MO_B_01
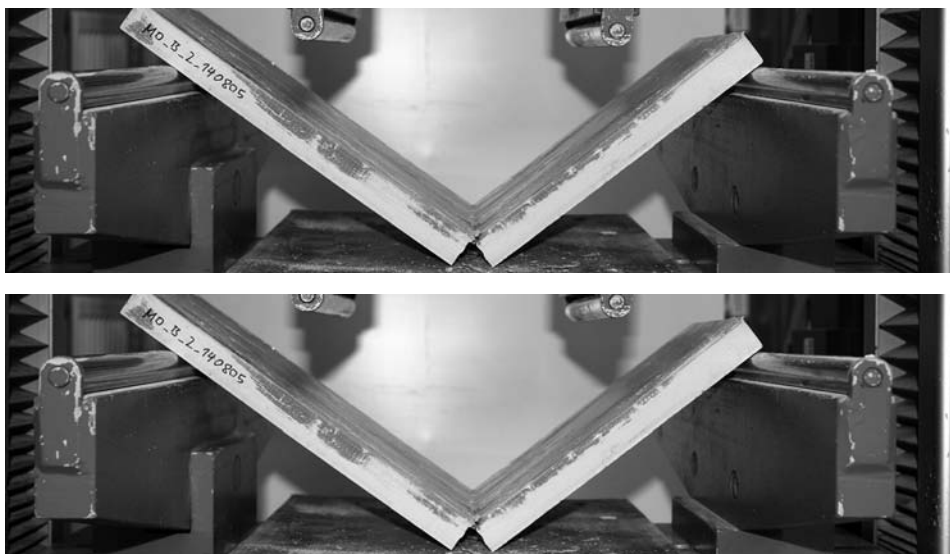
Figure E.6   Testing of specimen MO_B_02
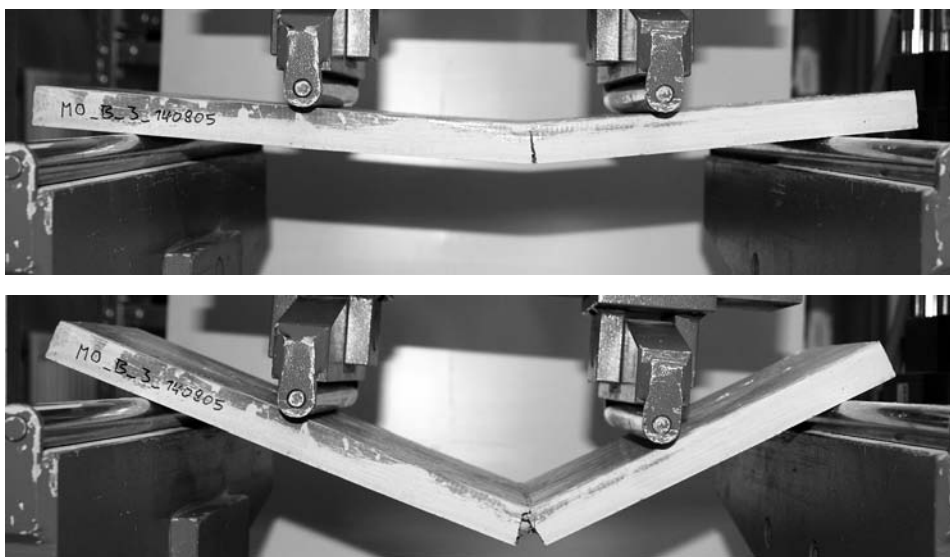
Figure E.7   Testing of specimen MO_B_03
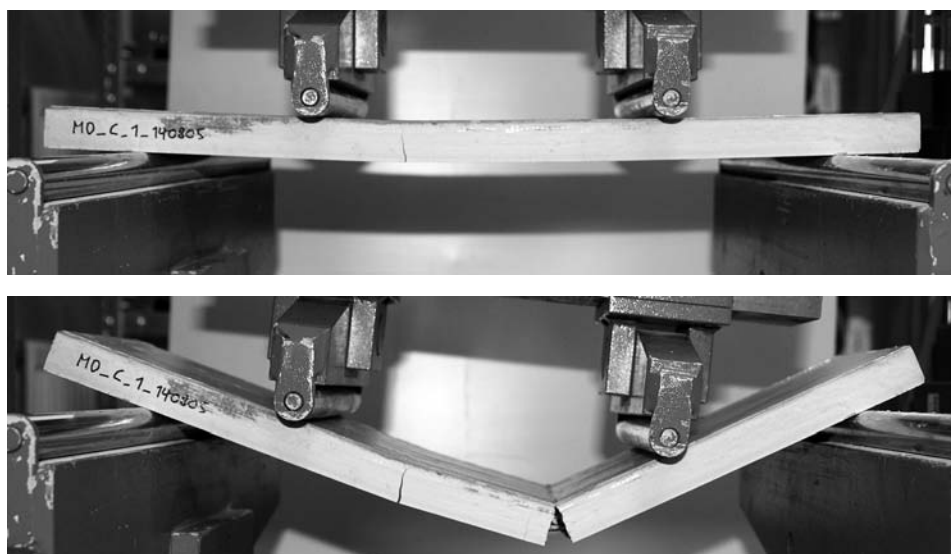
Figure E.8   Testing of specimen MO_C_01
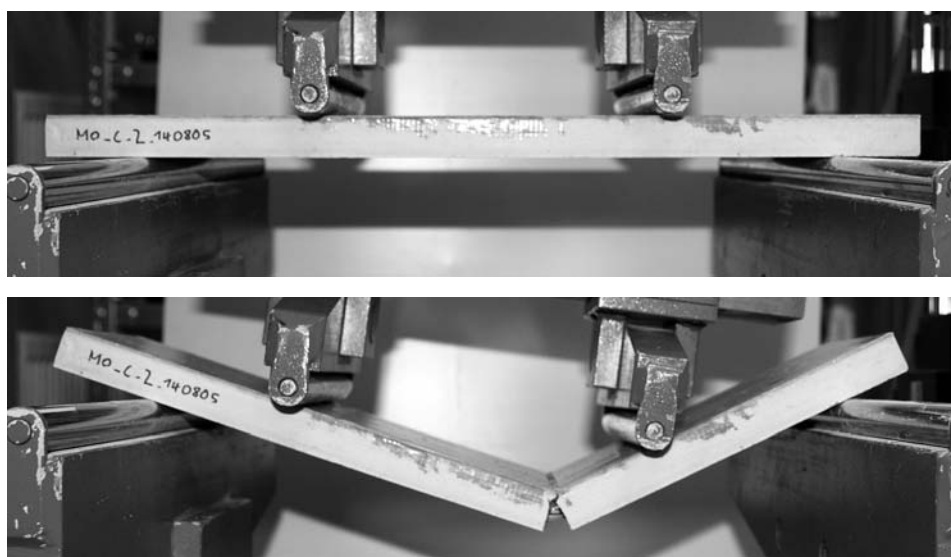
Figure E.9   Testing of specimen MO_C_02
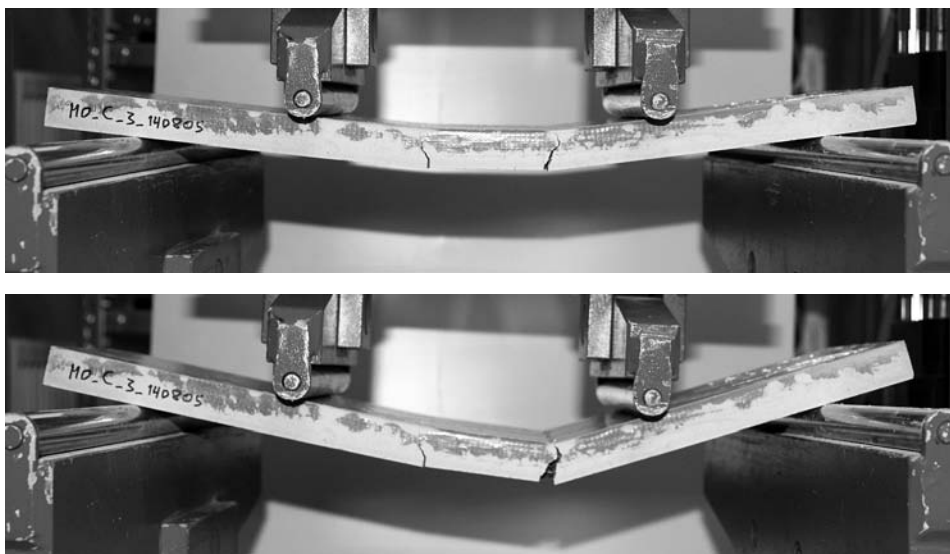
Figure E.10   Testing of specimen MO_C_03

Figure E.11   Testing of specimen MO_D_01
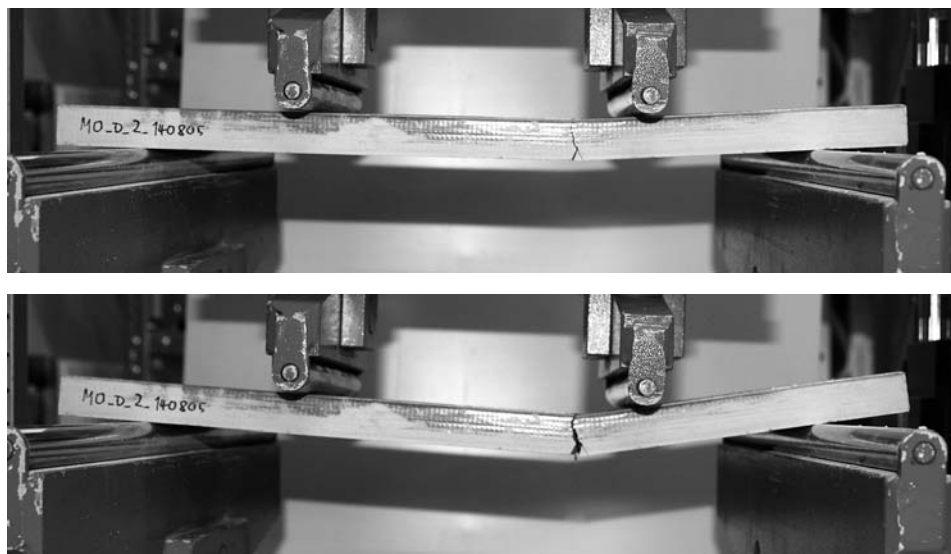
Figure E.12 Testing of specimen MO_D_02
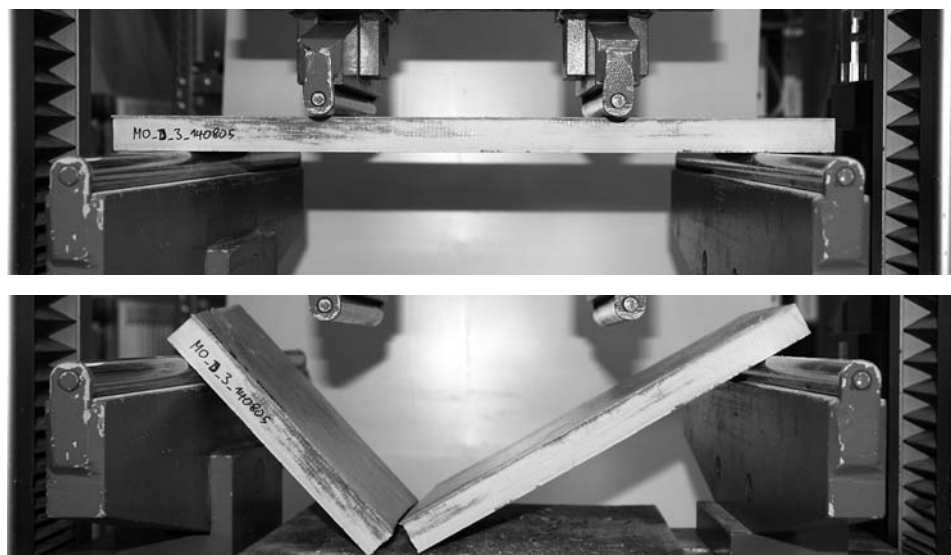
Figure E.13 Testing of specimen MO_D_03
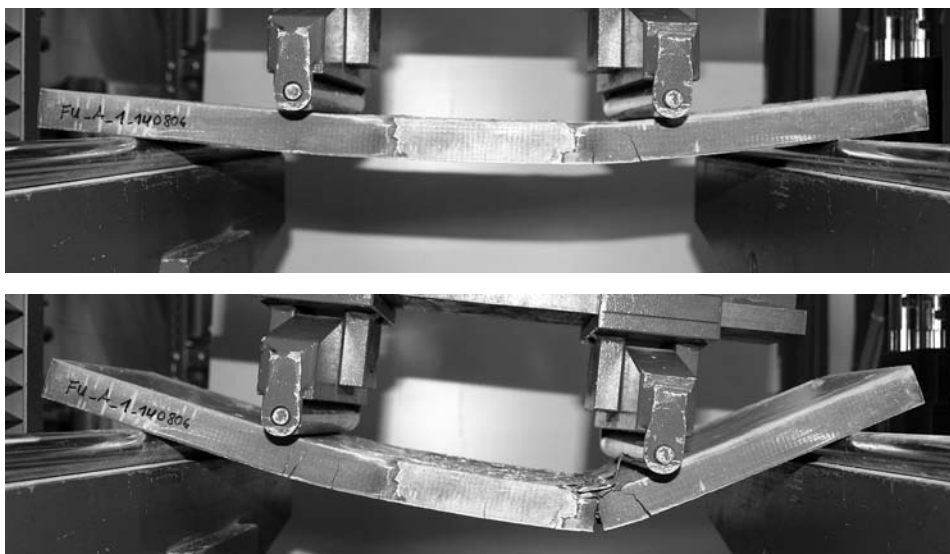
Figure E.14   Testing of specimen FU_A_01
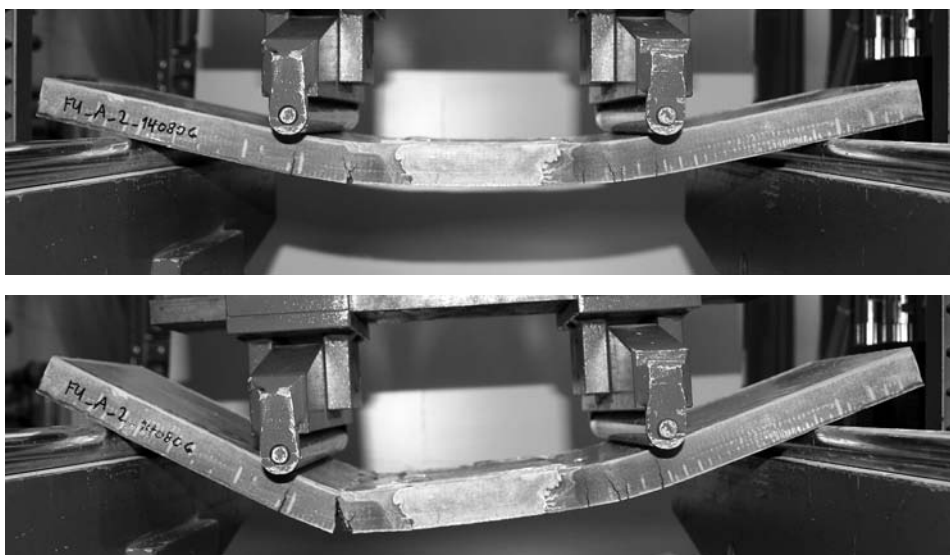
Figure E.15   Testing of specimen FU_A_02
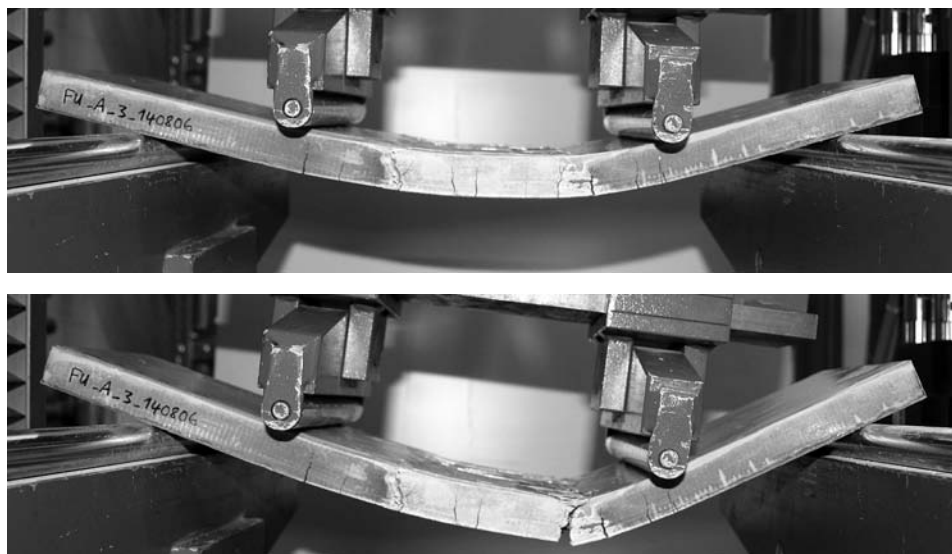
Figure E.16   Testing of specimen FU_A_03
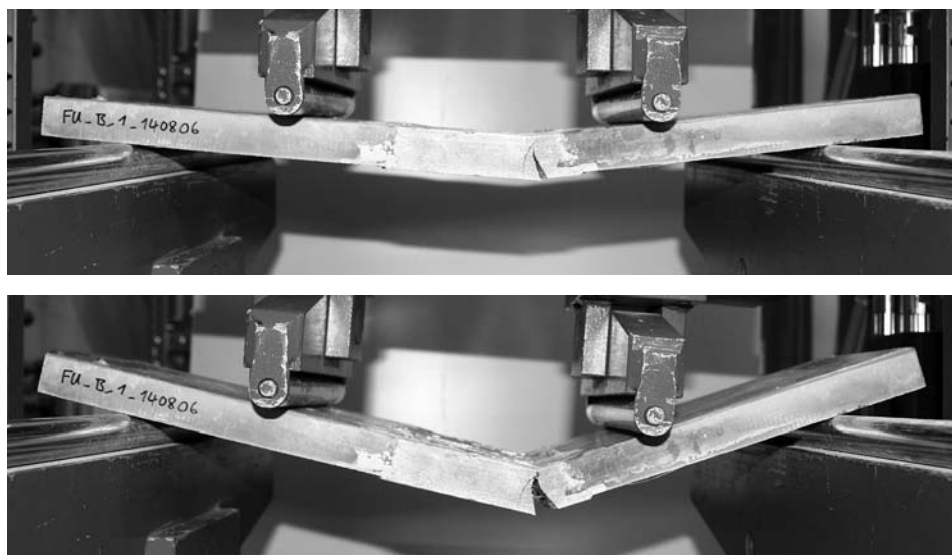
Figure E.17   Testing of specimen FU_B_01
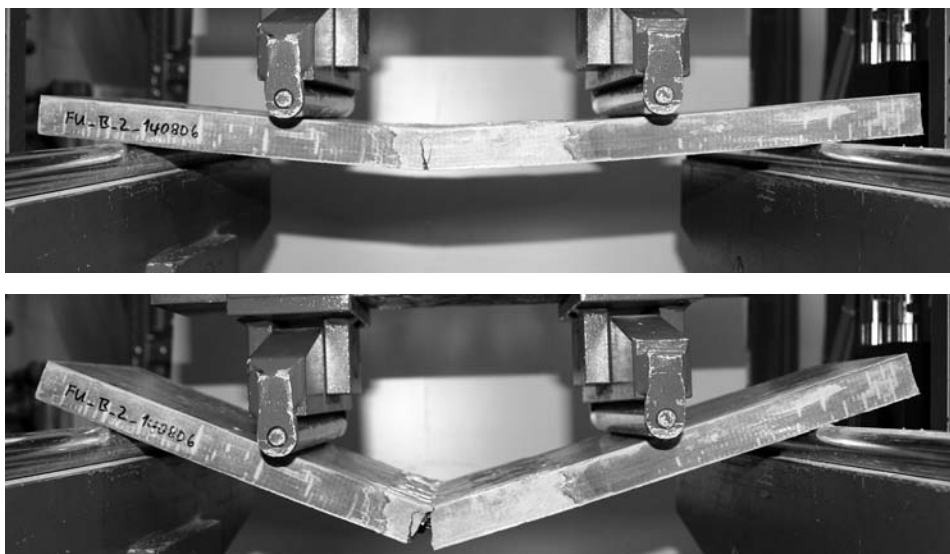
Figure E.18   Testing of specimen FU_B_02
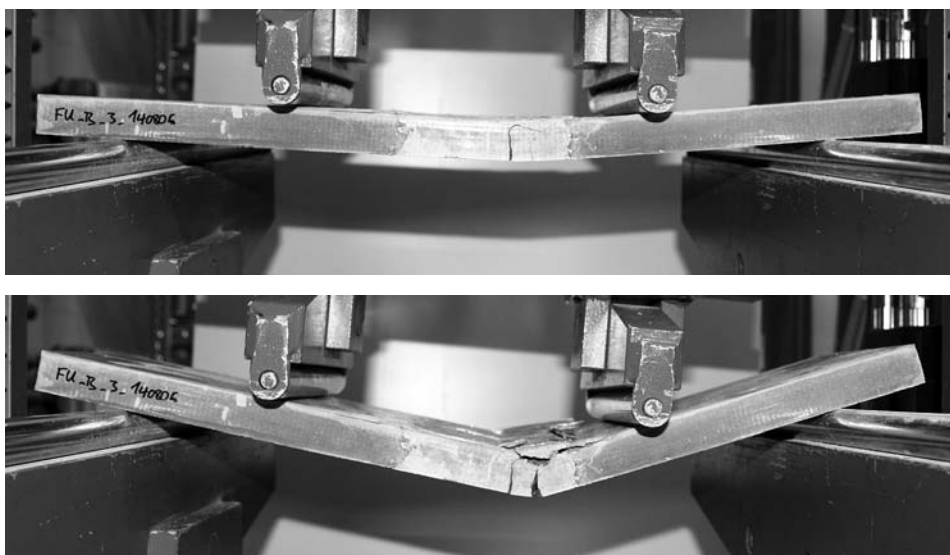
Figure E.19   Testing of specimen FU_B_03
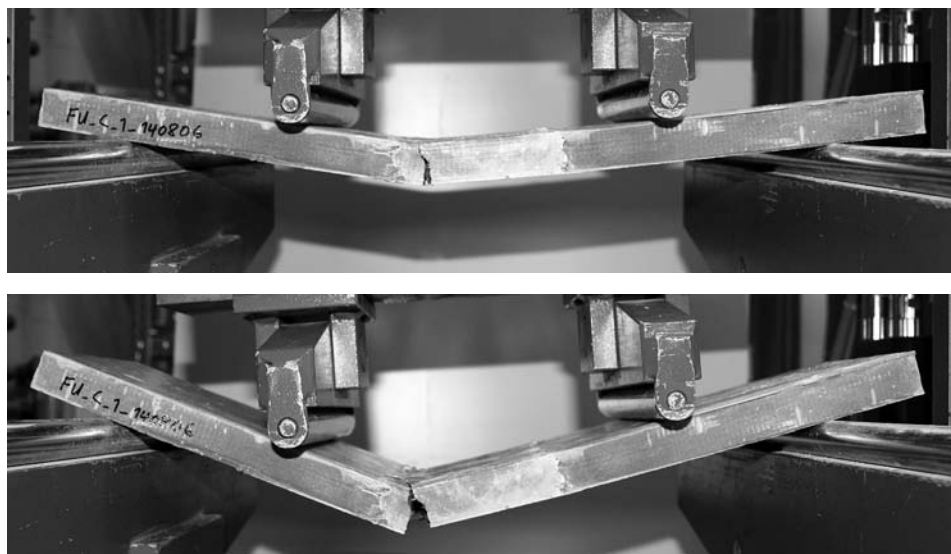
Figure E.20   Testing of specimen FU_C_01
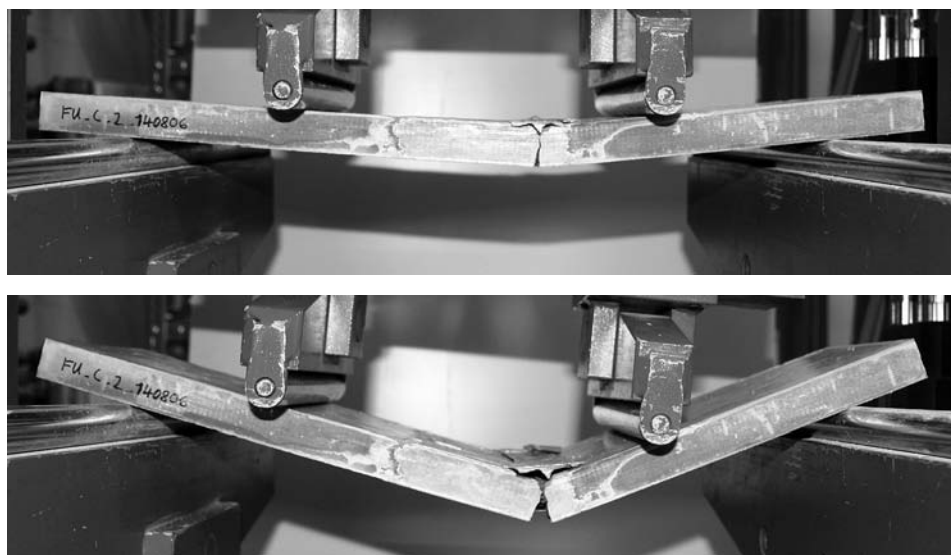
Figure E.21   Testing of specimen FU_C_02
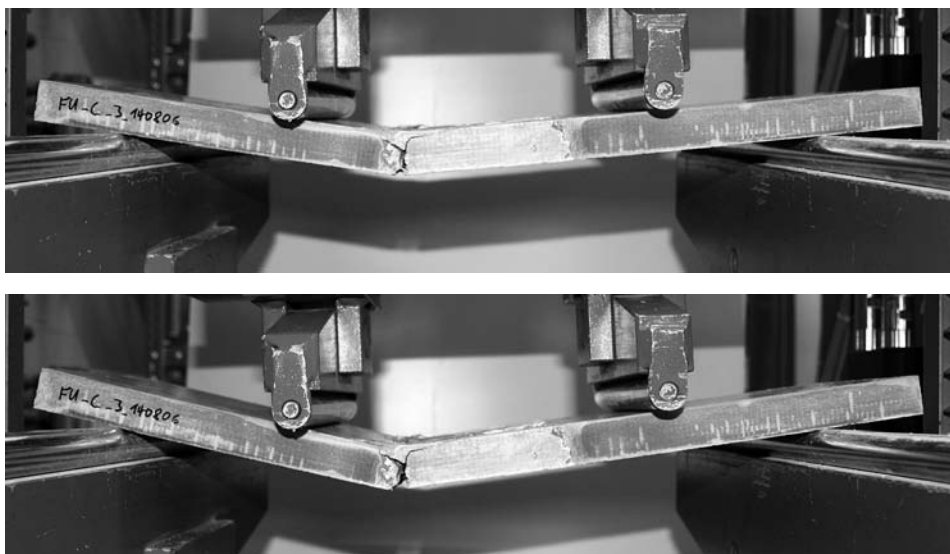
Figure E.22 Testing of specimen FU_C_03
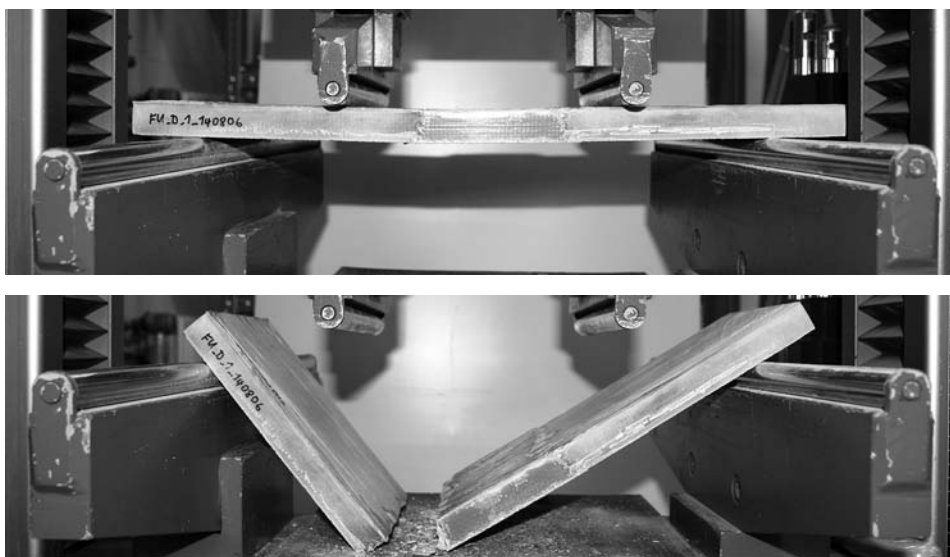
Figure E.23 Testing of specimen FU_D_01
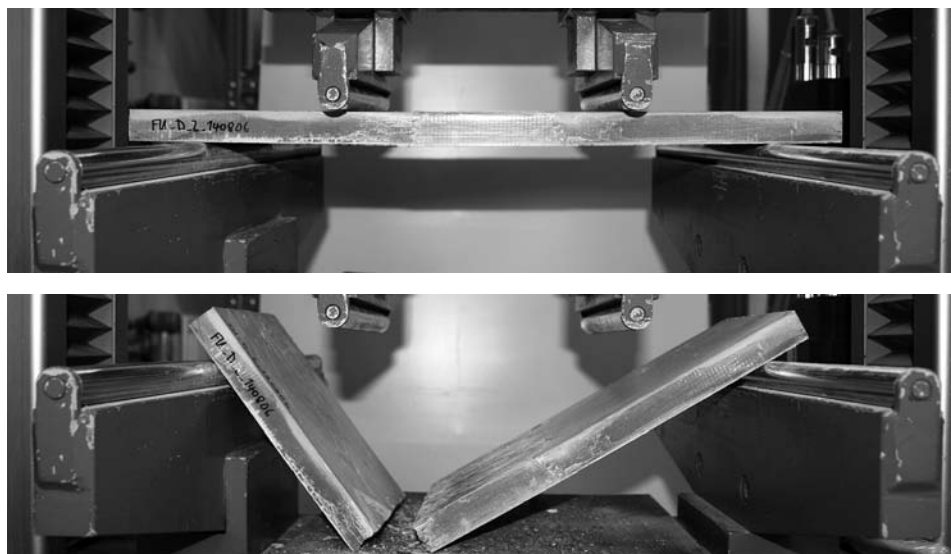
Figure E.24   Testing of specimen FU_D_02
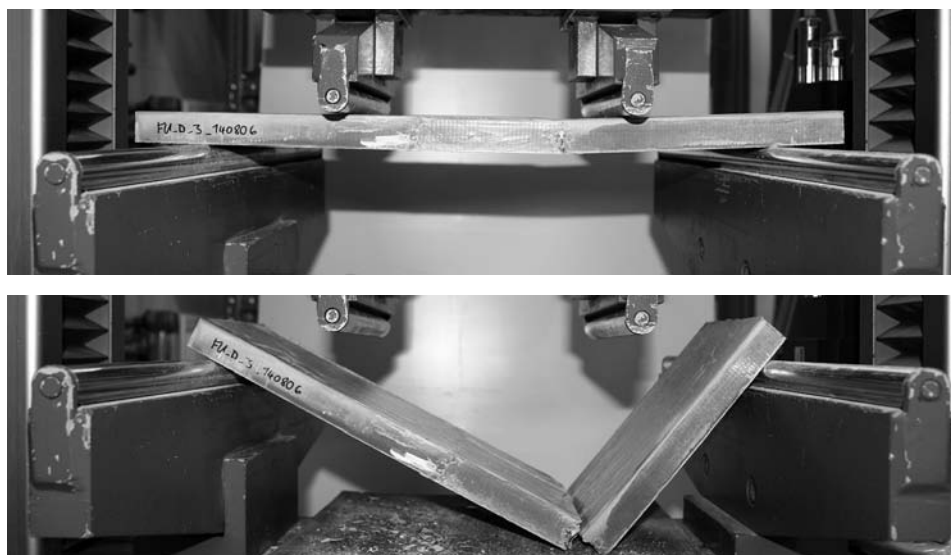
Figure E.25   Testing of specimen FU_D_03

E.2 Load – displacement evaluation and load bearing capacities

The load – displacement curves, which have been recorded from the four point bending investigations are completely given on the following pages. Each page comprises the plots of the single tests 1, 2 and 3 as well as a summarizing graph including the mean value graph $\overline{1,2,3}$. The sequence of the illustration starts with the specimen cast in one stage *MO* (pages 279–282), followed by the specimen cast in two stages *FU* (pages 283–286).

The load bearing capacities derived from the investigations undertaken are summarized tabularly. The results of the specimen cast in one stage *MO* can be found on page 287, the the results of the specimen cast in two stages *FU* on page 288.
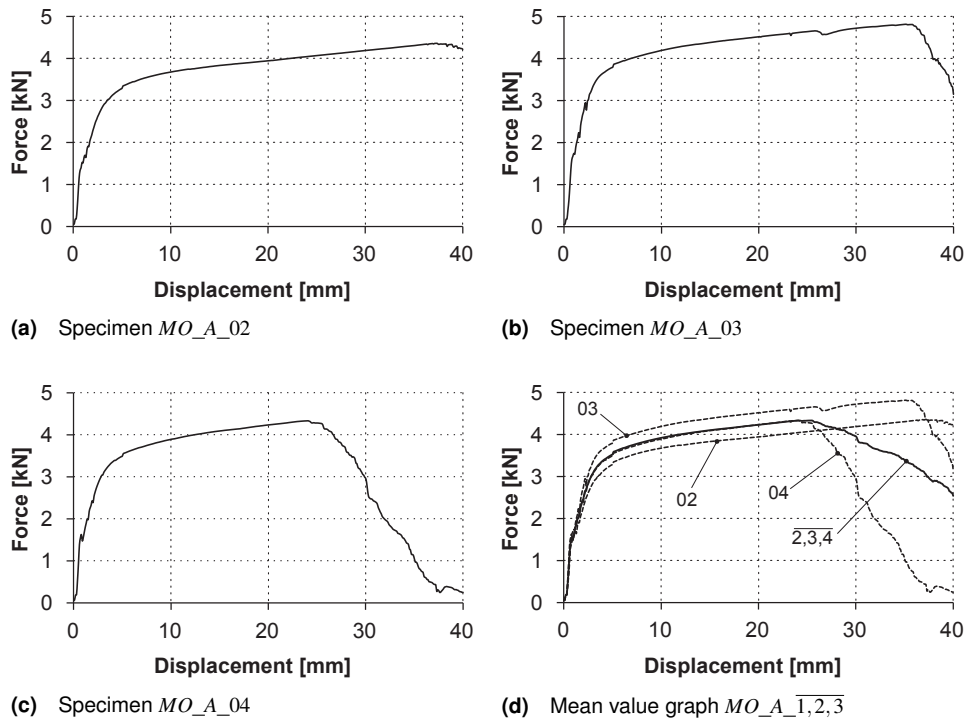
Figure E.26 Load−displacement plots for series cast monolithic (in one stage) *MO* with reinforcement arrangement *A*; plots *02*, *03*, *04* and mean value graph $\overline{2,3,4}$
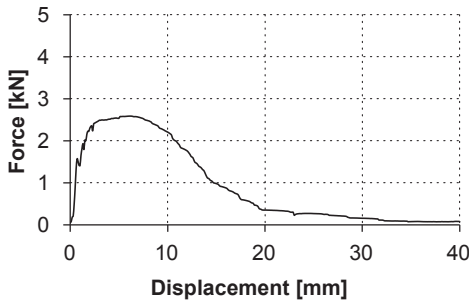
(a) Specimen MO_B_01
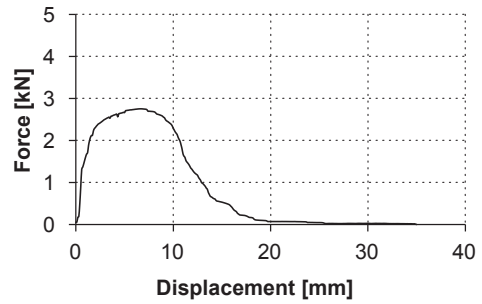
(b) Specimen MO_B_02
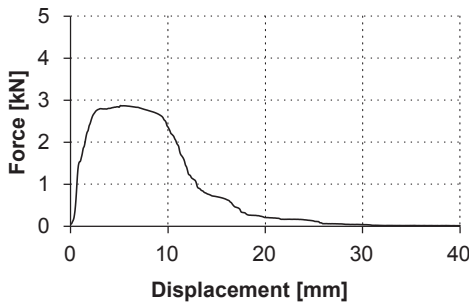
(c) Specimen MO_B_03
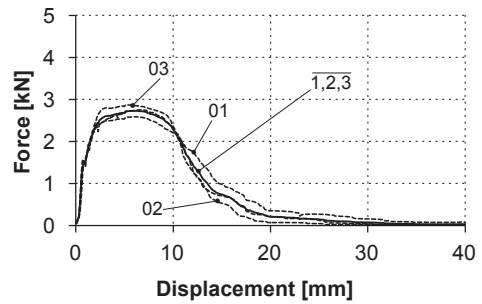
(d) Mean value graph $MO\_B\_\overline{1,2,3}$

Figure E.27 Load–displacement plots for series cast monolithic (in one stage) *MO* with reinforcement arrangement *B*; plots *01*, *02*, *03* and mean value graph $\overline{1,2,3}$

(a) Specimen MO_C_01

(b) Specimen MO_C_02

(c) Specimen MO_C_03

(d) Mean value graph $MO\_C\_\overline{1,2,3}$
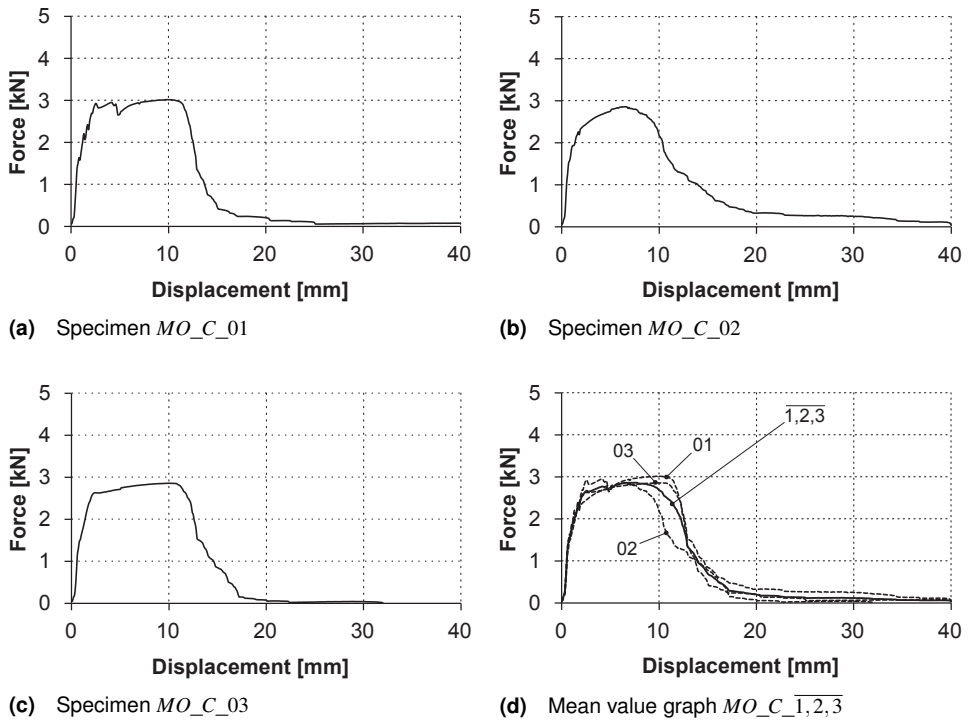
Figure E.28 Load–displacement plots for series cast monolithic (in one stage) *MO* with reinforcement arrangement *C*; plots *01*, *02*, *03* and mean value graph $\overline{1,2,3}$
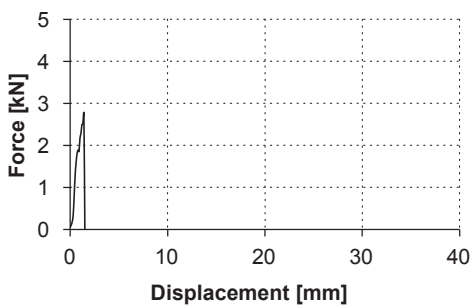
(a) Specimen MO_D_01
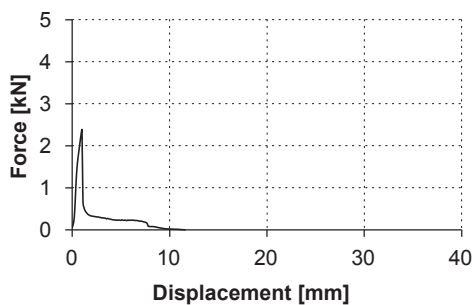
(b) Specimen MO_D_02
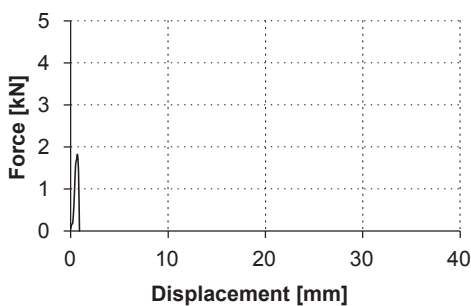
(c) Specimen MO_D_03
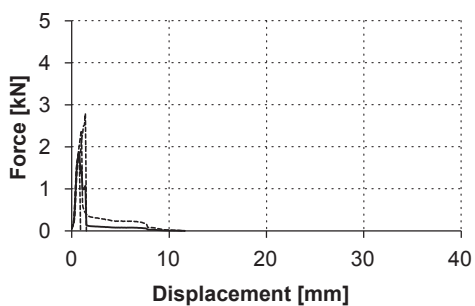
(d) Mean value graph $MO\_D\_\overline{1,2,3}$

Figure E.29 Load−displacement plots for series cast monolithic (in one stage) *MO* with reinforcement arrangement *D*; plots *01*, *02*, *03* and mean value graph $\overline{1,2,3}$
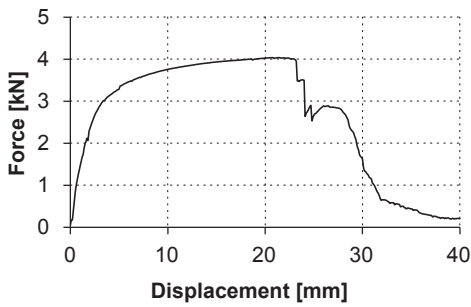
(a) Specimen FU_A_01
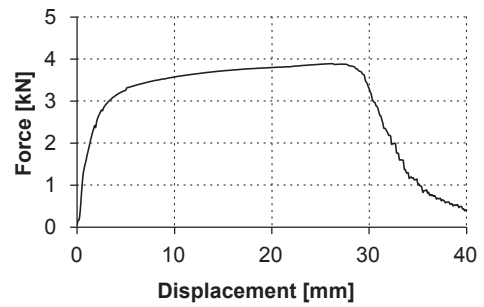
(b) Specimen FU_A_02
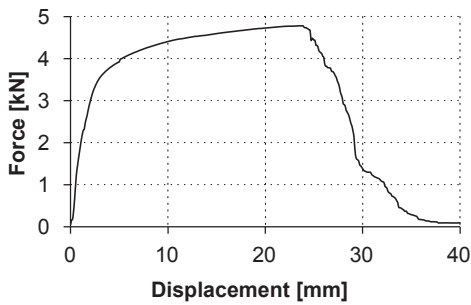
(c) Specimen FU_A_03
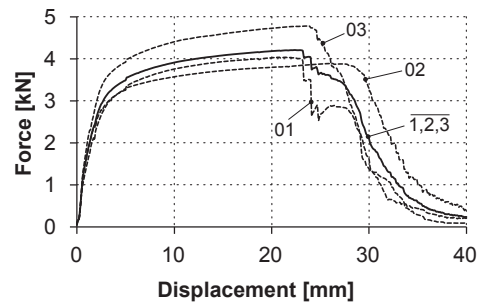
(d) Mean value graph $FU\_A\_\overline{1,2,3}$

Figure E.30 Load–displacement plots for series cast in two stages FU with reinforcement arrangement A; plots 01, 02, 03 and mean value graph $\overline{1,2,3}$
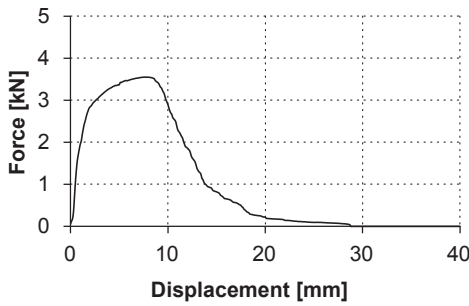
(a)　Specimen FU_B_01
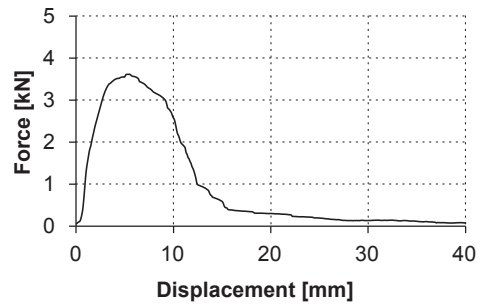
(b)　Specimen FU_B_02
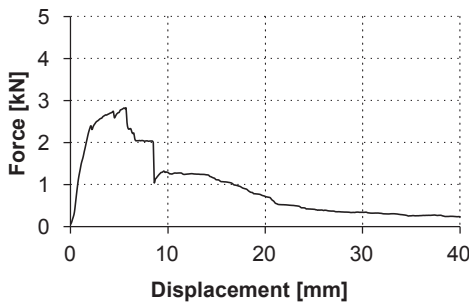
(c)　Specimen FU_B_03
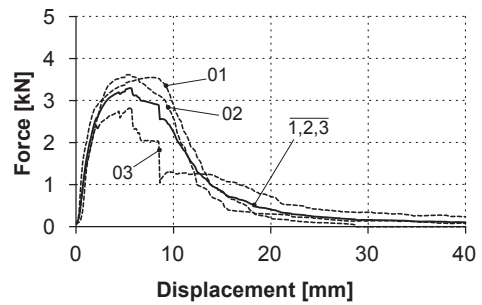
(d)　Mean value graph $FU\_B\_\overline{1,2,3}$

Figure E.31　Load−displacement plots for series cast in two stages FU with reinforcement arrange-ment B; plots 01, 02, 03 and mean value graph $\overline{1,2,3}$

(a) Specimen FU_C_01

(b) Specimen FU_C_02

(c) Specimen FU_C_03

(d) Mean value graph $FU\_C\_\overline{1,2,3}$
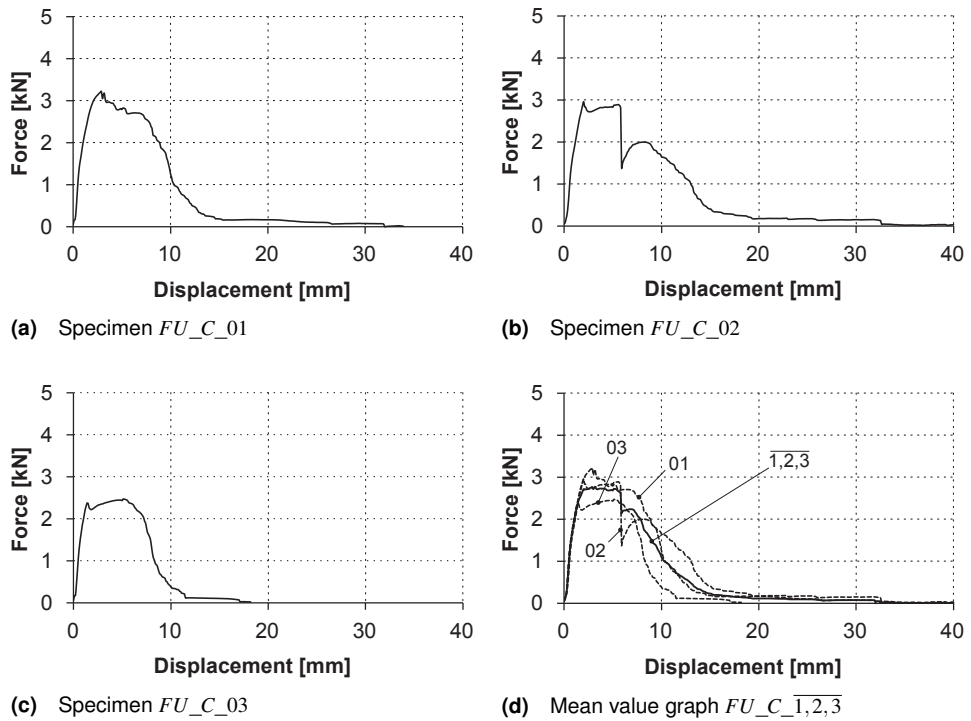
Figure E.32 Load – displacement plots for series cast in two stages FU with reinforcement arrangement C; plots 01, 02, 03 and mean value graph $\overline{1,2,3}$
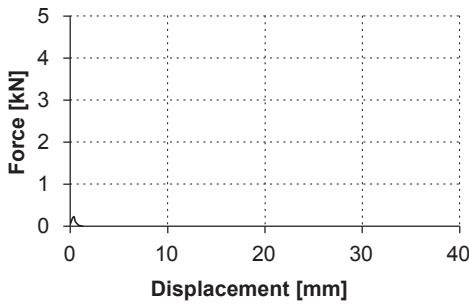
(a) Specimen *FU_D*_01
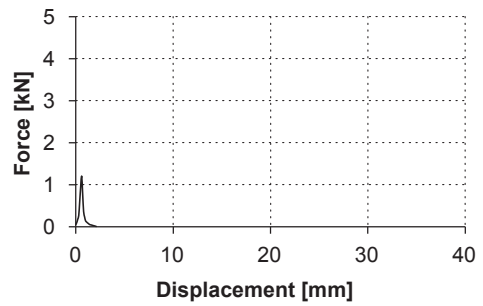
(b) Specimen *FU_D*_02
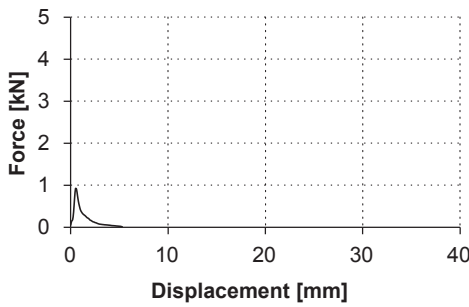
(c) Specimen *FU_D*_03
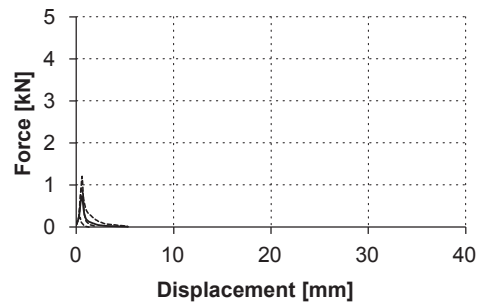
(d) Mean value graph $FU\_D\_\overline{1,2,3}$

Figure E.33 Load–displacement plots for series cast in two stages *FU* with reinforcement arrangement *D*; plots *01*, *02*, *03* and mean value graph $\overline{1,2,3}$

Table E.1 Bending tensile strength investigated with four point bending tests, samples *MO, A*

no.	length [mm]	width [mm]	height [mm]	mass [g]	density $[kg/m^3]$	F_{max} [kN]	M_{max} [Nm]	W_y $[mm^3]$	β_{BT} $[N/mm^2]$
MO_A_1	500	151,1	21,4	4 092	2 534	3,9	193,5	11 504	16,8
MO_A_2	500	151,1	21,9	4 045	2 447	4,4	218,0	12 055	18,1
MO_A_3	500	151,4	24,0	4 357	2 401	4,8	240,5	14 506	16,6
MO_A_4	500	151,2	23,3	4 270	2 427	4,3	216,5	13 644	15,9
$\overline{x}$	500	151,2	22,6	4 191	2 452	4,3	217,1	12 927	**16, 8**

Table E.2 Bending tensile strength investigated with four point bending tests, samples *MO, B*

no.	length [mm]	width [mm]	height [mm]	mass [g]	density $[kg/m^3]$	F_{max} [kN]	M_{max} [Nm]	W_y $[mm^3]$	β_{BT} $[N/mm^2]$
MO_B_1	500	151,4	22,6	4 188	2 444	2,6	129,5	12 933	10,0
MO_B_2	500	151,9	23,5	4 270	2 398	2,8	137,5	13 920	9,9
MO_B_3	500	151,5	23,3	4 241	2 407	2,9	143,5	13 661	10,5
$\overline{x}$	500	151,6	23,1	4 233	2 416	2,7	136,8	13 505	**10, 1**

Table E.3 Bending tensile strength investigated with four point bending tests, samples *MO, C*

no.	length [mm]	width [mm]	height [mm]	mass [g]	density $[kg/m^3]$	F_{max} [kN]	M_{max} [Nm]	W_y $[mm^3]$	β_{BT} $[N/mm^2]$
MO_C_1	500	152,7	23,1	4 277	2 430	3,0	151,0	13 529	11,2
MO_C_2	500	151,3	23,5	4 322	2 432	2,9	143,0	13 914	10,3
MO_C_3	500	151,2	22,9	4 277	2 465	2,9	143,0	13 265	10,8
$\overline{x}$	500	151,7	23,2	4 292	2 442	2,9	145,7	13 569	**10, 7**

Table E.4 Bending tensile strength investigated with four point bending tests, samples *MO, D*

no.	length [mm]	width [mm]	height [mm]	mass [g]	density $[kg/m^3]$	F_{max} [kN]	M_{max} [Nm]	W_y $[mm^3]$	β_{BT} $[N/mm^2]$
MO_D_1	500	151,7	23,6	4 235	2 368	2,9	143,5	14 056	10,2
MO_D_2	500	151,1	23,6	4 283	2 399	2,4	121,5	14 063	8,6
MO_D_3	500	151,2	24,2	3 902	2 129	1,9	94,0	14 807	6,4
$\overline{x}$	500	151,3	23,8	4 140	2 299	2,4	119,7	14 309	**8, 4**

Table E.5 Bending tensile strength investigated with four point bending tests, samples *FU, A*

no.	length [mm]	width [mm]	height [mm]	mass [g]	density [kg/m^3]	F_{max} [kN]	M_{max} [Nm]	W_y [mm^3]	β_{BT} [N/mm^2]
FU_A_1	500	152,3	23,7	4 045	2 239	4,0	202,0	14 291	14,1
FU_A_2	500	151,3	23,7	4 076	2 272	3,9	194,5	14 177	13,7
FU_A_3	500	151,5	24,0	4 337	2 384	4,8	239,0	14 566	16,4
x̄	500	151,7	23,8	4 153	2 298	4,2	211,8	14 345	**14, 8**

Table E.6 Bending tensile strength investigated with four point bending tests, samples *FU, B*

no.	length [mm]	width [mm]	height [mm]	mass [g]	density [kg/m^3]	F_{max} [kN]	M_{max} [Nm]	W_y [mm^3]	β_{BT} [N/mm^2]
FU_B_1	500	151,5	24,6	4 349	2 330	3,6	177,5	15 329	11,6
FU_B_2	500	151,7	24,4	4 221	2 279	3,6	180,5	15 075	12,0
FU_B_3	500	152,1	24,0	4 160	2 281	2,8	141,5	14 585	9,7
x̄	500	151,7	24,4	4 243	2 297	3,3	166,5	14 996	**11, 1**

Table E.7 Bending tensile strength investigated with four point bending tests, samples *FU, C*

no.	length [mm]	width [mm]	height [mm]	mass [g]	density [kg/m^3]	F_{max} [kN]	M_{max} [Nm]	W_y [mm^3]	β_{BT} [N/mm^2]
FU_C_1	500	151,8	24,8	4 356	2 319	3,2	161,0	15 499	10,4
FU_C_2	500	151,1	24,4	4 235	2 298	3,0	150,0	14 981	10,0
FU_C_3	500	152,2	24,2	4 258	2 313	2,5	123,5	14 851	8,3
x̄	500	151,7	24,5	4 283	2 310	2,9	144,8	15 110	**9, 6**

Table E.8 Bending tensile strength investigated with four point bending tests, samples *FU, D*

no.	length [mm]	width [mm]	height [mm]	mass [g]	density [kg/m^3]	F_{max} [kN]	M_{max} [Nm]	W_y [mm^3]	β_{BT} [N/mm^2]
FU_D_1	500	151,5	24,6	4 145	2 229	0,3	16,0	15 215	1,1
FU_D_2	500	151,3	24,7	4 241	2 270	1,3	65,5	15 373	4,3
FU_D_3	500	152,1	24,5	4 172	2 235	1,0	47,5	15 268	3,1
x̄	500	151,6	24,6	4 186	2 245	0,9	43,0	15 285	**2, 8**

F Evaluation of prestressing connection investigation

F.1 Procedure of load bearing investigations – approach $^{\#}$01 / low tensioning

F.1.1 Experiments 'vertical' arrangement

The investigation approaches 'vertical' illustrate the failure behaviour of the concrete elements, connected with a low prestressing. The system proofs a buckling out of plane. However the capacity is sufficient for the exhibition object *Stable Equilibrium*. Within the elastic range (fig. F.1a on the following page), where the system remains within its initial form configuration, a safety factor of about 2,7 is achieved.

With beginning failure the systems does not 'fall down', since a catenary develops, as shown on fig. F.1b and fig. F.1c.
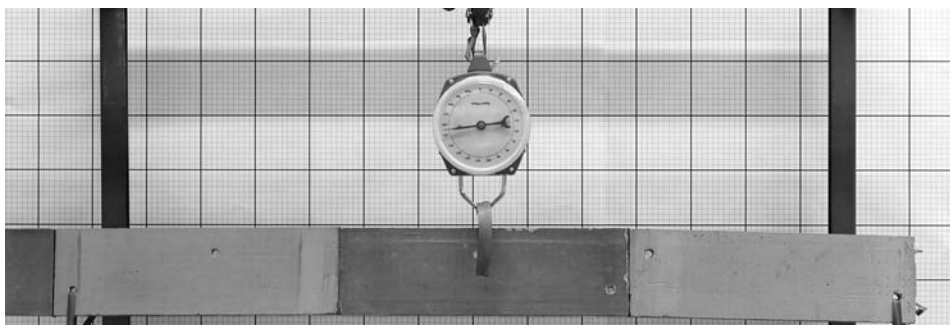
(a) End of elastic range; $u = 13\,\text{mm}$, $F = 1{,}55\,\text{kN}$ ($M_y = 564\,\text{N m}$)
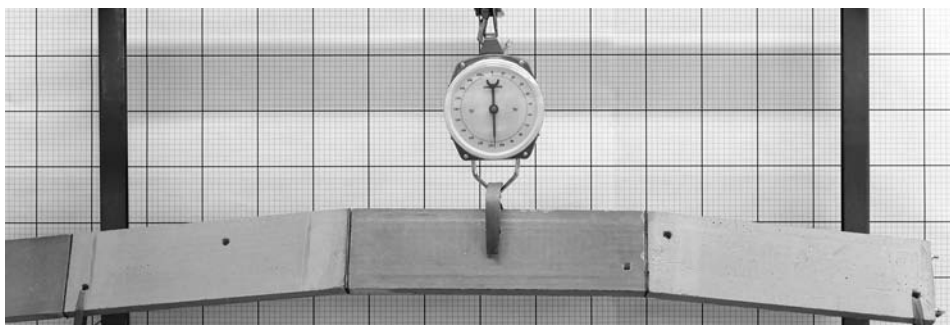
(b) End of bending out of plane; $u = 21\,\text{mm}$, $F = 1{,}07\,\text{kN}$ ($M_y = 389\,\text{N m}$)
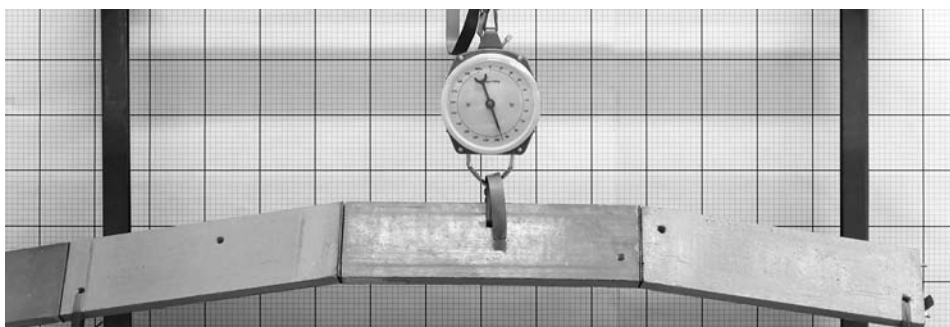
(c) Collapse point; $u = 55\,\text{mm}$, $F = 0{,}93\,\text{kN}$ ($M_y = 339\,\text{N m}$)

Figure F.1 Testing sequence of approach [#]01 'vertical'

Table F.1 Applied test loads and investigated deflections in approach $^\#$01 'vertical', see load-displacement curve in fig. 7.10 on page 201

increment	test load F	equiv. M_y	deflection u	range
[-]	[N]	[Nm]	[mm]	
1	330	120	2,0	
2	560	204	5,0	
3	680	248	6,0	
4	780	284	7,0	
5	890	324	8,0	
6	980	357	9,0	elastic
7	1 070	389	9,5	
8	1 150	419	10,0	
9	1 280	466	10,0	
10	1 370	499	11,0	
11	1 460	531	12,0	
12[a]	1 550	564	13,0	
13	1 280	466	15,0	
14	1 150	419	18,0	bending out of plane
15[b]	1 070	389	21,0	
16	1 090	397	29,0	
17	1 060	386	33,0	collapse
18[c]	930	339	55,0	

[a] refer fig. F.1a on page 290
[b] refer fig. F.1b
[c] refer fig. F.1c

Table F.1 illustrates the applied load and metered displacements during the investigation. The corresponding load – displacement graph is given in fig. 7.10 on page 201.

F.1.2 Experiments 'horizontal' arrangement

The following photographs are illustrating the testing sequence of the investigations with 'low tensioning' and 'horizontal' arrangement of specimens.

table F.2 illustrates the applied load and metered displacements during the investigation. The corresponding load – displacement graph is given in fig. 7.13 on page 204.
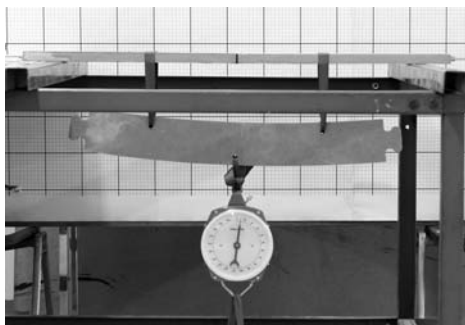
(a) Start of elastic range; $u = 4\,\text{mm}$, $F = 50\,\text{N}$ ($M_z = 5\,\text{N}\,\text{m}$)
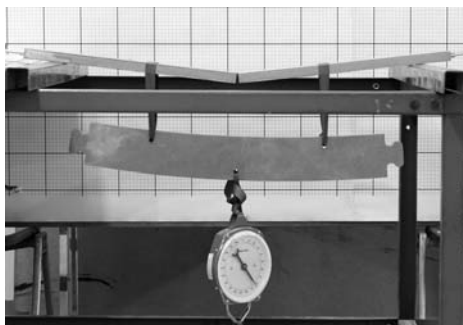
(b) First cracking occurs; $u = 55\,\text{mm}$, $F = 820\,\text{N}$ ($M_z = 82\,\text{N}\,\text{m}$)
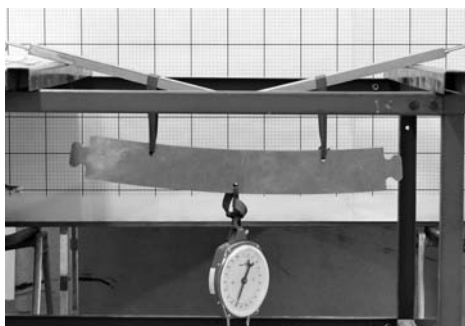
(c) End of plastic range; $u = 120\,\text{mm}$, $F = 1190\,\text{N}$ ($M_z = 119\,\text{N}\,\text{m}$)
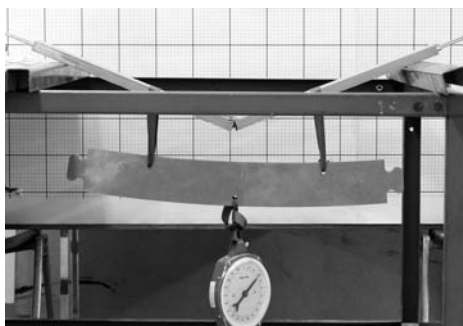
(d) Collapse; $u = 150\,\text{mm}$, $F = 320\,\text{N}$ ($M_z = 32\,\text{N}\,\text{m}$)

Figure F.2   Testing sequence of approach $^{\#}01$ 'horizontal'

Table F.2 Applied test loads and investigated deflections in approach #01 'horizontal', see load-displacement curve in fig. 7.13 on page 204

increment	test load F	equiv. M_z	deflection u	range
[-]	[N]	[Nm]	[mm]	
1[a]	50	5	4,0	
2	100	10	4,0	
3	200	20	6,0	
4	240	24	7,0	
5	270	27	8,0	
6	300	30	13,0	
7	380	38	17,0	
8	430	43	19,0	
9	420	42	19,0	
10	490	49	23,0	elastic
11	500	50	25,0	
12	540	54	27,0	
13	600	60	30,0	
14	660	66	32,0	
15	700	70	34,0	
16	730	73	40,0	
17	770	77	47,0	
18	800	80	50,0	
19	860	86	54,0	
20[b]	820	82	55,0	
21	880	88	55,0	
22	920	92	59,0	
23	970	97	77,0	
24	1 010	101	85,0	
25	1 050	105	93,0	plastic
26	1 090	109	97,0	
27	1 150	115	97,0	
28	1 160	116	107,0	
29	1 180	118	111,0	
30[c]	1 190	119	120,0	
31[d]	320	32	150,0	collapse

[a] refer fig. F.2a on page 292
[b] refer fig. F.2b; first cracking occurs
[c] refer fig. F.2c; end of plastic range
[d] refer fig. F.2d; collapse

F.2 Procedure of load bearing investigations – approach $^{\#}$02 / high tensioning

F.2.1 Determination of coefficient of creep

The coefficient of creep $\varphi(t,t_0)$ for constant stress levels as used for the readjusting of the screws in section 7.6.2.3 on page 211 is determined according to the guide line in *DAfStb*, issue 525 [DAf10, 60]. The coefficient of creep to an arbitrary time is calculated with following equation:

$$\varphi(t,t_0) = \varphi_0 \cdot \beta_c(t,t_0) \tag{F.1}$$

The values of φ_0 and $\beta_c(t,t_0)$ are determined as:

$$\varphi_0 = \varphi_{\mathrm{RH}} \cdot \beta(f_{\mathrm{cm}}) \cdot \beta(t_0) \tag{F.2}$$

and

$$\beta_c(t,t_0) = \left[\frac{(t-t_0)/t_1}{\beta_H + (t-t_0)/t_1} \right]^{0,3} \tag{F.3}$$

The input parameters are as follows:

$t = 183\,\mathrm{d}$ concrete age at time of interest

$t_0 = 181\,\mathrm{d}$ concrete age at time of loading

$\mathrm{RH} = 50\,\%$ indoor humidity

$b/h = 150\,\mathrm{mm}/22\,\mathrm{mm}; A_c = 3300\,\mathrm{mm}^2; u = 344\,\mathrm{mm}$

$h_0 = 2 \cdot A_c/u = 19{,}2\,\mathrm{mm}$ effective thickness

$f_{\mathrm{ck}} = 80\,\mathrm{N/mm}^2$ characteristic cylinder concrete strength

$f_{\mathrm{cm}} = f_{\mathrm{ck}} + 8\,\mathrm{N/mm}^2 = 88\,\mathrm{N/mm}^2$ median cylinder concrete strength

$\alpha = 1$

This gives:

$$\alpha_1 = \left[\frac{35}{f_{cm}}\right]^{0,7} = 0,524$$

$$\alpha_2 = \left[\frac{35}{f_{cm}}\right]^{0,2} = 0,832$$

$$\alpha_3 = \left[\frac{35}{f_{cm}}\right]^{0,5} = 0,631$$

$$\beta_H = 150 \cdot \left[1 + \left(1,2 \cdot \frac{RH}{100}\right)^{18}\right] \cdot \frac{h_0}{h_1} + 250 \cdot \alpha_3 = 186,44 \leq 1500 \cdot \alpha_3$$

$$t_{0,eff} = t_0 \cdot \left[\frac{9}{2 + (t_0/t_1)^{1,2}} + 1\right]^{\alpha} = 184,2\,d \geq 0,5\,d$$

$$\beta(t_0) = \frac{1}{0,1 + (t_{0,eff}/t_1)^{0,2}} = 0,340$$

$$\beta(f_{cm}) = \frac{16,8}{\sqrt{f_{cm}}} = 1,791$$

$$\varphi_{RH} = \left[1 + \frac{1 - RH/100}{\sqrt[3]{0,1 \cdot (h_0/h_1)}} \cdot \alpha_1\right] \cdot \alpha_2 = 1,646$$

Using eq. (F.3) and eq. (F.2) gives

$$\beta_c(t, t_0) = 0,2557$$

and

$$\varphi_0 = 1,0034$$

Finally, inserting in eq. (F.1) gives the creep coefficient

$$\varphi(t, t_0) = 0,2566$$

F.2.2 Four point bending tests and load – displacement evaluation

The following photographs are illustrating the testing procedures of the four point bending tests undertaken.

The images are arranged starting with the continuous 'prestressed sections' *PS* (pages 296–299) followed by the 'prestressed joints' *PJ* (pages 299–302).

The load – displacement curves, which have been recorded from the four point bending investigations are completely given, comprising the plots of the single tests 1, 2 and 3 as well a summarizing graph including the mean value graph $\overline{1,2,3}$. The sequence of the illustration starts with the continuous 'prestressed sections' *PS* (pages 303–304), followed by the 'prestressed joints' *PJ* (pages 305–306)
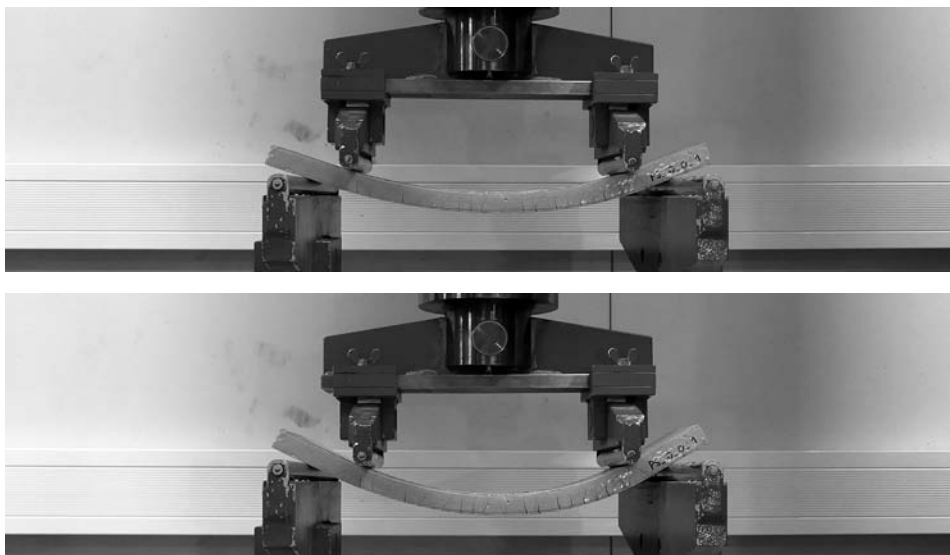
Figure F.3   Testing of specimen PS_0_0_01
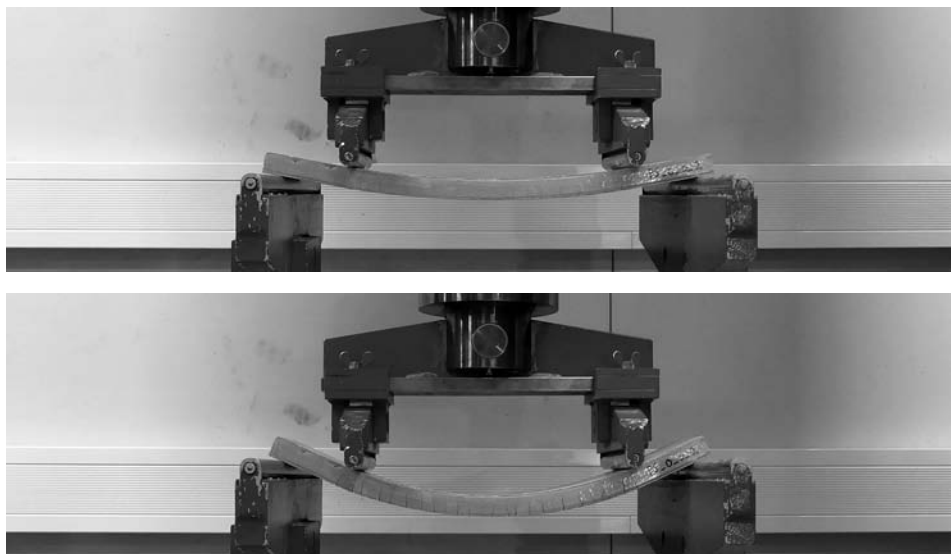
Figure F.4 Testing of specimen PS_0_0_02
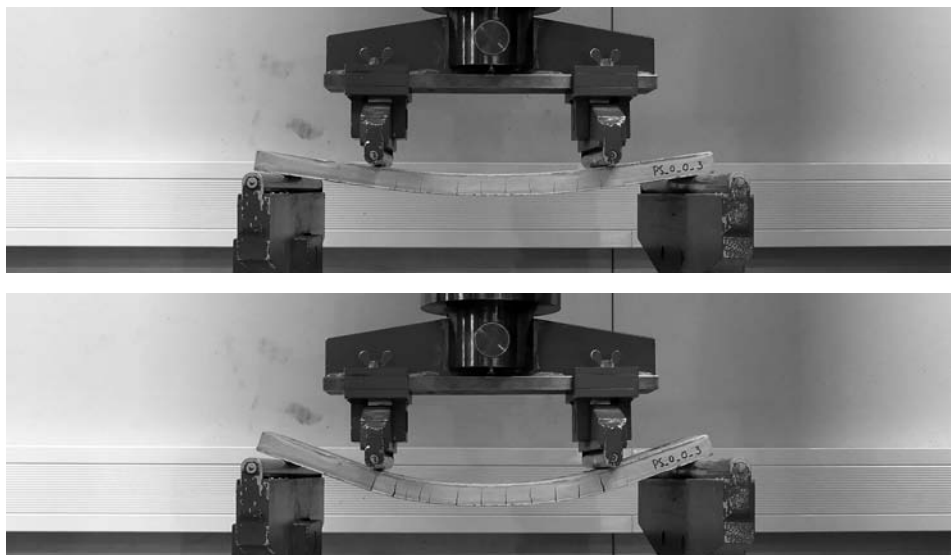
Figure F.5 Testing of specimen PS_0_0_03
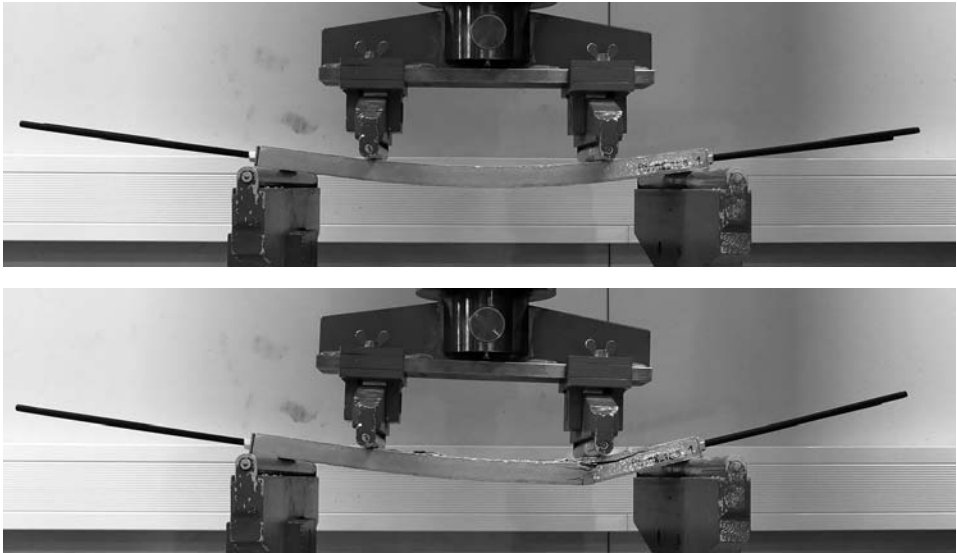
Figure F.6   Testing of specimen PS_M8_12.9_01
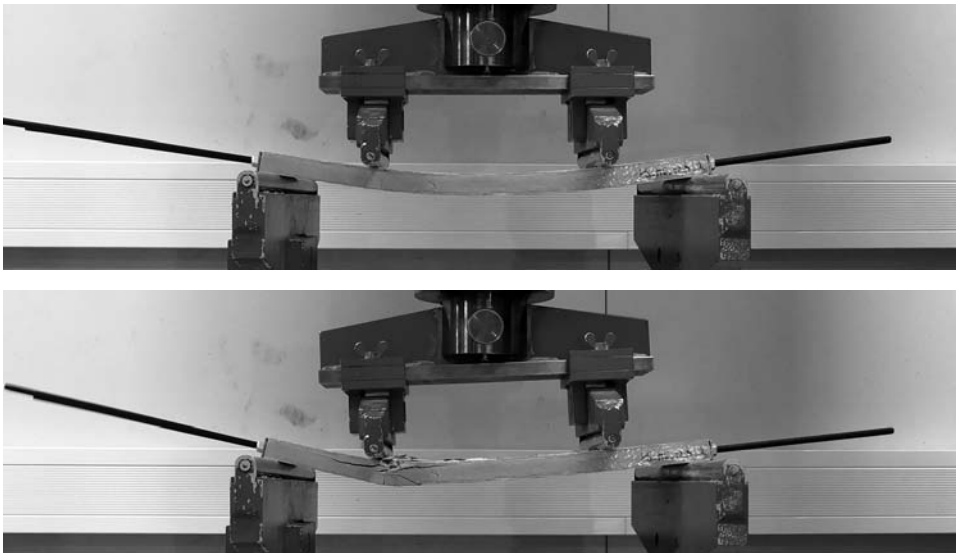
Figure F.7   Testing of specimen PS_M8_12.9_02
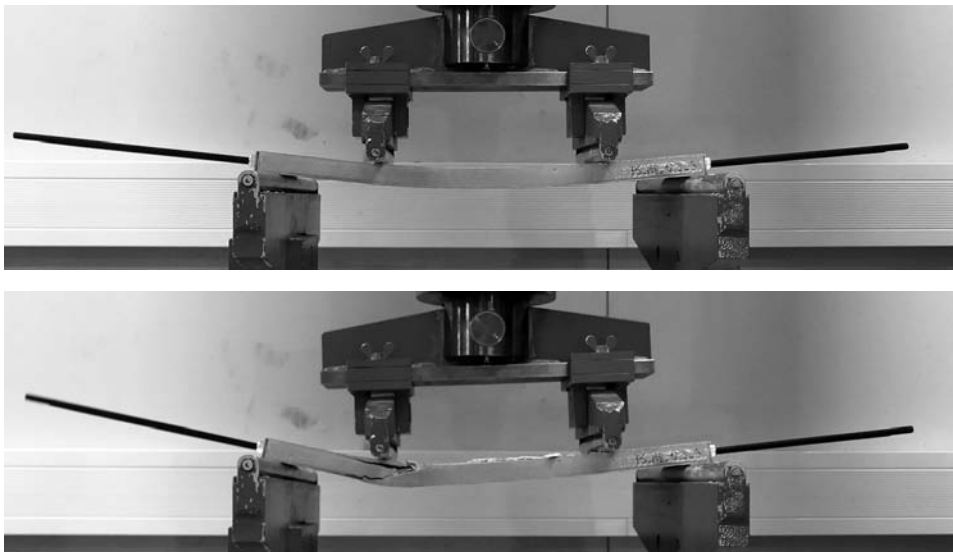
Figure F.8 Testing of specimen PS_M8_12.9_03
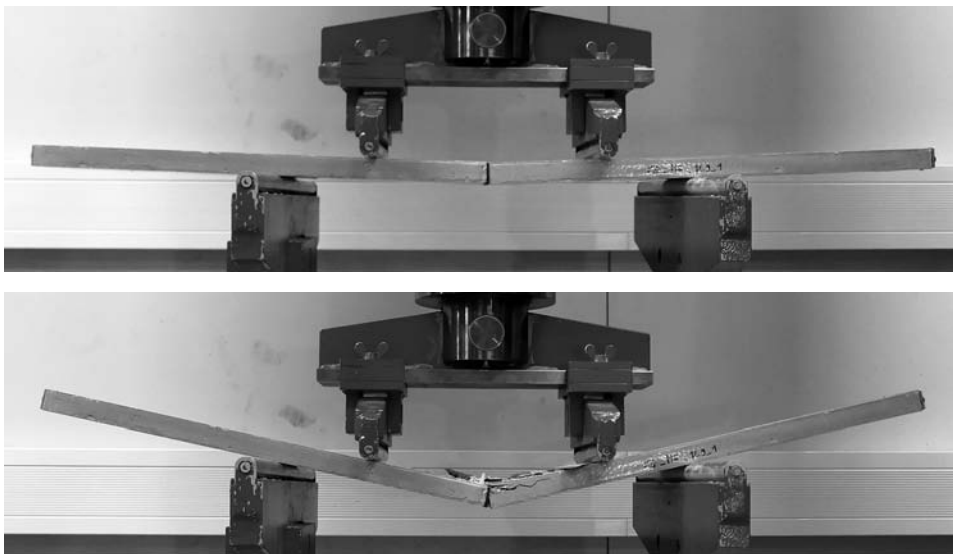
Figure F.9 Testing of specimen PJ_M8_12.9_01
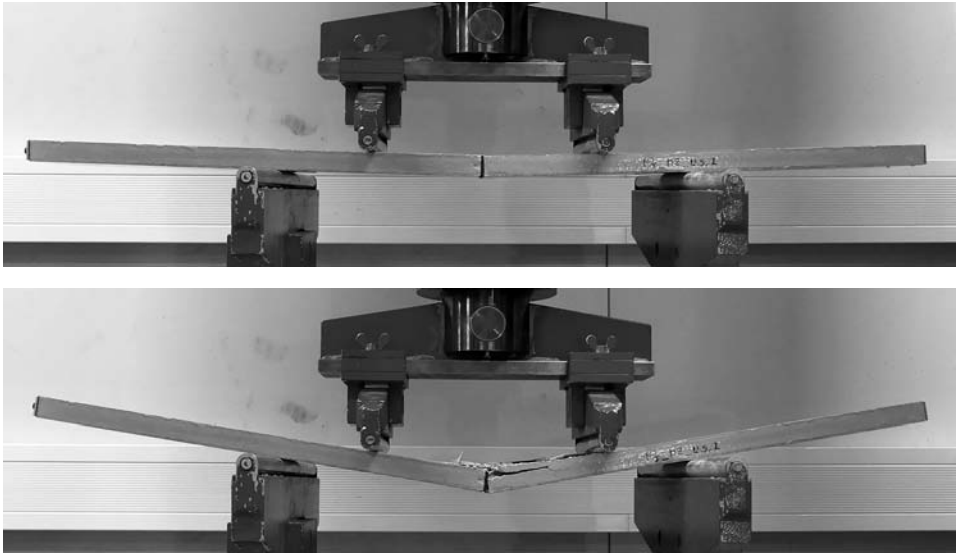
Figure F.10   Testing of specimen PJ_M8_12.9_02
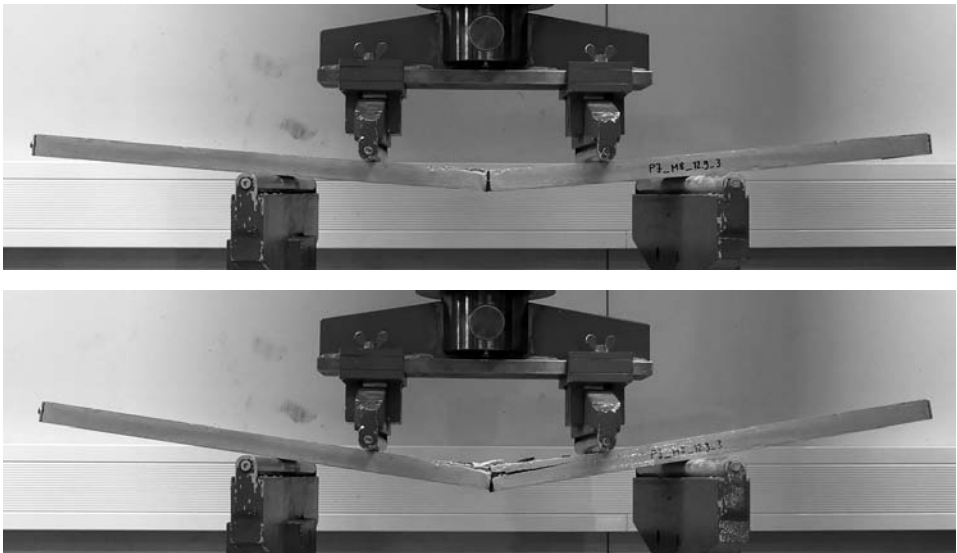
Figure F.11   Testing of specimen PJ_M8_12.9_03
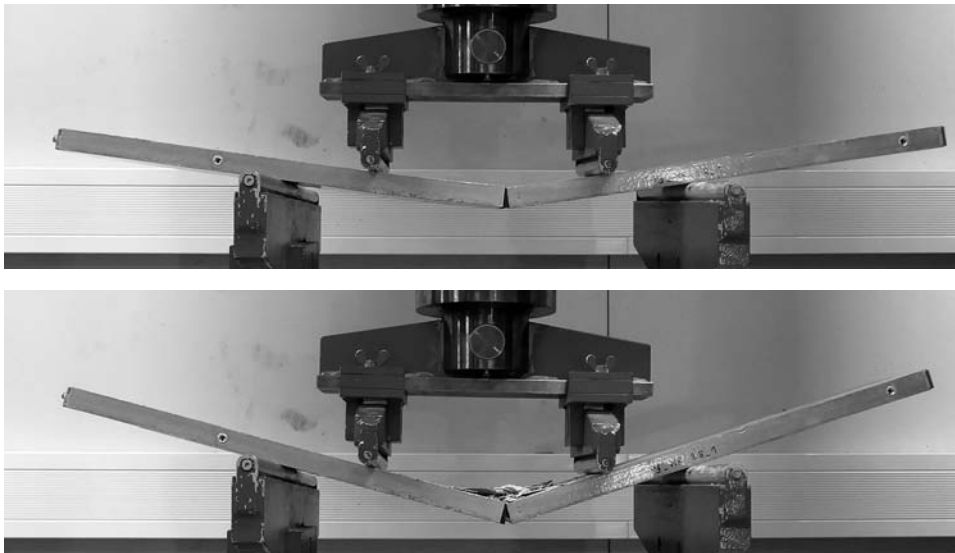
Figure F.12   Testing of specimen PJ_M8_8.8_01
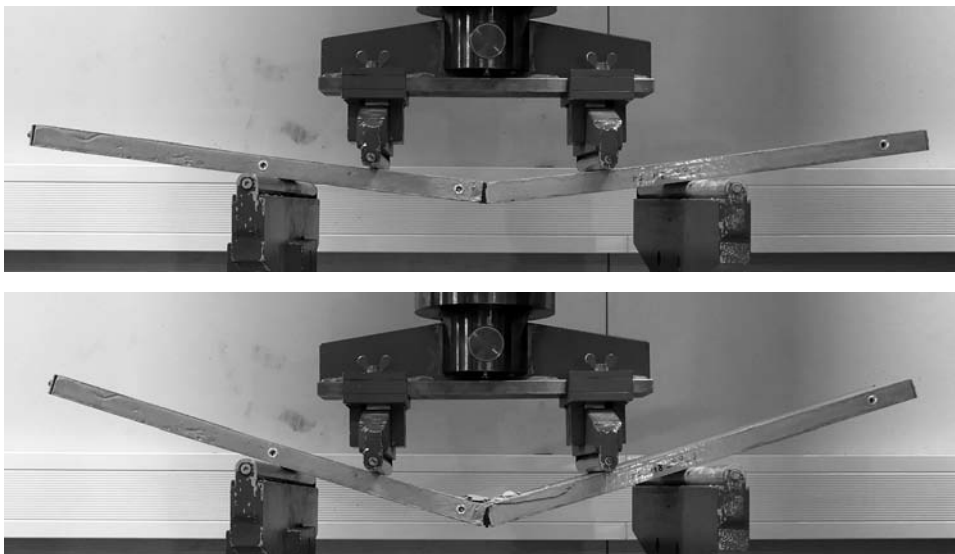
Figure F.13   Testing of specimen PJ_M8_8.8_02
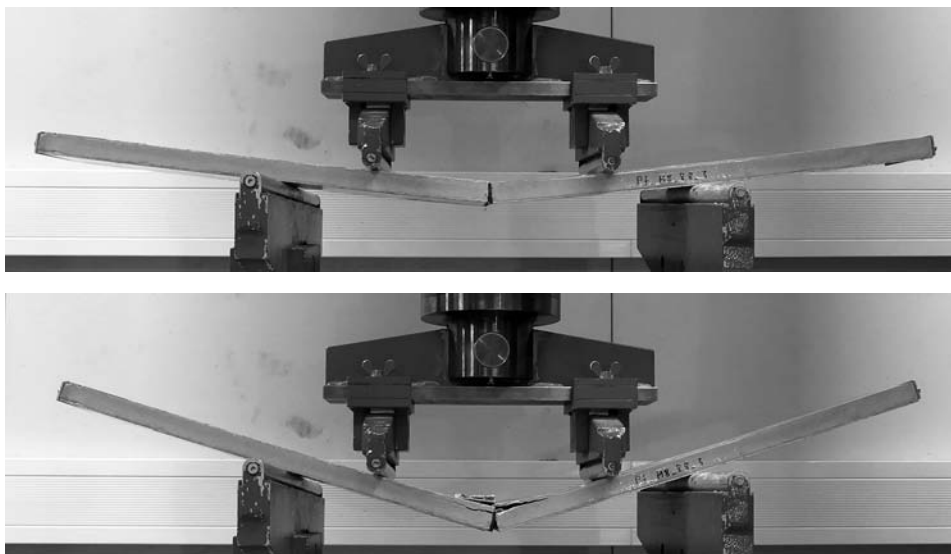
Figure F.14   Testing of specimen PJ_M8_8.8_03
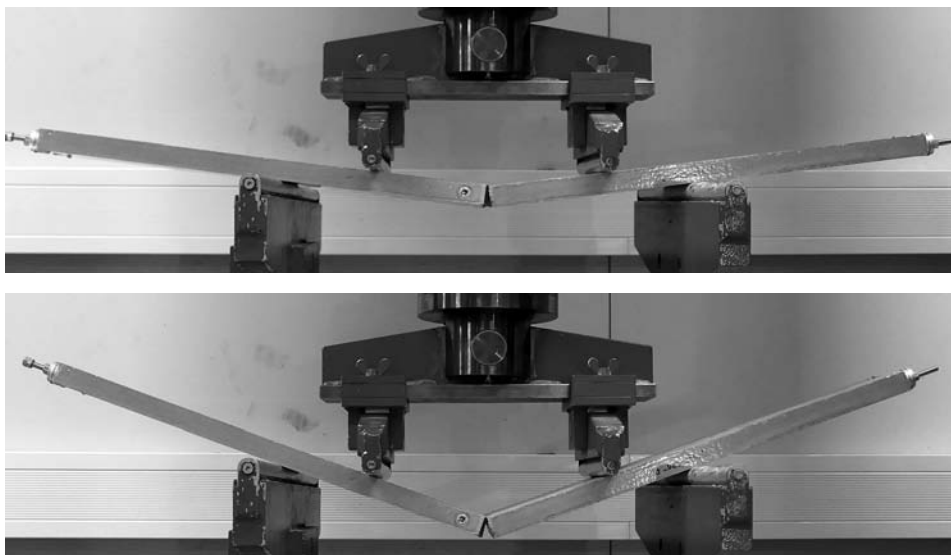
Figure F.15   Testing of specimen PJ_D2_1570_01
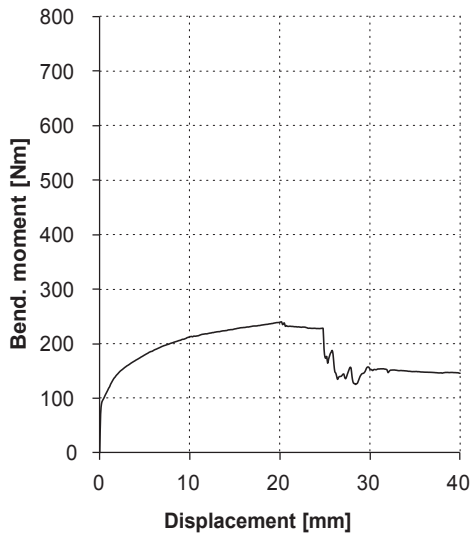
(a) Specimen *PS_0_0_01*
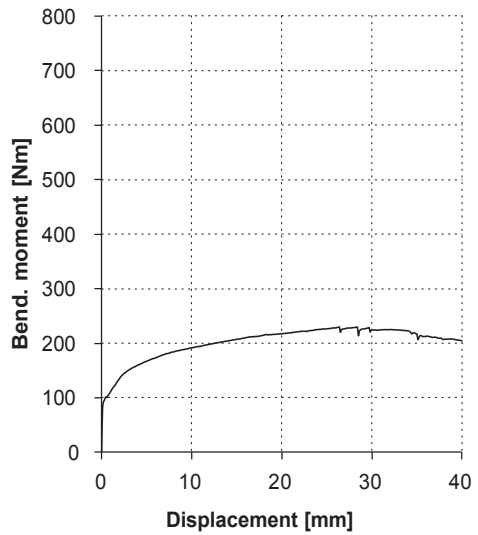
(b) Specimen *PS_0_0_02*
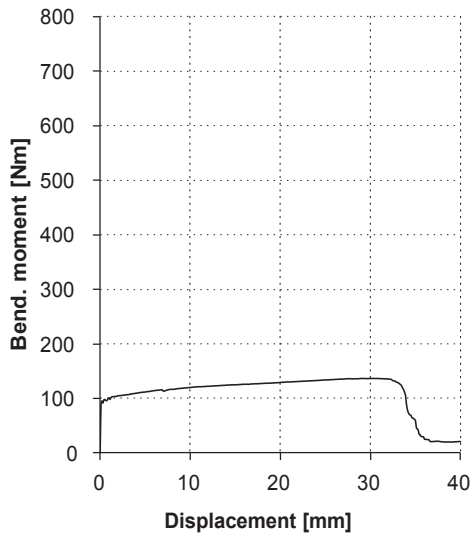
(c) Specimen *PS_0_0_03*
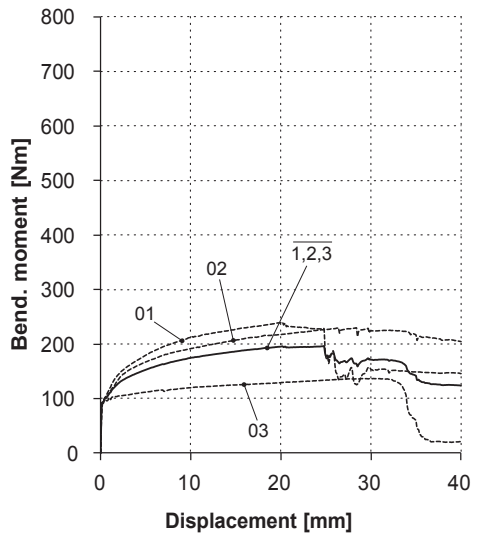
(d) Mean value graph *PS_0_0_$\overline{1,2,3}$*

Figure F.16 Load – displacement plots for concrete sections *PS* with no prestressing; plots *01*, *02*, *03* and mean value graph $\overline{1,2,3}$
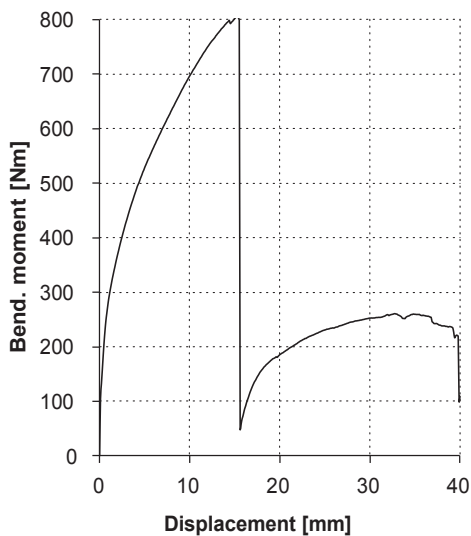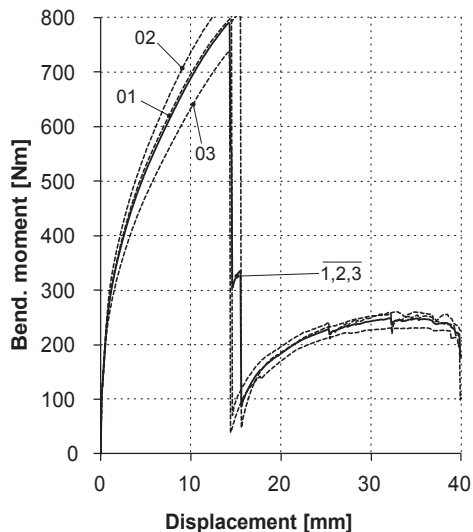
(a) Specimen *PS_M*8_12.9_01
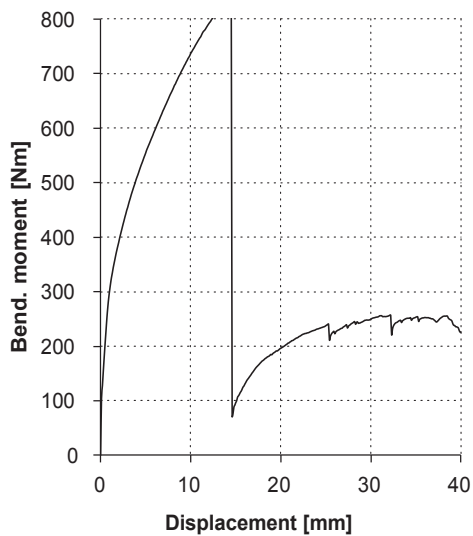
(b) Specimen *PS_M*8_12.9_02
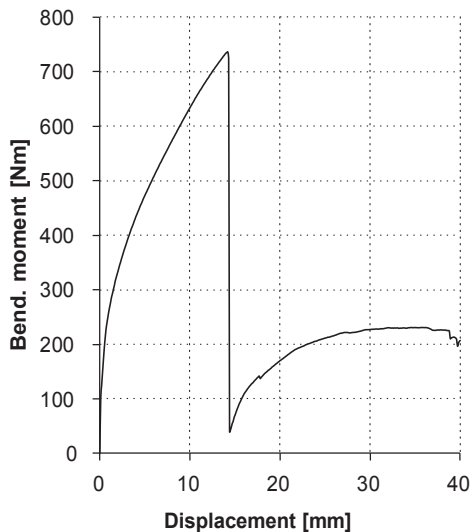
(c) Specimen *PS_M*8_12.9_03

(d) Mean value graph *PS_M*8_12.9_$\overline{1,2,3}$

Figure F.17 Load–displacement plots for concrete sections *PS* prestressed with *M8, grade 12.9*; plots *01*, *02*, *03* and mean value graph $\overline{1,2,3}$
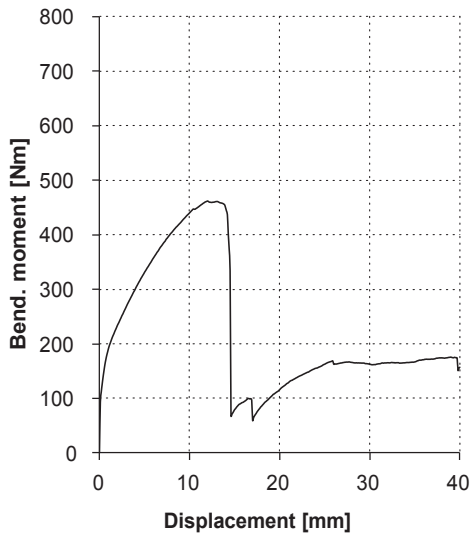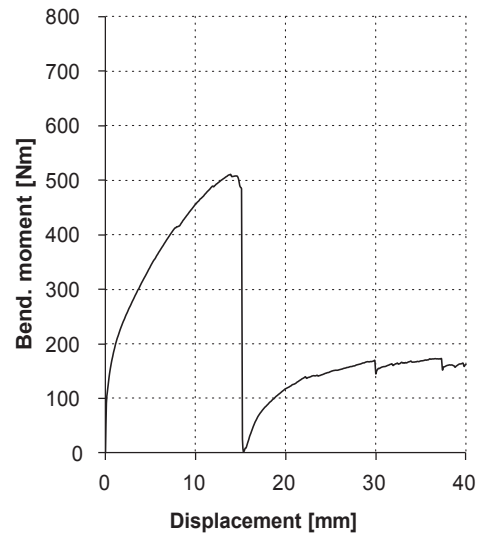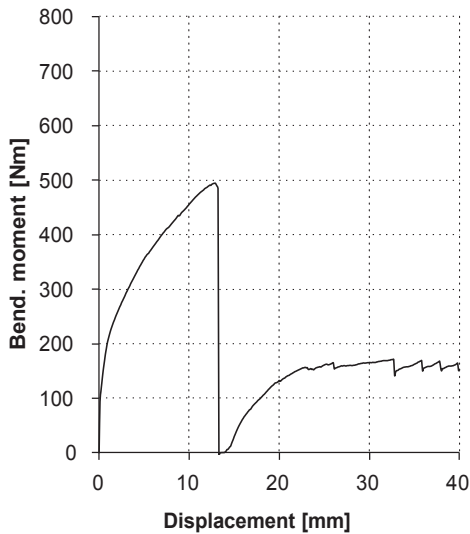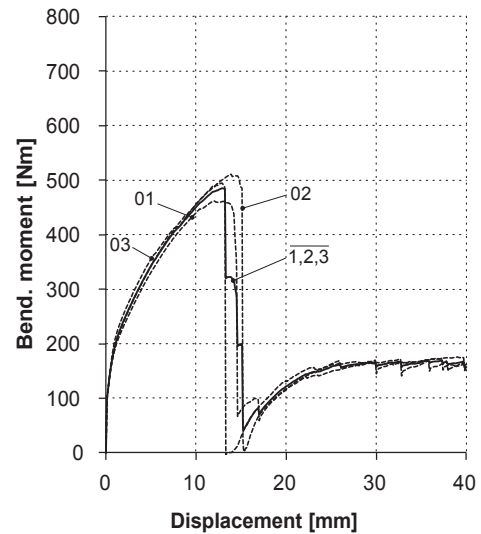
(a) Specimen *PJ_M*8_12.9_01

(b) Specimen *PJ_M*8_12.9_02

(c) Specimen *PJ_M*8_12.9_03

(d) Mean value graph *PJ_M*8_12.9_$\overline{1,2,3}$

Figure F.18 Load – displacement plots for connected elements *PJ* prestressed with *M8, grade 12.9*; plots *01*, *02*, *03* and mean value graph $\overline{1,2,3}$

(a)   Specimen *PJ_M*8_8.8_*01*

(b)   Specimen *PJ_M*8_8.8_*02*

(c)   Specimen *PJ_M*8_8.8_*03*

(d)   Mean value graph *PJ_M*8_8.8_$\overline{1,2,3}$

Figure F.19   Load–displacement plots for connected elements *PJ* prestressed with *M8, grade 8.8*; plots *01*, *02*, *03* and mean value graph $\overline{1,2,3}$
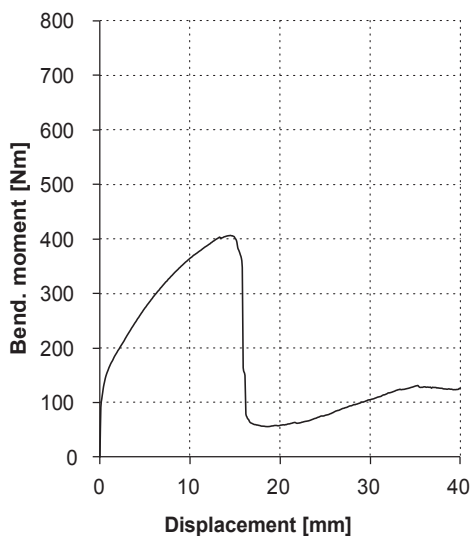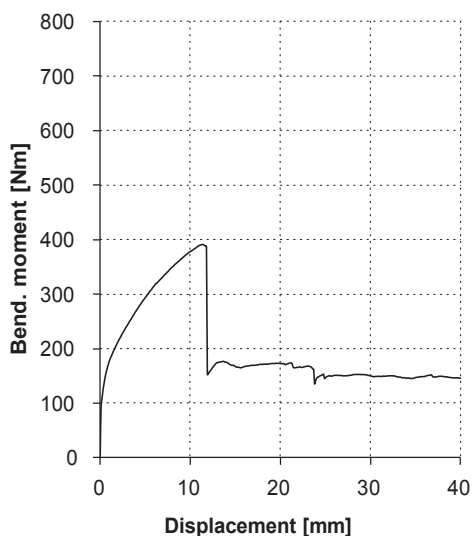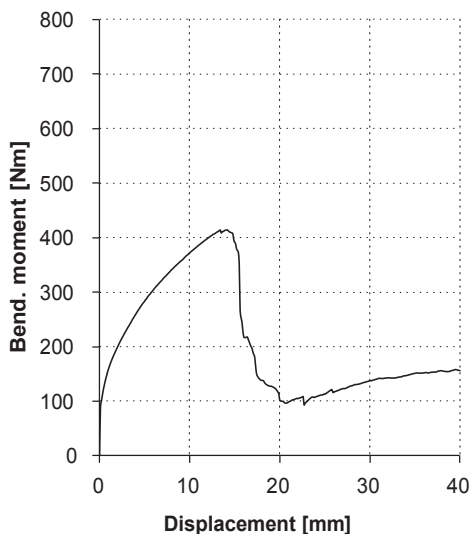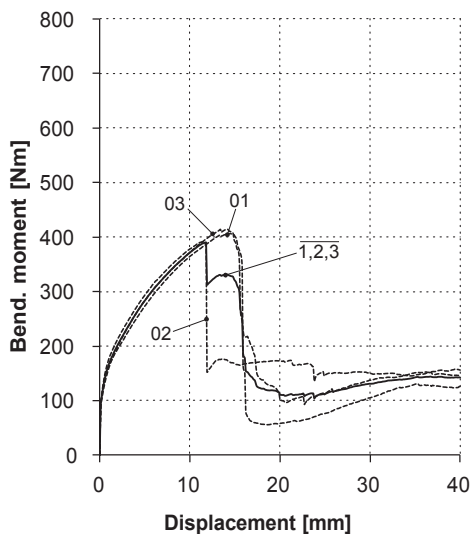
G Published work in thesis context

Conference papers

Philipp Eisenbach, Ragunath Vasudevan, Manfred Grohmann, Klaus Bollinger, Stephan Hauser. *Parapluie – Ultra Thin Concrete Shell Made of UHPC by Activating Membrane Effects*, Proceedings of the International Association for Shell and Spatial Structures (IASS) Symposium, Wroclaw, Poland, 2013 "Beyond the Limits of Men", J.B. Obrębski and R. Tarczewski (Eds.), 2013.

Philipp Eisenbach. *Parapluie und Möbiusban(k)d – Entwicklung und Realisierung ultraschlanker Schalentragwerke aus Stahlbeton*, Tagungsband CiA – Composites in Architecture, 6. Internationales Symposium Leipzig, Germany, December 2014.

Philipp Eisenbach, Manfred Grohmann, Moritz Rumpf, Stephan Hauser. *Seamless rigid connections of thin concrete shells – a novel stop-end construction technique for prefab elements*, Proceedings of the IASS2015 Annual International Symposium on Future Visions, Amsterdam, Netherlands, August 2015.

Manfred Grohmann, Philipp Eisenbach, Moritz Rumpf, Magdalena Hellmann. *Stable Equilibrium – on-site mounting technique of lightweight concrete structures*, Proceedings of the IASS2015 Annual International Symposium on Future Visions, Amsterdam, Netherlands, August 2015.

Moritz Rumpf, Manfred Grohmann, Philipp Eisenbach, Stephan Hauser. *Structural Surface – multi parameter structural optimization of a thin high performance concrete object*, Proceedings of the IASS2015 Annual International Symposium on Future Visions, Amsterdam, Netherlands, August 2015.

Oliver Tessmann, Manfred Grohmann, Philipp Eisenbach, Moritz Rumpf, Topi Äikäs. *Negotiate My Force Flow – Designing with dynamic concrete formwork*, eCAADe 2016, 34th Annual Conference "Complexity & Simplicity", Oulu, Finland, August 2016.

Manfred Grohmann, Philipp Eisenbach, Moritz Rumpf, Cynthia Ward. *Hinged Folded Festival Pavilion – Membrane Bearing in Lightweight Dismountable Structures*, Proceedings of the IASS Annual Symposium 2016 "Spatial Structures in the 21st Century", Tokyo, Japan, September 2016.

Journal articles

Philipp Eisenbach, Ragunath Vasudevan, Manfred Grohmann, Klaus Bollinger, Stephan Hauser; Winning paper of the 2013 Tsuboi Award for the outstanding paper published in the proceedings of the annual IASS Symposium "Beyond the Limits of Men", September 2013, Wroclaw, Poland. *Parapluie – Ultra Thin Concrete Shell Made of UHPC by Activating Membrane Effects*, Journal of the International Association for Shell and Spatial Structures (J. IASS), Vol. 55 (2014) No. 4 December n. 182, ISSN: (Electronic Version) 1996-9015, (Print Version) 1028-365X, Sergio Pellegrino (Ed. in Chief), p. 201–212.

Philipp Eisenbach, Ragunath Vasudevan, Manfred Grohmann, Klaus Bollinger, Stephan Hauser. *Parapluie – Realisierung einer ultraschlanken Betonschale durch Aktivierung einer Membrantragwirkung*, Beton- und Stahlbetonbau, Heft 01 2014, S. 53–59.

Philipp Eisenbach, Manfred Grohmann. *Structural implementation of slender concrete shells with prefabricated elements*, Journal of the International Association for Shell and Spatial Structures (J. IASS), special issue "New directions for shell structures", est. publication March 2017.

Books

Philipp Eisenbach: *Processing of slender concrete shells – fabrication and installation*, Dissertation at the University of Kassel, FB06 Architektur–Stadtplanung–Landschaftsplanung, January 2017.

Manfred Grohmann, Philipp Eisenbach, Moritz Rumpf: *Structural Surface – Computational design, optimization and realization of a freeform object from high performance concrete*, University of Kassel, Blurb Inc. San Franzisco, est. publication February 2017.

Exhibition

Manfred Grohmann, Philipp Eisenbach, Moritz Rumpf: *Stable Equilibrium – Concrete Mobile*, Exposition of Symposium Contest of the IASS2015 Annual International Symposium on Future Visions, Muziekgebouw Amsterdam, Netherlands, 27. June–23. August 2015.

Public recognition and cited work

Publik online. *Studierende bauen "Möbius-Bank"*, Universität Kassel Kommunikation Presse und Öffentlichkeitsarbeit, `www.uni-kassel.de/uni/universitaet/pressekommunikation/publik-online/aktuelles/campus-details/article/studierende-bauen-moebius-bank.html`, July 2014.

Competitionline Wettbewerbe und Architektur. *Möbiusban(k)d – Gewinner Kategorie I. Studienarbeiten 2015*, competitionline Verlags GmbH, `www.competitionline.com/de/beitraege/97658`, 22. Jan. 2015.

Charlotte Knoll. *MÖBIUSBAN(K)D – Entwicklung durch Evolution*, Competition Magazin, Ausgabe 11, April-June 2015, April 2015, p. 26–27

Eric   Sturm.   *Ein   Möbiusband   als   "Möbius-Bank"*,   Blog Be-
ton/Campus   (B/C),   `www.beton-campus.de/2015/09/`
`ein-moebiusband-als-moebius-bank`, 01. September 2015.

Stephan Hauser. Möbiusbank, Parapluie and TSUBOI Award in *Duktiler Hochleis-
tungsbeton als Sicherheits- und Architekturbeton beim Neubau des World-Trade
Centers*, Beton- und Stahlbetonbau, Heft 12, (109) 2014, p. A4–A8.

Ragunath Vasudevan, Mark Fahlbusch, Michael Schumacher, Klaus Bollinger,
Michael Grimm. Parapluie and Möbiusbank in *Computational systems for de-
sign and production of complex geometries with large-format roll-bent aluminum
plates*, Proceedings of the IASS Annual Symposium 2016 "Spatial Structures in
the 21st Century", Tokyo, Japan, September 2016.

Lectures

*Parapluie – Ultra Thin Concrete Shell Made of UHPC by Activating Membrane
Effects*, International Association for Shell and Spatial Structures (IASS) Sympo-
sium "Beyond the Limits of Men", Wroclaw, Poland, 26. September 2013.

*Parapluie und Möbiusban(k)d – Entwicklung und Realisierung ultraschlanker Scha-
lentragwerke aus Stahlbeton*, CiA – Composites in Architecture, 6. Internationales
Symposium Leipzig, Germany, 02. December 2014.

Structural Surfaces, Digital Design Unit (DDU) in the Faculty of Architecture,
TU – Darmstadt, Germany, 02. June 2015.

*Seamless rigid connections of thin concrete shells – a novel stop-end construc-
tion technique for prefab elements*, International Association for Shell and Spatial
Structures (IASS) Symposium on Future Visions, Amsterdam, Netherlands, 18.
August 2015.

Stable Equilibrium – on-site mounting technique of lightweight concrete structures, International Association for Shell and Spatial Structures (IASS) Symposium on Future Visions, Amsterdam, Netherlands, 20. August 2015.

Thin walled concrete structures – Implementation features, Nottingham PhD Summer School; DESIGN + TECTONICS: Working in the Space between Theory and Practice, Nottingham, England, 05. July 2016.

Processing of slender concrete shells – fabrication and installation, Disputation, University of Kassel, Faculty of Architecture, Kassel, Germany, 30. January 2017.

Awards

Tsuboi Award. For the outstanding paper presented and published in the Proceedings of the 2013 IASS symposium, Wroclaw 'Beyond the Limits of Men', Poland. Parapluie – Ultra Thin Concrete Shell Made of UHPC by Activating Membrane Effects, Brasilia, September 2014.

Competition Campus Award. Möbiusban(k)d, Competitionline Wettbewerbe und Architektur Verlags GmbH, Berlin, Germany, January 2015.

Lightweight structures and material optimized systems are of major relevance in the building industry and particularly in the design of concrete structures. This is not only for aesthetic reasons, but also to use material in a resource conserving way. The increase of strength characteristics, as one measure to reduce cross section dimensions, postulates the prefabrication of cementitious materials under laboratory conditions. This thesis examines the contradiction of the possibility to realize slender concrete elements and the complexity of the discontinued homogeneity arising from necessary segmentations. Proposals of implementation strategies are demonstrated and verified on the basis of selected case studies.

Philipp Eisenbach studied civil engineering at the Technical University Darmstadt, the University of New South Wales in Sydney and the École Polytechnique Fédérale de Lausanne. Since his graduation in 2006 he has practiced in structural engineering and realized several national and international renowned projects. In 2017 he received his doctorate from the University of Kassel under the supervision of Manfred Grohmann.